NON-LINEAR BEHAVIOUR OF RECTANGULAR ORTHOTROPIC PLATES UNDER TRANSVERSE AND IN-PLANE LOADS

A thesis presented for the degree of

Doctor of Philosophy

of the University of London

in the Faculty of Engineering

by

Bijan AALAMI, B.Sc.(Eng.)

Imperial College of Science and Technology,
London.

November, 1966

ABSTRACT

A treatment is presented for the elastic non-linear behaviour of rectangular orthotropic (including isotropic) plates subjected simultaneously to transverse and inplane loads, the non-linearity being due to large deflections.

Boundary restraints are introduced which can be rotational, extensional, tangential, or normal to the plane of the plate, and their specifications cover a wide range of plate problems. Uniform and concentrated distributions of transverse pressure are considered. The inplane loading may be in the form of either an applied edge-compression, or an applied edge-displacement, or a combination of both. Initial deformations are also allowed for.

The von-Karman differential equations of plates are appropriately modified, non-dimensionalised and expressed in terms of finite differences. Graded meshes are used where suitable. The resulting equations are solved by an iterative process using the University of London Atlas Computer. Close agreement was found in the comparison of results with the few existing solutions.

A selected range of problems have been solved and discussed in detail. Numerical results are given which enable non-linear plate behaviour in many other practical cases to be predicted.

The investigation shows the influence on behaviour of the inplane boundary conditions, the extent of which has not been fully recognised previously. It has been demonstrated that in many cases the extensional boundary conditions can be at least as important as the flexural conditions.

The scope of treatment is such that many other outstanding plate problems are capable of solution.

ACKNOWLEDGEMENTS

The research reported in this thesis was carried out in the Civil Engineering Department of Imperial College under the direction of Dr. J.C. Chapman, to whom the author is greatly indebted for his valuable suggestions and constant guidance. The project was sponsored by the British Ship Research Association; the author wishes to thank the Association for their financial support.

The author is deeply grateful to Professor S.R. Sparkes for giving the opportunity of this research work.

The proposal to undertake full-time research was arrived at following discussions with Dr. E.H. Brown to whom the author is thankful for this valuable suggestion.

On the experimental aspect of the work, thanks are due to Mr. N.D. Scott for construction of the model, to Messrs. P.F. Taylor and P. Guile for discussions on the design of the loading rig, and to Messrs. T. Wells and L. Billinghurst for their great skill and devoted perseverance in the construction of the loading rig and preparation of the test arrangements.

The author is also grateful to Mr. P.G. Dowling for useful discussions on the research project, to Mr. D.G. Williams for his general assistance in the preparation of the thesis, to Mr. M. Oshidari for his help in plotting the graphs and proof-reading, and finally to Mrs. S. A. Thomas for typing.

CONTENTS

		Page No.
NOTATION		9
CHAPTER I	Introduction	21
	Origins and scope of the Present Research	36
CHAPTER II	Theory	40
	List of Figures and Tables	61
CHAPTER III	Theoretical Results	63
CHAPTER IV	Conclusions	89
CHAPTER V	Experimental Work	95
REFERENCES		101
APPENDIX A	Notation	107
APPENDIX B	Derivation of the Non-Linear Plate Equations	108
APPENDIX C	Finite Difference Solution	136
APPENDIX D	Transformation of the Orthotropic Plates	163
APPENDIX E	Comparison of Results and Accuracy Checks	168
APPENDIX F	Solution by Digital Computer	188
APPENDIX G	Numerical Examples	191
FIGURES		193
TABLES		266

NOTATION

x, y, z	Cartesian coordinates, being normal to the plane of the plate
$u, v, \bar{w}$	Displacements of mid-surface of plate in x, y and z directions respectively caused by the applied loading
w_o	Initial deformations of plate corresponding to w
w	$= \bar{w} + w_o$. Total displacement of the middle surface of plate in z-direction
a	Length of plate in x direction
b	Length of plate in y direction
h	Thickness of plate
q	Intensity of lateral pressure at the point (x, y)
p_x	Intensity of applied load in x direction per unit width in y direction at $x = \pm a/2$, positive when tensile
p_y	Intensity of applied load in y direction per unit width in x direction at $y = \pm \frac{b}{2}$, positive when tensile
M_x, M_y	Bending moments in x and y directions per unit width of plate in y and x directions respectively
M_{xy}	Twisting moment per unit width of plate
N_x, N_y	Membrane forces in x and y directions per unit width of plate in y and x directions respectively, positive when tensile
N_{xy}	Inplane shear force per unit width of plate
σ_x, σ_y	Membrane stresses in x and y directions
σ_{xy}	Inplane shear stress
ν_{xb}, ν_{yb} or μ_{xb}, μ_{yb}	Poisson ratios in bending associated with applied bending moment in x and y directions respectively

ν_{xm}, ν_{ym} or μ_{xm}, μ_{ym}	Poisson ratios in extension associated with applied tension in x and y directions respectively
e_x, e_y	Strains in mid-surface of plate in x and y directions respectively, positive when tensile
γ'_{xy}	Shearing strain of mid-surface of plate
E	Young's Modulus of elasticity
C_x	$= N_x / e_x$ Forces to produce unit strain with transverse
C_y	$= N_y / e_y$ deformations unrestrained, $(Eh)^*$
C_1	$= -\frac{C_x}{\nu_{xm}} = -\frac{C_y}{\nu_{ym}}$, $(\frac{Eh}{\nu})^*$
C_{xy}	Shearing rigidity, $(Gh = \frac{Eh}{2(1+\nu)})^*$
H_m	$= 1/(\frac{1}{C_1} + \frac{1}{2C_{xy}})$, $(Eh)^*$
P_{xy}, P_{yx}	Applied inplane shear forces per unit width of plate at $x = \pm a/2$ and $y = \pm b/2$ respectively
u_a, v_a	Applied displacements at $x = \pm a/2$ and $y = \pm b/2$ in x and y directions respectively
Q_x, Q_y	Normal shear forces per unit width of plate in y and x directions respectively
V_x, V_y	Normal reactions per unit width of plate, associated with Q_x and Q_y, at $x = \pm a/2$ and $y = \pm b/2$ respectively

*Values in parenthesis relate to isotropic plates

B_x	$= M_x / \frac{\partial^2 w}{\partial x^2}$	Bending moments to produce unit curvature with anticlastic curvatures unrestrained, $(Eh^3/12)$*
B_y	$= M_y / \frac{\partial^2 w}{\partial y^2}$	
D_x	$= B_x/(1 - \nu_{xb} \cdot \nu_{yb})$	Flexural rigidities in x and y directions respectively, $(Eh^3/12(1-\nu^2))$*
D_y	$= B_y/(1 - \nu_{xb} \cdot \nu_{yb})$	
D_1	$= \nu_{xb} D_y = \nu_{yb} D_x$, $(\nu EH^3/12(1-\nu^2))$*	
D_{xy}	Torsional rigidity, $(Eh^3/24(1+\nu))$*	
H_b	$= 2D_{xy} + D_1$, $(Eh^3/12(1-\nu^2))$*	
f	Airy's stress function	
ε or ρ	$= a/b$	
X	$= x/a$	Dimensionless coordinates
Y	$= y/b$	
W	$= w\sqrt{C_x/D_x}$	Dimensionless total deflection, $(3.305\ w/h)$*
W_o	$= w_o\sqrt{C_x/D_x}$	Dimensionless initial deformation $(3.305\, w_o/h)$
Q	$= \frac{a^4}{D_x}\sqrt{\frac{C_x}{D_x}} \cdot q$	Dimensionless intensity of applied transverse load (pressure ratio), $(36.09 \frac{a^4}{h^4} \cdot \frac{q}{E})$*
P_x	$= \frac{P_x a^2}{D_x}$	Dimensionless intensity of the applied inplane loading at $x = \pm \frac{a}{2}$ and $y = \pm \frac{b}{2}$ respectively, $(10.92 \frac{a^2}{h^2} \cdot \frac{\sigma x}{E})$*
P_y	$= \frac{P_y a^2}{D_x}$	

* Values in parenthesis relate to isotropic plates

U	$= au\frac{C_x}{D_x}$	Dimensionless intensity of the displacements at $x = \pm a/2$ and $y = \pm b/2$ respectively
V	$= av\frac{C_x}{D_x}$	
U_a	$= a \cdot \frac{C_x}{D_x} \cdot u_a$	Dimensionless applied displacements corresponding to u_a and v_a respectively, $(10.92\frac{a^2}{h^2} \cdot \frac{u}{a})$
V_a	$= a \cdot \frac{C_x}{D_x} \cdot v_a$	
F	$= f/D_x$	Dimensionless stress function

k_{rx} Stiffness of elastic restraint against rotation at $x = \pm \frac{a}{2}$, being equal to moment per unit length to produce unit rotation of the restraint

k_{ry} Stiffness of elastic restraint against rotation at $y = \pm \frac{b}{2}$, being equal to moment per unit length to produce unit rotation of the restraint

k_{dx} Stiffness of elastic restraint against displacement perpendicular to the plane of the plate at $x = \pm a/2$, being equal to the force per unit width of plate to displace the restraint a unit length

k_{dy} Stiffness of elastic restraint against displacement normal to the plane of the plate at $y = \pm \frac{b}{2}$, being equal to the force per unit width of plate to displace the restraint a unit length

k_{mx} Stiffness of elastic restraint at $x = \pm \frac{a}{2}$ against movement in x direction, being equal to the force per unit width of plate to produce unit extension or compression of the restraint

k_{my} Stiffness of elastic restraint at $y = \pm b/2$ against movement in y direction, being equal to the force per unit width of plate to produce unit extension or compression of the restraint

k_{sx} Stiffness of elastic restraint at $x = \pm \frac{a}{2}$ against movement parallel to y axis, being equal to the tangential force per unit width of plate to produce unit displacement of the restraint

k_{sy} Stiffness of elastic restraint at $y = \pm \frac{b}{2}$ against movement parallel to x axis, being equal to the tangential force per unit width of plate to produce unit displacement of the restraint

t_{rx}, t_{ry} Torsional rigidity of the edge beams at $x = \pm a/2$ and $y = \pm b/2$, being equal to the torque required to produce unit twist per unit length of the edge beams respectively

b_x, b_y Flexural stiffness of the edge beams at $x = \pm a/2$ and $y = \pm b/2$, being equal to the bending moments required to give unit curvatures to the beams in y-z and x-z planes respectively

$K_{rx} = a\, k_{rx}/D_x$, $K_{ry} = a\, k_{ry}/D_y$ Coefficients of rotational edge restraints, (constant along the edges)

$K_{dx} = a^3 k_{dx}/D_x$, $K_{dy} = a^3 k_{dy}/D_y$ Coefficients of edge restraints against normal displacement to the plante of the plate, (constant along the edges)

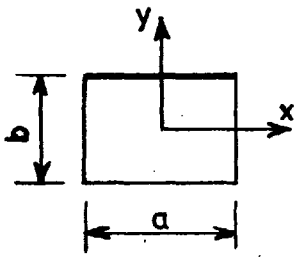
$K_{mx} = a\, k_{mx}/C_x$, $K_{my} = b\, k_{my}/C_y$ Coefficients of extensional edge restraints, (constant along the edges)

K_{sx}	$= a\, k_{sx}/C_y$	Coefficients of shear edge restraints, (constant along the edges)
K_{sy}	$= a\, k_{sy}/C_x$	
T_{rx}	$= t_{rx}/aD_x$	Torsion coefficients of edge beams
T_{ry}	$= t_{ry}/aD_x$	
B_{dx}	$= b_{dx}/a\, D_x$	Flexibility coefficients of edge beams
B_{dy}	$= b_{dy}/a\, D_x$	
K_1	$= C_x/C_y$	
K_2	$= C_x/H_m$	
K_4	$= H_b/D_x$	
K_5	$= D_y/D_x$	
λ	$= \sqrt[4]{D_y/D_x}$	
ε' or ρ'	$= \frac{a\lambda}{b}$, virtual side ratio	
a	$= H_b/\sqrt{D_y D_x}$, equivalent flexural stiffness ratio	
β	$= \sqrt{C_x C_y}/H_m$, equivalent extensional stiffness ratio	
γ	$= \sqrt[4]{C_y/C_x}\,/\sqrt{D_y/D_x}$	
W'	Deflection ratio	
Q'	Pressure ratio	
M'_x, M'_y M'_{xy}	Bending moment ratios	For definition
N'_x, N'_y, N'_{xy}	Inplane lead and membrane force ratios	see
U', V'	Inplane displacement ratios	Appendix D

P_e $= \frac{4\pi^2 D_x}{a^2}$, critical buckling force for a simply supported square plate under uniaxial compression with inplane movements in the transverse direction unrestrained

U_e $= \frac{\pi^2}{6(1-\nu^2)} \cdot \left(\frac{h}{a}\right)^2 \cdot a$, critical strain for a simply supported square plate under uniaxial compression with inplane movements in the transverse direction unrestrained

Symbols for limiting flexural boundary conditions.



Symbol	boundary condition
———	rigidly supported, hinged edge.
═══	rigidly supported, fixed edge
— — —	unsupported, hinged edge.
═══ — — —	unsupported, fixed edge

FIG. A - 1

Symbols for the more common cases of transverse loading.

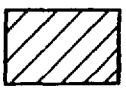
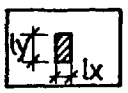
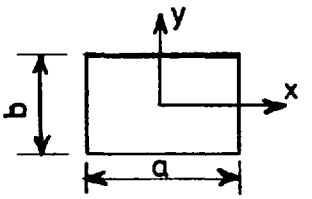
Symbol	Transverse loading
	Uniformly distributed load on the whole surface
	central patch load of dimensions lx and ly

FIG. A - 2

Symbols for limiting inplane boundary conditions



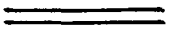
symbol	boundary condition
———	zero direct stress, zero shear stress
	zero extension, zero shear stress
	zero extension, zero tangential displacement
	zero direct stress, zero tangential displacement
	edge remains straight with zero total direct force , zero shear stress.
	edge remains straight with zero total direct force, zero tangential displacement

Fig. A - 3

Symbols for the more common inplane loading conditions

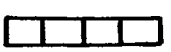
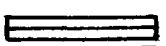
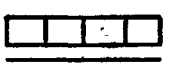
Symbol	Inplane loading
	uniform direct stress , zero shear
	uniform edge displacement , zero shear
	uniform edge displacement under specified total direct force , zero shear

Fig. A - 4

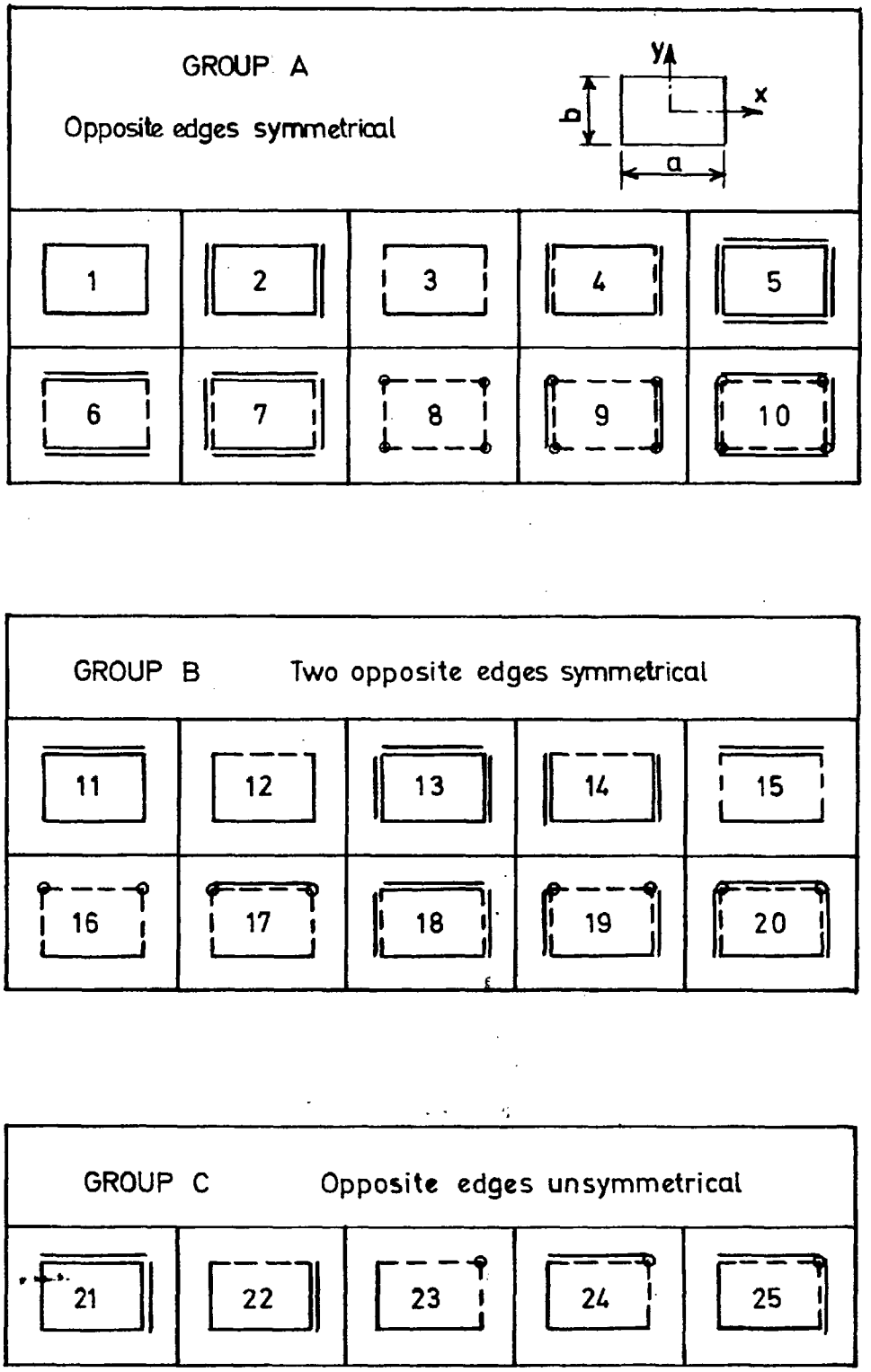


Fig. A- 5 Rectangular plates with limiting flexural boundary conditions. (those within the scope of the present analysis are shown)

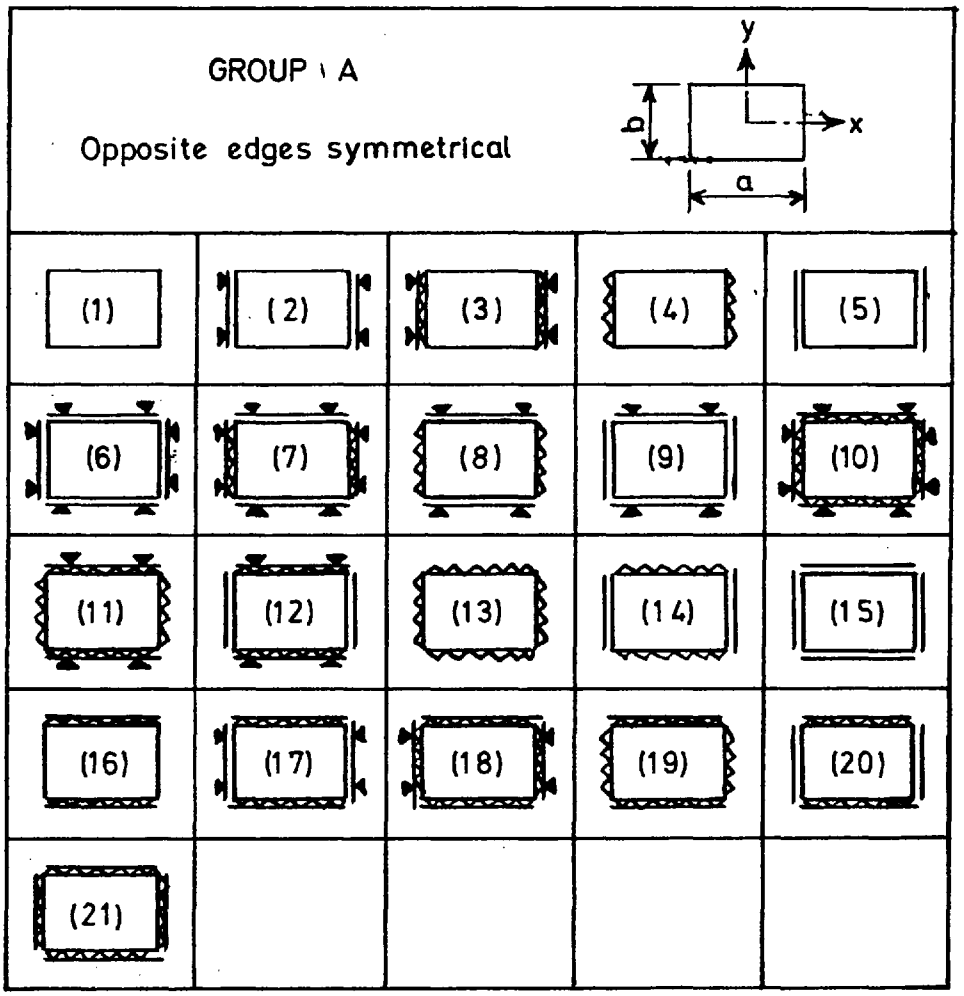


Fig. A-6 Limiting membrane boundary conditions of transversely loaded rectangular plates.

(those within the scope of the present analysis are shown)

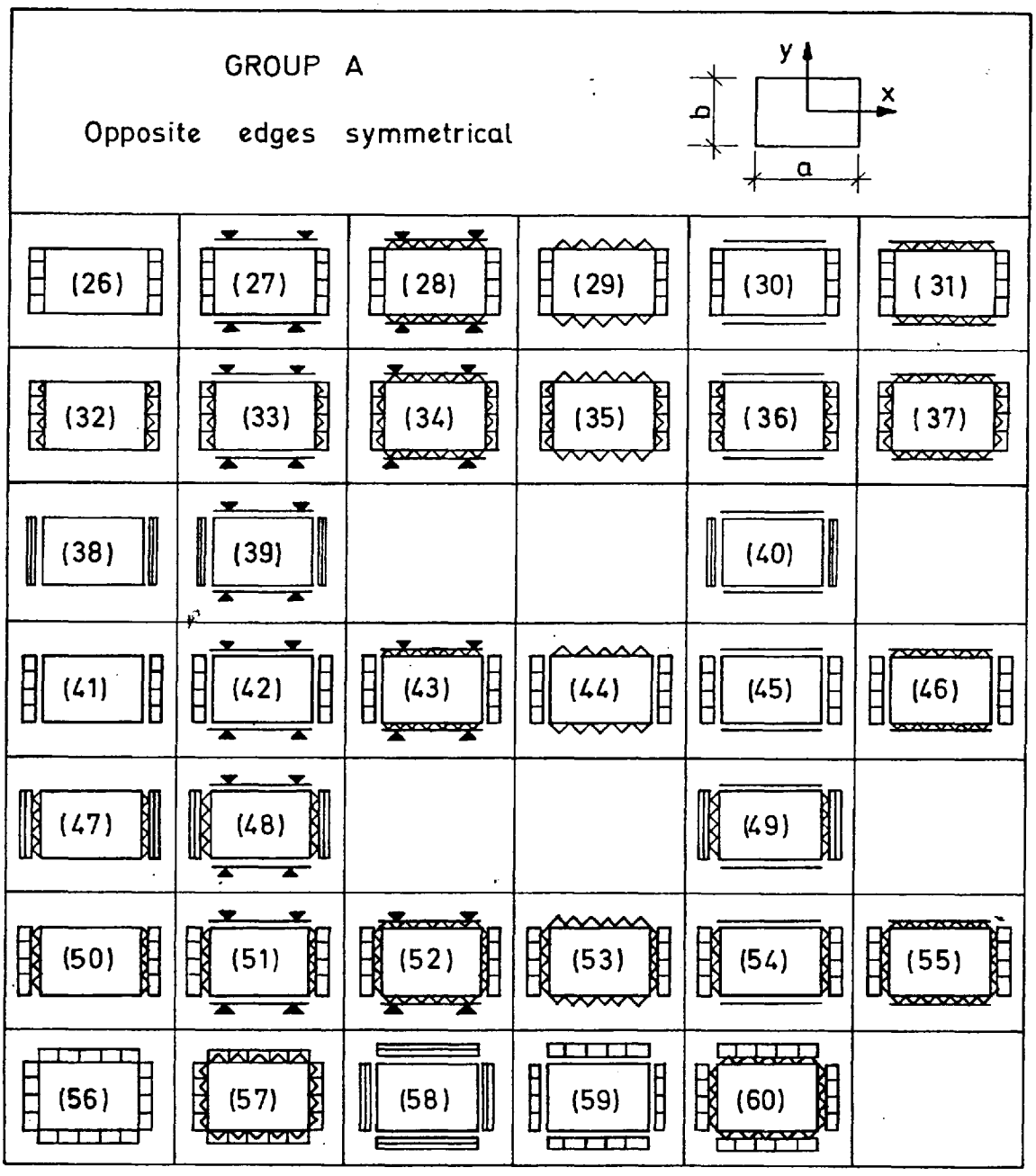


FIG. A - 7 Limiting membrane boundary conditions and inplane loading of rectangular plates under uniform edge compression or edge displacement.

CHAPTER I

INTRODUCTION

General

Certain structures are made up of grid or framework systems which are skinned with panels of plating. The structural function of the plating in such assemblies is twofold. Firstly the plates may receive direct transverse pressure which is then transferred to the rest of the system by bending and possibly by membrane action; secondly they may be subjected to thrusts in their planes due to the overall deformation of the whole structure in sustaining the applied load.

Plate panels which form the outside shell of the bottom of ship hulls are under direct transverse loading due to water pressure, and inplane loading partly as a result of the overall bending of the ship and partly due to the transverse bending of the bottom.

The plate panels covering the wings and the fuselage of aircraft are similarly loaded.

In bridge decks constructed of stiffened plating, the plating receives as direct transverse pressure the wheel load of the vehicles, and in acting as the compression flange of the deck and of the main girders is subjected to simultaneous inplane loading.

As a result of handling, construction and welding, the finished plate panels are rarely flat. The deviation from flatness is frequently of the same order of magnitude as the thickness of the plate. Alternatively the plate panels may have been deliberately dished for structural reasons. The behaviour of these plates when subjected to end thrust is analogous to that of flat plates

under inplane and transverse loading. The method of analysis used for flat plates under combined loading may, therefore, be extended to be applicable to initially deformed plates.

The assemblies in which the stiffeners are closely spaced can be idealised for the purpose of their overall stress analysis as orthotropic plates. The loading of these orthotropic plates may also be combined as already discussed for the constituent plate panels.

In the analysis of plates under transverse pressure and edge compression, it is frequently assumed that, provided the deflection of the plate remains small relative to its thickness, the stresses due to bending may be found from the classical small deflection theory of transversely loaded plates; and for stresses due to edge compression plane stress analysis may be used. The results obtained separately may then be superimposed to give the final state of stresses in the plate.

The edge compression, however, reduces the flexural stiffness of the plate and consequently results in higher deflection and bending stresses due to transverse pressure, even when the deflections are small. The methods of analysis which incorporate the reduction of stiffness in bending due to the in-plane loading, instead of the superimposition of the effects, are a more exact approach to the problem and are referred to as small deflection, linear or linearised solutions.

In fact, as soon as the plate deflects, membrane forces set in. By the time the deflection of the plate reaches 0.1 - 0.5 of its thickness, the membrane forces become a predominant factor in the behaviour of the plate. Their influence extensively alters the original distribution of stress based on the small deflection (linearised) solutions, where effects of membrane forces are neglected. The position of maximum stress may shift considerably and stress reversals may occur. The behaviour (e.g. load-deflection relationship) of such plates is

non-linear. The solutions, in which the effects of the membrane forces are accounted for are generally called non-linear solutions, reflecting the nature of the results they give. It is important to note that here the non-linearity is due to the change of the geometry of the plate under the applied loading.

A characteristic of plates under inplane loading is instability. Initially flat plates buckle at their critical buckling loads and sustain further loading in their post-buckling region. For initially deformed plates and plates under simultaneous transverse loading, there are also specific values of inplane thrust for which the plates become unstable (i.e. the applied loading can be resisted by an alternative deflected profile by less energy). The instability of such plates is more difficult to analyse.

Depending on the dimensions and loading of the individual plate panels, at a certain stage of loading the development of the membrane forces is accompanied by the yielding of the material of the plate at the region of high stresses. The behaviour of the plate is thereafter affected by a second factor of non-linearity, namely, plasticity. Some panels of plating especially if they are thin or initially deformed, may develop extensive membrane forces before the onset of plasticity.

The work presented in this thesis, however, is limited to the elastic behaviour of the plating, the study of which is necessary in order to determine the state of stresses and specially the position of maximum stress for further elasto-plastic and ultimate load analysis.

The non-linear behaviour of plates under the combined action of inplane and transverse loading is very complex. The nature of the inplane loading (applied edge displacement, applied force or a combination of both) and the membrane boundary conditions have to be closely examined and clearly defined for any particular plate problem. Each plays a prominent part in the behaviour

of the plate which is not possible to predict from small deflection and plane stress solutions alone.

The equations governing the elastic non-linear behaviour of isotropic homogeneous plates were first derived by von Karman[1] in the form of two fourth order simultaneous partial differential equations in terms of the transverse deflection of the plate and a stress function for the membrane action of the plate. G. G. Rostovcev[2] derived the same equations as applicable to homogeneous orthotropic plates. Soper[3] presented the derivation of the governing equations for stiffened plates treated as orthotropic plates.

The methods of approach to the treatment of plate problems fall initially under two categories, namely, those aimed at some kind of solution of the governing differential equations, and those in which the plate is substituted by a theoretical model whose behaviour can be related to the actual plate and is less cumbersome to analyse.

In the following a concise review of the work done so far on the non-linear behaviour of plates is given. The review is restricted to the methods in which solutions for von Karman's differential equations in their original, elaborated or simplified forms are sought.

Methods of Solution

The direct solution of the von Karman equations is lengthy and involved even for simple cases of loading and boundary conditions. It becomes almost impossible for general loading and complicated boundary conditions. Several methods, some approximate and indirect, have been put forward by the previous investigators in this field. The major methods of the treatment of the problem are

(i) Ritz energy method. Solutions based on this method assume expressions for the three displacements (u, v, w) in the form of algebraic polynomials with unknown coefficients. The polynomials are chosen such that they satisfy the boundary conditions. The unknown coefficients are then determined by minimizing, with respect to the coefficients, the total potential energy of the plate.

(ii) Fourier series method. Deflection and the stress functions for the plate are expressed in terms of infinite trigonometrical series with unknown coefficients. The coefficients are subsequently evaluated by substituting the assumed series in the governing equations and solving the resulting set of simultaneous equations.

(iii) Finite difference method. The plate is subdivided into a mesh. The differential equations of the plate, together with the boundary conditions, are converted into finite difference expressions at the nodes of the mesh. The resulting sets of simultaneous equations are solved either by a relaxation technique or directly.

Large Deflection of Transversely Loaded Plates

Kaiser[4] obtained a finite difference solution for a simply supported square plate with edges free from inplane shear and direct stresses under uniform transverse pressure. The author's theoretical solution (for one specific value of pressure only) agreed closely with his experimental results.

Marguerre[5] employed the Ritz energy method to investigate a similar problem, namely, that of a simply supported square plate in which the edges remain straight while they are permitted to move in a direction perpendicular to themselves. Also, instead of the direct stresses themselves vanishing, their integral along each boundary vanishes. This is a boundary condition less

laborious to formulate and solve than the stress free boundary condition by this method.

Again by means of the Ritz energy method Way[6] succeeded in solving the case of transversely loaded plates clamped against rotation and inplane movements. Way obtained solutions for three aspect ratios, 1, 1.5 and 2.

General solutions were later obtained by Levy[7],[8],[10],[11] and Levy and Greenman[9] for simply supported and clamped rectangular plates under the combined action of transverse pressure and inplane thrust using a double Fourier series. The method presented has the disadvantage of restricting the satisfaction of all the membrane boundary conditions. In the solutions given the edges must either have zero displacement or must remain straight during translation. In the latter case, the edges may either be subjected to a self-equilibrating stress distribution, as assumed by Marguerre[5], or an applied end thrust. The method involves a considerable amount of numerical computation and a maximum of six terms of the double Fourier series are considered in the calculations.

The first successful application of finite difference approximations to the large deflection behaviour of plates was made by Wang[12], by forming two sets of simultaneous equations. These equations were solved by two methods, namely, the method of successive approximations and the relaxation method. In the former the author developed a useful iterative procedure which forms the basis of later investigations on the subject using finite difference approximations. Numerical results were obtained for two cases, a simply supported square plate with edges free from inplane stresses and a clamped square plate with edges fully fixed against extensional and tangential displacements. The plates are subdivided into a very coarse mesh to make the numerical computations feasible and, therefore, the results are not very accurate. Subsequently Wang[13] applied the same method in obtaining solutions for

simply supported rectangular plates with aspect ratios 1.5 and 2, in which the edges were assumed to have zero extensional displacements and zero inplane shear.

Soper[3] extended Levy's method (Fourier series) to the solution of rectangular stiffened plates. The stiffened plates were idealised into homogeneous orthotropic plates for which the author modified von Karman equations accordingly. Elastic rotational restraints were introduced at the boundaries to cover the range of simply supported to clamped plates. Solutions were obtained which agreed well with the tests conducted on an aluminium model.

Eggwertz and Norr[14] considered a square plate under normal pressure provided with edge frames of finite stiffness in the plane of the plate. Using energy methods and neglecting the bending of the plate, the authors derived simple formulae for plate deflection and membrane forces. Subsequently the bending moments and their contribution to the transmission of the applied pressure to the supports were estimated roughly.

Basu and Chapman[15],[16] extended Wang's (finite differences) computational method and obtained solutions for the large deflection behaviour of a wide range of orthotropic and isotropic plates. The plates are initially transformed into a suitably chosen coordinate system in a similar manner to Girkman's[17] transformation of orthotropic plates, and non-dimensionalised to give more general numerical results. Apart from the elastic rotational and extensional restraints, tangential edge restraints were introduced at the boundaries. Solutions were given and compared for a combination of various flexural and membrane boundary conditions.

Bauer[18] also employed the finite difference method and obtained solutions for simply supported plates with zero inplane direct and shear stresses at the boundaries by using an iterative process. To obtain solutions, the two fourth order partial differential equations are converted into a system of four

second order differential equations. The type of solution presented has the limitation that its applicability is based on the simple boundary conditions assumed. Solutions are given for plates with aspect ratios 1 and 2.

Plates under Inplane and Transverse Loading

Because of the extensive use of stiffened plates in engineering structures, the problem of the behaviour of plates under inplane and transverse loading is of great importance. Due, however, to the complexity of the theoretical analysis, so far very little work is done on this subject, and there are relatively few solutions available. Most of the investigators have neglected in their analysis the effect of membrane forces due to bending and have limited the investigation to the reduction in stiffness of the plate in bending due to the presence of the end thrust.

Levy[10] extended his general method for the analysis of the large deflection of transversely loaded plates to cover plates under combined loading, and obtained solutions for a simply supported plate under transverse pressure and uniaxial edge compression, in which the edges of the plate remain straight but are free to translate. The author gave numerical results for a square plate with two values of transverse pressure. The transverse pressure was first introduced and kept unaltered while the inplane thrust was raised incrementally to 1.30 times the critical buckling load of the plate in the first case of transverse load and 2.96 times the critical load in the second case. In the same publication, the author solved the problem of a 3:1 rectangular plate loaded along its shorter sides, again for two values of transverse pressure where in each case the edge compression was raised to the critical load of the plate.

Later Woolley, Corrick and Levy[19] extended the method presented by Levy[10] to obtain solutions for a 4:1 clamped rectangular plate subjected to inplane and transverse loading. The calculations were carried out for two

values of transverse pressure and in each case the edge compression was raised above the critical buckling load of the plate. It was concluded that the effect of normal pressure on the axial load for a given edge strain is negligible.

Timoshenko[20],[21] solved the problem of plates under inplane and transverse loading by assuming that the membrane forces in the plate are initially uniform and remain so during the bending of the plate. The problem is thus simplified to the solution of the governing equation of plate in bending only. A double Fourier series is used and linearised (small deflection) solutions are obtained in the form of magnification factors of the effects in bending alone. These magnification factors approach infinity when the critical buckling load of the plate is being reached. Another limitation imposed by the method is that the membrane boundary conditions do not enter the analysis and their effects are completely neglected.

Conway[22] solved the same equations as Timoshenko for simply supported rectangular plates using a single Fourier series and presented the linearised solutions obtained in the form of design charts which special reference to the ship plating. The charts refer to plates under uniaxial compression. The edge compression may assume values up to 75% of the plate's critical buckling load.

Lockwood[23] used a double Fourier series and with simplifying assumptions obtained magnification factors for the bending moments in the plate. The method, which is a linearised solution, was extended to include clamped plates under uniaxial compression. The author gives numerical results for simply supported plates with three aspect ratios, namely, $\frac{1}{2}$, 1, $1\frac{1}{2}$, and for square and long clamped plates with edge compressions up to two-thirds of the plate's critical load.

Marguerre's theory of plates was extended by Bleich[24] to include the effect of transverse pressure. Bleich derived a cubic equation in terms of the plate's central deflection and the transverse pressure. Using the results of

this equation, the author suggested that for the design of ship's plating a simplified linearised solution could be sufficiently accurate. A design formula, similar to the beam column formula, was therefore developed for the magnification of the central deflection and moment of the plate on the basis of which a comprehensive design manual was compiled.[25]

A more exact linearised solution for plates under inplane and transverse loading was put forward by Chang and Conway[26]. The deflected profile of the plate was assumed to be the product of two functions, each dependent on one of the Cartesian axes only. Making use of the Marcus method, by a system of successive approximations, solutions were obtained for clamped rectangular plates under biaxial tension or compression. The solutions entail a considerable amount of computation for any particular problem.

Using a method similar to Timoshenko's, Taylor[27] has given solutions for simply supported and clamped plates with aspect ratios 0.5, 1 and 1.5. The numerical results given refer to edge compressions up to 0.5 P_e.

Initially Deformed Plates under End Thrust and Post-Buckling of Initially Flat Plates

There are more non-linear solutions available for initially deformed plates than for flat plates under inplane and transverse loading. This may be due to the fact that it is usually assumed that the initial deformation is of the same form as the final deflected shape of the plate and this leads to some simplifications in the analysis. The extension of von Karman equations to include initial deformation of the plates was first achieved by Marguerre[28].

Hu, Lindquist and Batdorf[29] extended Levy's method[7] to the non-linear behaviour of simply supported plates under uniaxial compression and obtained solutions for initially deformed plates with several degrees of deviation from

flatness (w_o centre/h up to O.1). The authors discussed the evaluation of the critical buckling load of the plates from the load-deflection curves obtained, as well as the effective width of the initially deformed plates. It was concluded that:

(i) The effect of initial deformation is most pronounced around the flat plate's critical buckling load, otherwise the behaviour of the plate is very much the same as flat plate.

(ii) The larger the initial deviation from flatness, the smaller the experimental critical load.

(iii) The Southwell plot for predicting the critical buckling load from experimental results is in general not satisfactory for flat plates.

(iv) The effective width for stiffness against further compression is less than that of flat plates for loads below the critical buckling and greater at loads above.

Coan[30] investigated the buckling behaviour of an initially deformed simply supported plate under uniaxial compression. Three different methods of application of edge compression were considered, namely, applied uniform stress and applied uniform displacement, where in the latter case a distinction was made between the condition when displacement is given and the condition when the loaded edges translate perpendicular to themselves under a given total force. An attempt was made to illustrate the significance of each type of loading. The method of solution was based on Levy's, and it is the first series solution in which the unloaded edges are allowed to distort. Numerical results were given for w_o centre/h = O.1.

Solutions for the non-linear buckling of initially deformed orthotropic plates were later presented by Yussuf[31] for square laminated fibre glass

plates. The von Karman equations were modified to take into account the anisotropic properties of the plate as well as the initial deformations, and were subsequently solved by a double Fourier series based on an extension of the method developed by Levy[7] and his successors[29],[30]. In the analysis, the loaded edges remain straight, whereas the unloaded edges can be either stress free or kept straight.

Falconer and Chapman[32] studied the post-buckling behaviour of simply supported long rectangular plates loaded at their shorter sides and having any degree of longitudinal and transverse stiffening. The stiffeners were assumed closely spaced such that local instability could not develop and the plate could be treated as a homogeneous orthotropic plate. The unloaded edges were assumed stress free. Making some simplifying assumptions, solutions were obtained by means of an energy method for the critical buckling load, membrane and bending stresses in the buckled condition and the buckling amplitude of long stiffened plates, which may be initially deformed or flat.

Levy and Coan's works were later extended by Yamaki[33] to obtain solutions for rectangular plates with the sides either all clamped, or all simply supported, or two opposite sides clamped and the other two simply supported. The membrane boundary conditions investigated were, that the loaded edges remain straight and the unloaded edges may either be stress free or be kept straight. Numerical results are given for the non-linear variation of the central deflection and stresses in the plate with end-thrust. The plates may be initially flat or deformed. The shortening of the plate under the applied loading is determined, and hence the effective width of the plate discussed. Formulae for the ultimate load of the square plate were derived for each case by using the maximum shear theory for the beginning of yielding. Experiments conducted to confirm the results are also reported[34]. The analysis, however, does not consider transverse loading.

Bauer[35] transformed the von Karman equations into two pairs of second order simultaneous equations as described before, and by using a finite difference technique obtained solutions for the post-buckling behaviour of initially flat simply supported rectangular plates subjected to uniaxial end thrust.

Critical Buckling Loads of Plates

The problem of the critical buckling of plates has been attempted by many investigators. A full account of the methods of treatment of the problem and the range of available solutions are given in the standard text books[20],[24]. The methods of solution initially proposed mainly refer to the standard cases of simply supported or clamped plates under uniform end thrust. When the loading is not uniform and the plate is not isotropic, the rigorous solution may become practically impossible. Approximate methods were later devised and widely used, giving upper bounds and lower bounds of the critical loads.

Richardson[36] suggested a finite difference procedure for the determination of the characteristic values of the differential equations, which is applicable to the evaluation of the critical buckling load of the plates. Collaz[37] independently investigated the use of the finite differences for the same purpose. Southwell[38] presented the relaxation method for obtaining the critical buckling loads. Later, Boley[39] developed three numerical methods similar to the Southwell's relaxation procedure.

Salvadori and Baron[40] made a comprehensive study of the application of finite difference approximations to the buckling problem. The authors reduced the problem to the solution of a system of simultaneous algebraic equations, and by means of a successive approximation technique which was greatly improved by a simple method of extrapolation obtained solutions for several nonstandard cases.

The Analysis of the "Double-Bottom" of Ships

The "double-bottom" which constitutes the bottom of most dry cargo ships is made up of an inner and outer plating connected by means of web members. The webs may be solid or provided with holes for lightening and inspection purposes. Webs in the transverse direction spanning the sides of the ship are called floors and are usually placed at approximately 9 feet centres. Webs in the longitudinal direction are referred to as centre girder (if at centre) or intercostals and may be spaced at 15 feet intervals. In addition, there are struts which serve to maintain the skins at a fixed distance; and brackets which provide local stiffening of the structure. Bulkheads, which are transverse diaphragms and subdivide the ship into compartments are made up of stiffened or corrugated plates. The bulkheads could be spaced at 1.5 times the width of the ship.

The double bottom structure is extremely complex. This is in part due to the constructional considerations and details.

The external loads on sections of double bottom bounded by the sides of the ship and two adjacent bulkheads are primarily:

(i) Transverse loading, due to water pressure from outside and due to cargo from inside.

(ii) Longitudinal end-thrust due to the overall bending of the ship.

The structural analysis of the double-bottom may be regarded to consist of the study of the overall behaviour of the section under the external loading, and the study of the behaviour of the constituent components of the structure (local behaviour). In this thesis attention is focussed on the local behaviour of the plating of the outer shell (skin).

For the purpose of the analysis of the overall behaviour of the double-bottoms, investigators have considered the effects of the transverse loading and the end-thrust separately. For the evaluation of the stresses due to transverse

bending, beam and grillage approaches have been frequently used. It was only recently that attempts were made to utilise the plating's substantial contribution to the bending and torsional rigidities of the basic grid structure in the theoretical analysis.

Schade[41],[42],[43] approximated the double-bottom as a homogeneous orthotropic plate, the stiffnesses of which are the same as those of the actual double-bottom assumed to be uniformly spread. By means of an energy method the author obtained solutions for the orthotropic plate's differential equations and presented design curves and tables for double-bottom structures, from which deflections, bending and shear stresses can be estimated. The boundary conditions of the orthotropic plates considered were, all edges simply supported, all edges clamped or two opposite edges clamped and the others simply supported. Provision is made in the analysis to account for the variation in bending stiffness across the width of the plate for the cases when the centre girder is stiffer than the intercostals.

Orthotropic plate theory was later applied by Chapman[44] to the overall behaviour of doubly-plated grillages in order to investigate the influence of the distribution of material between the flanges and the webs. The theoretical results obtained were confirmed by a model test.

More elaborate models tests were subsequently carried out and reported with reference to stiffened plates in ship structures and in conjunction with theoretical analysis[45],[46],[47],[48]. A survey of recent developments in the structural design of ships and a comprehensive list of references is given in Ref.(49).

The plate panels of the outer shell may have unstiffened spans of 30 in. and are normally between $\frac{1}{4}$ in. to $\frac{3}{4}$ in. thick. They may be initially deformed. The maximum deviation from flatness of a panel is in the order of 0.1 in. As for their loading, the panels are subjected to transverse pressure

due to water and simultaneous biaxial thrust in their planes. The axial thrust is partly due to the transverse bending of the double-bottom and partly due to the overall bending of the ship. For their stress analysis, the panels may be treated as initially deformed plates under inplane and transverse loading.

Lockwood[27] applied the small deflection theory of plates under inplane and transverse loading to the ship's outer plating. The method of approach and the results obtained are discussed before.

A full theoretical investigation of the behaviour of the outer shell plating was undertaken by Bleich[24],[25]*. Murray[50] has, after a discussion on the build up of permanent set in the plate panels of the outer shell, proposed a theoretical approach for the evaluation of the effective load carried by the plate panel in compression. The effect of the rotational restraint exerted by the adjacent panels is taken into consideration.

Young[51] conducted several plate tests to verify the few theoretical solutions available for the plates under combined loading. The author concludes that the linearised solution put forward by Bleich[24] is sufficiently accurate for design purposes.

Origins and Scope of the Present Research

It is clear from the foregoing review that a very small number of solutions are available for the non-linear behaviour of plates subjected simultaneously to inplane and transverse loading. The available solutions are those due to Levy and Bleich.

---

*See page 29.

In Levy's solutions the plate is initially subjected to a uniform transverse pressure; the end-thrust is then introduced and raised. It appears from the literature that only three cases have been attempted so far. Numerical results are available for two specific values of transverse pressure in each case.

In Bleich's presentation, for given values of end-thrust, the central deflection and stresses are given for increasing values of transverse pressure. The solutions are obtained with extensive simplifications. The analysis does not account for the membrane boundary conditions.

In view of the importance of the subject, the apparent shortcomings in the theoretical analysis and the rarity of the available solutions, some fruitful objectives would be the following:

(i) To give an overall picture of stresses in the plates necessary for the full comprehension of the non-linear behaviour of plates.

(ii) To examine the influence of some of the more important factors in the non-linear behaviour of plates, such as the description of loading and boundary conditions.

(iii) To give results for the extension of the available published knowledge on the subject.

The present research started with the intention of studying the overall and local behaviour of ship's double-bottom structure. A one-eighth scale model, to be tested in bending and compression, was under construction. The project embraced both experimental and theoretical analysis forming part of a research programme sponsored by the B.S.R.A.[15],[55]. The author was engaged in planning the test programme, the design of the loading rig and the instrumentation of the model. The progress of construction, together with the preliminary theoretical results were reported a year later in Ref.(52).

Construction of the model, design and fabrication of the loading rig, and the instrumentation, were major undertakings. By the time the construction was complete, preliminary tests conducted and the first loading stage started two and a half years had elapsed. At this stage it was decided that the author should henceforth concentrate on the extension of the theoretical analysis; the scope of which exceeded the original expectation and encouraged this shift in emphasis[53].

Mr. D. Williams then took charge of the model and prepared a report on the first stage of the tests[54].

As far as the author was concerned thereafter, the object of the research was to provide a theoretical basis for the analysis of the elastic non-linear behaviour of rectangular plates under the combined action of inplane and transverse loading, with special reference to the double-bottom structure; and in doing so

(i) To allow for continuity of the plate beyond its supports by introducing rotational, sinking, extensional and tangential restraints at the boundaries.

(ii) To consider the boundary condition relating to individual plate elements within an array of such elements under symmetrical loading.

(iii) To study the significance of methods by which the inplane loading may be specified, namely, applied force, applied displacement, or a combination of both. Also, to examine the influence of membrane boundary conditions on the linearised solutions and the influence of flexural and membrane boundary conditions on the non-linear solutions.

(iv) To develop a method for the effective representation of concentrated transverse loading.

(v) To account for initial deviations from flatness in the analysis of plates.

(vi) For the purpose of design to examine the effective width concept for accounting for the loss of stiffness against end-thrust due to transverse deflection of plates. This may be due to transverse pressure, initial deformation or buckling.

(vii) To extend the method of analysis to the evaluation of the critical buckling loads of orthotropic plates under general inplane loading.

Clearly, a treatment of this generality will find applications in many fields of the structural engineering, and some of these have already been instanced (page 9).

CHAPTER II

THEORY

General. The elastic non-linear behaviour of plates can be expressed by two simultaneous fourth order partial differential equations. The equations are in terms of the transverse deflection of the plate and a stress function (Airy) related to the state of membrane stresses in the plate. From the solution of these equations together with the specified boundary conditions, the flexural actions (bending moments and normal shear) and the membrane stresses (inplane direct and inplane shear stresses), and also the displacements can be evaluated. The equations were first derived by von Karman[1] for isotropic plates; later they were modified to be applicable to other types of plates[2],[3],[28]. The direct solution of these equations in the general case is unknown; however, few approximate solutions of the problem are available as discussed in chapter I.

In this chapter the present method of solution, the scope of its application, and the fac tors considered in the analysis are outlined.

Scope of analysis

1) Continuity. Plates are seldom used singly, but are normally built and act as part of an assembly. Details of the joints, and the way in which the plate panels resist the external loading varies extensively. The assessment of the boundary conditions of individual plates within an assembly and their theoretical treatment is itself a problem often more difficult than the analysis of the interior of the plate.

To consider the effect of continuity of the plating beyond its supports, elastic flexural and membrane restraints are assumed at the boundaries. These

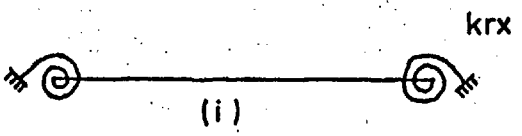
are edge-restraints against (i) rotation, (ii) displacement perpendicular to the plane of the plate, (iii) inplane extension, and (iv) inplane displacement of edges parallel to themselves (tangential displacements). These edge-restraints may be represented in the form of discrete elastic springs of uniform stiffness along the edges as shown in Figure (II-1). The stiffness of the edge-restraints of the opposite sides is assumed to be the same. The edge-restraints chosen are necessary and sufficient to exhibit all the possible types of movement of the edges.

If the stiffness of a particular spring is assumed either zero or infinity, the two limiting boundary conditions which correspond to the movement of that spring emerge (e.g. simply supported or clamped respectively in the case of elastic rotational edge-restraints). Thus edge-restraints type (i) and (ii) together can describe four limiting flexural boundary conditions which are considered in the analysis, and are designated as shown in Figure (A-1) of the notation. The remaining two edge-restraints give rise to four limiting extensional boundary conditions which are shown on the first four rows of the Figure (A-3) of the notation. In addition, two other membrane boundary conditions are considered which are listed in the same figure.

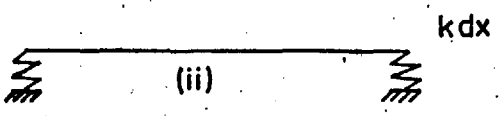
For the purpose of theoretical analysis, panels in an assembly are analysed in isolation. The restraint exerted on a given panel, by the structural elements adjacent to it, can be estimated and approximately represented by elastic edge-restraints at the boundaries of the theoretically isolated panel. In this case, the plate is referred to as having intermediate boundary conditions.

2) Loading. Both transverse and inplane loadings are considered. In most cases these are assumed to be symmetrical about the centre lines.

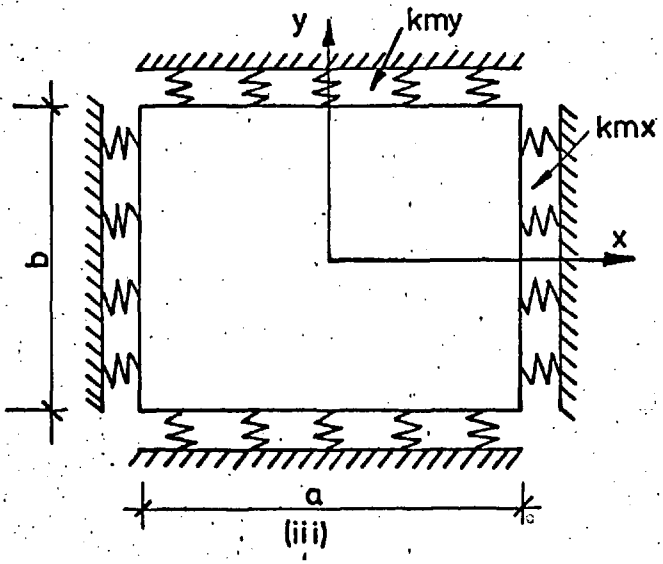
i) Transverse loading. For transverse loading the analysis allows any patch load of any shape and area to be closely approximated. Line loads and uniformly distributed loads form special cases of a general patch load.



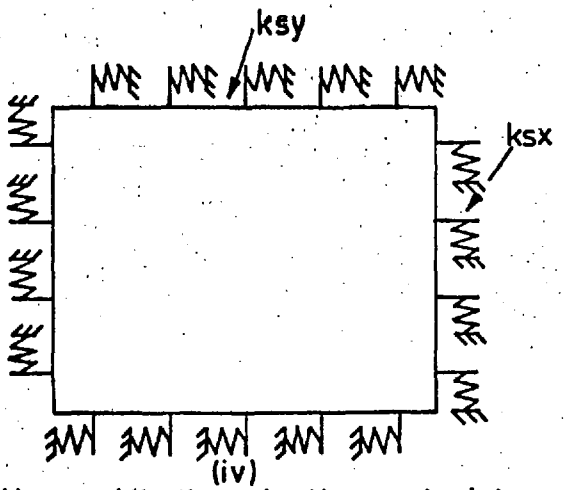
krx, kry = Stiffness of elastic restraint against rotation per unit length of the edge.



kdx, kdy = Stiffness of elastic restraint per unit length of the edge against displacement perpendicular to the plane of the plate.



kmx, kmy = Stiffness of elastic restraint against extension per unit length of the edge.



ksx, ksy = Stiffness of elastic restraint against movement parallel to the edge per unit length of the edge.

Note: All the elastic restraints are assumed uniform along the edges and of equal stiffness for the oposite sides.

FIG. II-1 Elastic restraints at the boundaries.

At the boundary, any distribution of slope or any distribution of applied bending moment may be specified.

In addition, provision is made for the deflected profiles of the unsupported edges to be prescribed.

ii) Inplane loading may be applied in one of the following three forms: (a) any distribution of direct stress, (b) any distribution of edge displacement, and (c) edge remains straight and translates under the action of a total specified force. The loading and the boundary conditions of individual members of assemblies made up of identical plate members may be approximated by loading condition (c).

Uniform end-thrust or uniform edge displacement are special cases of the above loading conditions.

3) Initial deviations from flatness. The analysis accounts for the initial deformation of plates which may be described (i) by a trigonometrical expression, (ii) by an algebraic polynomial, or (iii) the actual deflection contour of the plate may be given.

4) Anisotropic properties. In the analysis the plates are assumed to be homogeneous and orthotropic; further, the orthotropic properties are assumed to be orthogonal and parallel to the sides of the plate. Stiffened plates in which the distribution of stiffness is uniform and also the stiffeners are closely spaced are idealised as orthotropic plates for the analysis of their overall behaviour.

Isotropic plates are treated as special cases of orthotropic plates.

Formulation

i) Equations. The derivation of the non-linear equations of initially deformed orthotropic plates is given in appendix B. From equilibrium and compatibility considerations of an element of plate subjected simultaneously

to flexural actions and membrane forces (Figure B-1), the two governing equations (B-14) and (B-15) are derived. The former equation refers to the bending of the plate and the latter to the membrane action. The boundary conditions considered are also derived and discussed in the same appendix.

To increase the applicability of the solutions obtained, the governing equations together with the boundary conditions are non-dimensionalised, using the non-dimensional ratios defined in the notation (equations (B-16) and (B-17)). The non-dimensionalised sectional actions (flexural actions and membrane forces) and loading are also given in appendix B. Thus, the results of specific plate problems solved become applicable to the range of plates having the same non-dimensional parameters.

The generality of the solutions can be increased even further if plates to be analysed are first transformed into a new coordinate system which is appropriately chosen so as to reduce the number of plate parameters required to obtain specific solutions. This transformation is discussed in appendix D.

ii) Finite difference approximations. In order to obtain numerical solutions, the governing equations (B-16) and (B-17) and the boundary conditions are expressed in terms of first order finite difference approximations. Central differences are used throughout. To increase the accuracy of solutions for plates in which the boundary conditions involve the rotation of the edges, slopes at the boundaries are expressed in terms of four node points instead of three (see appendix E for improvement in the solutions).

The finite difference approximations are derived for an orthogonal mesh of unequal mesh lengths (graded mesh), and are given in a general form in appendix C. Graded meshes are employed in the following cases to improve the accuracy.

a) For transverse patch loading the mesh is concentrated under the load, in order to accommodate the local rapid change of curvature, and in order to closely describe the patch.

b) Adjacent to the boundary of clamped plates the mesh is made finer.

c) For plates with unsupported edges, the mesh is made finer in the vicinity of the edges and consequently at the corners of the plate.

The governing equations of the plate, and the boundary conditions, expressed in terms of the finite difference approximations are given in appendix C.

Solution

The governing equations are non-linear because the flexural action equation (B-16) involves, besides terms in W, products of W and F, and because the membrane action equation (B-17) contains F and products of F and W. This mathematical non-linearity reflects the physical non-linearity of the problem.

If in the first equation F is assumed zero, or assigned a given value, the equation becomes linear with one unknown in W and can be solved independently. In the case of F being zero, the equation describes the classical small deflection behaviour of transversely loaded plates, when values assigned to F relate to the distribution of membrane stress in the initially flat plate under the action of inplane loading alone, solutions obtained are linearised solutions.

Similarly in the membrane action equation, when W is assumed zero or given a finite value a linear equation in F results which can be solved completely. The former case refers to the extensional problems of flat plates.

From the foregoing discussion it is evident that the solution consists of several stages, (i) small deflection of transversely loaded plates, (ii) plane stress problem of flat plates, (iii) linearised solutions of plates under combined loading, and (iv) the non-linear solution of plates. The first three stages may each be regarded as a special case of stage (iv). In the work presented in this thesis the first stages were developed and examined separately, and subsequently

incorporated in stage (iv). In addition, the work was extended to include the evaluation of the critical buckling load of plates in stage (v), which is essential for the analysis of plates under combined loading.

Stage (i) Small deflection solutions of transversely loaded rectangular orthotropic plates.

This stage of the analysis is developed and programmed allowing for the following parameters to be designated.

a) Length to breadth ratio of the plate.

b) Number of divisions of the mesh in x and y directions. The mesh may be uniform or graded; if graded, the mesh lengths must be defined.

In obtaining solutions, the matrices formed are partitioned. This reduces the computation time and storage needed, and consequently it permits a finer mesh to be used. The maximum number of nodes used was about 420 (in a quarter of plate) in the case of a plate subjected to a patch load of varying intensity. In most of the plate problems, however, 60 to 100 nodes (in a quarter of plate) gave sufficiently accurate results for design purposes.

c) Flexural rigidities of orthotropic plates may be specified.

d) Plates may assume any of the 25 cases of limiting flexural boundary conditions given in figure (A-5). For intermediate boundary conditions the stiffness coefficients of elastic rotational edge-restraints and of elastic edge-restraints against displacements perpendicular to the plane of the plate must be given. The coefficients of edge-restraints on opposite edges are to be the same. For plates of group B in figure (A-5) only the opposite symmetrical boundaries may take intermediate boundary conditions. For group C of the same figure only the limiting boundary conditions may be specified.

e) Transverse loading to be specified is as discussed before in this chapter. The designation of slopes or moments, however, applies only to the boundaries which may assume intermediate conditions.

Although only one quarter of the plate is programmed, solutions for the unsymmetrical loading cases may be obtained by resolving the load into symmetrical and antisymmetrical components and using the principle of superposition of effects.

Two examples of the small deflection of plates under transverse loading are given in chapter III.

Stage (ii) Plane stress solutions of rectangular orthotropic plates.

In this stage of the analysis in anticipation of the later incorporation of various stages, the specification of the plate parameters is chosen to be very much the same as in the previous stage. The relevant parts of stage (i) therefore hold true for the extensional problems. The matrices set up, however, are not partitioned, because of the foreknowledge that the inversion operation needs to be carried out only once for the later non-linear analysis of any specific plate problem; and also because it was found that the accuracy of the results obtained is not very sensitive to the mesh fineness.

The loading specifications are as discussed before in this chapter.

Stage (iii) Linearised solutions of orthotropic plates under combined loading.

Stages (i) and (ii) are combined. The distribution of membrane stresses in the plate is determined by treating the case as a plane stress problem (from equation (B-17)). With this distribution, which is assumed to remain unchanged, the flexural action equation of the plate is solved.

It must be noted, however, that the principle of superposition does not hold true for this stage of the analysis or for the non-linear behaviour of plates.

Stage (iv) Non-linear solutions of rectangular orthotropic plates under combined loading.

This is an extension of stage (iii), and the parameters already discussed may also be specified for this stage of analysis. In contrast to the linearised solutions, in this stage for each specific value of loading a new solution must be obtained, due to the non-linearity of the problem. The counteraction of plate to increments of loading is governed by the state of stresses in the plate, and possibly the loading history.

For each specific value of combined loading the solution is obtained by an iterative process, based on the preceding state of membrane stress and the deflected profile of the plate. The method consists of alternate and repeated solutions of the flexural action and membrane action equations. Each equation, when being solved, is made linear by assigning to W or F their latest values and by treating them as constants. Solutions obtained for each cycle (one solution of the flexural and one of the membrane action equation) are compared with those of the previous cycle. The comparison is made for all the nodes of the mesh, including the fictitious nodes. If the values (of W or F) are found to have improved less than a specified accuracy, the solution is assumed to have converged. The load is then incremented to the next value and the procedure repeated. But, if the comparison reveals that the accuracy is not reached, the values of W or F obtained are appropriately modified and used in the next cycle.

The present work has been developed, such that the loading (transverse or inplane in any of the forms described before in this chapter) may be applied in any sequence and incremented in combination or individually.

The plate parameters and the boundary conditions together with the various types and sequences of loading describe numerous plate problems which can

readily be analysed by the present work. In studying the non-linear behaviour of plates under combined loading previous investigators have always first introduced either transverse pressure or inplane loading. While the magnitude of the initial load is kept constant, the other type of loading is applied and raised incrementally. For the examples given in this thesis the same procedure is adopted and the solutions obtained are divided into (i) those with constant inplane loading and (ii) those with constant transverse loading.

A list of the rectangular plates under uniform inplane loading which could be solved by the present analysis is shown in figure (A-7).

The large deflection behaviour of transversely loaded plates and the behaviour of initially deformed plates subjected to end -thrust are special cases of this stage of the analysis. Figure(A—6) shows the rectangular plates with various limiting membrane boundary conditions which can be treated by this stage of the analysis. For initially deformed plates, however, it must be noted that the initial deformations specified must also be assumed symmetrical about the centre lines of the plate if the transverse loading is so assumed.

Stage (v) Critical buckling load of rectangular orthotropic plates.

Several numerical methods exist for the evaluation of the critical buckling loads of plates. The method adopted here is the one most suitable for extending the analysis already undertaken.

In stage (iii) of the analysis, the eigenvalues of the square matrix formed from the flexural action equation correspond to the buckling loads of the plate, the lowest being the critical buckling load. The eigen-vectors correspond to the deflected profiles. The eigenvalues together with the eigen-vectors of such matrices can be determined using the available standard iterative methods.

In the present case, however, due to considerations in the analysis of the non-linear behaviour of plates, the problem is so formulated that the eigenvalues can be readily determined, leaving the eigenvectors (deflected profiles) to be evaluated separately.

The square matrix set up in stage (iii) of the analysis will be singular for its eigenvalues. These are evaluated using a method of successive approximations as follows. For increasing values of the inplane loading (usually starting from zero) the determinant of the matrix is evaluated and noted. A change of sign in the value of the determinant indicates the interception of a characteristic value of the matrix. Guided by this change of sign the last increment of inplane loading (within which the characteristic value lies) is repeatedly halved, the inplane loading accordingly adjusted and the determinant newly evaluated, until the change in two successive values of the inplane loading is less than a specified percentage of the last value. The solution is then noted and the incrementation of the inplane loading continued in order to intercept the next characteristic value corresponding to a higher mode of buckling.

In appendix E, examples of the critical buckling loads of plates using the above method are given.

Due to other commitments and shortage of time the second phase of this stage of analysis (determination of the buckled profile) is not developed at the time of the preparation of this thesis.

Computation

The bulk of the work is programmed for the University of London Atlas computer using EMA (Extended Mercury Autocode) language. Series solutions are programmed for the Imperial College IBM 7090 computer using Fortran IV.

A description of the iterative method used in the analysis is given in appendix F.

As far as the computation time is concerned, this is primarily a function of the number of nodes in the mesh chosen for any specific plate problem, and of course the number of times the problem is being solved. The following is an approximate estimate made on the basis of the present computer arrangements and the author's programs.

For small deflection solutions of transversely loaded plates with a quadrant of plate covered by 225 nodes (as in the examples given in this thesis) the computer's execution time for each plate problem is approximately 45 seconds. If the number of nodes is increased to 420, the time is 1 min.

The non-linear analysis of plates subdivided into 64 nodes ($\frac{1}{4}$ of plate), and subjected to 11 load increments takes 3 mins. execution time. For the same problem a subdivision into 100 nodes, takes 5 mins. At the end of each load increment, from the values of deflection and stress function to which the solution has converged the bending moments and membrane stresses at all the nodes, and the extension and rotation of the plate at the boundaries are evaluated. This is followed by checks on the equilibrium of membrane forces in the plate.

The storage required is approximately equal to the space taken by two square matrices, the dimensions of which equal the number of the nodes.

Accuracy

In all the non-linear solutions given in this thesis an accuracy of 0.5% has been specified. This means that the numerical values obtained are within 0.5% of the value to which the present solution would have converged. The mode of convergence is as in damped oscillations. No exact solutions are available for the non-linear results; these are therefore compared with the few available approximate solutions. Agreement with these solutions is very good.

Also in cases other than the non-linear solutions, the results obtained were examined for their accuracy and were found to be very satisfactory in this respect.

Appendix E deals with details of the accuracy checks made for each stage of the analysis.

Presentation of results

The theoretical results obtained are given graphically and in tables. Most of the graphs show the variation of central deflection and moment with the applied loading, and also the profiles of the deflection, moment, and membrane forces along the centre lines and boundaries for maximum loading reached. The numerical values obtained for sectional actions and displacements are given in the tables with the corresponding external loading.

The results given can be interpreted in three ways: they may refer to (i) isotropic plates, (ii) groups of orthotropic plates non-dimensionalised as in Appendix B, and (iii) groups of transformed orthotropic plates as denoted in appendix D. PLATE PARAMETERS. Generally five plate parameters must be specified in order to obtain non-linear solutions for a given plate problem. These parameters which are defined in the notation are as follows:

ε',(ρ'). Virtual side ratio. For isotropic plates it equals the actual side ratio (ε or ρ).

α Equivalent flexural stiffness ratio. This is a measure of the torsional rigidity of plate relative to the flexural stiffnesses, and is equal to 1 for isotropic plates.

β Equivalent extensional stiffness ratio. The inverse of β is a measure of the inplane shear rigidity of plate relative to its extensional rigidities. It equals 1 for isotropic plates.

γ This parameter relates flexural and extensional rigidities and is equal to 1 for isotropic plates.

Poisson's ratios. For the membrane action, these are specified in the form of $\sqrt{\nu_{x_m} \cdot \nu_{y_m}}$ for transformed plates. For plates non-dimensionalised according to appendix B, they are designated individually. In the case of membrane boundary conditions being defined in terms of stresses, Poisson's ratios for membrane action need not be specified. For plates on flexible supports, however, Poisson's ratios in bending must be given. In most of the solutions obtained (although not necessary for deflection) Poisson's ratios in bending were both assigned a value of (O.3) in order to evaluate bending moments of the special isotropic cases.

BOUNDARY CONDITIONS AND LOADING. For each particular plate problem solved, the boundary conditions and loading are represented symbolically on the graphs and in the tables. The symbols used are defined in the notation. They are denoted by means of two rectangles, having the same aspect ratios as the special isotropic case to which the results refer. The first rectangle, bearing the cartesian coordinates, describes the flexural boundary conditions and the transverse loading. The second rectangle indicates the membrane boundary conditions and the inplane loading. A numbering system as shown in the notation is used in conjunction with the symbols to assist in the identification of each problem. Each non-linear problem is described by two numbers separated by a dot. The first number refers to the flexural boundary conditions and the second number identifies the membrane boundary conditions and the inplane loading.

MESH. The fineness of the mesh used for each problem is indicated in the tables by (2 I) x (2 J) denoting the number of subdivisions of plate in x and y

directions respectively. Graded meshes are assigned numbers and are shown at the end of figures of the theoretical results.

ACCURACY. This refers to the limiting accuracy specified in the iterations.

POSITIONS OF SECTIONAL ACTIONS AND DISPLACEMENTS. The sectional actions and displacements appearing in the graphs and the tables are each assigned a numerical suffix to indicate the position in the plate to which they refer.

Suffix 1 refers to the position $x = 0, \quad y = 0$

" 2 " " " " $x = a/2, \quad y = 0$

" 3 " " " " $x = 0, \quad y = b/2$

" 4 " " " " $x = a/2, \quad y = b/2$

The coefficients relating to isotropic plates are based on Poisson's ratio of 0.3; in the figures these coefficients are given in parenthesis. For plates with other values of Poisson's ratio, where applicable, the factors can be readily recalculated. The quantities given in the graphs or the tables are given in the following.

DEFLECTION. The deflection ratio W' is

(i) For isotropic plates $W' = 3.305\, w/h.$

(ii), (iii) For orthotropic plates $W' = \sqrt{C_x/D_x}.w$

TRANSVERSE LOAD. The transverse pressure ratio represented by Q' is

(i) for isotropic plates $Q' = 36.09 \frac{a^4}{h^4} . \frac{q}{E}$

(ii), (iii) for orthotropic plates $Q' = \frac{a^4}{D_x} . \sqrt{C_x/D_x} . q$

For patch loads, Q' is the intensity of the transverse loading over the loaded area.

BENDING MOMENT. The solutions would have been more general if curvatures, directly derivable from the deflections, were given instead of bending moments, from which the latter can be found for known values of Poisson's ratio. In this thesis, however, on the assumption that the results will be referred to more frequently for isotropic plates with Poisson's ratio equal to 0.3, bending moment ratios are given. For orthotropic plates, therefore, curvatures and subsequently bending moments must be calculated from the given bending moment ratios using the following relationships.

(i) for isotropic plates $M'_x = 36.09 \frac{a^2}{Eh^4} M_x$

$$M'_y = 36.09 \frac{a^2}{Eh^4} M_y$$

$$M'_{xy} = 36.09 \frac{a^2}{Eh^4} M_{xy}$$

(ii) for non-dimensionalised plates according to appendix B as for (iii) below with $\lambda = 1$.

(iii) for transformed plates

$$M'_x = a^2 . \sqrt{C_x / D_x} \left(\frac{\partial^2 w}{\partial x^2} + \nu_{yb} \lambda^2 \frac{\partial^2 w}{\partial y^2} \right)$$

$$M'_y = a^2 . \sqrt{C_x / D_x} \left(\lambda^2 \frac{\partial^2 w}{\partial y^2} + \nu_{xb} \frac{\partial^2 w}{\partial x^2} \right)$$

$$M'_{xy} = 2 \frac{a^2}{D_x} . \sqrt{C_x / D_x} . \lambda D_{xy} \frac{\partial^2 w}{\partial x \partial y}$$

Bending stresses can be found from the bending moments in the usual manner.

MEMBRANE STRESSES, INPLANE LOADING. The membrane stress ratios are

(i) for isotropic plates, $N'_x = 10.92\frac{a^2}{h^2}.\frac{\sigma_x}{E}$

$$N'_y = 10.92\frac{a^2}{h^2}.\frac{\sigma_y}{E}$$

$$N'_{xy} = 10.92\frac{a^2}{h^2}.\frac{\sigma_{xy}}{E}$$

(ii) for plates non-dimensionalised according to appendix B as for (iii) with $\lambda = 1$.

(iii) for transformed plates $N'_x = \frac{a^2}{D_x}.N_x$

$$N'_y = \frac{a^2}{D_x}.\frac{1}{\lambda^2}.N_y$$

$$N'_{xy} = \frac{a^2}{D_x}.\frac{1}{\lambda}.N_{xy}$$

TOTAL FORCE. Total inplane force along each edge is represented in the same way as membrane stresses, with the difference that the former refers to total force per side instead of force per unit width as in the latter.

INPLANE DISPLACEMENTS. The inplane displacement ratios are

(i) for isotropic plates $U' = 10.92\frac{a}{h^2}.u$

$$V' = 10.92\frac{a}{h^2}v$$

(ii) for plates non-dimensionalised according to appendix B as for (iii) with $\lambda = 1$.

(iii) for transformed plates $U' = a\lambda\frac{C_x}{D_x} \cdot u$

$$V' = a\lambda^2\frac{C_x}{D_x} \cdot v$$

PROFILES. Profiles of the deflected shape of the plate, the distribution of membrane stress, and the inplane displacements at the boundaries as given refer to all the plates of the transformed group, whereas the bending moment profiles refer only to the special isotropic cases. It must be noted, however, that in the case of membrane stresses, the profiles relate to the distribution across the base line.

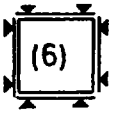
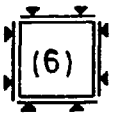
CENTRAL DEFLECTION. Unless otherwise specified, values given for w correspond to the deflection at centre of plate.

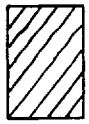
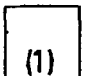
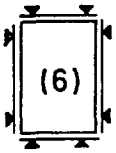
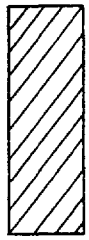
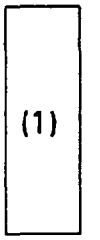
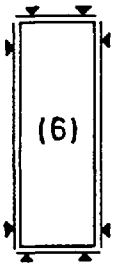
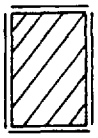
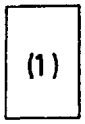
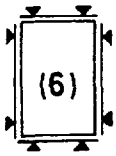
EXAMPLES. Numerical examples for the use of tables and figures are given in appendix G.

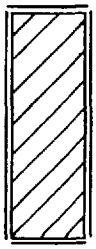
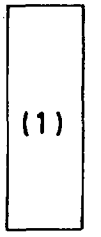
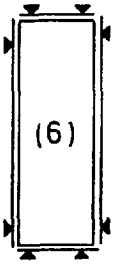
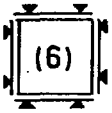
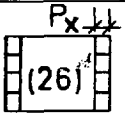
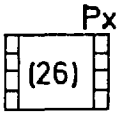
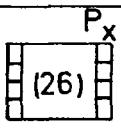
RESULTS

In the following figures, the plate problems which are discussed in this thesis are listed. They are selected to serve three purposes, (i) to demonstrate the scope of the present analysis, (ii) to study the influence of a variety of factors on the non-linear behaviour of plates, and (iii) to provide numerical results to be consulted in the design of plates under combined loading.

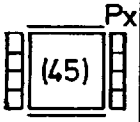
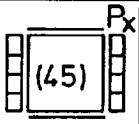
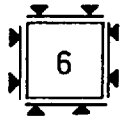
Due to limitations in time the potentialities of the analysis have not yet been fully exploited.

Boundary conditions		Plate Parameters					Loading	Table	Figure	Text
Flexural	Membrane	ε	α	β	γ	$\sqrt{\nu_{xm}\cdot\nu_{ym}}$				
 1	 (1)	1	1	1	1	0·3	U. D. L.	1	1 – 6	64
	 (6)	1	1	1	1	0·3	U. D. L.	2		
	 (13)	1	1	1	1	0·3	U. D. L.	3		
	 (15)	1	1	1	1	0·3	U. D. L.	4		
 5	 (1)	1	1	1	1	0·3	U. D. L.	5	7 – 12	65
	 (6)	1	1	1	1	0·3	U. D. L.	6		
	 (13)	1	1	1	1	0·3	U. D. L.	7		
	 (15)	1	1	1	1	0·3	U. D. L.	8		

Boundary conditions		Plate parameters					Loading	Table	Figure	Text
Flexural	Membrane	ω	α	β	γ	$\sqrt{\nu_{xm}\cdot\nu_{ym}}$				
 1	 (1)	1/1.5	1	1	1	0.3	U.D.L.	9	13 - 22	66
	 (6)	1/1.5	1	1	1	0.3	U.D.L.	10		
 1	 (1)	1/3	1	1	1	0.3	U.D.L.	11		
	 (6)	1/3	1	1	1	0.3	U.D.L.	12		
 5	 (1)	1/1.5	1	1	1	0.3	U.D.L.	13	23 - 32	67
	 (6)	1/1.5	1	1	1	0.3	U.D.L	14		

Boundary conditions		Plate parameters					Loading	Table	Figure	Text
Flexural	Membrane	ω	α	β	γ	$\sqrt{\nu_{xm}\cdot\nu_{ym}}$				
 5	 (1)	1/3	1	1	1	0·3	U. D. L.	15	23–32	67
	 (6)	1/3	1	1	1	0·3	U. D. L.	16		
 1	 (1)	1	1	1	1	0·3	Central patch load lx = ly, lx/a=0·1	17	33 – 40	68
 5	 (6)	1	1	1	1	0·3	Central patch load lx=ly, lx/a=0·1	18		
 1	 (26)	1	1	1	1	0·3	P_x/P_e = 0·25 + U.D.L.	19	41 – 47	70
	 (26)	1	1	1	1	0·3	$\frac{P_x}{P_e}$ = 0·5 + U.D.L.	20		
	 (26)	1	1	1	1	0·3	$\frac{P_x}{P_e}$ = 0·75 + U.D.L.	21		

Boundary conditions		Plate parameters					Loading	Table	Figure	Text
Flexural	Membrane	ω	α	β	γ	$\sqrt{\nu_{xm}\nu_{ym}}$				
1	(27) Px	1	1	1	1	0.3	$\frac{P_x}{P_e} = 0.5$ + U.D.L.	22	48 – 60	72
	(29) Px	1	1	1	1	0.3	$\frac{P_x}{P_e} = 0.5$ + U.D.L.	23		
	(38) U	1	1	1	1	0.3	$\frac{U}{U_e} = 0.5$ + U.D.L.	24		
	(39) U	1	1	1	1	0.3	$\frac{U}{U_e} = 0.5$ + U.D.L.	25		
5	(45) Px	1	1	1	1	0.3	$\frac{P_x \text{ total}}{P_e \text{ total}} = 0.1259$ + U.D.L.	26	61 – 65	77
1	(56) Py, Px	1	1	1	1	0.3	$P_x = P_y$, $\frac{P_x}{P_e} = 0.25$ + U.D.L.	27	66 – 69	78
5	(45) Px	1	1	1	1	0.3	Increasing P_x + U.D.L., Q=72.18	28	70 – 73	81
5	(45) Py	1/3	1	1	1	0.3	Increasing P_y + U.D.L. Q = 72.18	29	74 – 76	82
1	(45) Px	1	1	1	1	0.3	Increasing P_x, $\frac{W_{omax}}{h} = 0.1$	30	77 – 80	83

Boundary conditions		Plate parameters					Loading	Table	Figure	Text
Flexural	Membrane	ω	α	β	γ	$\sqrt{\nu_{xm}\cdot\nu_{ym}}$				
 5		1	1	1	1	0·3	Increasing P_x, $\frac{W_{omax}}{h} = 0.1$	31	81 - 86	84
		1	1	1	1	0·3	Increasing P_x, $\frac{W_{omax}}{h} = 0.5$	32		
 5		1	1	1	1	0·3	$\frac{W_{omax}}{h} = -1$ U. D. L.	33	87 - 89	85

Slab on four columns	Figs. 92 - 95 , P. 86
Slab on a central column	Figs. 96 - 98 , P. 88
Graded meshes.	Figs. 99 - 104

CHAPTER III

Theoretical Results

Most of the theoretical results given in this chapter are devoted to non-linear solutions of rectangular plates. Two examples of small deflection solutions of transversely loaded plates are included at the end. For plane stress problems and for the critical buckling load of plates, examples indicating the type of the solutions which can be obtained from the present analysis are given in appendix E. The same appendix is to be referred to for a discussion of accuracy of results and a comparison with the available solutions. For definition of the non-dimensional parameters used, "Notation" and "Presentation of results" in chapter II should be consulted.

Solutions presented are subdivided into groups as follows:

Non-linear solutions of transversely loaded plates

In order to have a basis of comparison for the influence of inplane loading on the behaviour of plates under combined loading, non-linear solutions were obtained for the same plates under transverse loading alone. Also the effects of boundary conditions and aspect ratio on the non-linear behaviour of plates may be studied tentatively before solutions become more involved due to the presence of inplane loading. This section being common to parts of previous work[15],[16] done on the subject has served in providing a check of the results before solutions were obtained with inplane loading. The solutions given in this section extend the range of existing results and reveal some phenomena in the large deflection of plates not previously observed.

The maximum value of transverse pressure was chosen such that under the intended combined loading the central deflection of each plate analysed would

be of the order of 2-3 times its thickness. The loading was, in most cases, raised to its maximum value in 10 increments.

1) Simply supported plate under transverse pressure. Solutions are given for four different membrane boundary conditions, namely, plate 1.(1), 1.(6), 1.(13) and 1.(15). Results are shown in figures 1-6 and listed in tables 1-4.

For plate 1.(15), in which the resultant direct membrane stress along each edge is zero, no finite difference solutions have been available before. This membrane boundary condition was developed to simulate the boundary conditions of individual plate elements of panels made up of identical arrays of such elements under symmetrical loading.

Figure 1 shows the variation of central deflection with transverse pressure. The tangent to the cruves at the origin is the linear solution. It can be seen that for a given transverse pressure, plates fixed at the edges against inplane movement deflect least, while the highest deflections are exhibited by plates free from membrane stresses along the edges. The central deflections of plates 1.(13) and 1.(15) lie between these two limiting cases.

In all the four cases membrane action has the effect of reducing curvatures at the centre relative to the regions away from it (figures 2 and 3) and consequently the position of maximum moment shifts from the centre towards the sides (for square and rectangular plate). For given values of transverse pressure, the shift in the position of maximum moment is most pronounced for plates 1.(1) and least for plates 1.(6).

Membrane stresses at the centre and total membrane forces at the boundaries, after the initial slow rate in their development, increase steadily with the applied transverse pressure (figures 4 and 5). The distribution of membrane stress across the centre lines and boundaries is shown in figure 6 relating to the maximum transverse pressure reached. For a given intensity of transverse loading, the maximum membrane stress is developed in plates with free edges

and occurs as compression along the mid-point of the edges. Since there is no external inplane loading, the membrane stresses shown are in self-equilibrium for all the four cases. In plates 1.(13), as a result of the tangential restraint of the unloaded edges, the direct membrane stresses along the mid-point of these edges are zero. High tensile stresses across the mid-point of the edges in plates 1.(6) and 1.(15) are evidence of the greater tendency of the central portion of the sides to move inwards under the applied loading. Maximum shear stress at the edges in plate 1.(13) is encountered at a distance of about one-sixth of the side from the corner.

2) Clamped plates under transverse pressure.

Clamped plates with four membrane boundary conditions are analysed, namely, plates 5.(1), 5.(10), 5.(13) and 5.(15). The results are shown in graphs 7-12 and are given numerically in tables 5-8.

The effect of membrane boundary conditions on the central deflection (figure 7) is the same as for simply supported plates. A similar influence is exhibited on the central moments (figure 8). The membrane boundary condition of edges fixed against inplane displacements (10), causes the highest tensile stress to occur at the centre of the plate (figure 9). The influence of membrane boundary conditions on curvatures and moments is also similar to the corresponding simply supported cases (figures 10 and 11). The variation of bending moments over the centre of plate becomes smoother with the increase in membrane action.

The distribution of membrane stress across or along the centre line and the boundary are shown in figure 12. For plates 5.(1) and 5.(10) the distributions are similar to 1.(1) and 6.(1) already discussed. In plates 5.(15), however, the magnitude of membrane stresses across the boundary are smaller than the corresponding values across the centre lines. The corners of plate, in this

case, are subjected to a direct tensile stress. A close examination of the extensional displacement profiles of the edges revealed that for simply supported plates 1.(1), the angle between the sides (originally 90 degrees) at the corners gradually reduces as the transverse pressure is incremented, whereas for clamped plates 5.(1) it gradually opens. From this observation it appears that for clamped plates, if the edges are forced to remain straight (as in 5.(15)), it is logical to expect a tensile stress at the corners immediately followed by compression.

3) Simply supported plates under transverse loading (variation of aspect ratio).

Simply supported plates with two membrane boundary conditions are considered, namely, the case of stress free boundaries 1.(1) and the case of edges fixed against extensional displacements but free from inplane shear stresses 1.(6). For each case three aspect ratios 1, 1 : 1.5 and 1 : 3 are analysed. Results are shown in figures 13-22 and are given in tables 9-12.

For the case of the stress-free membrane boundary condition, deviation from the linear solutions for central deflection and central transverse moment, as a result of the membrane action, is largest for plates with an aspect ratio of 1 : 1.5 (figures 13 and 14). It can be observed from the tables that, in this case, the sum of the principle tensile stresses at the centre of plate is a maximum for the aspect ratio 1 : 1.5. In the case of plates restrained at the edges against translation, however, this deviation is most pronounced for plates with an aspect ratio of 1 : 3 (figures 15 and 16). In this case, the sum of the principle membrane stresses at the centre of plate for a given transverse pressure is almost constant for the three aspect ratios. The transverse membrane stresses, however, are largest for an aspect ratio of 1 : 3.

For plates 1.(6) with an aspect ratio of 1 : 1.5 a central deflection equal to 1.5 times the plate thickness causes the maximum longitudinal moment (1/6b from the shorter sides) to become 70% more than the moment at centre (figure 18). The same effect is even more pronounced for plates with aspect ratios of 1 : 3, as shown in figures 19 and 20. In both cases, however, the absolute magnitudes of the moments are still substantially less than the maximum moment of plate as given by the linear theory.

The distributions of membrane stress are shown in figures 21 and 22. For plates 1.(1) with an aspect ratio of 1 : 3 the transverse direct membrane stresses are negligible at the centre, and the magnitudes of the longitudinal direct stresses are relatively small considering the magnitude of the central deflection (figure 22). The distribution of membrane stress within the central region of plate 1.(6) for an aspect ratio of 1:3 is similar to an infinitely long strip under transverse pressure with the same membrane boundary conditions.

4) Clamped plate under transverse pressure (variation of aspect ratio).

As in the previous case, three aspect ratios 1, 1 : 1.5 and 1 : 3, and two membrane boundary conditions are analysed. The boundary conditions are edges free from membrane stresses - plates 5.(1), and edges fixed against extensional displacements with zero inplane shear stresses - plates 5.(6). Results are given in figures 23-32 and tables 13-16.

The variations, with transverse pressure, of the central deflection and moments are shown in figures 23-26. In principle, the effects of membrane action on bending in this case are analogous to the corresponding cases of simply supported plates.

The central transverse moment of plate 5.(1) for an aspect ratio of 1:3 becomes even larger than the linear theory for increments of transverse pressure (figure 24). The deflection profile of this plate (figure 29) confirms the

above behaviour and shows that in contrast to plate 5.(6) the membrane action increases the curvature at centre relative to the region near the sides. In both directions, the absolute magnitudes of the moments at centre are slightly larger than the values given by the linear theory.

For an aspect ratio of 1 : 1.5 the deflected profiles of plates 5.(1) and 5.(6) are both flatter than the profiles obtained from the linear theory (figure 27).

The distributions of bending moment along the centre lines of the plates relating to the maximum load reached are given in figures 28 and 30. For the corresponding distributions in the case of square plates reference should be made to group 2 of the results in this section.

The distributions of membrane stress across the centre lines and across the boundaries are shown in figures 21 and 22. The significant features, when compared with the corresponding simply supported cases, are that for plates 5.(6) the membrane stress at the mid-point of the shorter side and in the transverse direction is negligible in magnitude, and that there is a rise in tensile stress at the boundaries in the vicinity of the corners. Further, for plate 5.(1) with an aspect ratio of 1:3 the direct membrane stress in the transverse direction at centre is compressive instead of the usual tension.

5) Plates under central patch load.

Two cases are treated, (i) a simply supported plate with edges free from membrane stresses, and (ii) clamped plate with edges fixed against translation but free from inplane shear. In both cases a central patch load with dimensions of one-tenth of the plate's sides is chosen. The transverse load was raised to give maximum deflections of the order of 3.5-4 times the plate thickness.

A 16 x 16 graded mesh (No.5) was used and the loaded area covered by 9 node points. In the case of linear solutions of simply supported plates, without

an increase in the total number of nodes, the grading has improved the error in the central deflection from 2% to O.88%, and that of the central bending moment from approximately 12% to 1% (see appendix E for accuracy of results). The same grading is used for clamped plates. The results are given in figures 33-4O and tables 17 and 18.

No solutions for the large deflection of clamped plates under a central patch load are available. In the case of simply supported plates the present results have greatly improved the accuracy of the existing solution[15].

The main effect of membrane action on bending is a rapid increase in curvatures under the load relative to the rest of the plate (figures 34 and 37), and consequently high localised bending moments in this region (figures 35 and 38). The absolute magnitudes of the central moments, however, are appreciably less than the values given by the linear theory (tables 17 and 18). In both cases, for the greatest value of central deflection reached the load is to a large extent resisted by the membrane action. This is evidenced by the high localised central curvature, surrounded by a relatively straight deflection profile and correspondingly low values of bending moments (figures 35 and 37). Towards the supports the curvatures increase in order to accommodate the plate within the imposed boundary, and hence tend to give a second rise in the bending moments in this region.

The distributions of membrane stress across the centre lines and the boundaries for the two boundary conditions are given in figures 39 and 4O and indicate the high central peak in the distribution of membrane stress, when compared with plates under uniform transverse pressure.

Non-linear solutions of plates under inplane and transverse loading.

Solutions are divided into two groups. In the first group the inplane loading is kept constant and variations in sectional actions and displacements are studied for increasing transverse pressure. In the second group the transverse pressure is kept constant and the behaviour of plate is investigated for varying inplane loading.

Variation of transverse pressure.

In all the solutions of this group the plate, taken as initially flat, is first subjected to a uniform inplane loading which is either in the form of a uniform edge-compression, or a uniform edge displacement, or a combination of both. The intensity of the inplane loading is expressed in non-dimensional form as a ratio of the critical buckling load of the plate if it were simply supported with inplane movements in the transverse direction unrestrained. Uniform transverse pressure is subsequently applied and raised incrementally in 10 steps to its maximum value.

1) Simply supported plate under uniform edge compression and transverse pressure.

This is the simplest case of plates under combined loading and is the first analysed in the study of the influence of edge compression on the behaviour of transversely loaded plates. The plate is assumed to be free from direct and shear inplane stresses at the unloaded edges, and free from inplane shear at the loaded edges.

Solutions are obtained for four different values of inplane loading, namely, P_x/P_e = O, O.25, O.5 and O.75, where P_x is the applied inplane stress and P_e the critical buckling stress of the plate. The maximum resulting central deflection reached is about three times the plate thickness.

Figure 41 shows the central deflection plotted against the intensity of transverse loading. The tangents to the curves at the origin are the small deflection solutions, the slopes of which are given in table E-4 of appendix E together with Bleich's results for comparison. For small transverse pressures (below $Q' = 400$), central deflection is found to be very sensitive to the magnitude of the edge-compression. For larger transverse pressures, however, the rate of change of central deflection is not greatly influenced by this value.

For a given value of transverse pressure, plates with larger initial edge-compression exhibit deflected profiles slightly flattened in the direction of applied loading and slightly sharpened in the perpendicular direction (figure 42).

Figure 43 shows the bending moments M_x and M_y at the centre of plate plotted against transverse pressure. Also in this case the tangents to the curves at the origin are the linearised solutions and are given in table E-4 of appendix E. In this case M_y can be seen to be consistently greater than M_x. The influence of the magnitude of edge-compression is again more pronounced at smaller transverse pressures, where the bending moments of the four cases considered differ considerably. For larger pressures, moments in the direction of applied compression for all four cases approach one another, whereas moments in the perpendicular direction, which have now become more distinguishable from the former, gradually increase and depart from the former in harmony. In all the four cases treated, for the largest transverse pressure reached, the maximum moment in the plate was found to act in the direction of applied loading at about $a/6$ from the edge (figure 44). The solutions obtained show that the translation of the position of maximum moment is fully achieved by the time the central deflection of the plate exceeds its thickness.

The build up and variation, with transverse pressure, of membrane stresses at the centre of plate and the middle of edges is shown in figure 45. It can be seen that the build up of membrane stresses plotted is slow for central deflections up to about half the plate's thickness, but thereafter the rate of growth increases and membrane stresses become a dominant factor in the behaviour of the plates. Due to transverse pressure, the initial compressive membrane stresses at the centre of plate may be converted to tension (for $k = 0.5$ conversion takes place at $w/h \approx 1.4$). Further increase in transverse pressure results in an extension of the central tensile zone and consequently, from equilibrium considerations, the accumulation of high compressive stresses near the sides with maximum compression at the mid-point of the unloaded edges in the direction of applied loading.

Figure 46 shows the distributions of membrane stress across the centre lines of the plate for the maximum transverse pressure reached. It can be concluded from this distribution that for a given transverse pressure, increments in edge compression reduce the tensile zone at the centre of plate only slightly and are mainly accumulated in the compression zone adjacent to the unloaded edges. It is important to note that this region of plate sustains not only the total applied edge-compression but also the compressive equilibrating force of the tensile stresses across the centre line.

Figure 47 shows the profiles of the extensional displacements of the edges. For increments of transverse pressure, changes in these profiles are more pronounced at the unloaded edges.

2) Simply supported plate under uniform inplane loading and transverse pressure (influence of the inplane boundary conditions and inplane loading).

In order to study the influence, on the non-linear behaviour of plates, of the membrane boundary conditions of the unloaded edges, and of the method

of application of the inplane loading, solutions were obtained for five different cases of simply supported plates. In each case the plate is initially loaded to half the critical value at which a fully unrestrained simply supported plate would have buckled. In three cases this is achieved by applying a uniform edge-compression, the unloaded edges being, (i) fully free from membrane stresses - plate 1.(26), (ii) fixed against translation with zero inplane shear-plate 1.(27), and (iii) restrained against tangential movement with zero direst stress - plate 1.(29). In the remaining two cases the plate is subjected to a uniform edge displacement with the unloaded edges being, (iv) stress free - plate 1.(38), and (v) fixed against translation with zero inplane shear - plate 1.(39). Solutions are given in figures 48-60 and tables 22-25.

Figure 48 shows the variation of central deflection of the plate with transverse pressure from which the extensive influence of the membrane boundary conditions on the central deflection is evident. Tangents to the curves at the origin are the linearised solutions and their slopes are given in table III-1. It is important to note that the linearised solutions vary by over 100%. The greatest stiffness is shown by plate 1.(29); plate 1.(39) on the other hand initially deflects 80% more than the standard case 1.(26).

The linearised solutions differ partly because the plates considered do not have the same critical buckling loads. This is due to different membrane boundary conditions. The solutions would therefore be more comparable if the plates, instead of being initially subjected to the same inplane loading, were acted upon by half their respective critical buckling loads. The present analysis covers the evaluation of the critical buckling load of plates with due consideration to the membrane boundary conditions.

Figure 49 shows the deflection profiles along the centre lines of the plates. The change of profile is more noticeable in the direction perpendicular to the applied loading.

The influence, on bending of the membrane boundary conditions can be seen clearly in Table III-1 for the linearised solutions and in figure 50 for the non-linear behaviour.

TABLE III-1

Loading	Plate	Magnification factor*		
		W	M_x	M_y
$\frac{P_x}{P_e} = 0.5$	1.(26)	2.032	2.105	2.118
	1.(27)	2.928	3.080	3.088
	1.(29)	1.717	1.727	1.777
$\frac{U}{U_e} = 0.5$	1.(38)	2.032	2.105	2.118
	1.(39)	3.608	3.815	3.826

*Bleich's magnification factor for simply supported plates loaded with $\frac{1}{2}P_e$ is 2.000, ref.24.

Plates 1.(27) and 1.(39) which are contained in their widths exhibit the largest initial bending moments. Plates tangentially restrained at the unloaded edges, such as plate 1.(29), transfer a part of the applied edge compression to these edges through shear and thus reduce the influence of the applied loading at the centre of the plate. At the centre of plates moments in the transverse direction are generally larger than moments in the direction of applied loading, except in plate 1.(38) where the former becomes less at $w/h \approx 2/3$. The crossing of the bending moment curves closely follows that of the deflection pattern in figure 48.

As noted before, the main influence of the inplane loading on a tangentially restrained plate - 1.(29) is near its point of application. For the highest value of transverse pressure reached (figure 51), the maximum bending moment

in this region is about 75% more than the moment at centre. Transverse to the direction of the applied inplane loading, the bending moment profile is affected most in the case of plates with unloaded edges fully free from membrane stresses and least when these are fixed against translation.

Variation, with transverse pressure, of the membrane stresses at the centre, the middle of edges, and the corner of plates are shown in figures 52 and 53.

Figure 52 shows plates with uniform edge compression only. It can be seen that the lowest membrane stresses are obtained for plate 1.(27) where the fixity of the unloaded edges against translation has greatly restrained the rise of membrane stresses. Due to the membrane boundary conditions of the unloaded edges, the plates are initially subjected to slightly different values of membrane stresses.

The value of central deflection at which the central tensile zone in the plate initiates is found to be affected slightly by the inplane boundary conditions and is between 1.4 to 1.7 times the plate's thickness for the cases under discussion.

The highest membrane compression is developed in plate 1.(29) at the mid-point along the loaded edges.

Figure 53 includes the plates with initial edge displacements. The main feature in this case is that, as the initial applied displacement is kept unaltered, the transverse deformation rapidly reduces the resultant initial compression of the plate until the action at the loaded edges is completely annulled. Thereafter the displaced edges act as a restraining device against transverse deformation rather than as a contributory external load. Tensile stresses initiate across the mid-point of the displaced edges, in the case of plate 1.(38) at $w/h \approx 0.9$, and for plate 1.(39) at $w/h \approx 0.8$. In none of the cases were the stresses along the edges fully converted to tension.

The distribution of the membrane stress across the centre lines and along or across the boundaries of the plates analysed are shown in figures 54 and 55 for the maximum value of transverse pressure reached. In plate 1.(29) - figure 54, the central tensile zone extends to the unloaded edges and consequently fully seals off the flow route of the applied compression via the plate itself. The edge compression at this stage is transferred by shear to the boundary which must also accommodate, in shear, the equilibrating force of the tensile stresses across the relevant centre line of the plate.

Distribution of inplane shear stresses for plate 1.(29) is shown in figure 56. Shear stresses are of low value in the central region of the plate, and gradually build up towards the unloaded edges. In all the other plates of this group the values of shear are found to be substantially less than those of plate 1.(29).

Figure 57 shows the extensional displacement profiles of the edges for the highest value of transverse load reached. It can be seen that these profiles are also extensively influenced by the inplane boundary conditions.

The distribution of inplane shear stress along the boundary of plate 1.(29) is shown in figure 58. Increments in transverse pressure cause the position of maximum inplane shear to shift from its initial position at the corner towards the centre of plate. The build up of total inplane shear force at the boundaries as the transverse pressure is increased is shown in figure 59. The total shear force increases steadily and exceeds the total applied edge-compression at $w/h \approx 1.8$.

Figure 60 shows the variation of the total direct forces across the sides with increasing transverse pressure. It can be seen for plates 1.(38) and 1.(39) that increasing transverse pressure rapidly reduces the initial compressive forces at the displaced edges where finally considerable tensile forces are

developed. The change of total compression to tension takes place in plate 1.(38) at w/h $\approx$ 1.1 and in plate 1.(39) at w/h $\approx$ 1.

3) Clamped plate under combined loading - plate 5.(45).

The plate analysed refers in its special case to a square isotropic clamped plate. The loaded edges remain straight and translate under a total specified end-thrust equal to 1.259 P_e. The unloaded edges remain straight and translate with a resultant direct membrane stress across them equal to zero. Inplane shear stresses are assumed to be zero along all the edges. This arrangement approximates an individual plate in an assembly made up of identical plates under constant uniaxial compression. Due to symmetry, the rotation and inplane shear stresses along the boundary of individual panels may be assumed to be zero. If the assembly is unrestrained in the transverse direction the resultant direct stress across the boundaries, parallel to the applied loading, may also be zero.

Results are shown in figures 61-65 and are given in table 26.

Increments in transverse pressure reduce in this case the curvature of the plate at the centre relative to the regions adjacent to the loaded edges (figures 62 and 63).

Distribution of membrane stress in the plate for the maximum value of transverse pressure reached is shown in figure 64. Also in this case, the effect of rotational fixity of the edges on the disttibution of membrane stress can be seen at the corners of the plate. The applied edge-compression, originally uniform along the loaded edges, is concentrated near the unloaded edges with maximum values adjacent to the corners.

Transverse pressure reduces the inplane stiffness of the plate and consequently the plate shortens further, as the transverse pressure is increased, under the total specified end-thrust. The effective width, defined as the

ratio of the actual inplane load carried by the plate to the load the plate would carry if it does not deflect, is evaluated and is shown in figure 65. It can be seen that a central deflection equal to the plate's thickness corresponds approximately to a 20% reduction in the effective width.

4) Simply supported plate under biaxial compression and transverse loading - plate 1.(56).

The plate which in its special case refers to a square isotropic plate is initially subjected to a uniform biaxial compression. Thereafter, an increasing uniform transverse pressure is applied. Results are given in figures 66-69 and table 27.

The loading in this case is comparable with the plate 1.(26) (table 20) already discussed and for which the inplane loading was uniaxial but with twice the intensity of the present case. There is a remarkable similarity between the flexural behaviour of the present plate and the plate loaded uniaxially. The difference between the central deflections and bending moments of the two cases is of the order of 1% of their values. This implies that the bending effects of a simply supported square plate under uniform biaxial compression may be closely approximated by that of a uniaxially loaded plate with twice the intensity of the inplane loading. An examination of the relevant governing equation (B-16) in appendix B confirms the above statement provided the deflected profiles of the uniaxially loaded plate can be assumed to be the same in both directions.

The similarity of behaviour becomes also evident from a comparison between figures of the case under discussion and the corresponding figures of plate 1.(26). The resemblance does not extend to the disttibution of membrane stress.

Variation of inplane loading.

The boundary conditions and loading of the two plates discussed in this

section are chosen with ship's bottom shell plating in mind. In their special cases, one of the plates relates to a square isotropic plate and the other to an isotropic plate with an aspect ratio of 1:3. The plates are assumed to be rigidly supported and rotationally fixed at the boundaries. The inplane loading and membrane boundary conditions are:zero inplane shear with edges remaining straight but free to translate-plate 5.(45).

From the information given in the Lloyd's Register of Shipping on the scantling of bottom shell plating (tables for length of ships, draft, and thickness of plating) the transverse pressure, due to still-water, to which a plating is subjected may be deduced. Figure III-1 shows the variation of transverse pressure ratio with length of ship for platings with one side equal to 30 inches. For the two cases analysed a transverse pressure ratio of 2($Q' = 72.18$) is chosen where this is approximately equal to that of the prototype, the model of which is under investigation.

The inplane loading to which the plating is subjected varies greatly and has been discussed in Chapter I. The critical buckling load and the inplane loading which causes overall yielding of such plates are used as a guide. The non-dimensional stress ratio corresponding to the critical buckling stress of square clamped plates is approximately 100, (a^2N_x/D_x). If the yield stress of the plating is assumed to be of the order of 20 tons/sq in., from the tables given in the Lloyd's Register of Shipping for the thickness of plating it can be deduced that the on-dimensional value of the inplane loading which will cause overall yielding of a 30 in. wide bottom shell plating varies from 215 to 17 for ships between 100 feet to 650 feet long respectively. For the particular case considered the inplane stress ratio is of the order of 40.

In the solutions obtained the inplane loading ratio is raised to 90 in the case of the square plate, and to 70 in the case of the 1:3 rectangular plate.

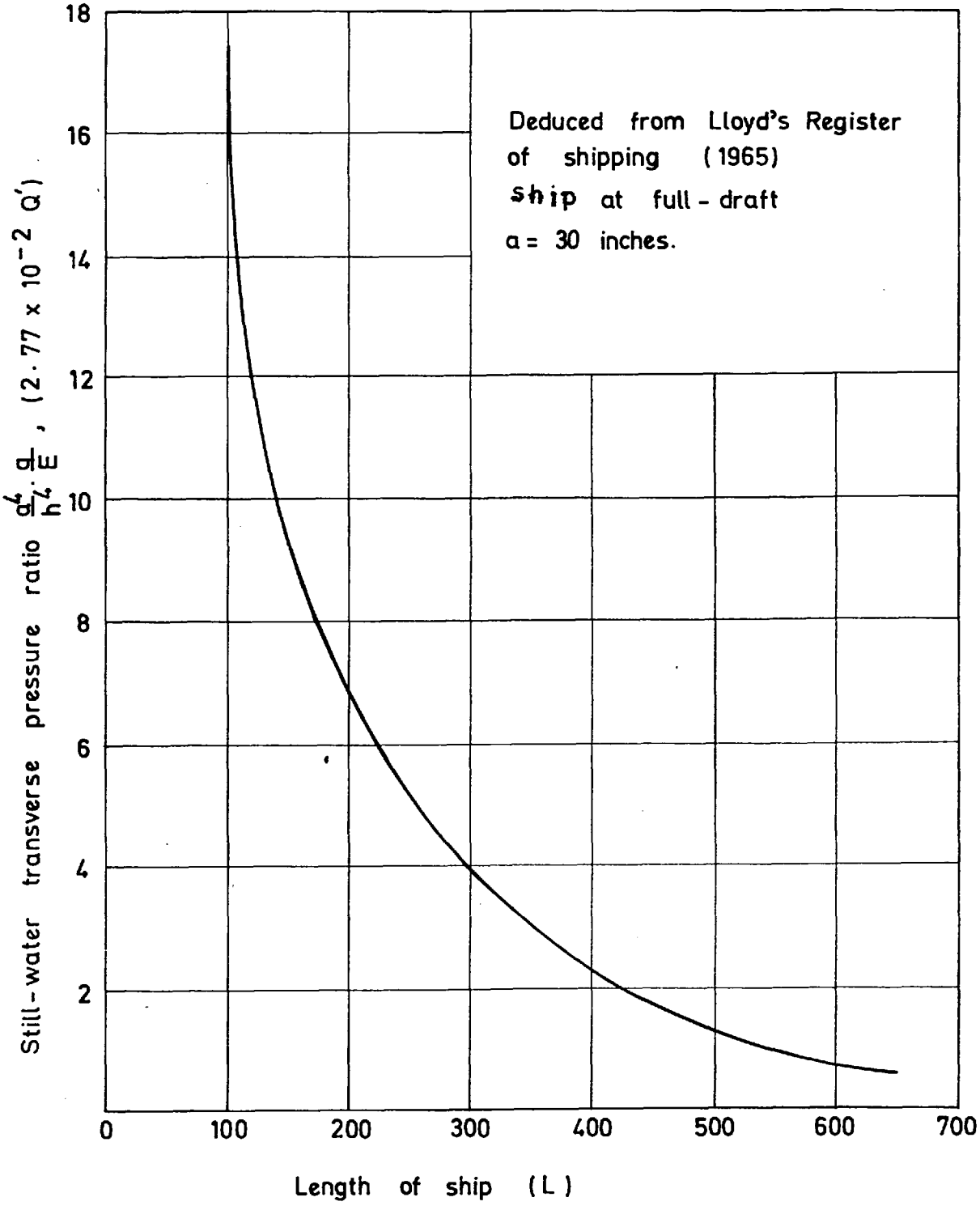


FIG. III - 1 Variation of length of ship with transverse pressure ratio for panels of double - bottom outer shell.

For the square plate the results are given in figures 70-73 and table 28.

In contrast to the cases when transverse pressure is varied, increments in the value of inplane loading sharpen the deflected profiles of the plate in both directions causing an increase in the rate of change of moment at the centre of the plate relative to the regions away from it (figure 71).

Figure 72 shows the bending moment profiles along the centre lines. It is important to note that the maximum moment in the direction of applied loading is at the centre of the plate, whereas in the linearised solution, the magnitude of the moment at the mid-point of the edges is over twice the value of the moment at the centre of the plate. Due to membrane action the position of maximum moment in the direction of applied loading shifts to the centre of plate for w/h above 0.1. For the maximum value of transverse pressure reached, the bending moment in the direction transverse to the inplane loading is still highest in the middle of the unloaded edges, although its ratio to the mid-span moment is reduced in comparison to the linearised solutions.

The change, for increasing values of end-thrust, in the distribution of membrane stress is not appreciable (figure 73), and consequently there is no significant reduction in the effective width due to transverse pressure. On the other hand, for the highest value of end-thrust reached the initial central deflection is increased by 11 times and the central bending moment by about 15 times due to inplane loading.

For values of inplane loading close to the critical buckling load of the flat plate the convergence of the solution was slow, and for loads above the critical value the solution converged to a deflected profile which did not appear to be the uninterrupted continuation of the previous load-deflection history of the plate. The new profile, however, satisfied the governing equations and the equilibrium of membrane forces. This could be due to

the fact that in the present analysis, for given magnitudes of inplane and transverse loading and by making use of the previous state of stress in the plate, deflection profiles are found that satisfy the governing equations and the boundary conditions. When for a combination of loading there exists more than one deflected profile that fulfils the imposed conditions, the previous history of the plate does not seem to have been represented in the analysis strongly enough to cause the solution to converge to the corresponding profile. This can be achieved, however, if the iteration method is modified such that for given magnitudes of central deflection and transverse pressure the inplane loading and the deflected profile are determined which satisfy the equilibrium considerations. In this case, instead of the inplane loading, the central deflection would be incremented. Due to a shortage of time this modification is not yet incorporated in the analysis.

The results of the 1:3 plate are shown in figures 74-76 and are given in table 29. As is evident from the figures, the flexural behaviour is extensively influenced by the inplane loading. Also, due to its aspect ratio the plate behaviour is very different from that for the square plate. Under a given value of transverse loading the plate deflects into a one half-wave as shown in figure 75. Increments of inplane loading initially magnify this profile (figure 74), but further increments reduce the central deflection of plate and the profile gradually approaches a three half-wave pattern which represents the incipient critical buckling mode of the plate.

For the maximum value of inplane load reached the central deflection has reversed sign and the plate has buckled into a three half-wave mode with signs of new waves emerging at the supports (figure 75).

The bending moment distribution shown in figure 76 reflects the same behaviour. The absolute magnitude of the bending moment at the mid-point

of the loaded edges reduces as the inplane loading is increased. In the interior of the plate bending moments vary extensively and the position of maximum moment is very sensitive to the magnitude of the applied end-thrust.

The influence of the transverse pressure on the distribution of membrane stress and on the stiffness of the plate against inplane loading is insignificant.

From the two cases treated it may be concluded that for the maximum loading considered the flexural behaviour is extensively affected by the inplane loading, whereas the membrane effects are not influenced by the presence of the transverse pressure to any great extent.

Initially deformed plates under end-thrust

Initially deformed plates under end-thrust are analysed for two different boundary conditions both of which are applicable to ships bottom plating. Initial deformations are assumed in the form of one half sine wave in both directions.

1) Simply supported plate under end-thrust, plate 1.(45).

The membrane boundary conditions and loading are that the edges remain straight in translation and are free from inplane shear stresses.

In bottom shell plating, due to initial deformations and loading, the adjacent panels may buckle either in the same way or in the opposite directions. In the latter case, for the purpose of theoretical analysis, the panels may be approximated as simply supported plates with the above membrane boundary conditions.

Maximum initial deformation is chosen to be 0.1 of the plate thickness.

Results are shown in figures 77-80 and in table 30.

The variation of central deflection with end-thrust is shown in figure 77 together with the available solutions. In plate 1.(41), which is given for

comparison, the direct membrane stresses across the unloaded edges are assumed to be zero instead of their resultant being zero as in the present case.

There is no appreciable change in the deflection profiles of the plate (figure 78). The curvatures in the direction of applied loading are slightly lower than in the perpendicular direction for the maximum loading reached. The corresponding curvatures in the two directions are, however, so close to one another throughout the incrementation of the inplane loading that the results may, from the previous conclusions, be used to estimate the bending stresses of the same plate under biaxial compression.

Distribution of membrane stress is shown in figure 80. For maximum loading reached there is a reduction of approximately 12% in the inplane stiffness of the plate (table 30 and figure 86). The magnitudes of the direct membrane stresses across the unloaded edges are small relative to the applied loading. This is the reason for the close agreement of the existing solution for plate 1.(41) with the present case.

2) Clamped plates under end-thrust, plate 5.(45).

The membrane boundary conditions are again chosen so as to approximate an interior panel of the outer shell plating. Solutions are obtained for two values of maximum initial deformation, namely, one-tenth and one-half of the plate's thickness. The magnitudes of these initial deformations are reasonable for ship's plating.

The results are given in figures 81-86 and in tables 31 and 32.

For given values of inplane loading, the plate with greater initial deformation exhibits larger moments and higher changes in membrane stresses. For the maximum value of loading reached, however, the central moments of the two cases approach one another (Tables 31 and 32).

As in the case of transversely loaded plate with increments of end-thrust, the rate of change of moment at mid-point of the loaded edges reduces relative to the moment at the centre. Maximum moment does, however, remain at the mid-point of the unloaded edges. It is important to note that for the same values of inplane loading the sectional actions are of higher magnitude in the case of the initially deformed plates than the case of the flat plate being subjected to a transverse pressure due to still-water for ship at full-draft (table 28). As the order of magnitude of initial deformations assumed are quite common in ship plates, the above results imply that the consideration of initial deviations from flatness may be of more significance in the design of ship plates than the presence of transverse pressure. In addition it can be seen from the tables that for given values of end-thrust the reduction in inplane stiffness of initially deformed plates is more than in the case of plates under transverse pressure. The above conclusions, however, are not general and only refer to magnitudes of transverse pressure and initial deformations relating to ship plates.

For several of the plates analysed the variation of the effective width with the central deflection is shown in figure 86, from which it can be seen that the effective width does not appear to be a simple function of the net or total central deflection of the plates analysed.

It is an interesting point to note that, in the cases analysed, the end-thrust initially widens the plates, but as the critical buckling load is approached the rate of widening decreases, and in the case of $w_o/h = 0.5$ the plate started to contract indicating the onset of incipient buckling (Table 32).

Cambered plate under uniform transverse pressure

A clamped plate which in its special case relates to a square isotropic plate is given an initial camber in the form of a half sine wave in both ways and with maximum rise equal to the plate thickness. It is subsequently

subjected to a uniform transverse pressure against the direction of camber. The edges are fixed against translation but are free from inplane shear. The problem approximates a single panel from an array of identical cambered plates under transverse loading. Results are shown in figures 87-90 and are given in table 32.

Figure 87 shows the variation of central deflection with transverse pressure. Initially, membrane action assists in resisting the applied pressure, but when the central deflection is reduced to about two-thirds of the plate thickness the rate of increase in deflection becomes greater than that given by linear theory.

Due to the rotational fixity of the edges, only the central region of the plate deflects below the datum line.

Two examples of transversely loaded plates

1) Square slab on four columns.

A square slab resting on four symmetrically located columns is considered. The moment rotation relationships of the slab at column-slab junctions, and the distribution, in the slab, of applied moments at column-slab junctions are determined.

For the purposes of analysis a fine mesh is used (one quarter of plate is subdivided into a 16 x 16 graded mesh as given in the results). Each interface of column and slab is covered by 25 nodes, and bending moments are represented by two triangular distributions of pressure (one positive and one negative) over each column area. This implicitly assumes that the columns exert no restraint on the deflection of slab at column-slab junction, and that the deformation of the interface is a continuation of the deformation curve of the slab. If, however, as the other extreme, columns are assumed as

infinitely rigid, an applied column moment results in a rigid body rotation of the column-slab junction (the plane of interface remains undeformed). In practice intermediate conditions, possibly closer to the latter extreme prevail.

Rotations are calculated along the columns' centre lines using a central five point finite difference formula for the first derivatives of the deflection function. Due to the method of application of moments and the evaluation of the resulting rotations, the solutions given are lower bound values of the stiffness of slab in resisting the applied moment.

Four cases are analysed, two for columns in the interior of the plate and two for columns immediately adjacent to the free edges. In each case solutions are obtained for applied moments at column-slab junctions both symmetrical or antisymmetrical about one centre line of the slab. Superposition gives the case when equal moments are applied at two of the four column-slab junctions on one side of a centre line only. Results are given in figures92-95.

For interior columns, figure 92 indicates that under symmetrical loading the slab exhibits greater stiffness when the columns are placed nearer the centre; for antisymmetrical moments there exists an optimum stiffness of slab for a column spacing between the two extremes analysed.

Equivalent beam stiffnesses are calculated on the assumption that the bending moment is applied uniformly across the slab about the axes through the centre of columns. The slab behaviour under such loading may then be approximated by that of a beam.

For cases when columns are located at the edges of the slab, maximum stiffness is shown for columns at corners in the case of symmetrical moment, and for columns at an intermediate position in the case of antisymmetrical moments (figure 93).

Figure 94 shows the extensive contribution of the overhanging part of the slab in resisting the applied moment. It is due to the influence of this region

of slab that, although the applied moment is concentrated over a small area, the stiffness exhibited by the plate is appreciable when compared with the equivalent beam in which the contribution of the relevant overhanging parts is zero. Maximum moments occur from the present analysis, in the direction of applied moment along the centre lines of the columns at the first node within the column area. For columns at the corners, however, the position of maximum moment is found to be one node closer to those edges which are perpendicular to the axis of the applied moment. In all the cases maximum transverse moment occurs along the centre line of columns at the first node outside the column area (figure 95).

2) Square slab on a central column

Using the same principles as in the previous example the moment rotation relationships are determined for a square slab on a central column and with three different boundary conditions, namely, all edges simply supported, all edges fully fixed, and finally the case of two opposite edges simply supported and others unsupported but with zero rotation. The third boundary condition may approximate an internal panel of a flat slab, under side loading (inplane), on columns spaced equally on an orthogonal grid.

In each case solutions are obtained for three different column dimensions. The smallest column area is represented by 25 nodes, the medium column by 49, and the large column by 81 nodes.

Results are given in figures 96-98, from which it can be seen that the distribution of bending moment in the vicinity of the column is not particularly sensitive to the boundary conditions chosen.

CHAPTER IV

Conclusions

An analysis has been made in terms of finite differences which enables the behaviour of rectangular orthotropic (isotropic) plates under any system of transverse and inplane loading and with any rotational, vertical (normal to the plane of the plate), extensional, and tangential restraints at the boundaries to be studied. The equations formed have been solved by digital computer.

A selected range of previously unsolved problems have been solved and these enable a number of conclusions concerning the physical behaviour of plates and the influence of boundary conditions to be drawn. The scope of the treatment is such that many other outstanding plate problems are capable of solution.

The influence of the inplane boundary conditions on the bending behaviour of plates has not been previously fully recognised. It has been demonstrated that in many cases the extensional boundary conditions can be as important as the flexural boundary conditions.

In the non-linear behaviour of transversely loaded plates, the effect of membrane boundary conditions on central deflection and moments is similar for both simply supported and clamped plates. The deviation from linear theory is greatest for plates with boundaries fully fixed against inplane movements (10) and is least for plates free from membrane stresses at the edges (1). For other membrane boundary conditions the deviations lie between these two limiting cases, where the central deflection of the tangentially restrained plates (13) is less than that of plates with straight edges and zero resultant direct stress at the boundaries (15).

For all the membrane boundary conditions considered, increments in transverse pressure reduce the rate of change of curvature at the centre relative to the rest of the plate. In the case of simply supported plates the position of maximum moment, originally at the centre, shifts towards the sides as the load increases. This translation of the position of maximum moment is manifested more strongly in the case of rectangular plates with edges restrained against inplane displacements. For a simply supported plate with an aspect ratio of 1:1.5 , a central deflection equal to 1.5 times the thickness of plate corresponds to a maximum longitudinal moment at one-sixth of the plate length away from the edges having an intensity of 70% more than the bending moment at the centre. The absolute magnitude of the moment, however, is still less than the maximum moment in the plate given by linear theory.

For clamped plates the corresponding effect is a flattening of the distribution of bending moment over the central region of the plate and an increase in the ratio of moment at mid-point of the edges to moment at the centre (for plate 5.(13) a central deflection of the order of plate thickness relates to a ratio of mid-edge to central moment of 3).

Within the range of aspect ratios considered (1:1, 1:1.5, 1:3), for both simply supported and clamped plates, the strongest restraining effect of membrane action on central deflection and moment is found, in the case of stress-free boundaries, for plates having an aspect ratio of 1:1.5, and in the case of boundaries fully fixed against inplane displacement for plates having an aspect ratio of 1:3.

For a given value of transverse pressure, maximum tensile membrane stress occurs at the centre of plate for the case of edges fully fixed against inplane displacements. Maximum compressive stress is exhibited along the mid-point of the edges for plates with edges free from membrane stress in the plate.

Due to membrane action, the angle between the sides of the plates at the corners reduces in the case of simply supported plates and opens in the case of clamped plates. Therefore clamped plates with edges forced to remain straight show a rise in the tensile membrane stresses at the corners.

In plates restrained against tangential displacements at the boundaries the maximum value of inplane shear occurs along the edges. The position of this maximum moves from the corner towards the quarter-points of the sides as the transverse pressure is increased.

In the case of simply supported plates under combined loading the shift of the position of maximum moment is even more pronounced, especially in the direction of the applied inplane loading.

For a simply supported plate under edge compression and low values of transverse pressure, the central deflection and moments are found to be very sensitive to the magnitude of the applied inplane loading. At higher values of transverse pressure, however, this sensitivity greatly diminishes. The magnitude of the central bending moment in the direction transverse to the applied inplane load is consistently higher than the corresponding central moment in the direction of this loading. Nevertheless the maximum moment in the plate occurs in the latter direction near the loaded edges.

Even for plates under constant inplane loading, increments in transverse pressure result in the formation of a tensile zone in the plate. In the case of plates tangentially restrained at the sides, this zone may extend across the full width of the plate, the inplane loading being resisted by the side as a shear force. The total shear at these edges then exceeds the applied loading.

The flexural behaviour of simply supported plates under uniform biaxial edge-compression closely resembles that of the same plate subjected to a

uniaxial edge-compression of twice the intensity of the biaxial case. Solutions obtained for simply supported plates under uniaxial end-thrust may therefore be used to predict the behaviour of the same plate acted upon by a biaxial edge-compression. The analogy does not, however, hold true for the membrane action or for clamped plates.

For clamped plates under combined loading, increments in inplane loading rapidly reduce the magnitude of moment at middle of the loaded edges relative to the centre of plate. In the case analysed (Table 28) the former became less than the central moment in magnitude at a central deflection of the order of O.1 of the plate thickness. The same phenomenon is exhibited in the transverse direction but is less pronounced.

For initially deformed plates considered, the reduction in effective width at a given value of central deflection is more for simply supported than for clamped plates with the same initial deformations.

For medium size ships (length of ship about 400 feet) the effect of transverse pressure, due to still-water, on the distribution of membrane stress in the bottom shell plating, due to end-thrust, is negligible. The effect of end-thrust on the bending of plating is, however, appreciable. In the case of the square plate analysed the bending effects are magnified several times due to inplane loading (table 28).

Initial deformations in ship plating (maximum deviations from flatness considered O.1-O.5 of plate thickness) result in a bigger reduction in the effective width of the plating against inplane loading than the reduction caused by transverse pressure due to still-water. The effects on bending of the inplane loading in such plates is also very significant. The consideration of initial deviations from flatness appears to be of more importance in the design of the outer shell plating than allowance for transverse pressure.

From the foregoing it is evident that the variation with the applied loading of central deflection and moments in a plate are not true representatives of the non-linear behaviour of the plate. It is also evident that a knowledge of the state of stress in the plate based on linear theory together with the knowledge of the above variation is not sufficient for the full comprehension of the behaviour and for design purposes. This is because the original distribution of stress may extensively change as the load increases with shifts in the position of maximum stress.

The linearised solution proposed by Bleich for simply supported plates yields reasonably accurate results when the plate is acted upon by a uniform edge-compression with the unloaded edges free from membrane stresses. For other membrane boundary conditions the solution may be grossly in error either overestimating or underestimating the true value. For example, for a simply supported plate under an end-thrust equal to $\frac{1}{2}P_e$, Bleich's magnification factors overestimate the central deflection by 16% in the case of the unloaded edges being tangentially restrained, and underestimate it by over 50% if the unloaded edges are restrained against translation (this is due to Poisson's ratio, assumed to be 0.3).

In extensional problems a relatively coarse mesh gives highly accurate solutions for the equilibrium of membrane forces.

In the case of the small deflection solutions of transversely loaded plates, the grading of mesh greatly improves the accuracy of results when

i) for plates under patch loading, the mesh is concentrated under the load (in the case of a simply supported plate under a central patch load

($l_x/a = 0.1$) a 16 x 16 mesh when graded improved the error in the central moment from over 12% to 1% - appendix E).

ii) For plates with unsupported edges, the mesh is concentrated adjacent to these edges.

For square slabs on four columns, located on the diagonals, the overhanging parts contribute substantially towards the resistance of the slab against bending moments at column-slab junctions. In the cases analysed, for equal moments at column-slab junctions, the greatest stiffness is realised when columns are closest to the centre in the case of symmetrical moments about one centre line of the slab, and when columns are placed at an intermediate position in the case of antisymmetrical moments.

For plates on a central column the magnitude and the distribution, in the vicinity of the column, of an applied moment at the column-slab junction is not greatly influenced by the boundary conditions of the slab if these are, all edges simply supported, all edges clamped, or two opposite edges simply supported and others unsupported but rotationally fixed. The moment rotation relationships at the column-slab junctions appear to be primarily a function of the column dimensions and not the boundary conditions of the slab.

Whenever possible the results obtained were compared with the existing theoretical solutions. The agreement has, in general, been very good.

CHAPTER V

Experimental work

To investigate the structural behaviour of a ship's double-bottom, a one-eighth scale model representing one complete hold of a single decked dry cargo ship was constructed.

The model, which is of welded steel construction, has a length-width ratio of 1.5:1 and is 10 ft. 10.5 in. long, 7 ft. 3 in. wide and 5.5 in. deep. The outer shell is 0.080 in. thick plate and the rest of the components (i.e. inner bottom, floors, angle stiffeners, struts, etc.) are from 0.064 in. thick plate. The principal dimensions of the model are shown in figure V-1.

The model was to be tested under transverse pressure and combinations of transverse pressure and end-thrust.

The main problem in the construction was to attach the second skin after the remainder of the structure had been welded, since it was not possible to weld internally. A method was devised in which the faying edges of all members attached to the outer shell and inner bottom (i.e. centre and intercostal girders, floors, bracket floors, and longitudinal stiffeners) have projecting teeth machined in their edges which fit into corresponding slots machined in the inner bottom and bottom shell plating. Figures V-2 and V-3 show the model during construction and when complete.

The model was suspended from a loading rig in an upright horizontal position, 1.7 in. above the floor, and a pressure bag to be used for applying the transverse pressure was accommodated in this gap. The model was simply supported along four edge tee sections running along the top of the margin brackets by an adjustable pin-ended column at each frame along the sides and

and at each stiffener or web at the ends (see figure V-4). The pin-ended columns at the middle of each side were restricted to movement along the centre lines of the model only. The edges of the model were therefore free to translate, while its centre lines were kept in position relative to the loading rig.

The weight of the model in the unloaded condition was balanced by means of 20 adjustable coil springs distributed along the edges and attached to the loading rig frame.

The pressure bag, which covered the flat portion of the double-bottom, was made up of two sheets of rubber 1/16 in. thick and sealed at the sides. The bag was filled with water.

The end-thrust is to be applied by means of 26 lapped rams, 13 at each end, spaced so as to give a uniform distribution of stress along the ends of the model. For this purpose the ends of the model were extended by a box beam suitably designed to receive the jacks and spread the load.

The vertical reactions of the model (due to the transverse pressure from underneath) are resisted by the beam and column arrangement of the loading rig. The columns are bolted to the floor at the feet. The reaction of the jacks (placed horizontally) is taken by concrete blocks which are also bolted to the floor.

The model has electrical resistance gauges fitted both internally and externally. Deflections were measured by means of dial gauges.

The experimental results are being analysed at the time of the preparation of this thesis and will be reported by Williams (see Chapter I).

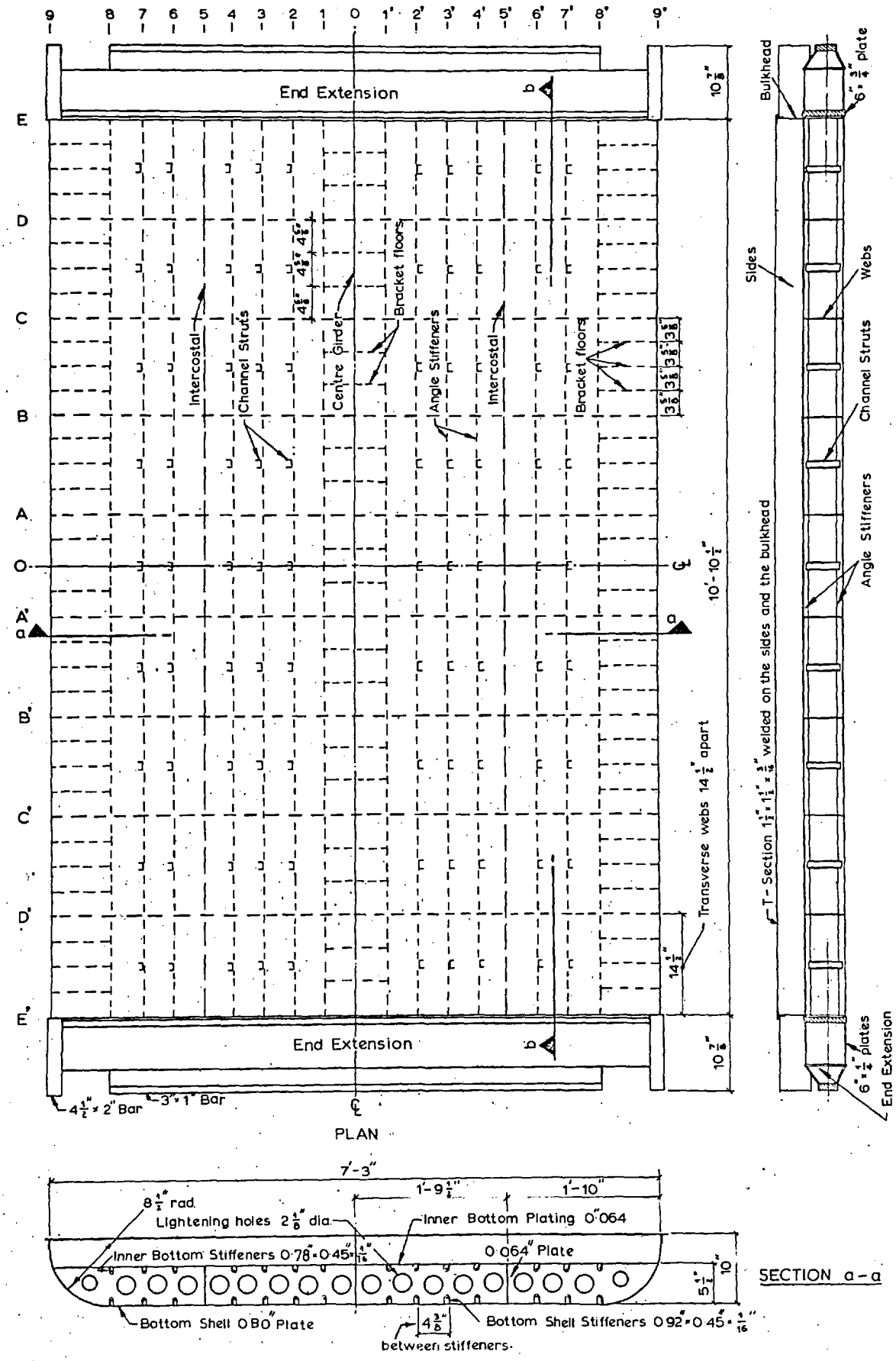


Figure V-1 Principal dimensions of the Double Bottom model

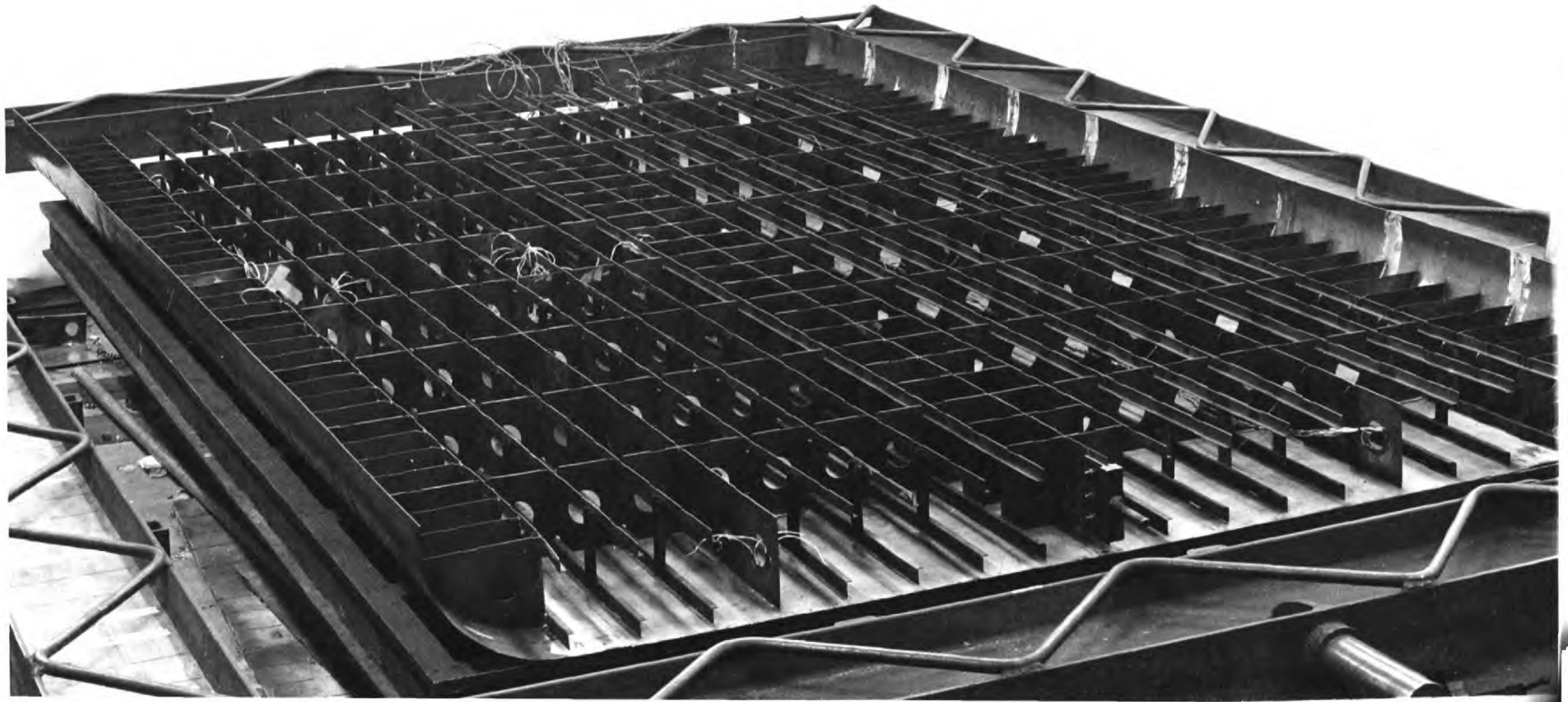


Figure V-2 Model During Construction



Figure V-3 Completed Model

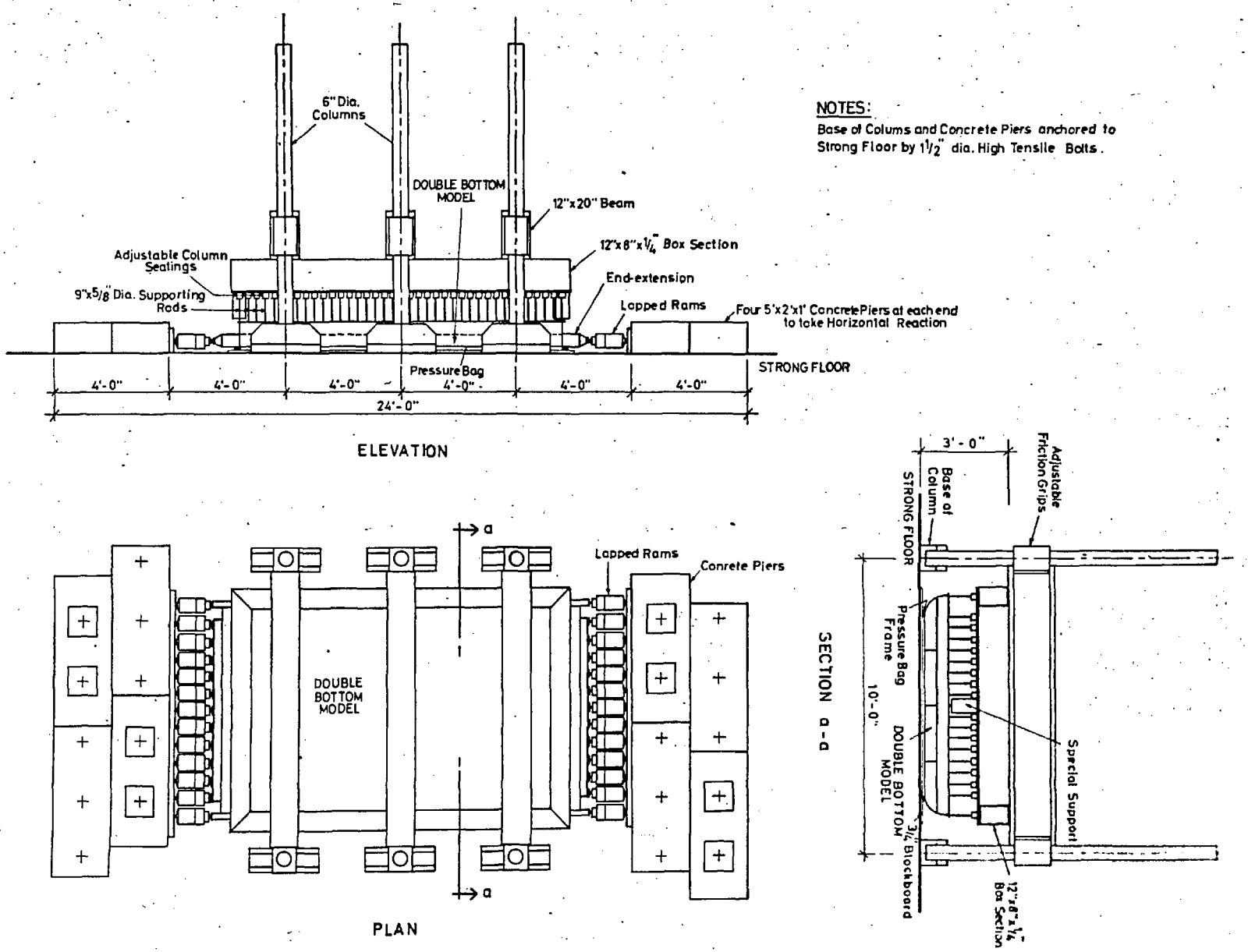


Figure V-4 The test arrangement

REFERENCES

1. von Karman, Th.
   Festigkeitsprobleme im Maschinenbau
   Encyklopaedie der Mathematischen Wissenschaften, IV (1910).

2. Rostovcev, G.G., cited by Iwinski, T. and Nowinski, J.
   The problem of large deflection of orthotropic plates
   Arch.Mech.Stoc., vol.9 (1957), (No.5).

3. Soper, W.G.
   Large deflection of stiffened plates
   Jour. of Appl.Mech., Dec.1958.

4. Kaiser, R.
   Rechnerische und experimentelle Ermittlung der Durchbiegung und Spannungen von quadratischen Platten bei Freier Auflagerung an den Raendern, gleichmaessig verteilter Last und grossen Ausbiegungen
   Z.f.A.M.M., Band 16, Heft 2, Ap.1936.

5. Marguerre, K.
   Die mittragende Breite der gedrueckten Platte
   Luftfahrt - Forschung, Vol.14, 1937.

6. Way, S.
   Uniformly loaded, clamped, rectangular plates with large deflection
   Proc.Fifth Int.Cong. of Appl.Mech., John Wiley and Sons, 1939.

7. Levy, S.
   Bending of rectangular plates with large deflections
   NACA, TN No.846, 1942.

8. Levy, S.
   Square plate with clamped edges under normal pressure producing large deflections
   NACA, TN No.847, 1942.

9. Levy, S. and Greenman, S.
   Bending with large deflection of a clamped rectangular plate with length width ratio of 1.5 under normal pressure
   NACA, TN No.853.

10. Levy, S.
Bending of rectangular plates with large deflections
NACA Report No.737, 1942.

11. Levy, S.
Square plate with clamped edges under normal pressure producing large deflections
NACA Report No.740, 1942.

12. Wang, C.T.
Non-linear large deflection boundary value problems of rectangular plates
NACA, TN No.1425, 1948.

13. Wang, C.T.
Bending of rectangular plates with large deflections
NACA, TN No.1462, 1948.

14. Eggwertz, E. and Norr, A.
Analysis of thin square plates with normal pressure and provided with edge frames of finite stiffnesses in the plane of the plates
Flygtekniska Foersoeksanstalten, Meddelande NR50, Stockholm 1953.

15. Basu, A.K.
The theory of orthotropic plates under lateral pressure and its application to corrugated plates
Ph.D. Thesis, London University, 1964.

16. Basu, A.K. and Chapman, J.C.
Large deflection behaviour of transversely loaded rectangular orthotropic plates
Proceedings of the Inst. of Civil Eng., Vol.35, Sept.1966.

17. Girkman, K.
Flaechentragwerke
Springer-Verlag, Wien, 1959.

18. Bauer, F., Bauer, L., Becker, W. and Reiss, E.L.
Bending of rectangular plates with finite deflections
IMM - New York University 332, Ap.1964.

19. Woolley, R.M., Corrick, J.N.,Levy, S.
Clamped long rectangular plate under combined axial and normal pressure
NACA, TN No.1047, 1946.

20. Timoshenko, S.P., and Gere, J.M.
Theory of elastic stability
McGraw-Hill Book Co., N.Y., 1961.

21. Timoshenko, S.P. and Woinowsky-Krieger, S.
Theory of plates and shells
McGraw-Hill Book Co., N.Y. 1959.

22. Conway, H.D.
Bending of rectangular plates subjected to a uniformly distributed lateral load and tensile or compressive forces in the plane of the plate
Jour.of Appl.Mech., Vol.16, Sept. 1949.

23. Lockwood, J.
Rectangular flat plates under combined bending and compression
The Shipbuilder and Marine Engine-Builder, Vol.57, Jan.1950.

24. Bleich, J.F.
Buckling strength of metal structures
London:McGraw-Hill Book Co., 1952.

25. Bleich, F.
A design manual on the buckling of metal structures
The Society of Naval Architects and Marine Engineers, N.Y.,
Technical and Research Bulletin, No.22, 1951.

26. Chang, C.C. and Conway, H. D.
The Marcus Method applied to solution of uniformly loaded and clamped rectangular plate subjected to forces in its plane
Jour.of Appl.Mech., Vol.19, 1952.

27. Taylor, J.L.
Rectangular flat plates under combined bending and compression
Shipbuilder, Vol.57, Jan. 1959.

28. Marguerre, K.
Zur Theorie der gekruemmter Platte grosser Formaenderung
Proceeding of the Fifth Int.Cong.for Appl.Mech., Cambridge, 1938.

29. Hu, P.C., Lindquist, E.E. and Batdorf, S.B.
Effect of small deviation from flatness on effective width and buckling of plates in compression
NACA, TN No.1124, 1946.

30. Coan, J.M.
Large Deflection theory for plates with small initial curvature loaded in edge compression
Trans.AMSE, Vol.73, 1951.

31. Yusuff, S.
Large deflection theory for orthotropic rectangular plates subjected to edge compression
Jour.of Appl.Mech., Vol19, 1952.

32. Falconer, B.M. and Chapman, J.C.
Compression buckling of stiffened plates
The Engineer, 5th and 12th June, 1953.

33. Yamaki, N.
Postbuckling behaviour of rectangular plates with small initial curvature loaded in edge compression
Jour.of Appl.Mech., Vol.26, Sept.1959, and Jour.of Appl.Mech., Vol.27, June, 1961.

34. Yamaki, N.
Experiments on the postbuckling behaviour of square plates loaded in edge compression
Transactions of the ASME, June 1961.

35. Bauer, L. and Reiss, E.L.
Nonlinear buckling of rectangular plates
IMM - New York University 316, Dec.1963.

36. Richardson, L.F.
The approximate arithmetical solution by finite differences of physical problems involving differential equations with an application to Masonary Dam.
Philosophical transactions of the Royal Society, London, Vol.210, 1911.

37. Collatz, L.
Zusamenfassender Bericht : Genaeherte Berechnung von Eigenwerten
Z.f.A.M.M., Vol.19, 1939.

38. Southwell, R.V.
Relaxation methods in engineering science
Clarendon Press, Oxford, 1940.

39. Boley, B.A.
Numerical methods for the calculation of elastic instability
Jour.of Aeronautical Sciences, June 1947.

40. Salvadori, M.G. and Baron, M.L.
Numerical computation of buckling loads by finite differences
Trans.of ASCE, Vol.116, 1931.

41. Schade, H.A.
Bending theory of ship bottom structure
Soc.Nav.Arch.Mar.Eng.Transactions, Vol.46, 1938.

42. Schade, H.A.
The orthogonally stiffened plate under uniform lateral load
A.S.M.E.Transactions, Vol.62, 1940.

43. Schade, H.A.
Design curves for cross stiffened plating under uniform bending load
Soc.Nav.Arch.Mar.Eng.Transactions, Vol.49, 1941.

44. Chapman, J.C.
Doubly plated grillages under uniform lateral pressure
B.S.R.A. Report R.B.1566, 1958.

45. Chapman, J.C.
The structural behaviour of ship's double bottom (failure test)
B.S.R.A. Report N.S.11,
Naval Architecture Report No.1, 1963.

46. Schulz, H.G.
Buckling and post-buckling behaviour of transversely stiffened ship hull model
Journal of Ship Research, Sept.1964.

47. Chapman, J.C., Ho, D. and Taylor, P.F.
Transverse bending of an element of a ship's double bottom
Trans.NECIES, 1965.

48. Harrison, R.P., Richardson, W.S.
Experiments on compression of double bottom plating: Part II
B.S.R.A. Report R.B.1582, S.S.190, 1958.

49. Chapman, J.C.
Developments in ship structures
The Structural Engineer, Feb.1966.

50. Murray, J.M.
Corrugation of bottom shell plating
Trans.of the Inst.of Nav.Arch., 1954.

51. Young, A.G.
Ship-plating subjected to loads both normal to, and inplane of the plate
Quart.Trans.of the Inst.of Nav.Arch., 1957.

52. Aalami, B. and Chapman, J.C.
The structural behaviour of a ship's double-bottom
Sixth progress report
B.S.R.A., NA/311/SS, 1965.

53. Aalami, B.
The structural behaviour of a ship's double bottom
Seventh progress report
B.S.R.A., NA/345/SS, 1966.

54. Williams, D.
The structural behaviour of a ship's double bottom
Eighth progress report
B.S.R.A., NA/346/SS, 1966.

55. Ho, D.
The buckling of perforated web plates
Ph.D. Thesis, London University, 1964.

56. Beinberg, D.B. and Beinberg, E.D.
Plastiny Diski Balki-Stenki
Kiev, 1959.

APPENDIX A

Notation

This appendix is withdrawn and is incorporated in the main text in pages 9-20.

APPENDIX B

Derivation of the non-linear plate equations

The deflection surface of a plate and the distribution of the membrane forces in it can be defined by a set of two simultaneous non-linear equations together with specified boundary conditions. A short historical account of the derivation and the application of these equations is given in Chapter I.

In this Appendix, the differential equations and the boundary conditions are derived for homogeneous rectangular orthotropic plates, and then converted into a non-dimensional form ready to be expressed in terms of the finite differences for obtaining solutions. The sectional forces and displacements are grouped and given in terms of W (the midplane deflection of the plate), and F (the stress function). The transformation of the orthotropic plates into groups of plates with a wider application is dealt with in Appendix D.

The governing non-linear differential equations of the plates can be obtained by either the equilibrium and compatibility considerations of an element of plate ,

APPENDIX B

Derivation of the non-linear plate equations

The deflection surface of a plate and the distribution of the membrane forces in it can be defined by a set of two simultaneous non-linear equations together with specified boundary conditions. A short historical account of the derivation and the application of these equations is given in Chapter I.

In this Appendix, the differential equations and the boundary conditions are derived for homogeneous rectangular orthotropic plates, and then converted into a non-dimensional form ready to be expressed in terms of the finite differences for obtaining solutions. The sectional

'ms
;he
›pic
ı is
of
and
,

ERRATUM - Appendix B

In equations B23, 24, 33, 34, 35, 36 D_1 must be replaced by (D_1+4D_{xy}). The results given remain unchanged as the error occurred in preparing the simplified notation for this appendix from the correct original notes.

or the principle of virtual displacements together with the strain energy expressions of the bent plate[17],[21]. Here, the former method, being shorter in length, is employed in deriving the equations.

The assumptions involved are those normally made in the theory of plates, namely:

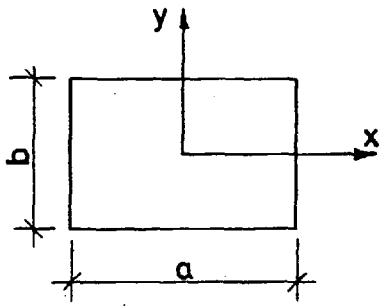
i Sections remain plane and perpendicular to the midplane of the bent and stretched plate.

ii The effect on bending of the normal direct stresses (N_z) and the normal shear forces (Q_x and Q_y) is negligible. This implies that the layers of the plate parallel to the mid-surface are in a state of plane stress, in which only N_x, N_y and N_{xy} may be non-zero.

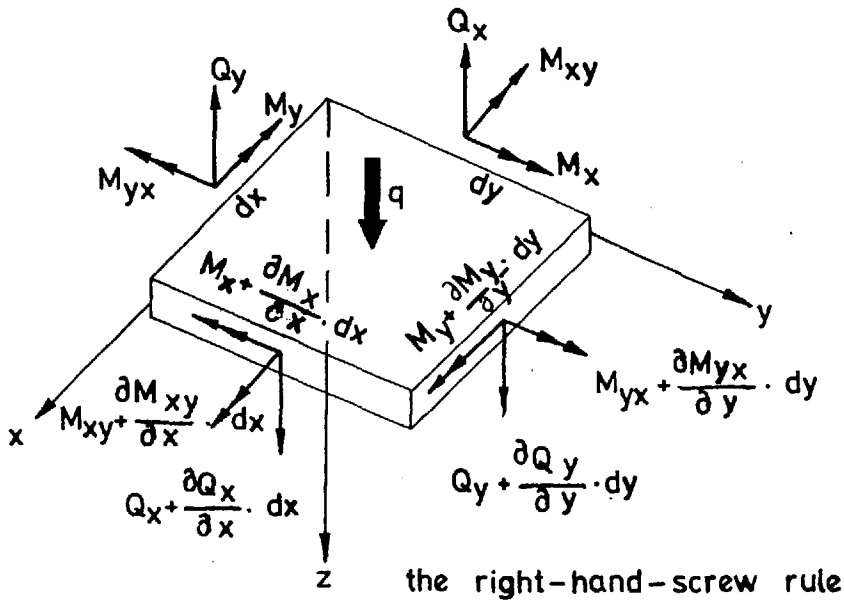
The sectional actions on an element of plate cut by two pairs of planes parallel to x-z and y-z planes of a Cartesian coordinate system are shown in the figures B-1-b and B-1-c. For clarity and convenience the sectional actions are shown separately, those due to the bending of the plate in Figure B-1-b and those due to the stretching of the midplane of the plate in Figure B-1-c.

The general equilibrium consideration of the forces on the element of plate leads to five independent equations of equilibrium as follows:

a)



b) Flexural actions.



the right-hand-screw rule is used for the direction of bending moments.

c) Membrane Forces.

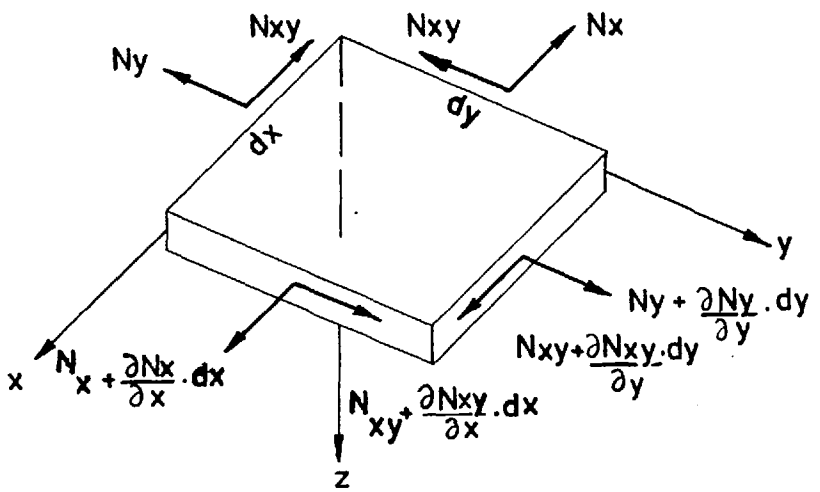


FIG. B-1. Sectional actions on an element of plate.

Taking moment of all the forces about x = dx axis

$$\frac{\partial M_x}{\partial x} \cdot dx\ dy + \frac{\partial M_{yx}}{\partial y} \cdot dx\ dy - Q_x \cdot dx\ dy = 0$$

which gives:

$$\frac{\partial M_x}{\partial x} + \frac{\partial M_{yx}}{\partial y} - Q_x = 0 \qquad \text{(B-1)}$$

similarly, taking moments about y = dy axis gives

$$-\frac{\partial M_y}{\partial y} + \frac{\partial M_{xy}}{\partial x} + Q_y = 0 \qquad \text{(B-2)}$$

From the equilibrium of the forces in x-direction

$$\frac{\partial N_x}{\partial x} \cdot dx\ dy + \frac{\partial N_{xy}}{\partial y} \cdot dx\ dy = 0$$

$$\frac{\partial N_x}{\partial x} + \frac{\partial N_{xy}}{\partial y} = 0 \qquad \text{(B-3)}$$

and in y direction

$$\frac{\partial N_y}{\partial y} + \frac{\partial N_{xy}}{\partial x} = 0 \qquad \text{(B-4)}$$

In the z-direction, the forces comprise the applied transverse pressure, the normal shear forces Q_x and Q_y and the normal components of the membrane forces.

The net components of the normal shear forces Q_x and Q_y are

$$\frac{\partial Q_x}{\partial x} \cdot dx\ dy + \frac{\partial Q_y}{\partial y} \cdot dx\ dy \qquad \text{(B-5a)}$$

The normal component of the membrane forces N_x is given by:

$$-N_x.\frac{\partial w}{\partial x}.dy + (N_x + \frac{\partial N_x}{\partial x}\,dx)(\frac{\partial w}{\partial x} + \frac{\partial^2 w}{\partial x^2}.dx)dy \ ,$$

which, when the terms higher than the second order are neglected, simplifies to

$$N_x \frac{\partial^2 w}{\partial x^2}.dx\ dy + \frac{\partial N_x}{\partial x}.\frac{\partial w}{\partial x}.dx\ dy \qquad \text{(B-5b)}$$

Similarly the normal components of the membrane forces N_y are:

$$N_y \frac{\partial^2 w}{\partial y^2}.dx\ dy + \frac{\partial N_y}{\partial y}.\frac{\partial w}{\partial y}.dx\ dy \qquad \text{(B-5c)}$$

The slopes of the two opposite faces of the element parallel to y-axis are $\frac{\partial w}{\partial y}$ and $\frac{\partial w}{\partial y} + \frac{\partial^2 y}{\partial x \partial y}.dx$, and hence the components in z-direction of N_{xy} forces, acting on these faces, are

$$-N_{xy} \frac{\partial w}{\partial y}.dy + (N_{xy} + \frac{\partial N_{xy}}{\partial x}.dx)(\frac{\partial w}{\partial y} + \frac{\partial^2 w}{\partial x \partial y}.dx)dy \ ,$$

after simplification

$$N_{xy} \frac{\partial^2 w}{\partial x \partial y}.dx\ dy + \frac{\partial N_{xy}}{\partial x}.\frac{\partial w}{\partial y}.dx\ dy \qquad \text{(B-5d)}$$

Similarly, the N_{xy} forces, on faces parallel to the x-axis, resolve in the z-direction to

$$N_{xy}\frac{\partial^2 w}{\partial x \partial y}.dx\,dy + \frac{\partial N_{xy}}{\partial y}.\frac{\partial w}{\partial x}.dx\,dy \qquad \text{(B-5e)}$$

Now, having derived all the components, the total force in z-direction must be equal to zero, i.e.

$$\left(\frac{\partial Q_x}{\partial x}.dxdy + \frac{\partial Q_y}{\partial y}.dxdy\right) + q + \left(N_x\frac{\partial^2 w}{\partial x^2}.dxdy + \frac{\partial N_x}{\partial x}.\frac{\partial w}{\partial x}.dxdy\right) +$$

$$\left(N_y\frac{\partial^2 w}{\partial y^2} + \frac{\partial N_y}{\partial y}.\frac{\partial w}{\partial y}.dxdy\right) + \left(2N_{xy}\frac{\partial^2 w}{\partial x \partial y}.dxdy + \frac{\partial N_{xy}}{\partial x}.\frac{\partial w}{\partial y}\,dxdy\right.$$

$$\left. + \frac{\partial N_{xy}}{\partial y}.\frac{\partial w}{\partial x}.dxdy\right) = 0 ,$$

after simplification

$$\left(\frac{\partial Q_x}{\partial x} + \frac{\partial Q_y}{\partial y}\right) + \left(q + N_x\frac{\partial^2 w}{\partial x^2} + 2N_{xy}\frac{\partial^2 w}{\partial x \partial y} + N_y\frac{\partial^2 w}{\partial y^2}\right) +$$

$$\left(\frac{\partial N_x}{\partial x} + \frac{\partial N_{xy}}{\partial y}\right)\frac{\partial w}{\partial x} + \left(\frac{\partial N_y}{\partial y} + \frac{\partial N_{xy}}{\partial x}\right)\frac{\partial w}{\partial y} = 0 .$$

The contents of the third and fourth brackets of the above expression, being the same as the equations (B-3) and (B-4) respectively, are equal to zero. Finally

$$\left(\frac{\partial Q_x}{\partial x} + \frac{\partial Q_y}{\partial y}\right) = -\left(q + N_x\frac{\partial^2 w}{\partial x^2} + 2N_{xy}\frac{\partial^2 w}{\partial x \partial y} + N_y\frac{\partial^2 w}{\partial y^2}\right) \qquad \text{(B-5)}$$

Substituting for the left hand side of equation (B-5) from equations (B-1) and (B-2), the equilibrium equation of the plate element is obtained

$$\frac{\partial^2 M_x}{\partial x^2} + \frac{\partial^2 M_{yx}}{\partial x \partial y} - \frac{\partial^2 M_{xy}}{\partial x \partial y} + \frac{\partial^2 M_y}{\partial y^2} = -\left(q + N_x\frac{\partial^2 w}{\partial x^2} + 2N_{xy}\frac{\partial^2 w}{\partial x \partial y} + N_y\frac{\partial^2 w}{\partial y^2}\right) \qquad \text{(B-6)}$$

The strains of the middle plane of the plate due to the applied load are

$$\left|\begin{array}{l} e_x = \frac{\partial u}{\partial x} + \frac{1}{2}\left(\frac{\partial \bar{w}}{\partial x}\right)^2 + \frac{\partial \bar{w}}{\partial x}\cdot\frac{\partial w_o}{\partial x} \\ \\ e_y = \frac{\partial v}{\partial y} + \frac{1}{2}\left(\frac{\partial \bar{w}}{\partial y}\right)^2 + \frac{\partial \bar{w}}{\partial y}\cdot\frac{\partial w_o}{\partial y} \\ \\ \gamma'_{xy} = \frac{\partial u}{\partial y} + \frac{\partial v}{\partial x} + \frac{\partial \bar{w}}{\partial x}\cdot\frac{\partial \bar{w}}{\partial y} + \frac{\partial \bar{w}}{\partial x}\cdot\frac{\partial w_o}{\partial y} + \frac{\partial w_o}{\partial x}\cdot\frac{\partial \bar{w}}{\partial y} \end{array}\right. \qquad \text{(B-7)}$$

Eliminating u and v from the above expressions gives the equation of compatibility of the stretched and bent plate as

$$\frac{\partial^2 e_x}{\partial y^2} + \frac{\partial^2 e_y}{\partial x^2} - \frac{\partial^2 \gamma'_{xy}}{\partial_x \partial_y} = \left(\frac{\partial^2 \bar{w}}{\partial x \partial y}\right)^2 - \frac{\partial^2 \bar{w}}{\partial x^2}\cdot\frac{\partial^2 \bar{w}}{\partial y^2} + 2\frac{\partial^2 \bar{w}}{\partial x \partial y}\cdot\frac{\partial^2 w_o}{\partial x \partial y} - \frac{\partial^2 \bar{w}}{\partial x^2}\cdot\frac{\partial^2 w_o}{\partial y^2} - \frac{\partial^2 w_o}{\partial x^2}\cdot\frac{\partial^2 \bar{w}}{\partial y^2} \qquad \text{(B-8a)}$$

If $\bar{w}$ (the net deflection) is substituted in terms of the total and initial deflections ($\bar{w} = w - w_o$), the equation (B-8a) reduces after simplification to

$$\frac{\partial^2 e_x}{\partial y^2} + \frac{\partial^2 e_y}{\partial x^2} - \frac{\partial^2 \gamma'_{xy}}{\partial x \partial y} = \left[\left(\frac{\partial^2 w}{\partial x \partial y}\right)^2 - \frac{\partial^2 w}{\partial x^2}\cdot\frac{\partial^2 w}{\partial y^2}\right] - \left[\left(\frac{\partial^2 w_o}{\partial x \partial y}\right)^2 - \frac{\partial^2 w_o}{\partial x^2}\cdot\frac{\partial^2 w_o}{\partial y^2}\right] \qquad \text{(B-8)}$$

The expressions derived so far are general and apply to any kind of plate subjected to the sectional actions specified. To derive the governing equations of the hcmogrneous orthotropic plates of constant thickness, their flexural and extensional rigidities are defined as follows:

the flexural rigidities

$$\left|\begin{array}{l} M_x = -\left(D_x \frac{\partial^2 \bar{w}}{\partial x^2} + D_1 \frac{\partial^2 \bar{w}}{\partial y^2}\right) \\ M_y = -\left(D_y \frac{\partial^2 \bar{w}}{\partial y^2} + D_1 \frac{\partial^2 \bar{w}}{\partial x^2}\right) \\ M_{xy} = -M_{yx} = 2D_{xy} \frac{\partial^2 \bar{w}}{\partial x \partial y} \end{array}\right. , \qquad \text{(B-9)}$$

and the extensional rigidities

$$\left|\begin{array}{l} e_x = \frac{N_x}{C_x} + \frac{N_y}{C_1} \\ e_y = \frac{N_y}{C_y} + \frac{N_x}{C_1} \\ \gamma'_{xy} = \frac{N_{xy}}{C_{xy}} \end{array}\right. . \qquad \text{(B-10)}$$

If Airy's stress function "f" is introduced at this stage and defined as

$$N_x = \frac{\partial^2 f}{\partial y^2} , \; N_y = \frac{\partial^2 f}{\partial x^2} \text{ and } N_{xy} = -\frac{\partial^2 f}{\partial x \partial y} , \qquad \text{(B-11)}$$

the expressions (B-10) become

$$\left|\begin{array}{l} e_x = \frac{1}{C_x}.\frac{\partial^2 f}{\partial y^2} + \frac{1}{C_1}\frac{\partial^2 f}{\partial x^2} \\ e_y = \frac{1}{C_y}.\frac{\partial^2 f}{\partial x^2} + \frac{1}{C_1}\frac{\partial^2 f}{\partial y^2} \\ \gamma'_{xy} = \frac{1}{C_{xy}}.\frac{\partial^2 f}{\partial x \partial y} \quad . \end{array}\right. \qquad \text{(B-12)}$$

Having defined the rigidities of the plate, the first of the non-linear equations is obtained by substitution, in the equation (B-6), for bending moments their values in terms of $\bar{w}$ from the equation (B-9), and for membrane forces their values in terms of the stress function "f" from (B-11).

$$D_x\frac{\partial^4\bar{w}}{\partial x^4} + 2(D_1 + 2D_{xy})\frac{\partial^4\bar{w}}{\partial x^2\partial y^2} + D_y\frac{\partial^4\bar{w}}{\partial y^4} =$$

$$q + \left(\frac{\partial^2 f}{\partial y^2}.\frac{\partial^2 w}{\partial x^2} - 2\frac{\partial^2 f}{\partial x\partial y}.\frac{\partial^2 w}{\partial x\partial y} + \frac{\partial^2 f}{\partial x^2}.\frac{\partial^2 w}{\partial y^2}\right) \qquad \text{(B-13a)}$$

The second governing equation is obtained when in equation (B-8) e_x, e_y and γ'_{xy} are substituted by their values in terms of "f" from the equations (B-12).

$$\frac{1}{C_x}.\frac{\partial^4 f}{\partial y^4} + \left(\frac{2}{C_1} + \frac{1}{C_{xy}}\right)\frac{\partial^4 f}{\partial x^2\partial y^2} + \frac{1}{C_y}\frac{\partial^4 f}{\partial x^4} =$$

$$\left[\left(\frac{\partial^2 w}{\partial x\partial y}\right)^2 - \frac{\partial^2 w}{\partial x^2}.\frac{\partial^2 w}{\partial y^2}\right] - \left[\left(\frac{\partial^2 w_o}{\partial x\partial y}\right)^2 - \frac{\partial^2 w_o}{\partial x^2}.\frac{\partial^2 w}{\partial y^2}\right] \qquad \text{(B-13b)}$$

Finally from (B-13a) and (B-13b) the two simultaneous non-linear equations expressed in terms of w, w_o and f are

$$D_x\frac{\partial^4 w}{\partial x^4} + 2H_b\frac{\partial^4 w}{\partial x^2\partial y^2} + D_y\frac{\partial^4 w}{\partial y^4} = \bar{q} + \left(\frac{\partial^2 f}{\partial y^2}\cdot\frac{\partial^2 w}{\partial x^2} - 2\frac{\partial^2 f}{\partial x\partial y}\cdot\frac{\partial^2 w}{\partial x\partial y} + \frac{\partial^2 f}{\partial x^2}\cdot\frac{\partial^2 w}{\partial y^2}\right) \tag{B-14}$$

$$\frac{1}{C_y}\cdot\frac{\partial^4 f}{\partial x^4} + \frac{2}{H_m}\cdot\frac{\partial^4 f}{\partial x^2\partial y^2} + \frac{1}{C_x}\frac{\partial^4 f}{\partial y^4} = \left[\left(\frac{\partial^2 w}{\partial x\partial y}\right)^2 - \frac{\partial^2 w}{\partial x^2}\cdot\frac{\partial^2 w}{\partial y^2}\right] - \left[\left(\frac{\partial^2 w_o}{\partial x\partial y}\right)^2 - \frac{\partial^2 w_o}{\partial x^2}\cdot\frac{\partial^2 w_o}{\partial y^2}\right] \tag{B-15}$$

where

$$\bar{q} = q + \left(D_x\frac{\partial^4 w_o}{\partial x^4} + 2H_b\frac{\partial^4 w_o}{\partial x^2\partial y^2} + D_y\frac{\partial^4 w_o}{\partial y^4}\right.$$

For the small deflection analysis of the transversely loaded plates equations (B-14) alone is used with terms involving the stress function "f" omitted. The governing equation of flat plates, in a state of plane stress only, is equation (B-15) in which curvature terms vanish.

Conversion of the governing equations to non-dimensional form

If the equations are non-dimensionalised, the solutions obtained will be more general and will cover all the plates which have the same non-dimensional plate parameters.

sectional
The boundary conditions, the / actions and the applied loading must also be expressed in a non-dimensional form to make a conforming system. The definition of the non-dimensional ratios chosen are given in the notation.

The plate's two governing equations become

$$\frac{\partial^4 W}{\partial X^4} + 2K_4 \cdot \rho^2 \frac{\partial^4 W}{\partial X^2 \partial Y^2} + K_5 \cdot \rho^4 \frac{\partial^4 W}{\partial Y^4} = Q + I_1 + (\rho^2 \frac{\partial^2 F}{\partial Y^2} \cdot \frac{\partial^2 W}{\partial X^2} - 2\rho^2 \frac{\partial^2 F}{\partial X \partial Y} \cdot \frac{\partial^2 W}{\partial X \partial Y} + \rho^2 \frac{\partial^2 F}{\partial X^2} \cdot \frac{\partial^2 W}{\partial Y^2}) \quad \text{(B-16)}$$

$$K_1 \frac{\partial^4 F}{\partial X^4} + 2K_2 \cdot \rho^2 \frac{\partial^4 F}{\partial X^2 \partial Y^2} + \rho^4 \frac{\partial^4 F}{\partial Y^4} = [(\rho \frac{\partial^2 W}{\partial X \partial Y})^2 - \rho^2 \frac{\partial^2 W}{\partial X^2} \cdot \frac{\partial^2 W}{\partial Y^2}] + I_2 \quad \text{(B-17)}$$

where

$$I_1 = (\frac{\partial^4 W_o}{\partial X^4} + 2K_4 \rho^2 \frac{\partial^4 W_o}{\partial X^2 \partial Y^2} + K_5 \rho^4 \frac{\partial^4 W_o}{\partial Y^4})$$

and

$$I_2 = -[(\rho \frac{\partial^2 W_o}{\partial X \partial Y})^2 - \rho^2 \frac{\partial^2 W_o}{\partial X^2} \cdot \frac{\partial^2 W_o}{\partial Y^2}]$$

The sectional forces in terms of W, W_o and F are

$$\frac{a^2}{D_x}\sqrt{\frac{C_x}{D_x}}M_x = -\left(\frac{\partial^2 W}{\partial X^2} + \frac{D_1}{D_x}\cdot\rho^2\frac{\partial^2 W}{\partial Y^2}\right) + \left(\frac{\partial^2 W_o}{\partial X^2} + \frac{D_1}{D_x}\cdot\rho^2\frac{\partial^2 W_o}{\partial Y^2}\right) \qquad \text{(B-18)}$$

$$\frac{a^2}{D_x}\sqrt{\frac{C_x}{D_x}}M_y = -K_5\left(\rho^2\frac{\partial^2 W}{\partial Y^2} + \frac{D_1}{D_y}\frac{\partial^2 W}{\partial X^2}\right) + K_5\left(\rho^2\frac{\partial^2 W_o}{\partial Y^2} + \frac{D_1}{D_y}\frac{\partial^2 W_o}{\partial X^2}\right) \qquad \text{(B-19)}$$

$$\frac{a^2}{D_x}\sqrt{\frac{C_x}{D_x}}M_{xy} = 2\frac{D_{xy}}{D_x}\cdot\rho\frac{\partial^2 W}{\partial X\partial Y} \qquad \text{(B-20)}$$

$$\frac{a^3}{D_x}\sqrt{\frac{C_x}{D_x}}Q_x = -\left(\frac{\partial^3 W}{\partial X^3} + \frac{H_b}{D_x}\cdot\rho^2\frac{\partial^3 W}{\partial X\partial Y^2}\right) + \left(\frac{\partial^3 W_o}{\partial X^3} + \frac{H_b}{D_x}\cdot\rho^2\frac{\partial^3 W_o}{\partial X\partial Y^2}\right) \qquad \text{(B-21)}$$

$$\frac{a^3}{D_x}\sqrt{\frac{C_x}{D_x}}Q_y = -K_5\left(\rho^3\frac{\partial^3 W}{\partial Y^3} + \frac{H_b}{D_y}\rho\frac{\partial^3 W}{\partial X^2\partial Y}\right) + K_5\left(\rho^3\frac{\partial^3 W_o}{\partial Y^3} + \frac{H_b}{D_y}\rho\frac{\partial^3 W_o}{\partial X^2\partial Y}\right) \qquad \text{(B-22)}$$

$$\frac{a^3}{D_x}\sqrt{\frac{C_x}{D_x}}V_x = -\left(\frac{\partial^3 W}{\partial X^3} + \frac{D_1}{D_x}\rho^2\frac{\partial^3 W}{\partial X\partial Y^2}\right) + \frac{\partial^3 W_o}{\partial X^3} + \frac{D_1}{D_x}\rho^2\frac{\partial^3 W_o}{\partial X\partial Y^2}\Big) \qquad \text{(B-23)}$$

$$\frac{a^3}{D_x}\sqrt{\frac{C_x}{D_x}}V_y = -K_5\left(\rho^3\frac{\partial^3 W}{\partial Y^3} + \frac{D_1}{D_y}\rho\frac{\partial^3 W}{\partial X^2\partial Y}\right) + K_5\left(\rho^3\frac{\partial^3 W_o}{\partial Y^3} + \frac{D_1}{D_y}\rho\frac{\partial^3 W_o}{\partial X^2\partial Y}\right) \qquad \text{(B-24)}$$

$$\frac{a^2}{D_x}N_x = \rho^2\frac{\partial^2 F}{\partial Y^2}$$

$$\frac{a^2}{D_x}N_y = \frac{\partial^2 F}{\partial X^2} \qquad \text{(B-25)}$$

$$\frac{a^2}{D_x}N_{xy} = -\frac{\partial^2 F}{\partial X\partial Y}$$

The formation of the expressions (B-23) and (B-24) are discussed later.*

The main displacement relationships in terms of W, W_o and F are

$$\left|\begin{aligned} e_x &= \frac{D_x}{a^2 C_x}\cdot\rho^2\frac{\partial^2 F}{\partial Y^2} + \frac{D_x}{a^2 C_1}\frac{\partial^2 F}{\partial X^2} \\ e_y &= \frac{D_x}{a^2 C_y}\cdot\frac{\partial^2 F}{\partial X^2} + \frac{D_x}{a^2 C_1}\cdot\rho^2\frac{\partial^2 F}{\partial Y^2} \\ \gamma'_{xy} &= -\frac{D_x}{a^2 C_{xy}}\cdot\rho\frac{\partial^2 F}{\partial X\partial Y} \end{aligned}\right. \qquad \text{(B-26)}$$

$$\frac{\partial u}{\partial x} = \frac{D_x}{a^2 C_x}\left[\rho^2\frac{\partial^2 F}{\partial Y^2} + \frac{C_x}{C_1}\frac{\partial^2 F}{\partial X^2} - \frac{1}{2}\left(\frac{\partial W}{\partial X}\right)^2 + \frac{1}{2}\left(\frac{\partial W_o}{\partial X}\right)^2\right]$$

$$\frac{\partial v}{\partial y} = \frac{D_x}{a^2 C_x}\left[\frac{C_x}{C_y}\cdot\frac{\partial^2 F}{\partial X^2} + \frac{C_x}{C_1}\cdot\rho^2\frac{\partial^2 F}{\partial Y^2} - \frac{1}{2}\left(\frac{\partial W}{\partial Y}\right)^2 + \frac{1}{2}\left(\frac{\partial W_o}{\partial Y}\right)\right] \qquad \text{(B-27)}$$

Finally the relative displacement u of two points x_1 and x_2 on a line parallel to x-axis, and v the relative displacement of y_1 and y_2 on a line parallel to y-axis are

---

*See page 127.

$$U = a\frac{C_x}{D_x}[u]_{x_1}^{x_2} = \int_{x_1}^{x_2}(\rho^2\frac{\partial^2 F}{\partial Y^2})dX + \frac{C_x}{C_1}[\frac{\partial F}{\partial X}]_{x_1}^{x_2} -$$

$$\frac{1}{2}\int_{x_1}^{x_2}(\frac{\partial W}{\partial X})^2 dX + \frac{1}{2}\int_{x_1}^{x_2}(\frac{\partial W_o}{\partial X})^2 dX$$

$$V = a\frac{C_x}{D_x}[v]_{y_1}^{y_2} = \frac{C_x}{C_y\rho}\int_{y_1}^{y_2}(\frac{\partial^2 F}{\partial X^2})dY + \frac{C_x}{C_1}[\rho\frac{\partial F}{\partial Y}]_{y_1}^{y_2} -$$

$$\frac{1}{2\rho}\int_{y_1}^{y_2}(\rho\frac{\partial W}{\partial Y})^2 dY + \frac{1}{2\rho}\int_{y_1}^{y_2}(\rho\frac{\partial W_o}{\partial Y})^2 \partial Y \qquad \text{(B-28)}$$

Boundary Conditions

The behaviour of the plate within the boundaries is described by the equations (B-16) and (B-17). The final deflection profile and the distribution of the membrane forces in the plate, however, are extensively influenced by the way in which it is supported at the boundaries.

At every point along a boundary, the plate, in general, is subjected to five external actions, each resulting in a corresponding displacement of the plate at that point. These actions and their displacements are shown in the following table.

TABLE B-1

	external action at the boundary	plate's displacement at the boundary
1	bending moment	rotation
2	normal shear	displacement perpendicular to the plane of the plate
3	twisting moment	tangential twist
4	inplane direct force	normal displacement in the plane of the plate
5	inplane shear force	tangential displacement in the plane of the plate

The first three affect the behaviour of the plate primarily in bending, and their definition at the boundary is referred to as the flexural boundary conditions. The remaining two are related to the membrane action of the plate and are specified at the boundaries as membrane or inplane boundary conditions. The above boundary conditions are independent from one another.

To obtain a complete solution of a plate problem, besides the equations (B-16) and (B-17), the supporting conditions of the plate must be fully specified. This involves the definition, from each set of the above boundary conditions, of either the action or the displacement or a relationship between the action and its corresponding displacement.

Mathematically, however, a fourth order differential equation permits the satisfaction of only two independent boundary conditions. The membrane boundary conditions, being two in number, can therefore be satisfied directly by the equation (B-17), leaving the three flexural boundary conditions to be catered for by the fourth order equation (B-16). The inability of the equation (B-16) to account for all the physically present actions at the boundaries of its domain of application, necessary to define itself in that domain, is due to the fact that, in its derivation, the effects of the normal shear forces on the deflection of the plate have been neglected; thus the order of this governing equation is reduced from sixth to fourth.

To overcome this problem, the widely used method proposed by Kirchhoff is adopted here. The normal shear force and the twisting moment at the boundary are combined

into an equivalent reaction, to which is related a sinking type displacement. Details of Kirchhoff's proposals and its physical interpretation are given in the standard text books[17][21]. The effects of this assumption on the behaviour of the plate, however, are discussed elsewhere in this thesis.

In the following each of the boundary conditions are formulated in terms of the action and its corresponding displacement. The two are assumed in the solutions obtained, to vary linearly with one another; the constant of linearity being the stiffness of the appropriate elastic restraint assumed at the boundary.

The boundary conditions are derived in the following for the edges $x = \frac{a}{2}$ and $y = b/2$ in the first quadrant of the plate. It is further assumed that, the elastic edge restraints of the opposite edges, the initial deformation and the transverse loading are about each of the centre lines of the plate either symmetrical or anti-symmetrical. For inplane loading, however, only the symmetrical case is considered.

a) Flexural boundary conditions

Bending moment and rotation. At $x = \frac{a}{2}$, from the definition of k_{rx}

$$M_x = -k_{rx} \cdot \frac{\partial \bar{w}}{\partial x} ,$$

Using relationship (B-18) and the non-dimensional form of the elastic restraint

$$\left(\frac{\partial^2 W}{\partial X^2} + \frac{D_1}{D_x} \cdot \rho^2 \frac{\partial^2 W}{\partial Y^2}\right) - K_{rx} \cdot \frac{\partial W}{\partial X} = \left(\frac{\partial^2 W_o}{\partial X^2} + \frac{D_1}{D_x} \cdot \rho^2 \frac{\partial^2 W_o}{\partial Y^2}\right) - K_{rx} \frac{\partial W_o}{\partial X} \qquad \text{(B-29)}$$

Similarly at $y = \frac{b}{2}$, the rotational boundary condition is given by

$$\left(\rho^2 \frac{\partial^2 W}{\partial Y^2} + \frac{D_1}{D_y} \frac{\partial^2 W}{\partial X^2}\right) - K_{ry} \cdot \rho \frac{\partial W}{\partial Y} = \left(\rho^2 \frac{\partial^2 W_o}{\partial Y^2} + \frac{D_1}{D_y} \cdot \frac{\partial^2 W_o}{\partial X^2}\right) -$$

$$K_{ry} \rho \frac{\partial W_o}{\partial Y} \qquad \text{(B-30)}$$

Simply supported boundary conditions are obtained if K_{rx} and K_{ry} are equated to zero. The above expressions then reduce to M_x or M_y being zero, which is the definition of the "action" at the boundary. For full fixity against rotation the coefficients of the rotational restraints are infinity. In this case the rotation "displacement" is specified at the boundary.

In some of the solutions obtained, at the boundaries, the plate is assumed to be rigidly connected to edge beams symmetrical about the mid-plane of the plate. In this arrangement, the bending moment in the plate is resisted by the torque induced in the edge beam, the variation of which (from equilibrium considerations) over an element of plate along the boundary must be equal and opposite to the bending moment of that element.

For an element of plate at $x = \frac{a}{2}$, the torque in the edge beam is equal to

$$-t_{rx}\frac{\partial^2 \bar{w}}{\partial x \partial y}$$

hence $$M_x = t_{rx}\frac{\partial^3 \bar{w}}{\partial x \partial y^2}$$

and in terms of W and W_o

$$\left(\frac{\partial^2 W}{\partial X^2} + \frac{D_1}{D_x}\rho^2\frac{\partial^2 W}{\partial Y^2}\right) + T_{rx}\rho^2\frac{\partial^3 W}{\partial X \partial Y^2} = \left(\frac{\partial^2 W_o}{\partial X^2} + \frac{D_1}{D_x}\cdot\rho^2\frac{\partial^2 W_o}{\partial Y^2}\right) + T_{rx}\rho^2\frac{\partial^3 W_o}{\partial X \partial Y^2} \qquad \text{(B-31)}$$

Similarly on $y = \frac{b}{2}$

$$K_5\left(\rho^2\frac{\partial^2 W}{\partial Y^2} + \frac{D_1}{D_y}\frac{\partial^2 W}{\partial X^2}\right) + T_{ry}\rho\frac{\partial^3 W}{\partial X^2 \partial Y} = K_5\left(\rho^2\frac{\partial^2 W_o}{\partial Y^2} + \frac{D_1}{D_y}\frac{\partial^2 W_o}{\partial X^2} + T_{ry}\rho\frac{\partial^3 W_o}{\partial X^2 \partial Y}\right) \qquad \text{(B-32)}.$$

When T_{rx} or T_{ry} equal to zero a simply supported boundary condition results, identical to the corresponding conditions in expressions (B-29) and (B-30) respectively.

When the torsion coefficients (T_{rx} or T_{ry}) of the edge beams approach infinity a clamped case solution is obtained, in which the variation of the twist of the plate along the boundary is equated to zero, as compared to the slope being zero in the previous case. The two imposed "displacement" conditions, nevertheless, yield the same results. The expression $\frac{\partial^3 W}{\partial X \partial Y^2} = 0$ along $x = \frac{a}{2}$ when integrated twice to give the slope in x-direction will have two constants of integration, which will both vanish when the geometry of the deflected plate is considered, giving $\frac{\partial W}{\partial X} = 0$ along the boundary.

Reaction and sinking of supports. At $x = \frac{a}{2}$, from the definition of k_{dx}

$$V_x = -k_{dx} w,$$

where, V_x (reaction) includes the effect of the twisting moment (at the edges) based on Kirchhoff's proposal

[illegible] of the plate at the boundary is assumed to be [illegible] load [illegible] ope [illegible] radians

In the case of a boundary resting on flexible support and where rotation could occur, the components of the external loading must be included in the expressions obtained for the normal reaction. This

involves the addition of the term $P_x \frac{\partial W}{\partial X}$ to the left hand side of equation B-33 and C20, and the addition of the term $P_y \rho \frac{\partial W}{\partial Y}$ to the left hand side of equation B-34 and C21.

After substitution and rearrangement of some of the terms

$$\left(\frac{\partial^3 W}{\partial X^3} + \frac{D_1}{D_x}\rho^2 \frac{\partial^3 W}{\partial X \partial Y^2}\right) - K_{dx} W = \left(\frac{\partial^3 W_o}{\partial X^3} + \frac{D_1}{D_x}\rho^2 \frac{\partial^3 W_o}{\partial X \partial Y^2}\right) - K_{dx} W_o \quad \text{(B-33)}$$

Similarly at $y = \frac{b}{2}$

$$\left(\rho^3 \frac{\partial^3 W}{\partial Y^3} + \frac{D_1}{D_y}\rho \frac{\partial^3 W}{\partial X^2 \partial Y}\right) - K_{dy} W = \left(\rho^3 \frac{\partial^3 W_o}{\partial Y^3} + \frac{D_1}{D_y}.\rho \frac{\partial^3 W}{\partial X^2 \partial Y}\right) - K_{dy} W_o \quad \text{(B-34)}$$

The two limiting boundary conditions are obtained when K_{dx} or K_{dy} are equated to zero or infinity; the former refers to the unsupported and the latter to the rigid support boundary condition.

If the plate is supported on edge beams, the reaction of the plate along its boundaries will act as a load on these beams.

At $x = \frac{a}{2}$, the differential equation of the edge beam is, therefore, given by

$$b_x \frac{\partial^4 \bar{w}}{\partial y^4} = - V_x$$

hence, after the necessary substitutions and rearrangement of terms

$$B_{dx} \cdot \rho^4 \frac{\partial^4 W}{\partial Y^4} - \left(\frac{\partial^3 W}{\partial X^3} + \frac{D_1}{D_x} \cdot \rho^2 \frac{\partial^3 W}{\partial X \partial Y^2} = B_{dx} \rho^4 \frac{\partial^4 W_o}{\partial Y^4} - \left(\frac{\partial^3 W_o}{\partial X^3} + \frac{D_1}{D_x} \cdot \rho^2 \frac{\partial^3 W_o}{\partial X \partial Y^2}\right) \right. \qquad \text{(B-35)}\times$$

Similarly, at $y = \frac{b}{2}$

$$B_{dy} \frac{\partial^4 W}{\partial X^4} - K_5 \left(\rho^3 \frac{\partial^3 W}{\partial Y^3} + \frac{D_1}{D_y} \rho \frac{\partial^3 W}{\partial X^2 \partial Y}\right) = B_{dy} \frac{\partial^4 W_o}{\partial X^4} - K_5 \left(\rho^3 \frac{\partial^3 W_o}{\partial Y^3} + \frac{D_1}{D_y} \rho \frac{\partial^3 W}{\partial X^2 \partial Y}\right) \qquad \text{(B-36)}\times$$

b) Membrane boundary conditions

Inplane load and extension. At every point along $x = \frac{a}{2}$, from equilibrium considerations and the definition of k_{mx}, the applied inplane force(P_x), the membrane force in the plate (N_x) and the movement of the edge (u) in x-direction are related together by the following expression.

$$p_x - N_x - k_{mx}u = 0 \qquad \text{(B-37)}$$

In this case again, the slope of the plate at the boundary is assumed to be small and its influence on the above expression is neglected. To be exact, however, N_x acts at an angle θ_x, the slope of the plate at the boundary. Its component $N_x \cos \theta_x$, being approximately equal to $N_x[1 - \frac{1}{2}(\frac{\partial w}{\partial x})^2 + \ldots]$, must be substituted for N_x in the above expression. In the solutions obtained, the maximum slope was found to be 0.1 radians, where the inclusion of $\cos \theta_x$ would have reduced the value of N_x by only $^1/200$th.

After substituting for N_x and u their values in terms of F, W and W_o from (B-25) and (B-28) the above expression becomes

$$\frac{D_x}{a^2}.\rho^2.\frac{\partial^2 F}{\partial Y^2} + k_{mx}\frac{D_x}{aC_x}\left[\int_0^{X=0.5}(\rho^2\frac{\partial^2 F}{\partial Y^2})dX + \frac{C_x}{C_1}\left.\frac{\partial F}{\partial X}\right|_{X=0.5}\right]$$

$$= p_x + k_{mx}\frac{D_x}{aC_x}\left[\frac{1}{2}\int_0^{X=0.5}(\frac{\partial W}{\partial X})^2 dX - \frac{1}{2}\int_0^{X=0.5}(\frac{\partial W_o}{\partial X})^2 dX\right]$$

In this expression $\frac{\partial F}{\partial x}$ is to be evaluated at $x = \frac{a}{2}$ only, because due to the symmetry of the problem about y-axis, its value vanishes at $x = 0$. After further simplification and substitution

$$K_{mx}\left[\int_0^{X=0.5}(\rho^2\frac{\partial^2 F}{\partial Y^2})dX + \frac{C_x}{C_1}\frac{\partial F}{\partial X}\Bigg|_{X=0.5}\right] + \rho^2\frac{\partial^2 F}{\partial Y^2} =$$

$$P_x + K_{mx}\left[\tfrac{1}{2}\int_0^{X=0.5}(\frac{\partial W}{\partial X})^2 dX - \tfrac{1}{2}\int_0^{X=0.5}(\frac{\partial W_o}{\partial X})dX\right] \qquad \text{(B-38)}$$

If, however, the external load is in the form of an applied displacement (u_a), the following relationships hold true and must be utilised instead of (B-38)

$[u]_o^{x=\frac{a}{2}} = u_a$, and in terms of F, W and W_o

$$\int_0^{X=0.5}(\rho^2\frac{\partial^2 F}{\partial Y^2})dX + \frac{C_x}{C_1}\frac{\partial F}{\partial X}\Bigg|_{X=0.5} = U_a + \tfrac{1}{2}\int_0^{X=0.5}(\frac{\partial W}{\partial X})^2 dX -$$

$$\tfrac{1}{2}\int_0^{X=0.5}(\frac{\partial W_o}{\partial X})^2 dX \qquad \text{(B-39)}$$

Similarly at $y = \frac{b}{2}$, the relationship (B-37) becomes

$$p_y - N_y - k_{my}v = 0 \qquad \text{(B-40)}$$

After substitution and simplification

$$K_{my}\left[\int_0^{Y=0.5}\left(\frac{\partial^2 F}{\partial X^2}\right)dY + \frac{C_y}{C_1}\rho\left(\rho\frac{\partial F}{\partial Y}\right)\Big|_{y=0.5}\right] + \frac{\partial^2 F}{\partial X^2} =$$

$$P_y + K_{my}\left[\frac{1}{2}\frac{C_y}{C_x}\int_0^{Y=0.5}\left(\rho\frac{\partial W}{\partial Y}\right)^2 dY - \frac{1}{2}\frac{C_y}{C_x}\int_0^{Y=0.5}\left(\rho\frac{\partial W_o}{\partial Y}\right)^2 dY\right] \qquad \text{(B-41)}$$

If the displacement v_a of the edge is given, $[v]_0^{y=\frac{b}{2}} = v_a$

$$\frac{C_x}{C_y}\cdot\frac{1}{\rho}\int_0^{Y=0.5}\left(\frac{\partial^2 F}{\partial X^2}\right)dY + \frac{C_x}{C_1}\left(\rho\frac{\partial F}{\partial Y}\right)\Big|_{y=0.5} = V_a + \frac{\rho}{2}\int_0^{Y=0.5}\left(\rho\frac{\partial W}{\partial Y}\right)^2 dY -$$

$$\frac{\rho}{2}\int_0^{Y=0.5}\left(\rho\frac{\partial W_o}{\partial Y}\right)dY \qquad \text{(B-42)}$$

A membrane boundary condition which is often encountered in practice is that referring to the boundaries of the individual plate units of panels, made up of an array of identical elements. Plate units between the stiffeners of the plated grids, forming the skin, are a good example. The loading and the arrangement of the plate units, in most cases, are such that the edges of the plate units may be assumed to remain straight while they move in a direction perpendicular to themselves under the applied loading.

The extensional boundary condition, in this case, will itself consist of two postulations. At $x = \frac{a}{2}$ there are

i) For every point along the boundary $\int_0^{x=\frac{a}{2}} \frac{\partial u}{\partial x}dx$ constant

ii) Along $x = \frac{a}{2}$, $2 \int_0^{y=\frac{b}{2}} N_x dy$ = external load .

In the first expression the magnitude of the "constant" depends, in each case, on the plate parameters and the loading, and will be determined by the solution. In the absence of external inplane loading, the second integral is equated to zero, and hence the edge will be subjected to a system of direct stresses, in self-equilibrium, necessary to keep the edge straight.

Expression (i) is essentially the same as (B-39) in terms of W, W_o and F. Expression (ii), however, is given by

$$2b\frac{D_x}{a^3}\int_0^{Y=0.5}(\rho^2\frac{\partial^2 F}{\partial Y^2})dY = \text{external load},$$

after integration

$$2\rho^2\frac{\partial F}{\partial Y}\Bigg|_{\substack{X=0.5,\\ Y=0.5}} = \frac{a^2}{D_x}.\frac{\text{external load}}{b} \qquad \text{(B-43)}$$

Inplane shear. Along $x = \frac{a}{2}$, the membrane shear stress (N_{xy}), the applied shear stress (P_{xy}) and the tangential force exerted by the elastic restraints at the boundary are related by the expression

$$N_{xy} - k_{sx}v = P_{xy} \qquad \text{(B-44)}$$

Differentiating with respect to y it gives

$$\frac{\partial N_{xy}}{\partial y} - k_{sx}\frac{\partial v}{\partial y} = \frac{\partial P_{xy}}{\partial y} .$$

Substituting for $\frac{\partial N_{xy}}{\partial y}$ and $\frac{\partial v}{\partial y}$ their values from (B-25) and (B-27), the above expression becomes

$$-\frac{D_x}{a^3}(\rho^2\frac{\partial^3 F}{\partial X \partial Y^2}) - k_{sx}\frac{D_x}{C_x a}[\frac{C_x}{C_y a}.\frac{\partial^2 F}{\partial X^2} + \frac{C_x}{C_1 a}(\rho^2\frac{\partial^2 F}{\partial Y^2})] =$$

$$\frac{\partial P_{xy}}{\partial y} + k_{sx}\frac{D_x}{C_x a}[-\frac{1}{2a}(\frac{\partial W}{\partial Y})^2 + \frac{1}{2a}(\frac{\partial W_o}{\partial Y})^2]$$

after simplification

$$-(\rho^2\frac{\partial^2 F}{\partial X \partial Y^2}) - K_{sx}[\frac{\partial^2 F}{\partial X^2} + \frac{C_y}{C_1}(\rho^2\frac{\partial^2 F}{\partial Y^2})] = \frac{a^3}{D_x}.\frac{\partial P_{xy}}{\partial y} +$$

$$K_{sx}[\frac{C_y}{C_x}.\frac{1}{2}(\frac{\partial W}{\partial Y})^2 + \frac{1}{2}\frac{C_y}{C_x}(\frac{\partial W_o}{\partial Y})^2] \qquad \text{(B-45)}$$

Similarly, at $y = \frac{b}{2}$

$$N_{yx} - k_{sy}u = p_{yx} , \qquad \text{(B-46)}$$

Differentiating with respect to x

$$\frac{\partial N_{yx}}{\partial x} - k_{sy}\frac{\partial u}{\partial x} = \frac{\partial p_{yx}}{\partial x} .$$

After the necessary substitutions and simplifications,

$$-\left(\rho\frac{\partial^3 F}{\partial X^2 \partial Y}\right) - K_{sy}\left[\left(\rho^2\frac{\partial^2 F}{\partial Y^2}\right) + \frac{C_x}{C_1}.\frac{\partial^2 F}{\partial X^2}\right] = \frac{a^3}{E_x}.\frac{\partial p_{yx}}{\partial x} +$$

$$K_{sy}\left[\tfrac{1}{2}\left(\frac{\partial W}{\partial X}\right)^2 - \tfrac{1}{2}\left(\frac{\partial W_o}{\partial X}\right)^2\right] \qquad \text{(B-47)}$$

By assigning values of zero or infinity to K_{sx} or K_{sy} the two limiting inplane shear boundary conditions are obtained. When the coefficient of shear restraint and the external inplane shear are both zero for a boundary, the edge will be free from membrane shear stresses and will be free to extend or contract along its length. The corners of the plate will, therefore, undergo movement relative to one another. When the coefficient of shear restraint is equated to infinity, it implies that, the plate is rigidly connected to a stiff structure, such that the movement of the points on each edge parallel to that edge is prevented. The corners of the plate will, therefore, remain stationary relative to one another. The edges do not necessarily remain straight due to this restraint and may distort, if the extensional boundary conditions so permit.

APPENDIX C

Finite Difference Solution

In this appendix the governing equations (B-16) and (B-17), and the boundary conditions of the plate are expressed in terms of the finite difference equations. Graded meshes are employed and the finite difference relationships derived for such meshes are given in a general form for reference. The numerical integration used for the evaluation of the inplane displacements of the plate, and the method of derivation of the finite difference relationships for the graded mesh are outlined at the end of the appendix.

To obtain numerical solutions, due to the symmetrical or the antisymmetrical loading assumed, only one quarter of the plate is considered. This portion of the plate is subdivided by mesh lines, graded where necessary, as shown on [illegible] The governing equations, together with the boundary conditions [illegible] nt for [illegible] uations [illegible]. At the independent [illegible] two

ERRATUM - Appendix C

In equations C-20 and C-21, Poisson's ratios must be replaced by $\left[2(1-\sqrt{\nu_{xb}\cdot\nu_{yb}}\,)\lambda^2+\nu_{yb}\right]$ and $\left[2(1-\sqrt{\nu_{xb}\cdot\nu_{yb}}\,)\lambda^2+\nu_{xb}\right]$ respectively. The results given in the thesis are evaluated using the correct expressions for equations C-20 and C-21.

$$\begin{bmatrix} B \end{bmatrix} \begin{bmatrix} F \end{bmatrix} = \begin{bmatrix} W'' \\ + \\ I_2 \end{bmatrix}$$

APPENDIX C

Finite Difference Solution

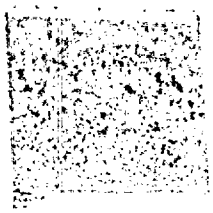
In this appendix the governing equations (B-16) and (B-17), and the boundary conditions of the plate are expressed in terms of the finite difference equations. Graded meshes are employed and the finite difference relationships derived for such meshes are given in a general form for reference. The numerical integration used for the evaluation of the inplane displacements of the plate, and the method of derivation of the finite difference relationships for the graded mesh are outlined at the end of the appendix.



To obtain numerical solutions, due to the symmetrical or the antisymmetrical loading assumed, only one quarter of the plate is considered. This portion of the plate is subdivided by mesh lines, graded where necessary, as shown on page 138. The governing equations, together with the boundary conditions are written for each node (intersection of the mesh lines). To account for the symmetrical or the antisymmetrical behaviour of the plate, the equations on the centre lines and the mesh lines next to them are duly modified. At the boundary a row of fictitious nodes are introduced, for which an extra independent equation is written for each node at the boundary.

The finite difference equations obtained are then arrayed into the two following matrix equations:

$$\begin{bmatrix} A \end{bmatrix} \begin{bmatrix} W \end{bmatrix} = \begin{bmatrix} Q \\ + \\ I_1 \end{bmatrix}$$



$$\begin{bmatrix} B \end{bmatrix} \begin{bmatrix} F \end{bmatrix} = \begin{bmatrix} W^{*} \\ + \\ I_2 \end{bmatrix}$$

where

$\begin{bmatrix} A \end{bmatrix}$ is a square matrix (O x O, O being the number of nodes). It comprises the LHS of equation (B-16) and the terms involving the function F on the RHS. It is, therefore, dependent on F.

$\begin{bmatrix} W \end{bmatrix}$ is a column matrix (O x 1) of the unknown deflection of the plate.

$\begin{bmatrix} Q \\ + \\ I_1 \end{bmatrix}$ is a column matrix (O x 1), each element being the sum of the transverse loading Q on the corresponding node and the initial deformation constant I_1 (except for nodes at the boundary).

$\begin{bmatrix} B \end{bmatrix}$ is a square matrix (O x O), representing the RHS of the equation (B-17).

$\begin{bmatrix} F \end{bmatrix}$ is the column matrix (O x 1) of the unknown stress function.

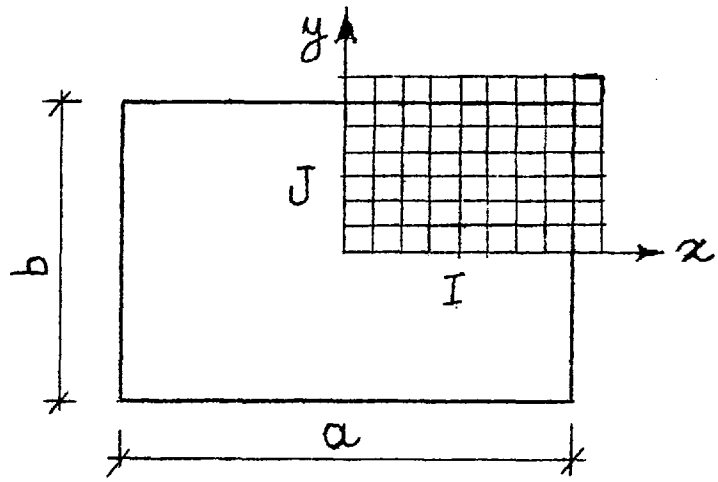
$\begin{bmatrix} W'' \\ + \\ I_2 \end{bmatrix}$ is a column matrix (O x 1). It represents the bending terms (W'') and the constants (I_2) due to the initial deformation of the plate.

The solutions of the above matrices are

$$\begin{bmatrix} W \end{bmatrix} = \begin{bmatrix} A \end{bmatrix}^{-1} \begin{bmatrix} Q \\ + \\ I_1 \end{bmatrix}$$

$$\begin{bmatrix} F \end{bmatrix} = \begin{bmatrix} B \end{bmatrix}^{-1} \begin{bmatrix} W'' \\ + \\ I_2 \end{bmatrix}$$

For every node (r) under consideration, the adjacent nodes are numbered and the mesh lengths labelled as shown on page 138. In each direction, the mesh lengths are represented by their ratio of the average mesh length in that direction. For simplicity in the expressions constants G_O - G_{11}, which depend on the mesh lengths in the vicinity of the node being examined are defined as given on page 139. The finite difference expressions are all written in terms of a length unit a_m, which in this case is assumed to be identical to the average mesh length in x-direction.



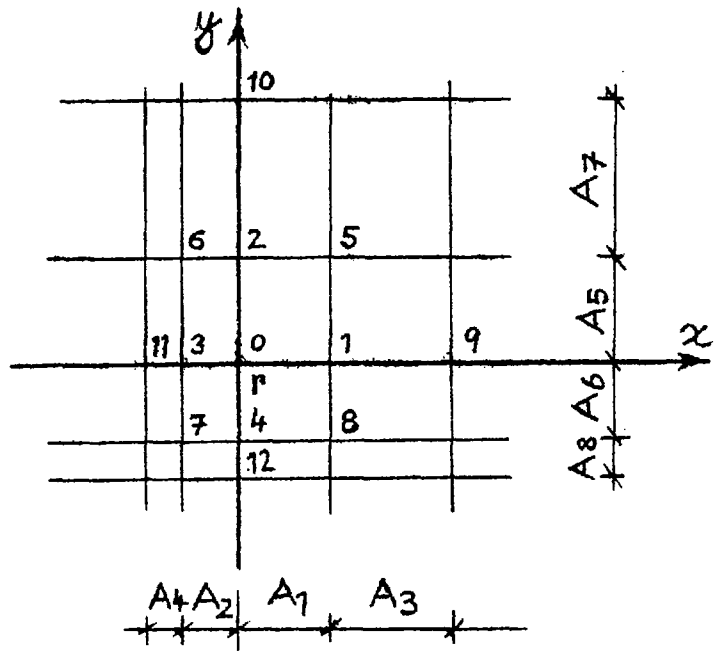
I in x-direction) Number of divisions in quarter
)
J in y-direction) of plate

O total number of nodes in quarter of plate = (I+2) (J+2)

$a_m = 1/2I$

$b_m = 1/2J$

Mean mesh lengths in x and y directions



A typical node (r) with graded mesh lines

A_1, A_2, A_3, A_4 = ratios of a_m

A_5, A_6, A_7, A_8 = ratios of b_m

Constants G_o to G_{11} are defined as follows:

$$G_o = {}^{am}/_{bm}$$

$$G_1 = \frac{2}{(A_1^2A_2 + A_1A_2^2)a_m^2}, \qquad G_9 = (A_1 + A_2)^2$$

$$G_2 = \frac{2}{(A_1^2A_3 + A_1A_3^2)a_m^2}, \qquad G_{10} = (A_5 + A_6)^2$$

$$G_3 = \frac{2}{(A_2^2A_4 + A_2A_4^2)a_m^2}, \qquad G_{11} = (A_1 + A_2)(A_5 + A_6)$$

$$G_4 = \frac{2G_o^2}{(A_5^2A_6 + A_5A_6^2)a_m^2}, \qquad G_5 = \frac{2G_o^2}{(A_7^2A_5 + A_7A_5^2)a_m^2}$$

$$G_6 = \frac{2G_o^2}{(A_6^2A_8 + A_6A_8^2)a_m^2}$$

The finite difference approximations for the derivations of a function ϕ at the node (r) are given by the following expressions:

$$\frac{\partial\phi}{\partial x} = \frac{G_1 a_m}{2}(A_2^2\phi_1 - (A_2^2 - A_1^2)\phi_o - A_1^2\phi_3) \qquad \text{(C-1)}$$

$$\frac{\partial\phi}{\partial y} = \frac{G_4 a_m}{2G_o}(A_6^2\phi_2 - (A_6^2 - A_5^2)\phi_o - A_5^2\phi_4) \qquad \text{(C-2)}$$

$$\frac{\partial^2\phi}{\partial x^2} = G_1(A_2\phi_1 - (A_1 + A_2)\phi_o + A_1\phi_3) \qquad \text{(C-3)}$$

$$\frac{\partial^2\phi}{\partial y^2} = G_4(A_6\phi_2 - (A_5 + A_6)\phi_o + A_5\phi_4) \qquad \text{(C-4)}$$

$$\frac{\partial^2 \phi}{\partial x \partial y} = \frac{G_1 G_4 a_m^2}{4 G_o} (A_2^2 A_6^2 \phi_5 + A_6^2 A_6^2 \phi_5 + A_6^2 (A_1^2 - A_2^2)\phi_2 - A_1^2 A_6^2 \phi_6$$

$$- A_1^2 (A_5^2 - A_6^2)\phi_3 + (A_1^2 - A_2^2)(A_5^2 - A_6^2)\phi_o + A_2^2 (A_5^2 - A_6^2)\phi_1$$

$$+ A_1^2 A_5^2 \phi_7 - A_5^2 (A_1^2 - A_2^2)\phi_4 - A_2^2 A_5^2 \phi_8) \qquad \text{(C-5)}$$

$$\frac{\partial^3 \phi}{\partial x^3} = \frac{G_1 a_m}{2} (G_2 A_1 A_2^2 \phi_9 - (G_2 A_2^2 (A_1 + A_3) + G_1 A_2 (A_2^2 - A_1^2))\phi_1 +$$

$$(G_2 A_2^2 A_3 - G_3 A_1^2 A_4 - G_1 (A_1 + A_2)(A_1^2 - A_2^2))\phi_o +$$

$$(G_3 A_1^2 (A_2 + A_4) + G_1 A_1 (A_1^2 - A_2^2))\phi_3 - G_3 A_1^2 A_2 \phi_{11}) \qquad \text{(C-6)}$$

$$\frac{\partial^3 \phi}{\partial y^3} = \frac{G_4 a_m}{2 G_o} (G_5 A_5 A_6^2 \phi_{10} - (G_5 A_6^2 (A_5 + A_7) + G_4 A_6 (A_6^2 - A_5^2))\phi_2 +$$

$$(G_5 A_6^2 A_7 - G_6 A_5^2 A_8 - G_4 (A_5 + A_6)(A_6^2 - A_5^2))\phi_o +$$

$$(G_6 A_5^2 (A_6 + A_8) + G_4 A_5 (A_5^2 - A_6^2))\phi_4 - G_6 A_5^2 A_6 \phi_{12}) \qquad \text{(C-7)}$$

$$\frac{\partial^3 \phi}{\partial x^2 \partial y} = \frac{G_1 G_4 a_m}{2 G_o} (-A_6^2 (A_2 + A_1)\phi_2 + A_2 A_6^2 \phi_5 + A_1 A_6^2 \phi_6 + A_2 (A_5^2 - A_6^2)\phi_1$$

$$+ (A_1 + A_2)(A_6^2 - A_5^2)\phi_o + A_1 (A_5^2 - A_6^2)\phi_3 + A_5^2 (A_1 + A_2)\phi_4$$

$$- A_2 A_5^2 \phi_8 - A_1 A_5^2 \phi_7) \qquad \text{(C-8)}$$

$$\frac{\partial^3 \phi}{\partial x \partial y^2} = \frac{G_1 G_4 a_m}{2}(A_2^2 A_6 \phi_5 + A_6(A_1^2 - A_2^2)\phi_2 - A_1^2 A_6 \phi_6$$

$$- A_2^2(A_5 + A_6)\phi_1 + (A_5 + A_6)(A_2^2 - A_1^2)\phi_o + A_1^2(A_5 + A_6)\phi_3$$

$$+ A_2^2 A_5 \phi_8 + A_5(A_1^2 - A_2^2)\phi_4 - A_1^2 A_5 \phi_7) \qquad \text{(C-9)}$$

$$\frac{\partial^4 \phi}{\partial x^4} = G_1(G_2 A_1 A_2 \phi_9 - (G_2 A_2(A_1 + A_3) + G_1 A_2(A_1 + A_2))\phi_1$$

$$+ (G_2 A_2 A_3 + G_3 A_1 A_4 + G_1(A_1 + A_2)^2)\phi_o - G_3 A_1(A_2 + A_4)\phi_3 +$$

$$G_3 A_1 A_2 \phi_{11}) \qquad \text{(C-10)}$$

one term missing

$$\frac{\partial^4 \phi}{\partial y^4} = G_4(G_5 A_5 A_6 \phi_{10} - (G_5 A_6(A_5 + A_7) + G_4 A_6(A_5 + A_6))\phi_2$$

$$+ (G_5 A_6 A_7 + G_6 A_5 A_8 + G_4(A_5 + A_6)^2)\phi_o - G_6 A_5(A_6 + A_8)\phi_4 +$$

$$G_6 A_5 A_6 \phi_{12}) \qquad \text{(C-11)}$$

one term missing

$$\frac{\partial^4 \phi}{\partial x^2 \partial y^2} = G_1 G_4(A_2 A_6 \phi_5 - A_6(A_1 + A_2)\phi_2 + A_1 A_6 \phi_6 - A_2(A_5 + A_6)\phi_1$$

$$+ (A_1 + A_2)(A_5 + A_6)\phi_o - A_1(A_5 + A_6)\phi_3 + A_2 A_5 \phi_8$$

$$- A_5(A_1 + A_2)\phi_4 + A_1 A_5 \phi_7) \qquad \text{(C-12)}$$

At the edges, to increase the accuracy, the slopes are expressed in terms of four points as follows:

$$\frac{\partial \phi}{\partial x} = \frac{k_1 \phi_1 - k_o \phi_o + k_3 \phi_3 + k_{11} \phi_{11}}{k a_m} \qquad \text{(C-13)}$$

where $k_1 = A_2^5 A_4 (A_2 + A_4)^2$

$$k_o = A_2^2 A_4 (A_1 + A_2)((A_2 + A_4)^2 (A_1^2 + A_2^2 - A_1 A_2) - A_1^2 (3A_2^2 + A_4^2 + 3A_2 A_4))$$

$$k_3 = -A_1^2 A_2^2 (A_2 + A_4)^2 (A_2^2 + A_1 A_2 + A_2 A_4)$$

$$k_{11} = A_1 A_2^5 (A_1 + A_2)$$

$$k = A_1 A_2^3 A_4 (A_1 + A_2)(A_2 + A_4)((A_2 - A_1)(A_2 + A_4) + A_1 (2A_2 + A_4))$$

Similarly,

$$\frac{\partial \phi}{\partial y} = \frac{G_O}{k a_m} (k_2 \phi_2 - k_o \phi_o + k_4 \phi_4 + k_{12} \phi_{12}) \qquad \text{(C-14)}$$

where $k_2 = A_6^5 A_8 (A_6 + A_8)^2$

$$k_o = A_6^2 A_8 (A_5 + A_6)((A_6 + A_8)^2 (A_5^2 + A_6^2 - A_5 A_6) - A_5^2 (3A_6^2 + A_8^2 + 3A_6 A_8))$$

$$k^4 = -A_5^2 A_6^2 (A_6 + A_8)^2 (A_6^2 + A_5 A_6 + A_6 A_8)$$

$$k_{12} = A_5 A_6^2 (A_5 + A_6)$$

$$k = A_5 A_6^3 A_8 (A_5 + A_6)(A_4 + A_8)((A_6 - A_5)(A_6 + A_8) + A_5 (2A_6 + A_8))$$

In all the solutions obtained, for simplification it is assumed that the row of fictitious points are as much away from the edge of the plate as the first row of internal nodes, i.e.

$$\text{at } x = \frac{a}{2} \quad A_1 = A_2, \text{ and}$$

$$\text{at } y = \frac{b}{2} \quad A_5 = A_6$$

The simplified relationships used are then:

$$\frac{\partial \phi}{\partial x} = \frac{1}{2A_1A_4(A_2 + A_4)(2A_2 + A_4)a_m} (A_4(A_2 + A_4)^2\phi_1 + 2A_2^3\phi_{11}$$

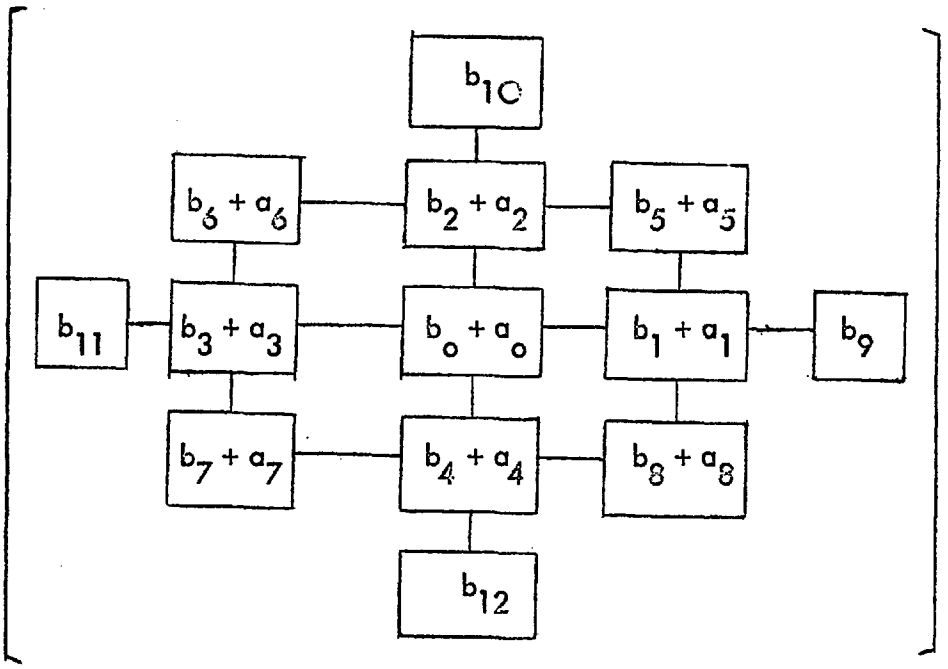
$$-(A_2+A_4)^2(2A_2 + A_4)\phi_3 + 2A_2A_4(2A_2 + A_4)\phi_o) \qquad \text{(C-15)}$$

$$\frac{\partial \phi}{\partial y} = \frac{G_o}{2A_5A_8(A_6+A_8)(2A_6+A_8)a_m} (A_8(A_6+A_8)^2\phi_2 + 2A_6A_8(2A_6+ A_8)\phi_o$$

$$- (A_6+A_8)^2(2A_6+A_8)\phi_4 + 2A_6^3\phi_{12}) \qquad \text{(C-16)}$$

Finite Difference Equations for Bending Action

For every internal node, the equation (B-16) can be written in the finite difference form (operating on W) as



$$W = Q + I_1 \qquad (C\text{-}17)$$

where, constants (b) refer to the bending action alone and remain unchanged throughout the analysis for any given plate. Constants (a) reflect the effects of the membrane action on bending, and need to be recalculated at every loading stage, and for any iteration from the latest distribution of the membrane stress in the plate.

The values of the constants (b) are:

$$b_O = G_1G_2A_2A_3 + G_1G_3A_1A_4 + G_1^2G_9 + K_5G_4(G_5A_6A_7 + G_6A_5A_8) + K_5G_4^2G_{10} + 2K_4G_1G_4G_{11}$$

$$b_1 = G_1G_2(A_2A_3 + A_1A_2) - G_1^2(A_1A_2 + A_2^2) - 2K_4G_1G_4A_2(A_5 + A_6)$$

$$b_2 = -K_5G_4G_5A_6(A_5 + A_7) - K_5G_4^2A_6(A_5 + A_6) - 2K_4G_4A_6(A_1 + A_2)$$

$$b_3 = -G_1G_3A_1(A_2 + A_4) - G_1^2A_1(A_1 + A_2) - 2K_4G_1G_4A_1(A_5 + A_6)$$

$$b_4 = -K_5G_4G_6A_5(A_6 + A_8) - K_5G_4^2A_5(A_5+A_6) - 2K_4G_1G_4A_5(A_1+A_2)$$

$$b_5 = 2K_4G_1G_4A_2A_6 \quad , \quad b_6 = 2K_4G_1G_4A_1A_6$$

$$b_7 = 2K_4G_1G_4A_1A_5 \quad , \quad b_8 = 2K_4G_1G_4A_2A_5$$

$$b_9 = G_1G_2A_1A_2 \quad , \quad b_{10} = K_5G_4G_5A_5A_6$$

$$b_{11} = G_1G_3A_1A_2 \quad , \quad b_{12} = K_5G_4G_6A_5A_6$$

If $$n_x = \frac{\partial^2 F}{\partial Y^2} = G_4(A_6F_2 - (A_5+A_6)F_O + A_5F_4)$$

$$n_y = \frac{\partial^2 F}{\partial x^2} = G_1(A_1F_3 - (A_1+A_2)F_O + A_2F_1)$$

$$n_{xy} = \frac{\partial^2 F}{\partial x \partial y} = \frac{G_1G_4a_m^2}{4G_O}(A_2^2A_6^2F_5 + A_6^2(A_1^2 - A_2^2)F_2 - A_1^2A_6^2F_6)$$

$$-A_1^2(A_5^2-A_6)F_3 + (A_1^2-A_2^2)(A_5^2-A_6^2)F_O + A_2^2(A_5^2-A_6^2)F_1$$

$$+ A_1^2A_5^2F_7 - A_5^2(A_1^2-A_2^2)F_4 - A_2^2A_5^2F_8)$$

then, the membrane constants (a) are given by:

$$a_O = -G_1(A_1+A_2)n_x - G_4(A_5 + A_6)n_y + G_{13}((A_2^2-A_1^2)(A_6^2-A_5^2))n_{xy}$$

$$a_1 = G_1A_2n_x + G_{13}A_2^2(A_5^2-A_6^2)n_{xy}$$

$$a_2 = G_4A_6n_y + G_{13}A_6^2(A_1^2 - A_2^2)n_{xy}$$

$$a_3 = G_1 A_1 n_x + G_{13} A_1^2 (A_6^2 - A_5^2) n_{xy}$$

$$a_4 = G_4 A_5 n_y + G_{13} A_5^2 (A_2^2 - A_1^2) n_{xy}$$

$$a_5 = G_{13} A_2^2 A_6^2 n_{xy} \quad , \quad a_6 = -G_{13} A_1^2 A_6^2 n_{xy}$$

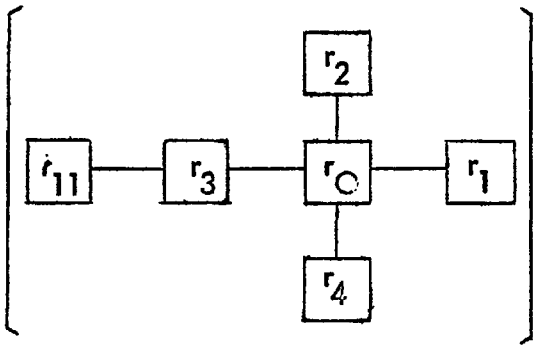
$$a_7 = G_{13} A_1^2 A_5 n_{xy} \quad , \quad a_8 = -G_{13} A_2^2 A_5^2 n_{xy}$$

where $G_{13} = \dfrac{G_1 G_4 a_m^2}{4G_o}$

I_1 which is a constant to be added to Q due to initial deformations of the plate is given by the same operator as in the LHS of equation (C-17) in which constants "a" are equated to zero and W is replaced by W_o.

Flexural Boundary conditions

At $x = \frac{a}{2}$, the rotational boundary condition is given from equation (B-29)



$$W = I_1 \qquad \text{(C-18)}$$

where $r_o = -2G_1 A_2 - \nu_{yb} G_4 (A_5 + A_6) - 2K_{rx} k_{11} A_2 A_4 (2A_2 + A_4)$

$$r_1 = G_1 A_2 - 2K_{rx} k_{11} (A_2 + A_4)^2 A_4 \quad , \quad r_2 = \nu_{yb} G_4 A_6$$

$$r_3 = G_1 A_2 + K_{rx} k_{11} (A_2 + A_4)^2 (2A_2 + A_4) \quad , \quad r_4 = \nu_{yb} G_4 A_5$$

$$r_{11} = -2K_{rx} k_{11} A_2^3$$

in which

$$k_{11} = {}^{1}/_{2}\, A_1 A_4 (A_2 + A_4)(2A_2 + A_4) a_m$$

I_1 is the constant due to initial deformation and is equal to the same array as on the left hand side of equation (C-18) operating on W_O.

Similarly at $y = {}^{b}/_{2}$, from the equation (B-30), the rotational boundary condition is:

$$\begin{bmatrix} & r_2 & \\ r_3 & r_O & r_1 \\ & r_4 & \\ & r_{12} & \end{bmatrix} \qquad W = I_1 \qquad \text{(C-19)}$$

where $r_O = -2G_4A_6 - \nu_{xb}G_1(A_1+A_2) - 2K_{ry}k_{12}A_6A_8(2A_6 + A_8)$

$$r_1 = \nu_{xb}G_1A_2 \;, \qquad r_2 = G_4A_6 - K_{ry}k_{12}A_8(A_6+A_8)^2$$

$$r_3 = \nu_{xb}G_1A_1 \;, \qquad r_4 = G_4A_6 + K_{ry}k_{12}(A_6+A_8)^2(2A_6+A_8)$$

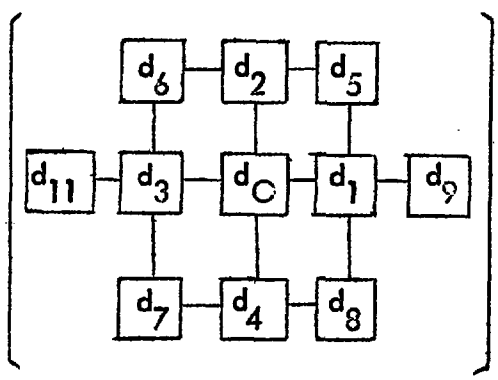
$$r_{12} = -2K_{ry}k_{12}A_6^2$$

in which

$$k_{12} = \frac{G_C}{2A_5A_8(A_6+A_8)(2A_6+A_8)a_m}$$

I_1, as in the previous case is equal to the array on the left hand side when operated on W_O.

For the reaction and the vertical displacement of the support the boundary condition at $x = a/2$, is given by the equation (B-33), and when expressed in terms of the finite differences it becomes:



$$W = \left[\text{Same as LHS}\right] W_O \qquad \text{(C-20)}$$

The values of constants (d) are:

$$d_O = 0.5a_m G_1(G_1(A_1+A_2)(A_2^2 - A_1^2) + G_2A_2^2A_3 - G_3A_1^2A_4)$$

$$+ 0.5a_m G_1\nu_{xb}G_4(A_5+A_6)(A_2^2-A_1^2) - K_{dx}$$

$$d_1 = -0.5a_m G_1(G_2A_2^2(A_2+A_3) + G_1A_2(A_1^2-A_2^2) + \nu_{xb}G_4A_2^2(A_5+A_6))$$

$$d_2 = + 0.5a_m G_1\nu_{xb}G_4A_6(A_1^2-A_2^2)$$

$$d_3 = +0.5a_m G_1(G_3A_1^2(A_2+A_4) + G_1A_1(A_1^2-A_2^2) + \nu_{xb}G_4A_1^2(A_5+A_6))$$

$$d_4 = 0.5a_m G_1\nu_{xb}G_4A_5(A_1^2-A_2^2)$$

$$d_5 = 0.5a_m G_1\nu_{xb}G_4A_2^2A_6 \quad , \quad d_8 = 0.5a_m G_1\nu_{xb}G_4A_2^2A_5$$

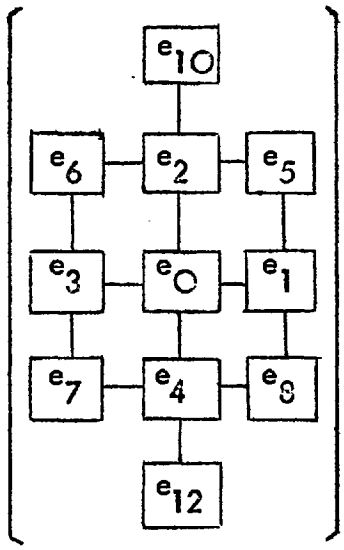
$$d_6 = -0.5a_m G_1 \nu_{xb} G_4 A_1^2 A_6 , \qquad d_9 = 0.5a_m G_1 G_2 A_1 A_2^2$$

$$d_7 = -0.5a_m G_1 \nu_{xb} G_4 A_1^2 A_5 , \qquad d_{10} = -0.5a_m G_1 G_3 A_1^2 A_2$$

The right hand side of the equation (C-20) gives the initial deformation constant I_1.

To eliminate point (9) corresponding to the second row of fictitious points, the governing equation (C-17), for the point being considered, is written and solved with the equation (C-20) for this purpose. The governing equation (C-17) and the equation (C-20) are added after the former is multiplied by $(-d_9)$ and the latter by (b_9).

Similarly at $y = b/2$, the normal shear boundary condition is given by:



$$W = \left[\text{Same as LHS}\right] W_O \qquad \text{(C-21)}$$

where

$$e_O = k_{13}(G_4(A_5+A_6)(A_6^2-A_5^2) + G_5 A_6^2 A_7 - G_6 A_5^2 A_8) +$$

$$\nu_{xb} k_{13} G_1 (A_1+A_2)(A_6^2-A_5^2) - K_{dy}$$

$$e_1 = \nu_{yb} k_{13} G_1 A_2 (A_5^2 - A_6^2)$$

$$e_2 = -k_{13}(G_5 A_6^2 (A_5 + A_6) - G_4 A_6 (A_5^2 - A_6^2) + \nu_{by} G_1 A_6^2 (A_1 + A_2))$$

$$e_3 = \nu_{yb} k_{13} G_1 A_1 (A_5^2 - A_6^2)$$

$$e_4 = k_{13}(G_6 A_5^2 (A_6 + A_8) + G_4 A_5 (A_5^2 - A_6^2) + \nu_{by} G_1 A_5^2 (A_1 + A_2))$$

$$e_5 = k_{13} \nu_{yb} G_1 A_2 A_6^2, \qquad e_8 = -k_{13} \nu_{yb} G_1 A_2 A_5^2$$

$$e_6 = k_{13} \nu_{yb} G_1 A_1 A_6^2, \qquad e_{10} = k_{13} G_5 A_5 A_6^2$$

$$e_7 = -k_{13} \nu_{yb} G_1 A_1 A_5^2, \qquad e_{12} = -k_{13} G_6 A_5^2 A_6$$

As in the previous case, G_o which refers to the second row of fictitious points parallel to $y = b/2$, is first eliminated by making use of the governing equation written for the point being considered.

Finite Difference Equations for Membrane Action

For all the internal points, the governing equation of the membrane action (B-17) is given by:

$$\begin{bmatrix} & & m_{10} & & \\ & m_6 & m_2 & m_5 & \\ m_{11} & m_3 & m_o & m_1 & m_9 \\ & m_7 & m_4 & m_8 & \\ & & m_{12} & & \end{bmatrix}$$

$$F = k_{21} + l_2 \qquad \text{(C-22)}$$

where m_O to m_{12} are constants independent of the loading and the state of stress in the plate. k_{21} represents the effect of bending of the plate on the membrane action, and l_2 is the constant due to initial deformation.

$$m_O = K_1G_1G_2A_2A_3 + K_1G_1^2G_9 + G_4(G_5A_6A_7 + G_6A_5A_8 + G_4G_{10}) + 2K_2G_1G_4G_{11} + K_1G_1G_3A_1A_4$$

$$m_1 = -K_1G_1G_2A_2(A_1+A_3) - K_1G_1^2A_2(A_1+A_2) - 2K_2G_1G_4A_2(A_5+A_6)$$

$$m_2 = -G_4G_5A_6(A_6+A_7) - G_4^2A_6(A_5+A_6) - 2K_2G_1G_4A_6(A_1+A_2)$$

$$m_3 = -K_1G_1G_3A_1(A_2+A_4) - K_1G_1^2A_1(A_1+A_2) - 2K_2G_1G_4A_1(A_5+A_6)$$

$$m_4 = -G_4G_6A_5(A_6+A_8) - G_4^2A_5(A_5+A_6) - 2K_2G_1G_4A_5(A_1+A_2)$$

$$m_5 = 2K_2G_1G_4A_2A_6, \qquad m_9 = K_1G_1G_2A_1A_2$$

$$m_6 = 2K_2G_1G_4A_1A_6, \qquad m_{10} = G_4G_5A_5A_6$$

$$m_7 = 2K_2G_1G_4A_1A_5, \qquad m_{11} = K_1G_1G_3A_1A_2$$

$$m_8 = 2K_2G_1G_4A_2A_5, \qquad m_{12} = G_4G_6A_5A_6$$

$$k_{2O} = \Big(\frac{G_1G_4a_m^2}{4G_O}(A_2^2A_6^2W_5 + A_6^2(A_1^2-A_2^2)W_2 - A_1^2A_6^2W_6 - A_1^2(A_5^2-A_6^2)W_3 + (A_1^2-A_2^2)(A_5^2-A_6^2)W_O + A_2^2(A_5^2-A_6^2)W_1 + A_1^2A_5^2W_7 - A_5^2(A_1^2-A_2^2)W_4 - A_2^2A_5^2W_8)\Big)^2$$

$$-G_1G_4(A_1W_3-(A_1+A_2)W_O + A_2W_1)(A_6W_2 - (A_5+A_6)W_O + A_5W_4)$$

I_2 is given by the same expression as k_{21}, in which W is replaced by W_O.

Extensional Boundary Conditions

At $x = \frac{a}{2}$, the equation (B-38) can be written as:

$$G_4A_6F_2 - K_{mx}\nu_{xm}k_{13}A_4(A_2 + A_4)^2F_1 - (2K_{mx}\nu_{xm}k_{13}A_2A_4(2A_2 + A_4)$$

$$+ G_4(A_5+A_6)\ F_O + G_4A_5F_4 + K_{mx}\nu_{xm}k_{13}(A_2 + A_4)^2(2A_2 + A_4)F_3$$

$$- 2K_{mx}\nu_{xm}k_{13}A_2^3F_{11} +$$

$$K_{mx}\sum_{r=O}^{r=n} B_r G_4(A_6F_2 - (A_5+A_6)F_O + A_5F_4) =$$

$$P_x + \frac{K_{mx}}{2}\sum_{r=O}^{r=n} B_r \frac{G_1^2a_m^2}{4}(A_2^2W_1 - (A_2^2-A_1^2)W_O - A_1^2)W_O - A_1^2W_3)^2 - I_2$$

(C-23)

where $k_{13} = \frac{1}{2A_1A_4(A_2+A_4)(2A_2+A_4)a_m}$, and

$\frac{C_x}{C_1}$ is substituted by its value $-\nu_{xm}$.

The first term on the LHS refers to the node at the boundary. Symbol ($\sum$) indicates the summation of the succeeding term, evaluated for nodes on the line (y = constant) from the centre line to the edge*. I_2 is the constant due to the initial deformation of the plate and equals the second term on the RHS when W is replaced by W_O (initial deformation). When the extension U of

*See page 159.

the plate is specified, in the above expression $K_{mx} = 1$, the terms without K_{mx} vanish and P_x is to be replaced by U.

Similarly at $y = b/2$, the equation (B-41) becomes:

$$-K_{my}\nu_{ym}k_{18}A_8(A_6+A_8)^2F_2 + G_1A_2F_1 - (2K_{my}\nu_{ym}k_{18}A_6A_8(2A_6+A_8) +$$

$$G_1(A_1+A_2))F_O + G_1A_1F_3 + K_{my}\nu_{ym}(A_6+A_8)^2(2A_6+A_8)F_4 - 2K_{my}\nu_{ym}A_6^3F_{12}$$

$$+ K_{my}\sum_{r=O}^{r=n} B_rG_1(A_2F_1 - (A_1+A_2)F_O + A_1F_3) =$$

$$P_Y + \frac{K_{my}}{2}\cdot\frac{C_y}{C_x}\sum_{r=O}^{r=n}\frac{B_rG_4^2a_m^2}{4G_O^2}(A_6^2W_2 - (A_6^2 - A_5^2)W_O - A_5^2W_4)^2 - I_2 \qquad (C\text{-}24)$$

where $k_{18} = \dfrac{G_O}{2A_5A_8(A_6+A_8)(2A_6+A_8)a_m}$

The significance of the terms in the above expression is the same as those in expression (C-23), but related to y-axis.

Inplane Shear Boundary Condition

The equations (B-45) and (B-47) for the inplane shears can be expressed as:

at $x = a/2$:

$$-k_{19}A_2^2A_6F_5+\left[K_{sx}\nu_{ym}G_4A_6-k_{19}A_6(A_1^2-A_2^2)\right]F_2+k_{19}A_1^2A_6F_6$$

$$-\left[K_{sx}G_1A_2+k_{19}A_2^2(A_5+A_6)\right]F_1+\left[K_{sx}G_1(A_1+A_2)+K_{sx}\nu_{ym}G_4(A_5+A_6)\right.$$

$$\left.-k_{19}(A_5+A_6)(A_2^2-A_1^2)\right]F_0-\left[K_{sx}G_1A_1+k_{19}A_1^2(A_5+A_6)\right]F_3$$

$$-k_{19}A_2^2A_5F_8-\left[k_{19}A_5(A_1^2-A_2^2)-K_{sx}\nu_{ym}G_4A_5\right]F_4+k_{19}A_1^2A_5F_7$$

$$=\frac{a^3\partial P_{xy}}{D_x\partial y}-\frac{K_{sx}}{8}\frac{C_y}{C_x}\cdot\frac{G_4^2a_m^2}{G_0^2}\left[A_6^2W_2-(A_6^2-A_5^2)W_0-A_5^2W_4\right]^2-I_2 \qquad \text{.. (C-25)}$$

where $k_{19}=\frac{G_1G_4a_m}{2}$,

I_2 is the same as the second term of the RHS when W is replaced by (W_0) the initial deformation,

and at $y = {}^{b}/2$

$$-k_{20}A_2A_6^2F_5+\left[k_{20}A_6^2(A_1+A_2)-k_{sy}G_4A_6\right]F_2-k_{20}A_1A_6^2F_6$$

$$-\left[k_{20}A_2(A_5^2-A_6^2)-K_{sy}\nu_{xm}G_1A_2\right]F_1-\left[k_{20}(A_1+A_2)(A_6^2-A_5^2)-\right.$$

$$\left.-K_{sy}G_4(A_5+A_6)+K_{sy\ xm}G_1(A_1+A_2)\right]F_0-\left[k_{20}A_1(A_5^2-A_6^2)-K_{sy\ xm}G_1A_1\right]$$

$$F_3+k_{20}A_2A_5^2F_8-\left[k_{20}A_5^2(A_1+A_2)+K_{sy}G_4A_6\right]F_4+k_{20}A_1A_5^2F_7=$$

$$\frac{a^3\partial P_{yx}}{D_x\partial x}+\frac{K_{sy}\cdot G_1^2a_m^2}{8}\left[A_2^2W_1-(A_2^2-A_1^2)W_0-A_1^2W_3\right]^2-I_2$$

.. (C-26)

where $G_{20}=\dfrac{G_1G_4a_m}{2G_0}$

I_2 is the constant due to the initial deformation being the same as its preceding term if W is replaced by W_0 (initial deformation.

Special Nodes

If the function to be expressed in the finite difference form is symmetrical about the centre lines of the plate, nodes falling outside the quarter of plate treated are eliminated by assuming that they have the same value and sign as their symmetrical counterparts within the quarter of plate. When the function is antisymmetrical, the values of the nodes to be eliminated are the same but of opposite sign to the corresponding interior points. It must be noted that, for plates with antisymmetrical bending about the centre line, the distribution of the direct membrane stresses remains symmetrical and the modification must not be duplicated for the stress function equations.

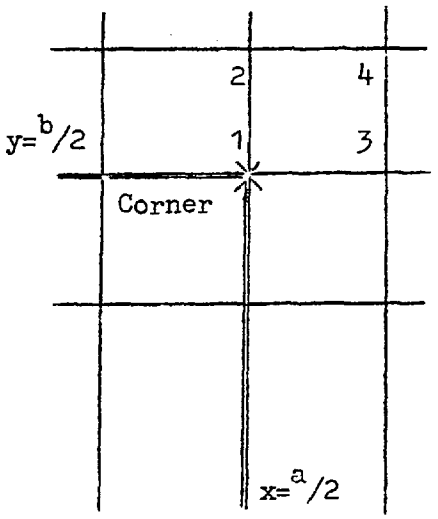
At the corner of plate, on the account that it lies both on $x = {}^{a}/2$ and $y = {}^{b}/2$, four equations can be written. But in order to obtain as solution the deflection of the plate relative to the corners, the equations formulated at this point are:

(a) In bending, at point 1

i) $W_1 = 0$

ii, iii) two rotational boundary conditions, one for each direction

iv) point 4 does not appear in any of the equations, and can be eliminated. It is, however, given an arbitrary value and formulated with the rest of the equations to simplify certain matrix operations (see solution by the digital computer).



(b) Similarly for the membrane action, at point 1

i) $F_1 = 0$

ii, iii) two equations for the extensional boundary conditions of the two sides

iv) point 4 is treated the same as in the previous case.

Numerical Integration

If the value of a function $\emptyset$ is given from the centre line of the plate to the side at n unequal intervals*, the integral of the function taken between the centreline and the side, in x-direction, can be expressed in the form of:

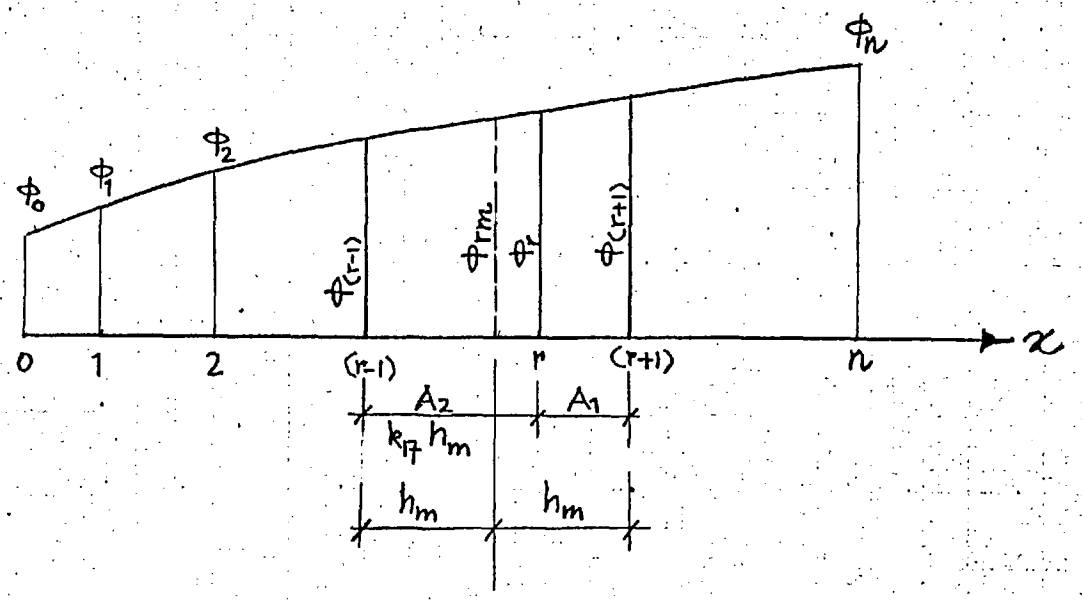
$$\int_{x=0}^{x=x_n} \emptyset_r dx = \sum_{r=0,1,2..n} B_r \emptyset_r \qquad .. (C-27)$$

where B_r is a constant to be evaluated for each point. The value of B_r, being independent of the function itself, is determined from the number and grading of the intervals. For any subdivision of the plate, the constants need be calculated once only and used when required.

The range of integration is considered as $\frac{n}{2}$ successive pairs of intervals (n to be even), each pair being treated individually.

The value of the function at the midpoint of the intervals being considered ($\emptyset_{rm}$) can be expressed, from a parabolic interpolation, in terms of the given ordinates*. The area underneath the function is from Simpson's integration formula, between the points (r-1) and (r+1), given by:

* See page 159



Function given at unequal intervals between x_0 and x_n

ϕ_{rm} = value of function at mid point of the pair of intervals being considered A_1, A_2, I as defined on page

$$h_m = \frac{A_1+A_2}{4I} \qquad \text{.. (C-28)}$$

$$k_{17} = \frac{A_2}{2Ih_m}$$

ϕ_{rm} is interpolated parabolically from $\phi_{(r-1)}$, ϕ_r and $\phi_{(r+1)}$

$$\phi_{rm} = k_{14}\phi_{(r-1)}+k_{15}\phi_r+k_{16}\phi_{(r+1)} \qquad \text{.. (C-29)}$$

where $$k_{14} = \frac{1-1.5\,k_{17}+0.5\,k_{17}^2}{4-2\,k_{17}}$$

$$k_{15} = \frac{1}{2k_{17}-k_{17}^2}$$

$$k_{16} = \frac{1-k_{17}}{4-2k_{17}}$$

$$\int_{x(r-1)}^{x(r+1)} \phi dx = B_{(r-1)}\phi_{(r-1)} + B_r\phi_r + B_{(r+1)}\phi_{(r+1)}$$

where $B_{(r-1)} = \frac{h_m}{3}(4k_{14}+1)$

$$B_r = \frac{h_m}{12} k_{15}$$

$$B_{(r+1)} = \frac{h_m}{3}(4k_{16}+1)$$

The values of h_m, k_{14}, k_{15} and k_{16} vary from point to point and have to be newly calculated for every pair. If the summation is then taken over the whole length, the coefficients become:

$$B_0 = \frac{h_m}{3}(4k_{14}+1)$$

$$B_{1,3,\ldots\ B_{(n-1)}} = \frac{h_m k_{15}}{12}$$

$$B_{2,4,\ldots\ B_{(n-2)}} = \frac{h_m}{3}(4k_{14}+1) + \frac{h_m}{3}(4k_{16}+1)$$

where the first term refers to the preceding and the second to the succeeding interval.

$$B_n = \frac{h_m}{3}(4k_{16}+1) \qquad \ldots (C\text{-}30)$$

Derivation of the Finite Difference Approximations

The value of the function ϕ, in the vicinity of node r* can be expressed from Taylor's expansion as:

$$\phi_1 = \phi_0 + A_1 a_m \left(\frac{\partial \phi}{\partial x}\right)_0 + \frac{A_1^2 a_m^2}{2!}\left(\frac{\partial^2 \phi}{\partial x^2}\right)_0 + \frac{A_1^3 a_m^3}{3!}\left(\frac{\partial^3 \phi}{\partial x^3}\right)_0 + \frac{A_1^4 a_m^4}{4!}\left(\frac{\partial^4 \phi}{\partial x^4}\right)_0 + \cdots \quad .. \text{(C-31)}$$

$$\phi_3 = \phi_0 - A_2 a_m \left(\frac{\partial \phi}{\partial x}\right)_0 + \frac{A_2^2 a_m^2}{2!}\left(\frac{\partial^2 \phi}{\partial x^2}\right)_0 - \frac{A_2^3 a_m^3}{3!}\left(\frac{\partial^3 \phi}{\partial x^3}\right)_0 + \frac{A_2^4 a_m^4}{4!}\left(\frac{\partial^4 \phi}{\partial x^4}\right)_0 - \cdots \quad .. \text{(C-32)}$$

After multiplying equation (C-31) by A_2^2 and equation (C-32) by A_1^2, adding and simplifying, if derivatives of the third and higher orders are neglected, it gives:

$$\left(\frac{\partial \phi}{\partial x}\right)_0 = \frac{A_2^2\phi_1 - (A_2^2 - A_1^2)\phi_0 - A_1^2\phi_3}{(A_1 A_2^2 + A_1^2 A_2)a_m}$$

For the second derivative, equation (C-31) is multiplied by A_2, equation (C-32) multiplied by A_1, the products are added and simplified to:

$$\left(\frac{\partial^2 \phi}{\partial x^2}\right)_0 = \frac{A_2\phi_1 - (A_1 + A_2)\phi_0 + A_1\phi_3}{(A_1^2 A_2 + A_1 A_2^2)a_m^2/2}$$

* See page 138

Higher derivatives are then derived from the above relationships when they are operated from one another.

The more accurate expressions for the first derivatives in terms of four points can be obtained by writing an extra expansion for the fourth point.

$$\phi_{11} = \phi_0 - (A_2+A_4)a_m\left(\frac{\partial\phi}{\partial x}\right)_0 + \frac{(A_2+A_4)^2 a_m^2}{2!}\left(\frac{\partial^2\phi}{\partial x^2}\right)_0 - \frac{(A_2+A_4)^3 a_m^3}{3!}\left(\frac{\partial^3\phi}{\partial x^3}\right)_0 + \cdots \quad .. \text{(C-33)}$$

The fourth order and higher derivatives are neglected. The three expressions (C-31), (C-32) and (C-33) are treated as a set of three simultaneous equations and solved for $\left(\frac{\partial\phi}{\partial x}\right)_0$, the value of which is given as expression (C-13).

The same procedure can be repeated for the derivatives in y-direction.

Cross derivatives are obtained when the operators in one direction apply to the derivatives in the perpendicular direction.

APPENDIX D

Transformation of the orthotropic plates

If the cartesian coordinates x' and y' are defined as $x' = x/a$ and $y' = y/\lambda a$, making use of the definition of the non-dimensionalised constants α, β, γ, ρ' and λ given in the notation, the governing equations (B-14) and (B-15) can then be transformed into the new coordinate system. They become

(D-1)

$$\frac{\partial^4 w'}{\partial x'^4} + 2\alpha \frac{\partial^4 w'}{\partial x'^2 \partial y'^2} + \frac{\partial^4 w'}{\partial y'^4} = \bar{q}' + \left(\frac{\partial^2 f'}{\partial y'^2}\cdot\frac{\partial^2 w'}{\partial x'^2} - 2\frac{\partial^2 f'}{\partial x' \partial y'}\cdot\frac{\partial^2 w'}{\partial x' \partial y'} + \frac{\partial^2 f'}{\partial x'^2}\cdot\frac{\partial^2 w'}{\partial y'^2}\right)$$

$$\frac{1}{\gamma^4}\frac{\partial^4 f'}{\partial x'^4} + \frac{2\beta}{\gamma^2}\frac{\partial^4 f'}{\partial x'^2 \partial y'^2} + \frac{\partial^4 f'}{\partial y'^4} = \left(\frac{\partial^2 w'}{\partial x' \partial y'}\right)^2 - \frac{\partial^2 w'}{\partial x'^2}\cdot\frac{\partial^2 w'}{\partial y'^2} - \left(\frac{\partial^2 w'_o}{\partial x' \partial y'}\right)^2 - \frac{\partial^2 w'_o}{\partial x'^2}\cdot\frac{\partial^2 w'_o}{\partial y'^2}$$

(D-2)

where $w' = w\sqrt{\frac{C_x}{D_x}}$, $w'_o = w_o\sqrt{\frac{C_x}{D_x}}$

$$f' = f/D_x\lambda^2$$

$$\bar{q}' = q' + \left(\frac{\partial^4 w'_o}{\partial x'^4} + 2\alpha \frac{\partial^4 w'_o}{\partial x'^2 \partial y'^2} + \frac{\partial^4 w'_o}{\partial y'^4}\right)$$

$$q' = \frac{a^4}{D_x} \cdot \sqrt{\frac{C_x}{D_x}}\, q$$

The boundary conditions as given in Appendix B can be readily transformed into the new system from their final form.

In the transformed boundary conditions for the membrane action, the Poisson's ratios appear in the form of $\sqrt{\mu_{xm}\mu_{ym}}$, as compared to μ_{xm} and μ_{ym} in the expressions derived in appendix B.

If at this stage the governing equations of the transformed plate (D-1) and (D-2) are manipulated in the same way as equations (B-14) and (B-15) in Appendix B, two new equations corresponding to (B-16) and (B-17) result. These equations are

$$\frac{\partial^4 W'}{\partial X'^4} + 2K'_4 \cdot \rho'^2 \frac{\partial^4 W'}{\partial X'^2 \partial Y'^2} + K'_5 \cdot \rho'^4 \frac{\partial^4 W'}{\partial Y'^4} = Q' + I'_1 + \left(\rho'^2 \frac{\partial^2 F'}{\partial Y'^2} \cdot \frac{\partial^2 W'}{\partial X'^2} - 2\rho'^2 \frac{\partial^2 F'}{\partial X' \partial Y'} \cdot \frac{\partial^2 W'}{\partial X' \partial Y'} + \rho'^2 \frac{\partial^2 F'}{\partial X'^2} \cdot \frac{\partial^2 W'}{\partial Y'^2}\right) \qquad (D\text{-}3)$$

$$K'_1 \frac{\partial^4 F'}{\partial X'^4} + 2K_2 \rho'^2 \frac{\partial^4 F'}{\partial X'^2 \partial Y'^2} + \rho'^4 \frac{\partial^4 F'}{\partial Y'^4} = \left(\rho' \frac{\partial^2 W'}{\partial X' \partial Y'}\right)^2 - \rho'^2 \frac{\partial^2 W'}{\partial X'^2} \cdot \frac{\partial^2 W'}{\partial Y'^2} + I'_2 \qquad (D\text{-}4)$$

where

$$I_1' = \left(\frac{\partial^4 W'_o}{\partial X'^4} + 2K_4'\rho'^2 \frac{\partial^4 W'_o}{\partial X'^2 \partial Y'^2} + K_5'\rho'^4 \frac{\partial^4 W'_o}{\partial Y'^4}\right) \quad \text{and}$$

$$I_2' = - \left(\rho' \frac{\partial^2 Wo'}{\partial X' \partial Y'}\right)^2 + \rho'^2 \frac{\partial^2 Wo'}{\partial X'^2} \cdot \frac{\partial^2 Wo'}{\partial Y'^2}$$

The solutions of the equations (D-3) and (D-4) give results which refer to the transformed plate and have to be reconverted to the values corresponding to the actual plate.

In the following table a summary of the relationships between the quantities in the actual plate, the non-dimensionalised plate according to appendix B, and the transformed plate are given.

TABLE D-1

Actual Plate	Transformed plate	Actual Plate	Transformed plate
Initial governing equations		Treated governing equations	
(B-14) (B-15)	(D-1) (D-2)	(B-16) (B-17)	(D-3) (D-4)
x	$x' = x/a$	$X = x/a$	$X' = \frac{x'}{a'} = \frac{x}{a}$
y	$y' = y/\lambda a$	$Y = y/b$	$Y' = \frac{y'}{b'} = \frac{y}{b}$
w	$w' = w\sqrt{C_x/D_x}$	$W = w\sqrt{C_x/D_x}$	$W' = w'\sqrt{\frac{C_x'}{D_x'}} = w\sqrt{\frac{C_x}{D_x}}$
q	$q' = \frac{a^4}{D_x}\sqrt{\frac{C_x}{D_x}}q$	$Q = \frac{a^4}{D_x}\sqrt{\frac{C_x}{D_x}}q$	$Q' = \frac{a'^4}{D_x'}\sqrt{\frac{C_x'}{D_x'}}q' = Q$
f	$f' = f/D_x\lambda^2$	$F = f/D_x$	$F' = f'/D_x' = f/D_x\lambda^2$
a	$a' = 1$	$K_1 = C_x/C_y$	$K_1' = \frac{C_x'}{C_y'} = 1/\gamma^4$
b	$b' = b/a\lambda$	$K_2 = C_x/H_m$	$K_2' = \frac{C_x'}{H_m'} = \beta/\gamma^2$
$\rho = a/b$	$\rho' = a'/b' = \frac{a\lambda}{b}$	$K_4 = H_b/D_x$	$K_4' = \frac{H_b'}{D_x'} = \alpha$
D_x	$D_x' = 1$	$K_5 = \frac{D_y}{D_x}$	$K_5' = \frac{D_y'}{D_x'} = 1$

Contd.over

TABLE D-1 (continued)

D_y	$D_y' = 1$
H_b	$H_b' = \alpha$
C_x	$C_x' = 1$
C_y	$C_y' = \gamma^4$
H_m	$H_m' = \frac{\gamma^2}{\beta}$

APPENDIX E

COMPARISON OF RESULTS AND ACCURACY CHECKS

This appendix deals with a comparison between the theoretical results obtained and the available solutions. Examples of equilibrium checks on the membrane forces, and examples for the examination of the validity of the solutions are given.

The results are examined under the following headings

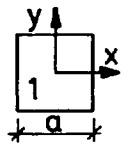
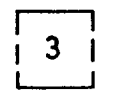
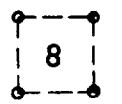
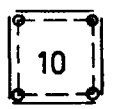
1) Small deflection solutions of transversely loaded rectangular orthotropic plates.
2) Plane stress solutions.
3) Non-linear solutions of transversely loaded plates.
4) Non-linear solutions of plates under combined loading.
5) Non-linear solutions of initially deformed plates subjected to end-thrust.
6) Critical buckling load of plates.
7) An example of equilibrium and displacement checks for a non-linear solution.

1) Small deflection solutions of transversely loaded orthotropic plates

i) Limiting flexural boundary conditions. Solutions obtained for several standard cases of plates under uniform transverse loading are given in table E-1. Available solutions are included for comparison. The cases listed in this table incorporate all the four limiting flexural boundary conditions considered. For the same uniform mesh used, the results of the plates with supported edges are more accurate.

TABLE E-1 Square isotropic plates under U.D.L.

mesh : 16 x 16, uniform

Plate	ν_{xb} = ν_{yb}	W_1 $=k_1\frac{a^4}{D_x}q\times10^{-3}$ k_1	W_2 $=k_2\frac{a^4}{D_x}q\times10^{-3}$ k_2	M_{x1} $=k_3a^2q\times10^{-2}$ k_3	M_{x2} $=k_4a^2q\times10^{-2}$ k_4	M_{y1} $=k_5a^2q\times10^{-2}$ k_5	M_{y2} $=k_6a^2q\times10^{-2}$ k_6
	0.3	4.06	0	4.77	0	4.77	0
		(4.06)*	(0)	(4.79)	(0)	(4.79)	0
	0.3	13.135	15.05	2.70	0	12.25	13.10
	0	13.06	13.06	0	0	12.50	12.50
	0.3	(13.09)	-	(2.71)	(0)	(12.25)	-
	0	(13.02)	(13.02)	(0)	(0)	(12.50)	(12.50)
	0.3	1.26	0	2.26	-5.13	2.26	-1.54
		(1.26)	(0)	(2.31)	(-5.13)	(2.31)	(-1.54)
	0.3	2.55	1.78	11.17	0	11.17	15.03
		(2.49)	-	(10.90)	(0)	(10.90)	(14.04)
	0.3	5.93	4.46	3.59	-1.29	3.59	4.81
		[5.80]⊗	[4.37]	[3.59]	[-1.29]	[3.59]	[5.12]

* ( ) from ref. 21 Timoshenko

⊗ [ ] from ref. 56 Beinberg

ii) Orthotropic properties of plates. To check whether the stiffness coefficients relating to the orthotropic properties of plates were correctly expressed in the finite difference expressions, the series solution given on page 372 of ref.(21) was programmed. Solutions given by the two approaches are compared for the case of the double bottom in Table E-2.

iii) Intermediate boundary conditions. The edges of the plate may be restrained against rotation and/or deflection. In both cases, due to difficulties in finding solutions for comparison, the results obtained were checked indirectly.

Solutions obtained for plates with edges on discrete elastic springs (corners on rigid supports) are compared with solutions of plates supported on elastic beams given in ref.(21), using the following argument.

For a plate supported on beams with flexural stiffness b_x the distribution of reaction of the plate on the beams may be assumed to be in the form of a half-sine wave. From simple beam theory the deflection of the beam at every point is, under the assumed loading, proportional to the reaction at that point. The beam can, therefore, be replaced by a series of elastic springs of uniform stiffness. From beam theory the stiffness of the substitute spring is

$$k_{dx} = \frac{\pi^4 b_x}{a^4} .$$

The results given for plates on elastic beams are expressed in terms of a non-dimensional beam factor $\frac{b_x}{aD_x}$ the corresponding non-dimensional stiffness of elastic restraint in the present solution is from definitions in the notation $K_{dx} = \pi^4$. beam factor.

For a square plate with two opposite edges simply supported and the other two on elastic beams with a beam factor = 10, the central deflection under uniform transverse pressure is from ref.21 (page 218) equal to $0.00434 \frac{a^4 q}{D_x}$. For the same plate with an elastic restraint $K_{dx} = 10\pi^4$ and with a uniform

12 x 12 mesh the present solution gives the central deflection as $0.00434 \frac{a^4 q}{D_x}$.

Solutions for plates with rotational restraints at the boundaries are checked in a similar manner, using the following argument.

For plates rigidly connected to rotationally stiff beams at the boundaries the distribution of bending moment at the shorter sides may be approximated by by a half sine wave[52]. From the simple beam theory the rotation caused at every point along the beam is proportional to the moment at that point. The beam in this case acts as an elastic rotational restraint, uniform in stiffness along its length. The stiffness of the equivalent spring is given by $k_{rx} = \frac{t_{rx} \pi^2}{b^2}$, where b is the length of the beam.

Independently, the equations of plates with torsionally stiff edge beams were programmed. It can be seen from the definitions given in the notation that using the above argument the relationship between the coefficient of rotational edge restraint (discrete springs) and the torsion coefficient of the edge beams at $x = \pm \frac{a}{2}$ is given by $K_{rx} = (\frac{a}{b})^2 \pi^2 T_{rx}$.

For the model analysed, the torsion coefficient of the edge beams along the shorter sides was estimated at $T_{rx} = 0.228$. Solutions obtained using both methods are given in Table E-3.

iv) Graded mesh. To study the improvement in the solutions obtained when graded mesh is used for plates under concentrated loading, and also to find the best grading of mesh, several cases were analysed.

Figure E-1 shows the variation of the error in central deflection and bending moment of a simply supported square plate under a central patch load with the dimensions of the load. It can be seen that for uniform mesh, the smaller the

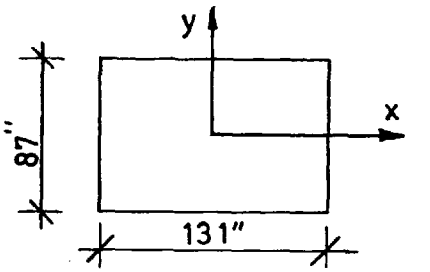
TABLE E - 2

$D_x = 41.7 \times 10^6$ lb in

$D_y = 37.8 \times 10^6$ lb in

$H = 36 \times 10^6$ lb in

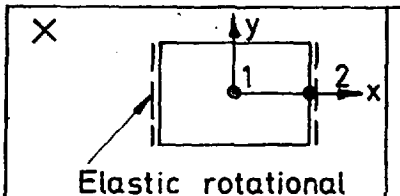
$\nu = 0.3$



		series solution	finite - ✳ difference solution
$W_{max} = k_1 \cdot q$ in	k_1	0.0121	0.0120
$M_{ymax} = k_2 \cdot q$ lb	k_2	627	627
$M_{xmax} = k_3 \cdot q$ lb	k_3	427	427

✳ mesh: 16 x 16

TABLE E-3

×  Elastic rotational restraint.	coef. of rotat -ional restraint	W_1 = k_1 q in k_1	M_{x1} = k_2 q lb in/in k_2	M_{x2} = k_3 q lbin/in k_3
discrete spring system	K_{rx} = -5.076	0.0102	402	-317
torsionally stiff edge beam	T_{rx} = 0.228	0.0102	402	-301

× Plate parameters same as in Table (E - 2)
mesh: 24 x 16 uniform

area of the patch the larger becomes the error in the solutions obtained. For two areas of patch loading graded meshes as shown in figure E-2 were used. Solutions obtained are marked in Figure E-1 for comparison. For the evaluation of errors, results were compared with those obtained from the following series solution

$$w = \frac{16q}{\pi^6} \sum_{m=1,3,..}^{\infty} \sum_{n=1,3,..}^{\infty} \frac{\sin\frac{m\pi x''}{a} \cdot \sin\frac{n\pi y''}{b} \cdot \sin\frac{m\pi l_x}{2a} \cdot \sin\frac{n\pi l_y}{2b} \cdot \sin\frac{m\pi x}{a} \cdot \sin\frac{n\pi y}{b}}{mn\left(D_x\frac{m^4}{a^4} + 2H\frac{m^2n^2}{a^2b^2} + D_y\frac{n^4}{b^4}\right)}$$

where x'' and y'' are coordinates of the centre of patch load. The above series is an extension of the expression given on page 372 of ref.(21) which was programmed for checking the finite difference solutions of orthotropic plates under patch loading. In obtaining numerical solutions, special attention was paid to the convergence of results.

v) Mesh fineness. To estimate the accuracy of the results and in order to choose a suitable mesh size for the later non-linear problems, solutions were obtained for several cases with different fineness of meshes. Figure E-3 shows the error in deflection and moment of square simply supported and clamped plates for various degrees of mesh fineness. The solutions are compared with those obtained from a program written for the above series expression. For clamped plates solutions obtained using more accurate finite difference expressions for the slope at the boundaries are also given.

2) Plane stress solutions

For simple boundary conditions and uniform loading at the edges accurate plane stress solutions are obtained, even when a relatively coarse mesh is used. To demonstrate the scope and accuracy of the results, the two following examples are given.

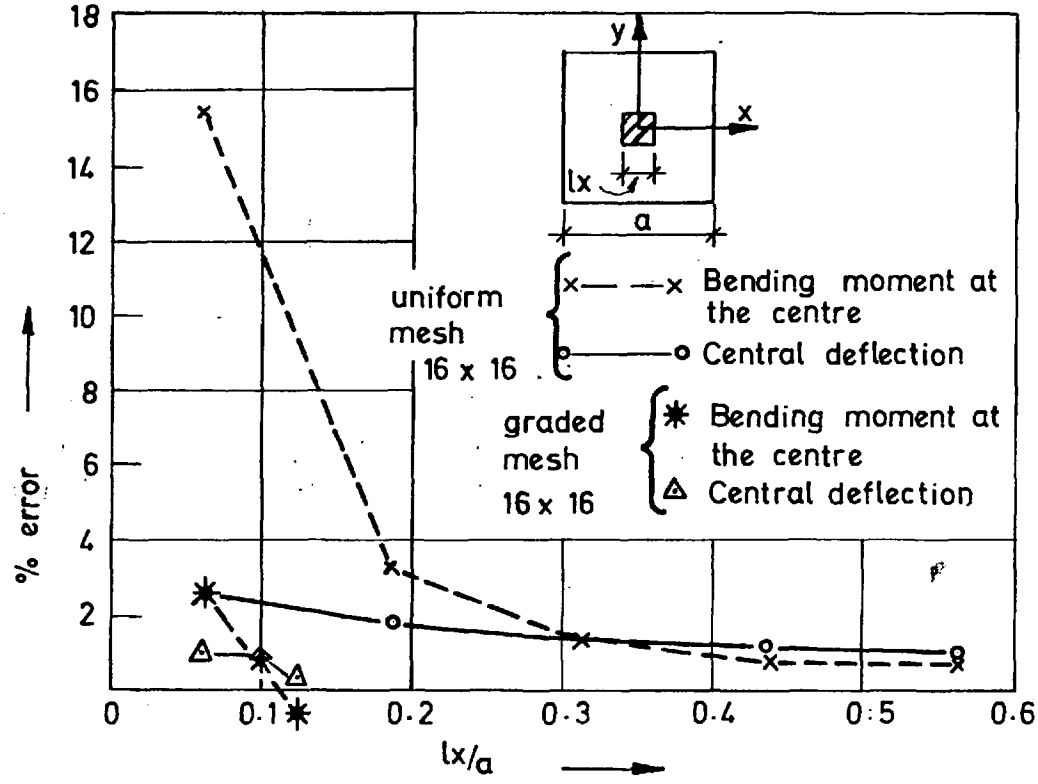
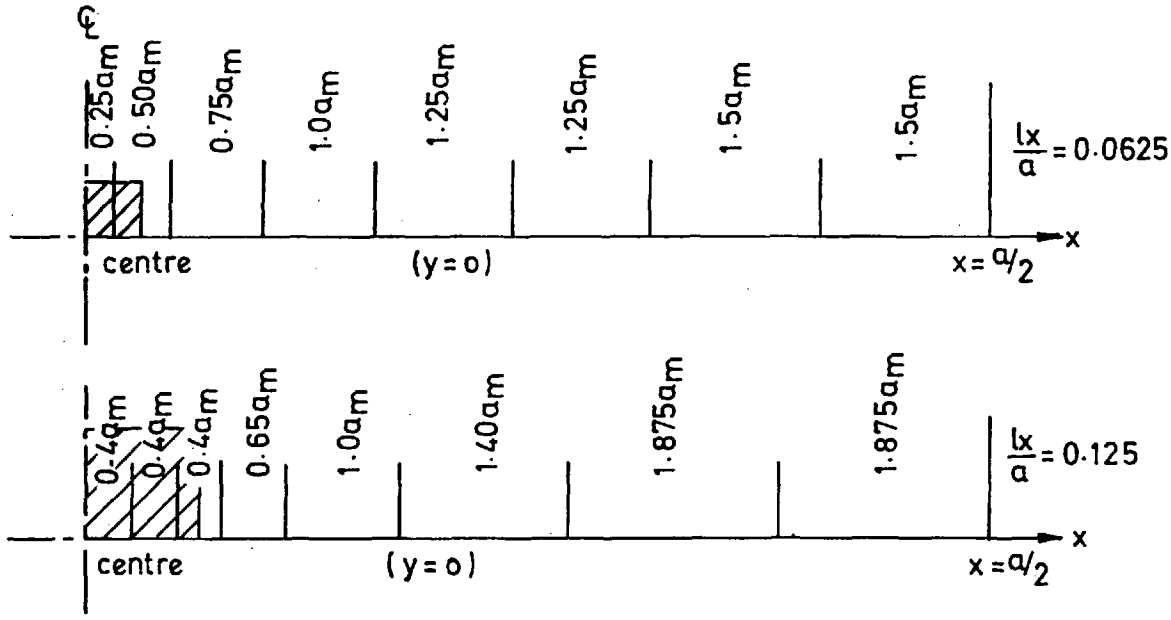


FIG. E-1



For $l_x/a = 0{\cdot}1$ see mesh No. 5

FIG. E-2

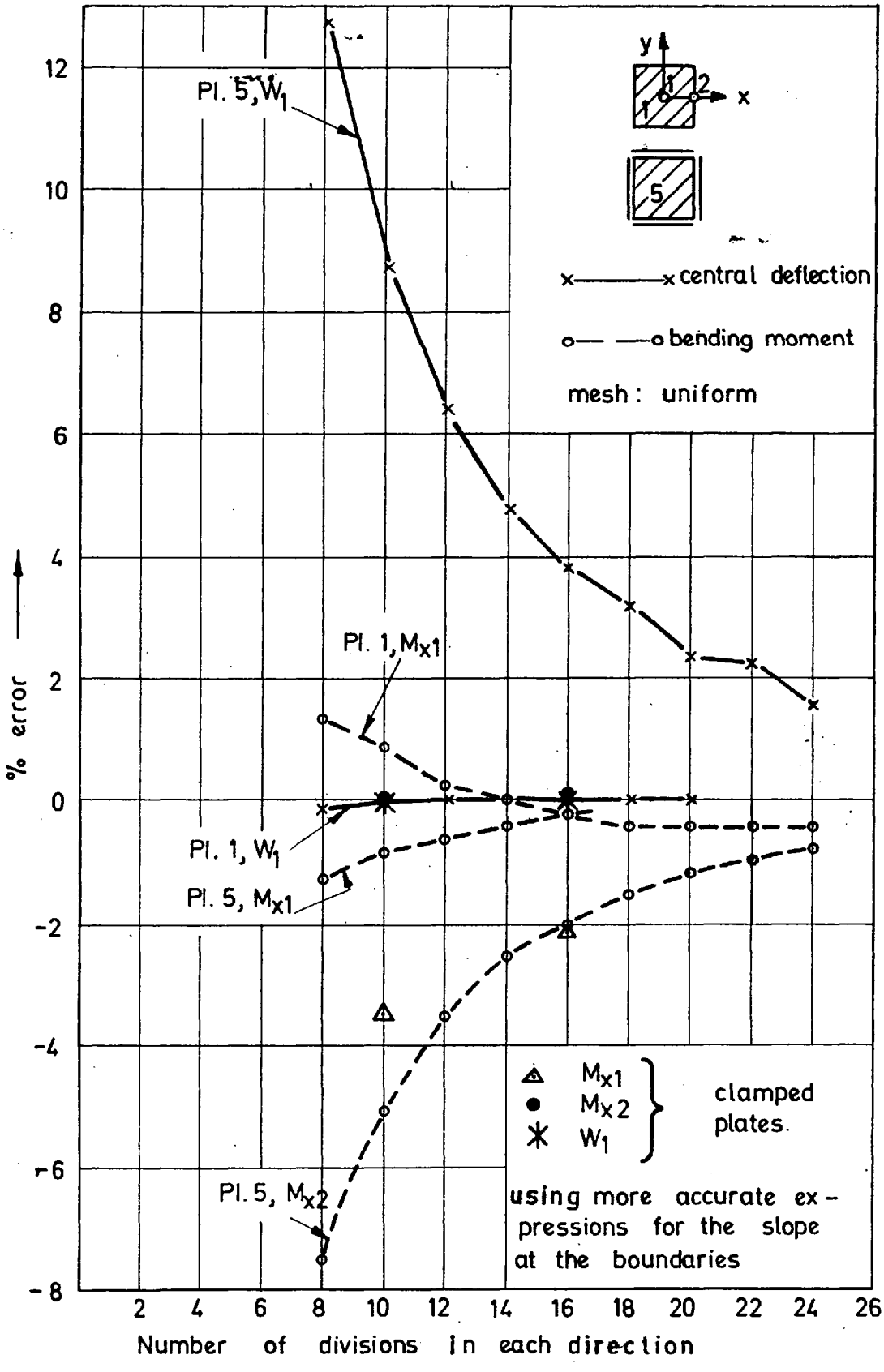


FIG. E-3 Square plates under U.D.L. Variation of error in deflection and moment with the fineness of the mesh.

i) Square plate pulled in the middle of two opposite sides. A uniform square mesh is used and the concentrated loads are applied to the nodes at the mid-point of the loaded edges. Solutions are obtained for 8 x 8, 10 x 10, 12 x 12 and 16 x 16 meshes. Figure E-4 shows the stress distribution obtained from a 12 x 12 mesh. The actual magnitude of the stresses found across the centre line and across the section $y = \frac{a}{4}$ are plotted. Simpson's integration formula is used to evaluate the total force for the equilibrium checks shown in the figure.

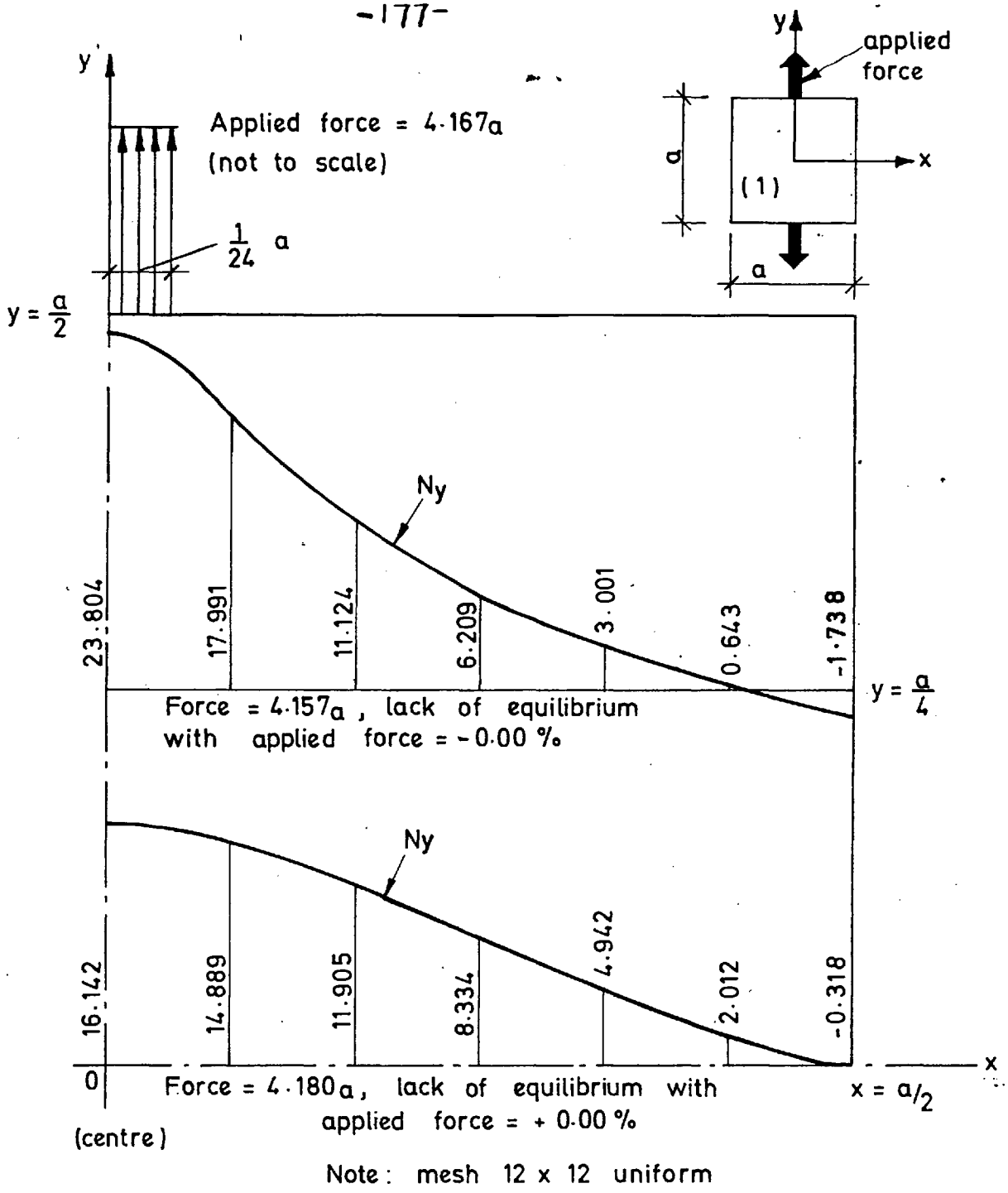
ii) Square plate, clamped and uniformly displaced on two opposite sides. The displaced edges are assumed to remain straight and fully restrained against movement parallel to themselves. The unloaded edges are assumed to be stress free. The distribution of stresses obtained from a uniform 12 x 12 mesh is shown in Figure E-5. Using the same method as in the previous case total forces across the centre lines and the boundary of the plate were evaluated. The maximum lack of equilibrium is about 1%.

In general the inplane boundary condition of edges fully restrained against tangential movement gives the least accurate results.

If the shear stresses at the boundaries were assumed zero, the uniform applied displacement U = 10 would have resulted in a uniform stress distribution throughout the plate with total $N_y = 10$. The present arrangement, however, gives an average total $N_y = 10.21$, indicating that the clamping of the edges increases the extensional rigidity of a square plate by approximately 2%.

3) Non-linear solutions of transversely loaded plates

In Figures 1 and 7 of the theoretical results, for square simply supported and clamped plates the numerical solutions available are also included. The available solutions are for Poisson's ratio of 0.316. It is, however, shown



Note: mesh 12 x 12 uniform

FIG. E-4 Square plate under uniaxial local tension.

Distribution of stress and equilibrium checks.

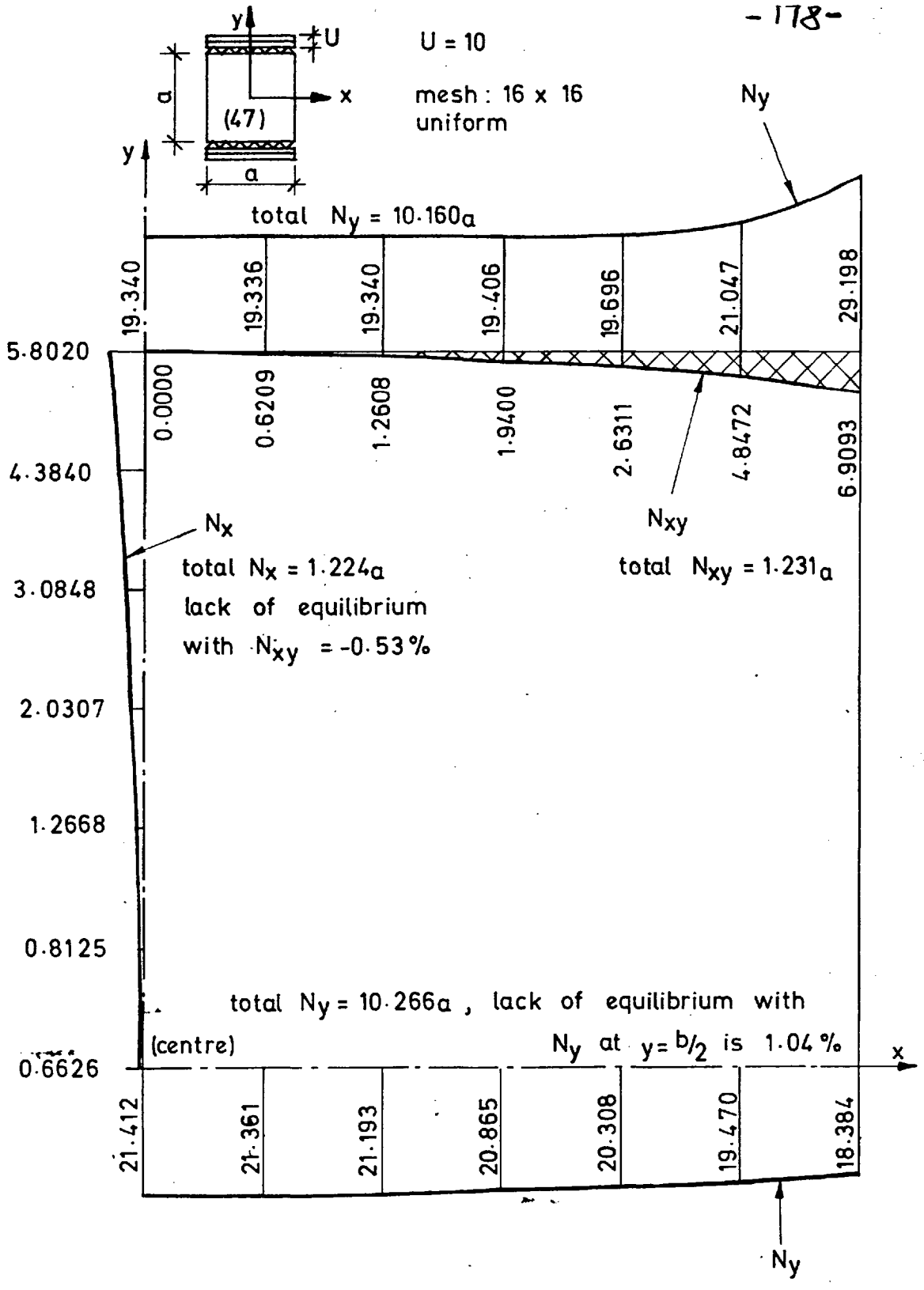


FIG. E-5 Square plate clamped and uniformly displaced on two opposite sides. Distribution of stress and equilibrium checks.

in ref.(15) that the change in Poisson's ratio from 0.3 to 0.316 does not affect the solutions appreciably. For clamped plates, the solution of plate 5.(10) is compared with that of plate 5.(6). The comparison is justified, as again in ref.(15) it is concluded that for plates fixed at the boundaries against inplane displacements the tangential restraints do not affect the central deflection of the plate. Using the same reasoning the results from ref.(13) for plate 1.(10) are shown in Figure 15 for comparison with the simply supported plates with aspect ratios 1/1.5.

In addition, present solutions which are common with refs.(15) and (16) were compared with the graphs given in these references and good agreement was observed.

4) Non-linear solution of plates under combined loading

Two examples are given, one is compared with Bleich's approximate solution and the other with one of the Levy solutions.

i) Simply supported square plate under combined loading (transverse pressure varies). The plate is initially subjected to an end-thrust equal to half of its critical buckling load. The variation of the central deflection with the intensity of the subsequent uniform transverse pressure obtained from the present solution is shown in figure E-6 together with Bleich's approximate solution calculated from the expression on page 482 of ref.(24). To indicate the sense and the order of magnitude of the errors in Bleich's solutions, variations of central deflection with transverse pressure are evaluated for zero inplane loading as well and are shown in the same figure. The errors become larger for higher deflections.

The tangents to the curves at the origin are the linearised solutions and their slopes are listed in table E-4, together with those obtained for two other magnitudes of inplane loading.

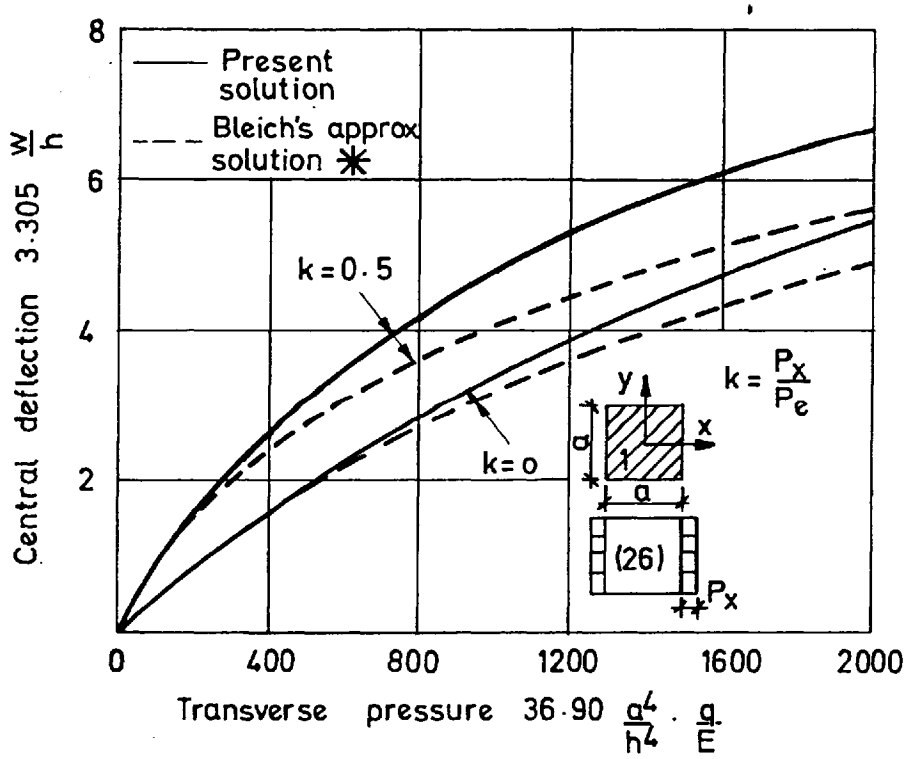


FIG. E - 6

TABLE E - 4

$\frac{P_x}{P_e}$	Magnification factors Pl. I. (26)			
	present solution			Bleich's approx. solution ✳
	W_1	M_{x1}	M_{y1}	W_1, M_{x1}, M_{y1}
0	1	1	1	1
0.25	1.342	1.366	1.370	1.333
0.5	2.032	2.105	2.118	2.000
0.75	4.140	4.384	4.405	4.000

✳ ref. 24

ii) Simply supported square plate under combined loading (end-thrust varied). To afford comparison with the available solutions, a simply supported plate with the same boundary conditions and loading as solved by Levy[10] was analysed. The plate is initially subjected to a uniform transverse pressure, followed by increments of compressive end-thrust. The variation of central deflection with end-thrust is shown in Figure E-7. Values of effective width of the plate in sustaining the inplane compression are given in table E-5 from both solutions for comparison.

The solutions agree very well, the maximum deviation being in the vicinity of the critical buckling load of the plate.

5) Non-linear solutions of initially deformed plates subjected to end-thrust

Results obtained from the present analysis for a simply supported square plate with an initial deformation in the form of one half sine wave in each direction are compared with two other available solutions. In all the three cases the maximum initial deformation is equal to one tenth of the plate thickness. Figure 77 shows the variation of central deflection with the end-thrust. The plate analysed by Yamaki[33] has identical membrane boundary conditions to the present solution. In the solution due to Coan[30], however, the unloaded edges are assumed to be stress free. No values for the effective width are given in the above references so that comparison could be made.

6) Critical buckling load of plates

To examine the program, and the method and accuracy of the results, solutions were obtained for several standard cases. Some of the more common cases are given in table E-6 together with the available solutions. In all the solutions an accuracy of 0.5% has been specified in the iterations.

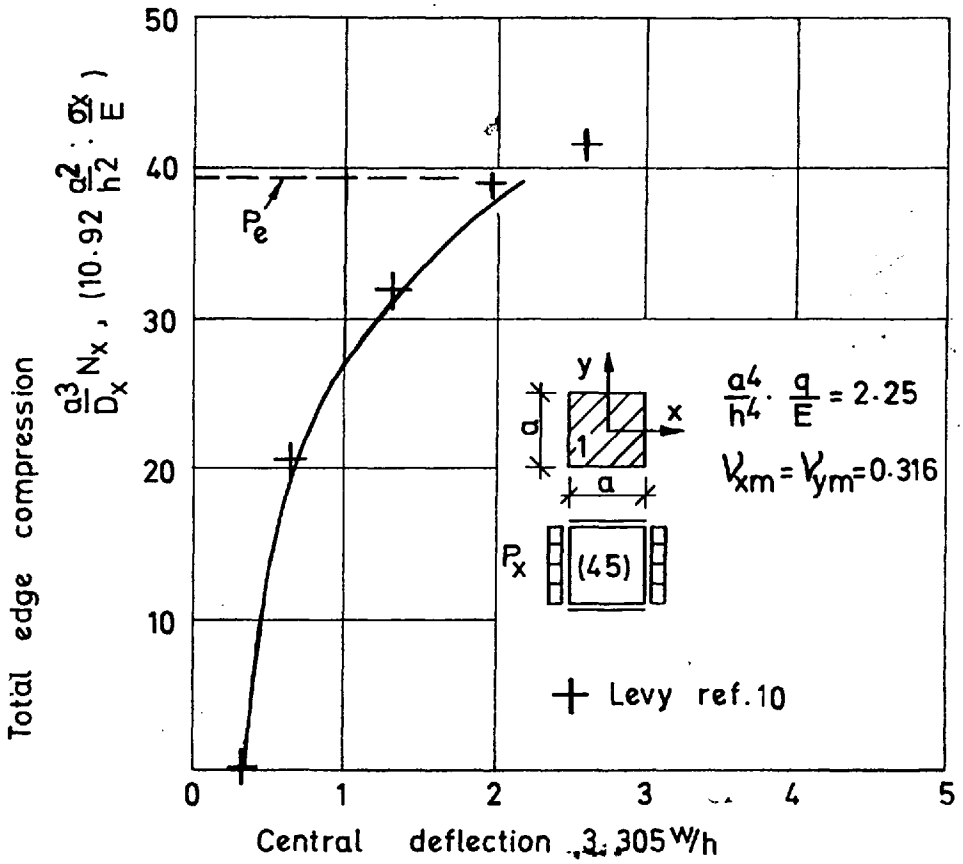
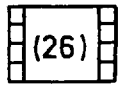
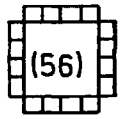
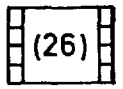
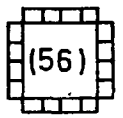
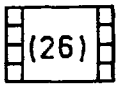
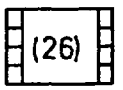


FIG. E - 7

TABLE E - 5

P_x total $= \frac{a^2}{D} N_x$	Effective width Pl. 1. (45)	
	present solution	Levy ref.10
−20.42	0.973	0.973
−32.00	0.932	0.935
−39.09	0.868	0.887

TABLE E - 6 Critical buckling load of plates

Boundary conditions and loading		P_x critical $= k \frac{Nx}{a^2 D_x}$ k	Poisson's ratio	Mesh size (uniform)
Flexural	Membrane			
 1	 (26)	- 39.30 (-39.48)*	——	12 x 12
 1	 (56)	-19.65 (-19.74)	——	12 x 12
 5	 (26)	- 97.66 (-99.39)	——	12 12
 5	 (56)	- 51.74 (-52.31) (-52.60)	——	12 x 12
 3	 (26)	-9.82 (-9.87)	0	16 x 8
 6	 (26)	- 38.84 (-39.48)	0	16 x 8

* refs. 20 and 24

7) An example of equilibrium and displacement checks for a non-linear solution

In all the solutions obtained, the equilibrium of the membrane forces along the boundaries and along the centre lines of the plates has been closely satisfied. In what follows the solution obtained for plate 1.(45) (the same solution was used in comparison with Levy's results, Fig.E-7) is examined in more detail for the equilibrium of membrane forces and for the validity of the displacements obtained at the boundaries.

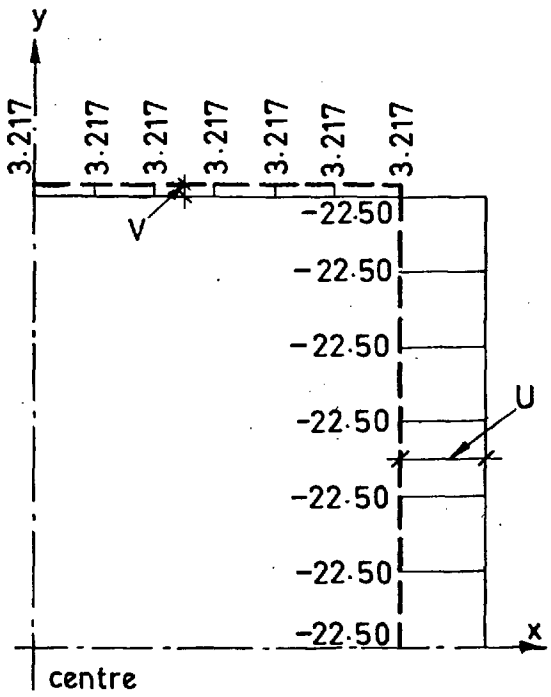
The distrihutions of membrane stress for the maximum load reached are shown in Figure E-8. The values given were obtained after a total of 20 iterations (each iteration involves one matrix inversion) and 4 loading levels. The total forces across the centre lines and the boundaries were calculated from the stress ordinates given using Simpson's integration formula, and are inserted in the figure. It can be seen that equilibrium is achieved in both directions within 0.00%.

The extensional displacements obtained along the edges are also shown in Figure 8. It can be seen that the displacements of the nodes at each boundary are constant along that boundary, indicating that the condition imposed on the edges to remain straight in their translation is satisfied. The values obtained for the displacements can be roughly checked as follows.

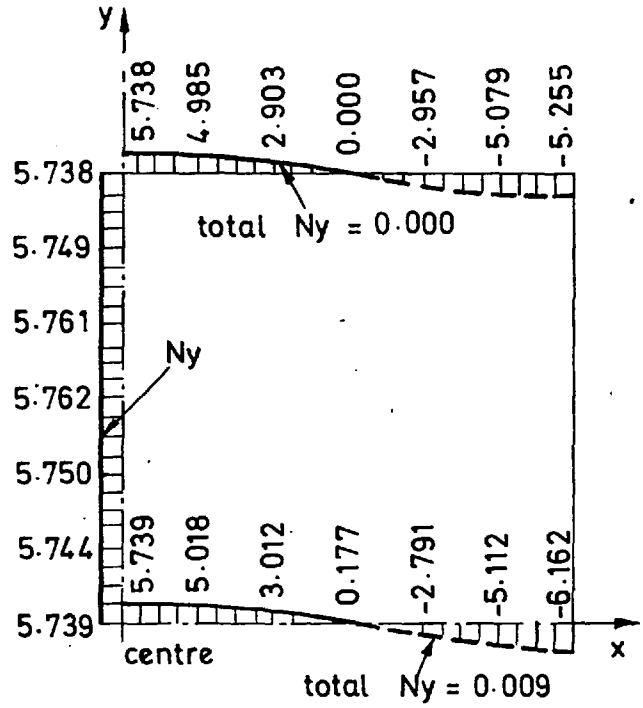
The extension U of the plate at $x = \frac{a}{2}$ is given by $U = U_w + U_m$, where U_w is the shortening due to transverse deflection and U_m is the extension caused by membrane forces.

Due to W, the shortening of the plate between the centre line and the edge is

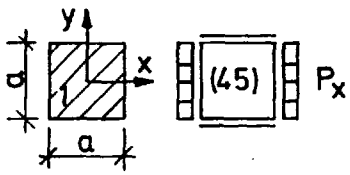
$$U_w = -\tfrac{1}{2} \int_0^{0.5} \left(\frac{\partial W}{\partial X}\right)^2 dX$$



i) Distribution of edge displacements



ii) Distribution of Ny



$\frac{a^4}{h^4} \cdot \frac{q}{E} = 2.25$

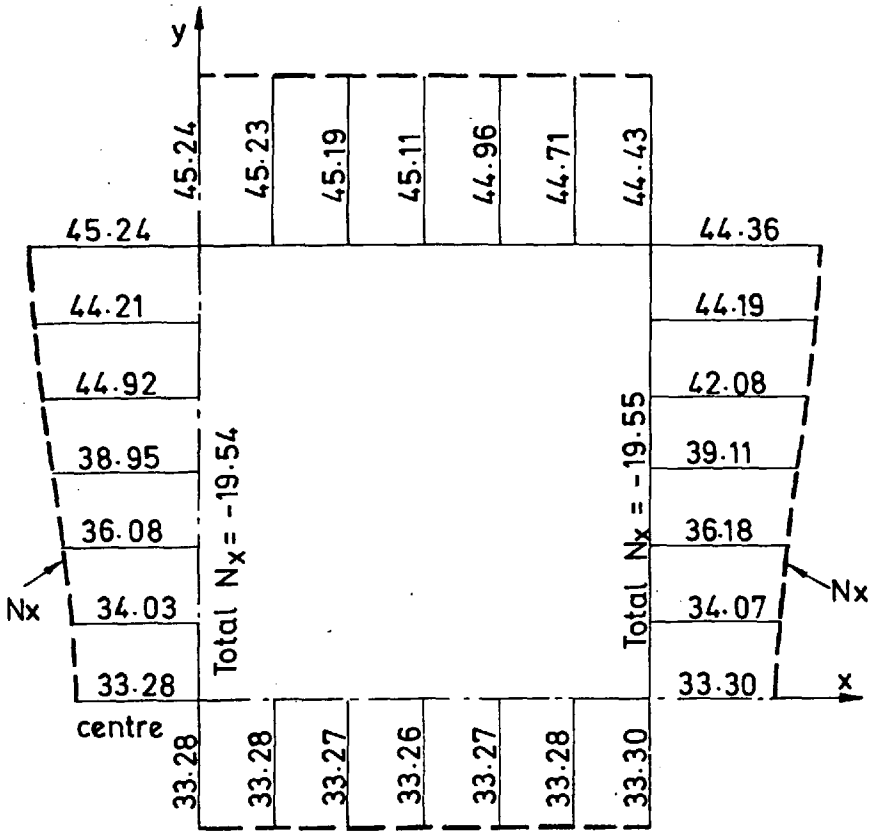
$\frac{a^2}{h^2} \cdot \frac{\sigma_x}{E} = -3.48$

$(\frac{a^2 N_x}{D_x} = -39.09)$

$V_{xm} = V_{ym} = 0.316$

$\frac{w'}{h} = 0.66$

$(W' = 2.182)$



iii) Distribution of Nx

FIG. E - 8

If W is assumed to be in the form of $W = W_1 \cos \pi X$, it can be shown that

$$U_w = -\frac{\pi^2}{8} W_1^2 = -1.23\, W_1^2.$$

In the present solution W_1 (central deflection) is 2.18, therefore

$$U_w = -1.23\,(2.18)^2 = -5.86$$

Due to membrane stresses, the extension u_m is given by

$$u_m = \frac{1}{E} \int_{x=o}^{x=a/2} (\sigma_x - \nu\sigma_y)dx$$

and in non-dimensional form

$$U_m = \int_0^{0.5} N_x dX - \nu \int_0^{0.5} N_y dX$$

Along the centre line y = O, the second term of the R.H.S. is zero (Figure E-8-ii). The first term of the R.H.S. can be evaluated from Figure E-8-ii in which the distribution of N_y may be assumed linear.

$$U_m = \frac{-(33.30 + 33.28)}{2} \cdot \tfrac{1}{2} = -16.64$$

Therefore, total U = -16.64 - 5.86 = - 22.50

Solution from computer - 22.50

Along y = b/2, as the edge is supported, using the same argument as above

$$U = U_m = \frac{-(45.24 + 44.43)}{2} \cdot \tfrac{1}{2} = -22.42$$

Solution from computer -22.50

Similarly V along the centre line x = O is given by $V = V_w + V_m$, in which $V_w = U_w = -5.86$ and

$$V_m = \int_O^{O.5} N_y dY - \nu \int_O^{O.5} N_x dY$$

If along this centre line the distribution of N_y is assumed linear (Figure F-8-ii), and the distribution of N_x assumed parabolic (Figure F-8-iii), V_m is given by

$$V_m = \frac{(5.738 + 5.739)}{2} \cdot \tfrac{1}{2} - O.316 \left[\frac{-33.28}{2} - \frac{2}{3} \cdot \frac{(45.24 - 33.28)}{2} \right]$$

$$= 9.387$$

Therefore $V = 9.387 - 5.86 = \underline{3.527}$

Solution from computer $\underline{3.217}$

$$Q' = 36.09 \left(\frac{30}{0.62}\right)^4 . 10.95 = 72.097$$

$$N_X' = - 10.92 \left(\frac{30}{0.62}\right)^2 . \frac{8.38 \times 2240}{30 \times 10^6} = - 16$$

Values of Q' and N_x' closely correspond to the third row of table 28, from which central deflection $w = \frac{0.112 \times 0.62}{3.305} = 0.021$ inches, central bending moment in the direction of applied loading

$$M_x = \frac{2.05(0.62)^4 \times 30 \times 10^6}{36.09 (30)^2} = 487 \text{ lb in/in.}$$

Maximum bending stress at centre is given by

$$\frac{487 \times 6}{(0.62)^2 \times 2240} = 3.39 \text{ tons/sq in.}$$

direct membrane stress at centre perpendicular to the direction of the applied loading

$$\sigma_y = 0.021 \left(\frac{0.62}{30}\right)^2 . \frac{30 \times 10^6}{10.92 \times 2240} = 0.011 \text{ tons/sq in.}$$

Similarly the rest of the coefficients in the table may be used.

Example 2

Given: initially deformed simply supported plate with the same parameters as in the previous example.

Central deviation from flatness = 0.062 inches, therefore

$w_o/h = 0.1$

Membrane boundary conditions as in example 1, the problem therefore refers to plate 1.(45).

Loading: average edge-compression = - 6.30 tons/sq in.

From the information given

$$N_x'' = -10.92 \left(\frac{30}{0.62}\right)^2 \cdot \frac{6.30 \times 2240}{30 \times 10^6} = -12$$

The above value relates to the third row of table 30 from which

central deflection $w = \frac{0.4735 \times 0.62}{3.305} = 0.089$ inches,

central moment $M_x = \frac{1.82 \times 30 \times 10^6 \times (0.62)^4}{(30)^2 \times 36.09} = 284$ lb in/in.

corresponding maximum bending stress $= \frac{284 \times 6}{(0.62)^2 \times 2240}$

$= 1.98$ tons/sq in.

$$\sigma_y = 0.143 \left(\frac{0.62}{30}\right)^2 \cdot \frac{30 \times 10^6}{10.92 \times 2240} = 0.075 \text{ tons/sq in.}$$

Example 3

If for a homogeneous plate with an aspect ratio of a:b = 0.840 the relationships between the extensional and flexural rigidities are given by $C_y/C_x = D_y/D_x = 2$, $H_b/D_x = H_m/C_x = 1.414$, it can be shown by direct substitution in the plate parameters given that the corresponding values of ε', α, β and γ are all equal to 1. The plate when transformed relates to a square isotropic plate.

APPENDIX F

Solution by digital computer

The governing equations (B-16) and (B-17) together with the boundary conditions and the applied loading are converted into the two following matrix equations as described in appendix C.

$$\begin{bmatrix} W \end{bmatrix} = \begin{bmatrix} A \end{bmatrix}^{-1} \begin{bmatrix} Q \\ + \\ I_1 \end{bmatrix} \qquad \text{(F-1)}$$

$$\begin{bmatrix} F \end{bmatrix} = \begin{bmatrix} B \end{bmatrix}^{-1} \begin{bmatrix} W'' \\ + \\ I_2 \end{bmatrix} \qquad \text{(F-2)}$$

From the plate parameters given matrix B can be readily formed and inverted. Initial deformation constants (I_1 and I_2) are also calculated and stored.

For any given value of transverse pressure and inplane loading the two simultaneous equations (F-1) and (F-2) can be solved for F and W as follows.

If, for example, at a certain stage of analysis the inplane loading is incremented, the initial values of deflection (W_i) due to this increment are estimated from the linear extrapolation of the values of W obtained previously. The solution then proceeds to the repetitive steps given below.

Step 1) With W_m (value of W to be used at each step) = W_i and the given inplane loading equation (F-2) is solved for F_1 (value of F at Step 1). Using F_1 matrix A is set up and W_1 is evaluated from equation (F-1).

Step 2) $W_m = 0.5\ (W_i + W_1)$ is used to find F_2 from equation (F-2). Using F_2 and equation (F-1) W_2 is evaluated.
Results are compared with W_1 and F_1, if the specified accuracy is not reached the procedure is repeated with $W_m = 0.5\ (W_2 + W_1)$ and so on.

The convergence of the solutions is fairly good and in practically all the cases they converged. Close to the buckling load, however, the convergence becomes slow, and for inplane loads above the critical buckling load the solution converges to a mode which is not physically feasible to be the continuation of the load-deflection history of the plate. The reason for this behaviour is still being sought.

In Chapter III a method is proposed for themodification of the iteration procedure which may overcome this problem.

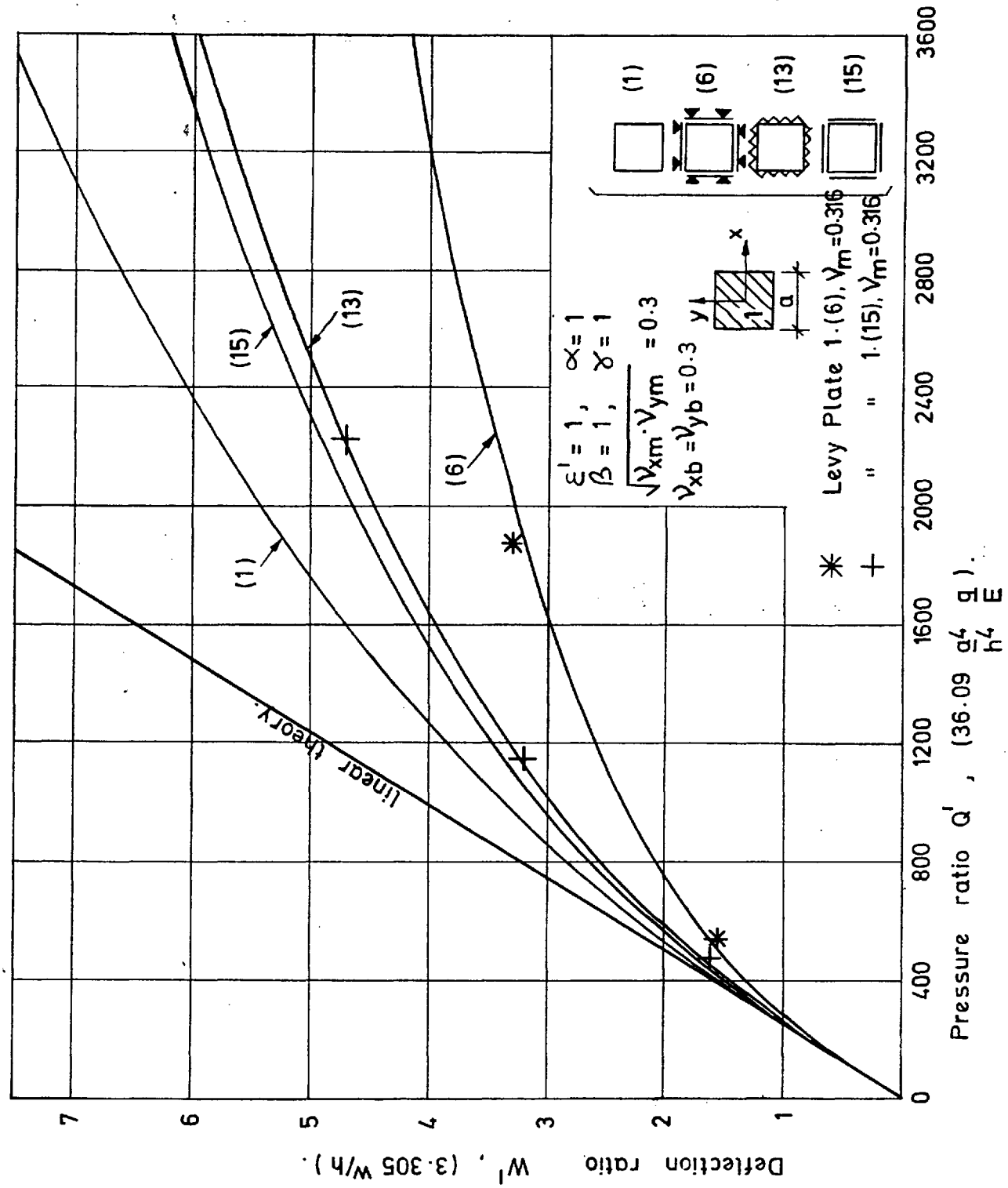


FIG. 1 Deflection at the centre of simply supported plates under uniform transverse pressure.

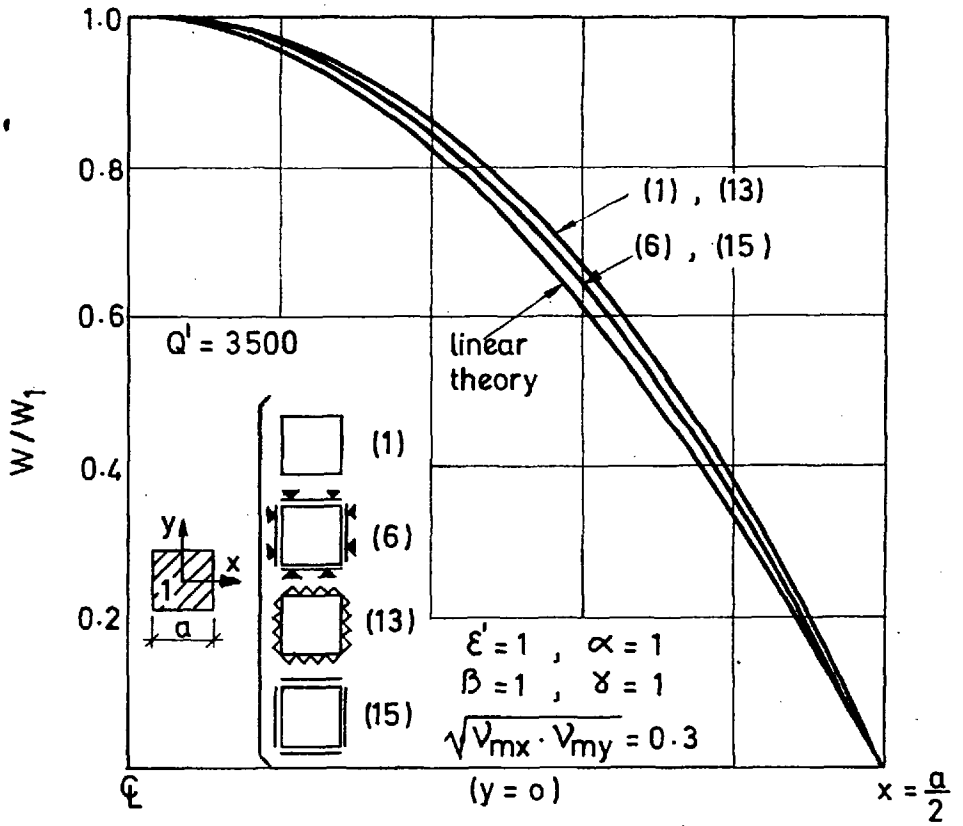


FIG. 2 Deflection profiles along the centre lines of simply supported plates under uniform transverse pressure.

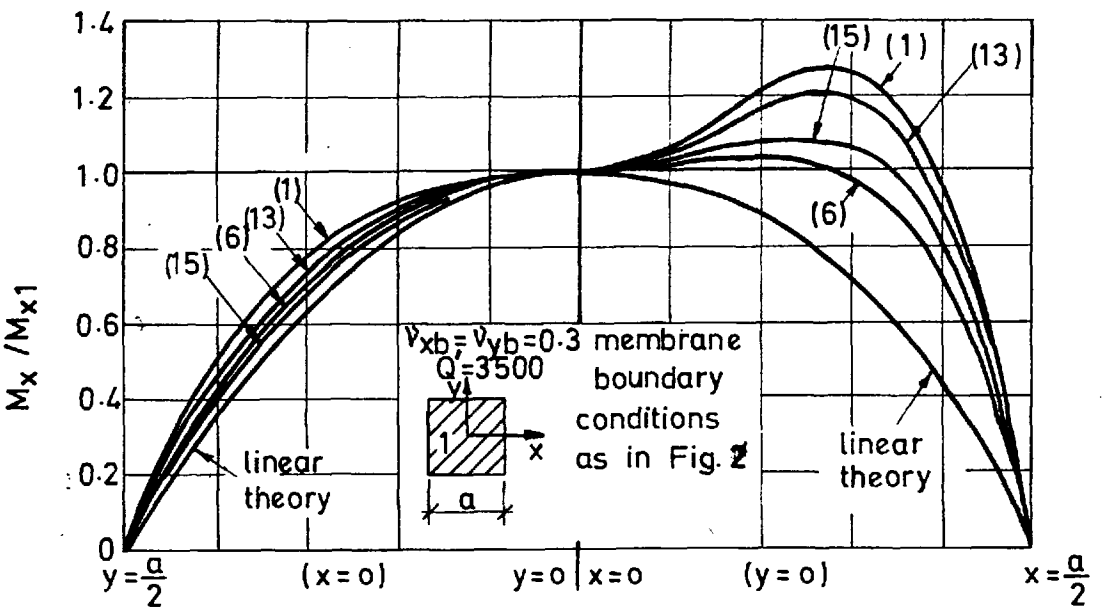


FIG. 3 Bending moment profiles along the centre lines of simply supported square plates under uniform transverse pressure.

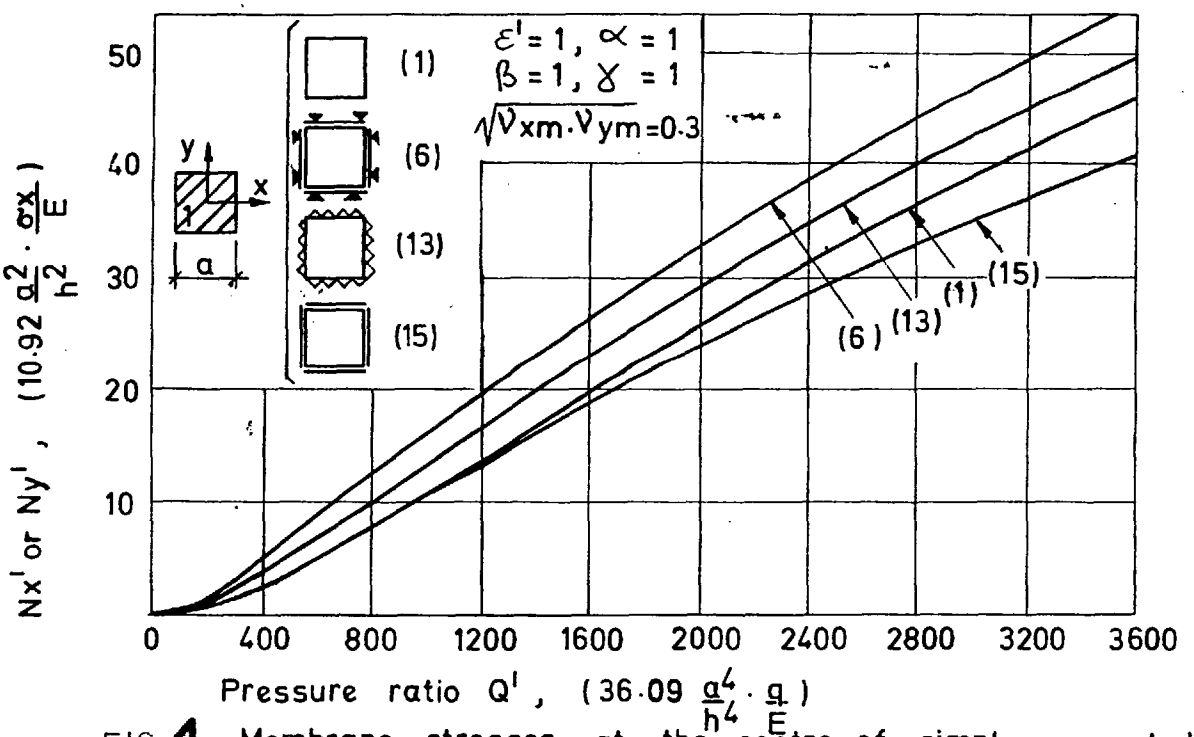


FIG. 4 Membrane stresses at the centre of simply supported plates under uniform pressure.

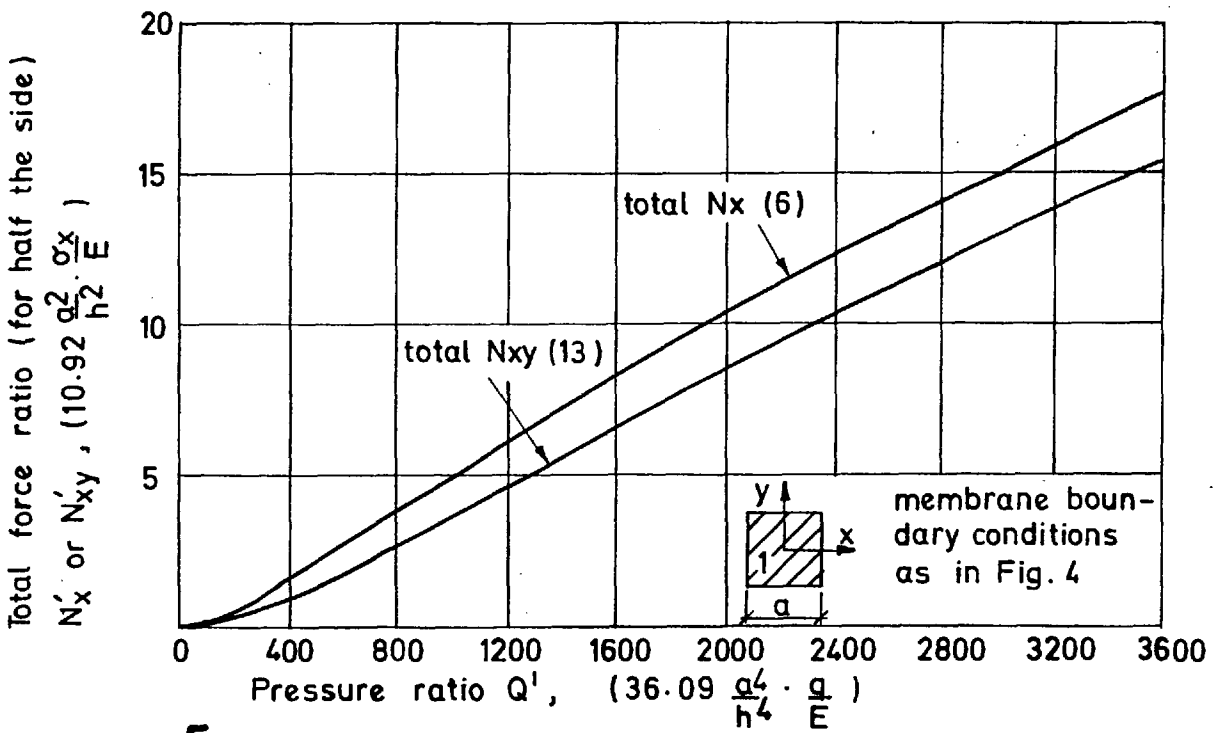


FIG. 5 Total extensional and tangential forces at the boundaries of simply supported plates under uniform transverse pressure.

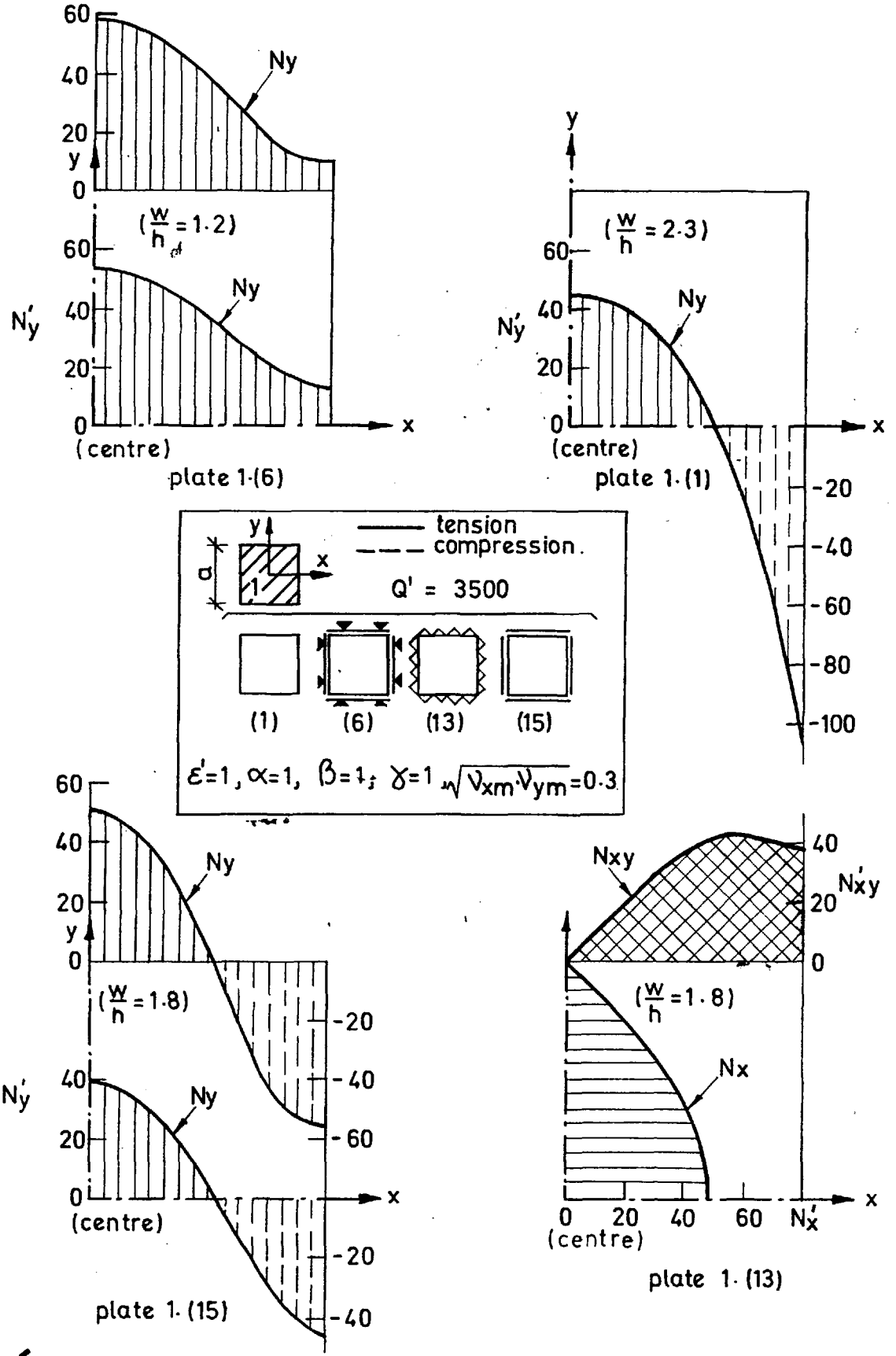


FIG. **6** Distribution of membrane stress along the centre lines and the boundaries of simply supported plates under uniform transverse pressure.

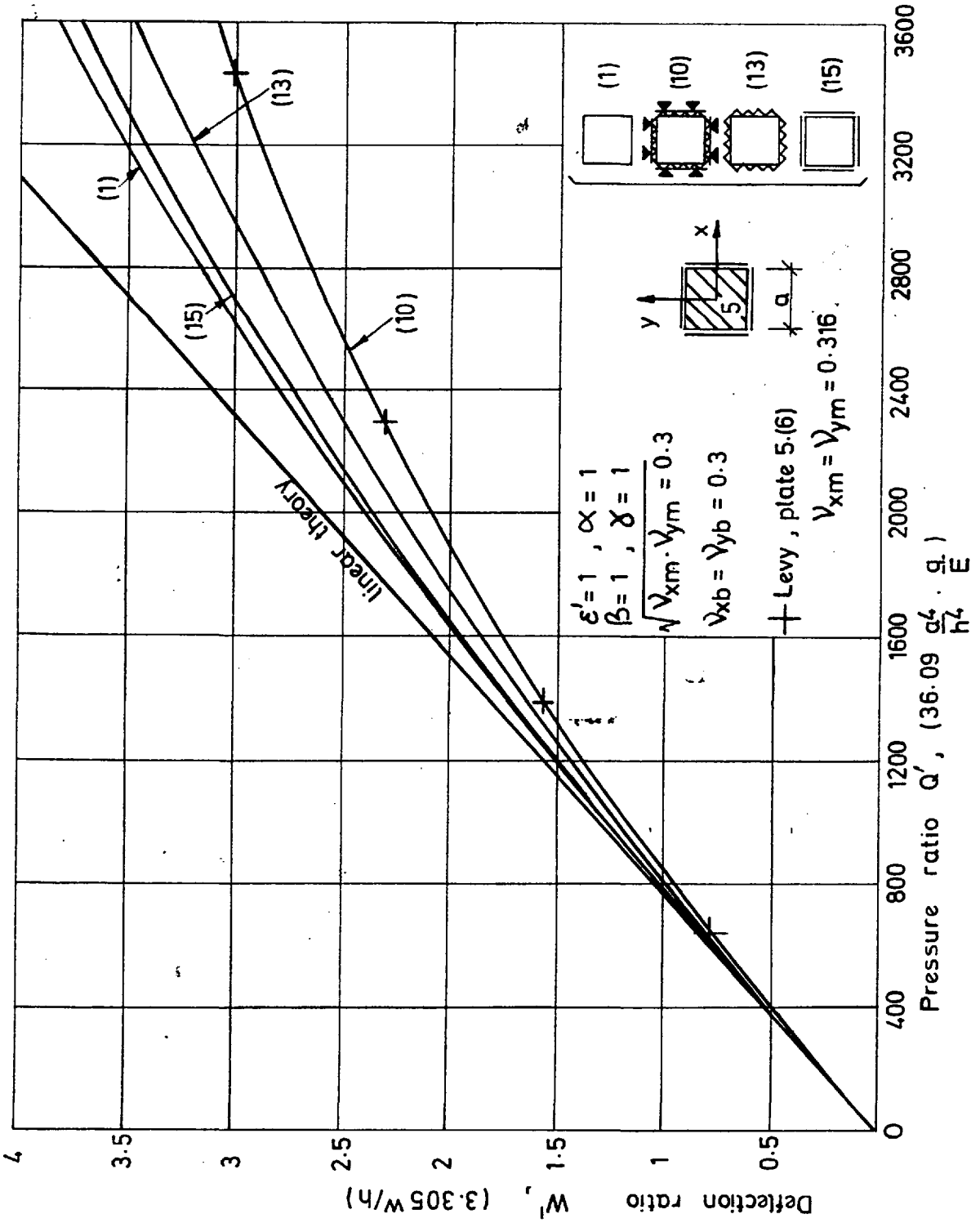


FIG. 7 Deflection at the centre of clamped plates under uniform transverse pressure.

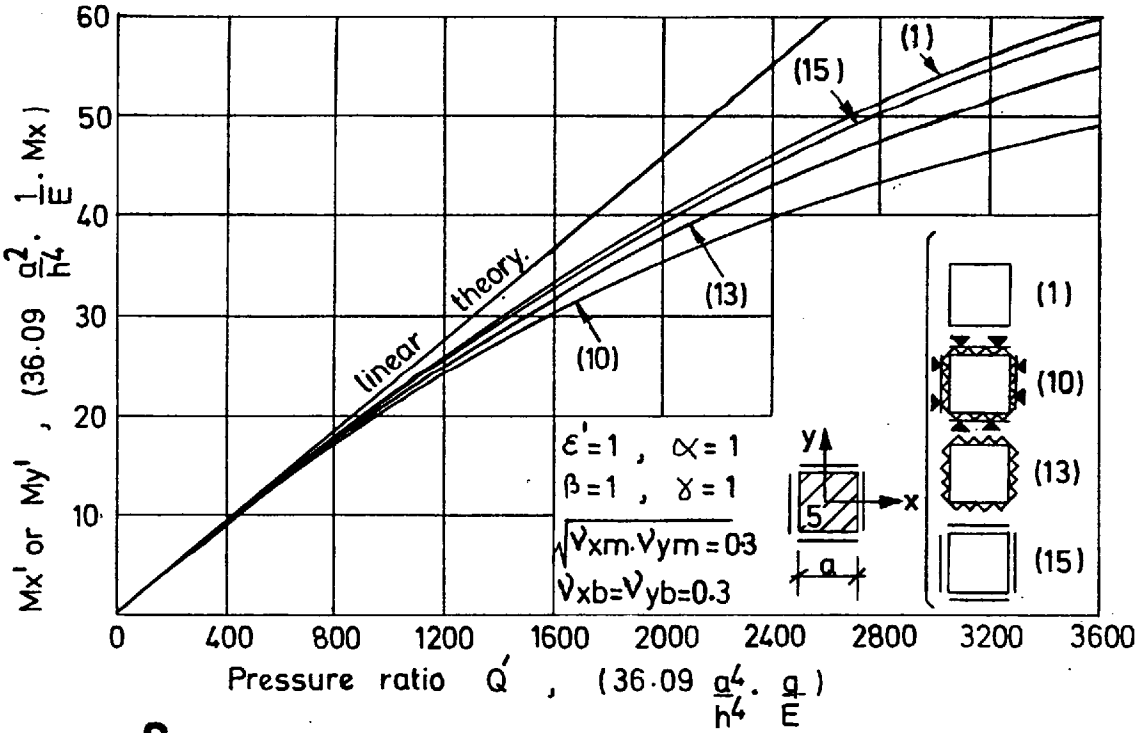


FIG. **8** Bending moment at the centre of clamped square plates under uniform transverse pressure.

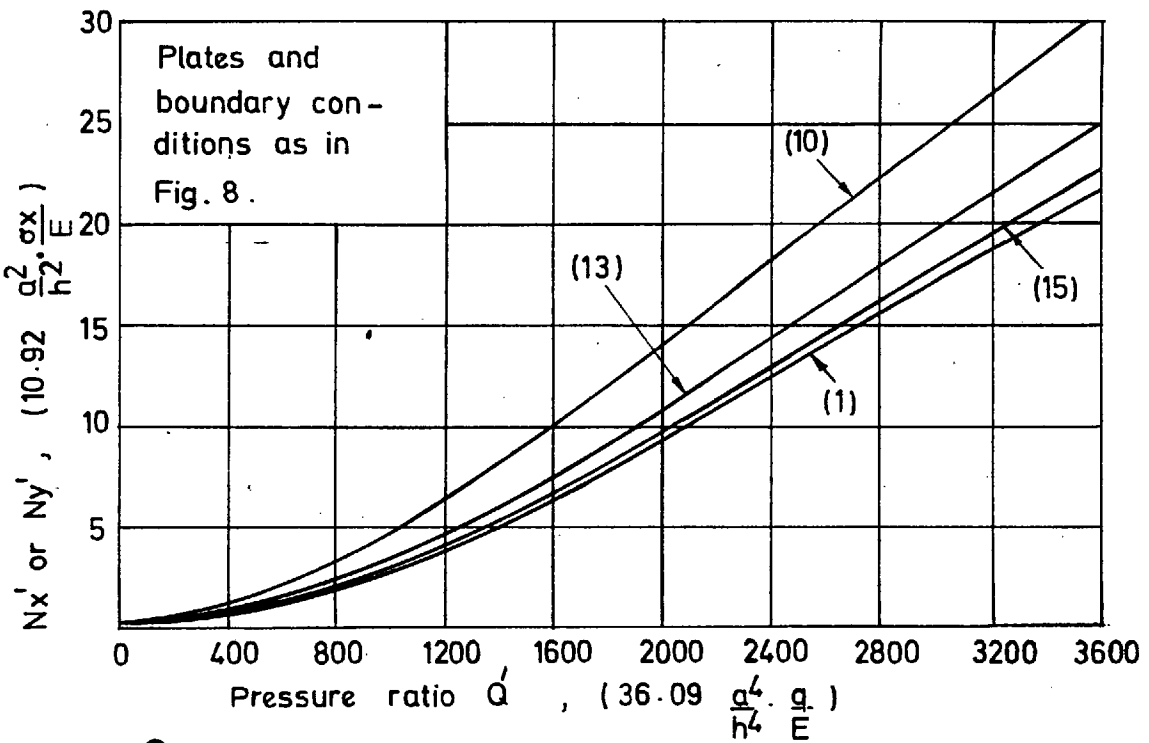


FIG. **9** Membrane stresses at the centre of clamped plates under uniform transverse pressure.

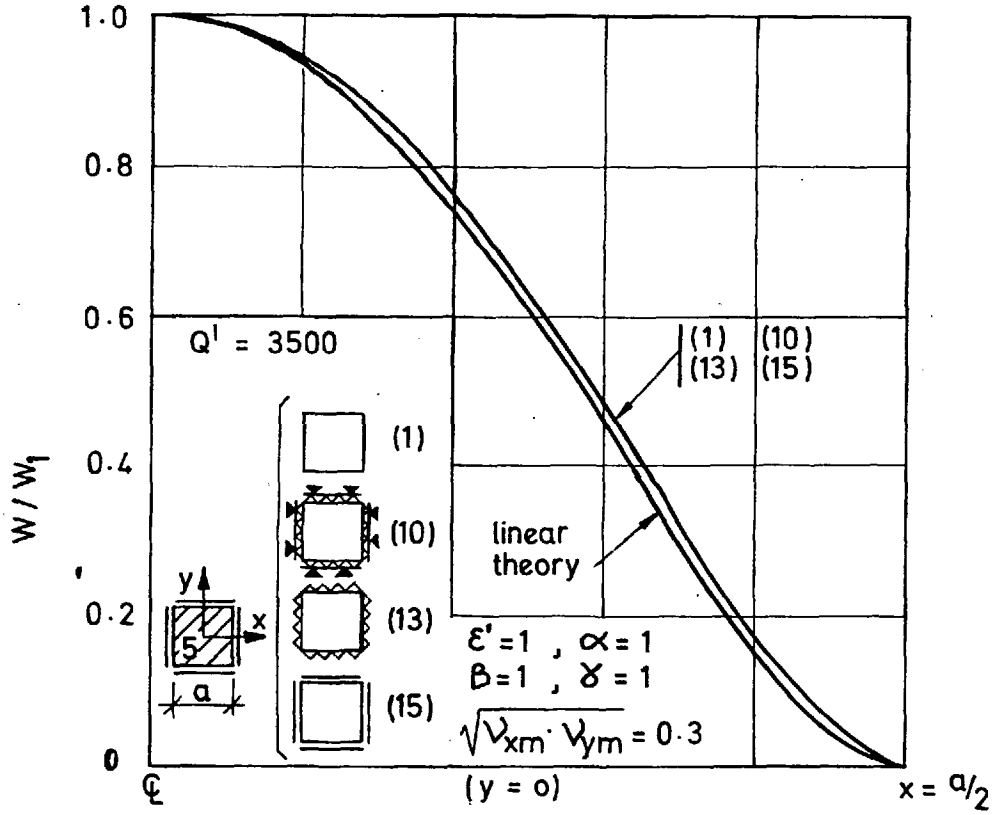
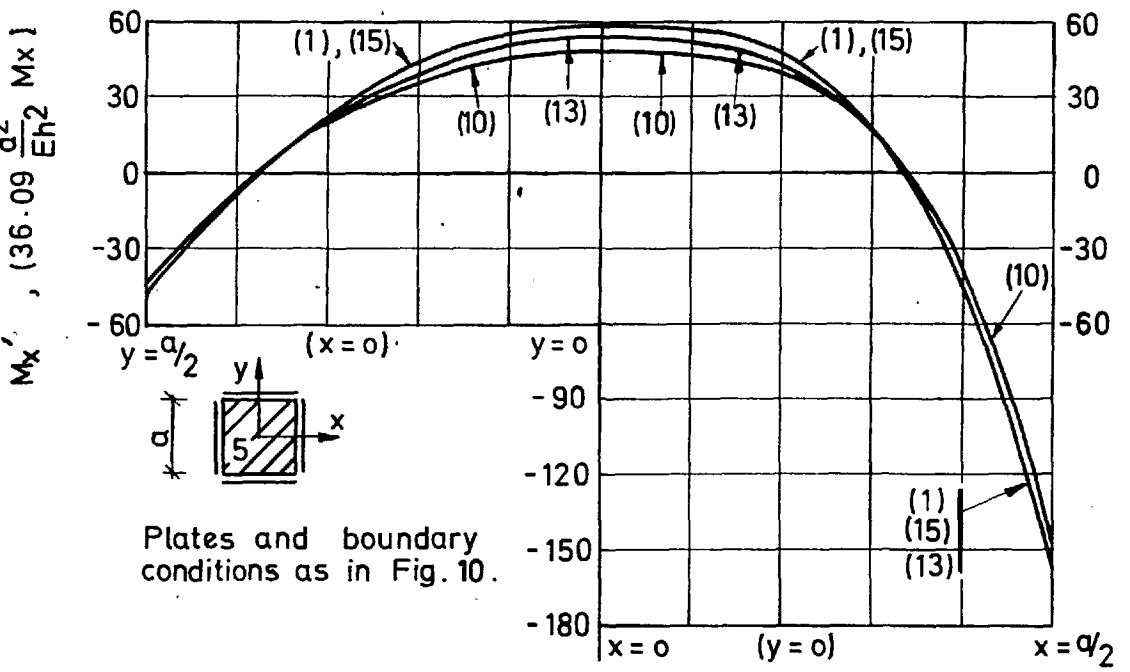


FIG. **10** Deflection profiles along the centre lines of clamped plates under uniform transverse pressure.



Plates and boundary conditions as in Fig. 10.

FIG. **11** Distribution of bending moment along the centre lines of clamped square plates under uniform transverse pressure.

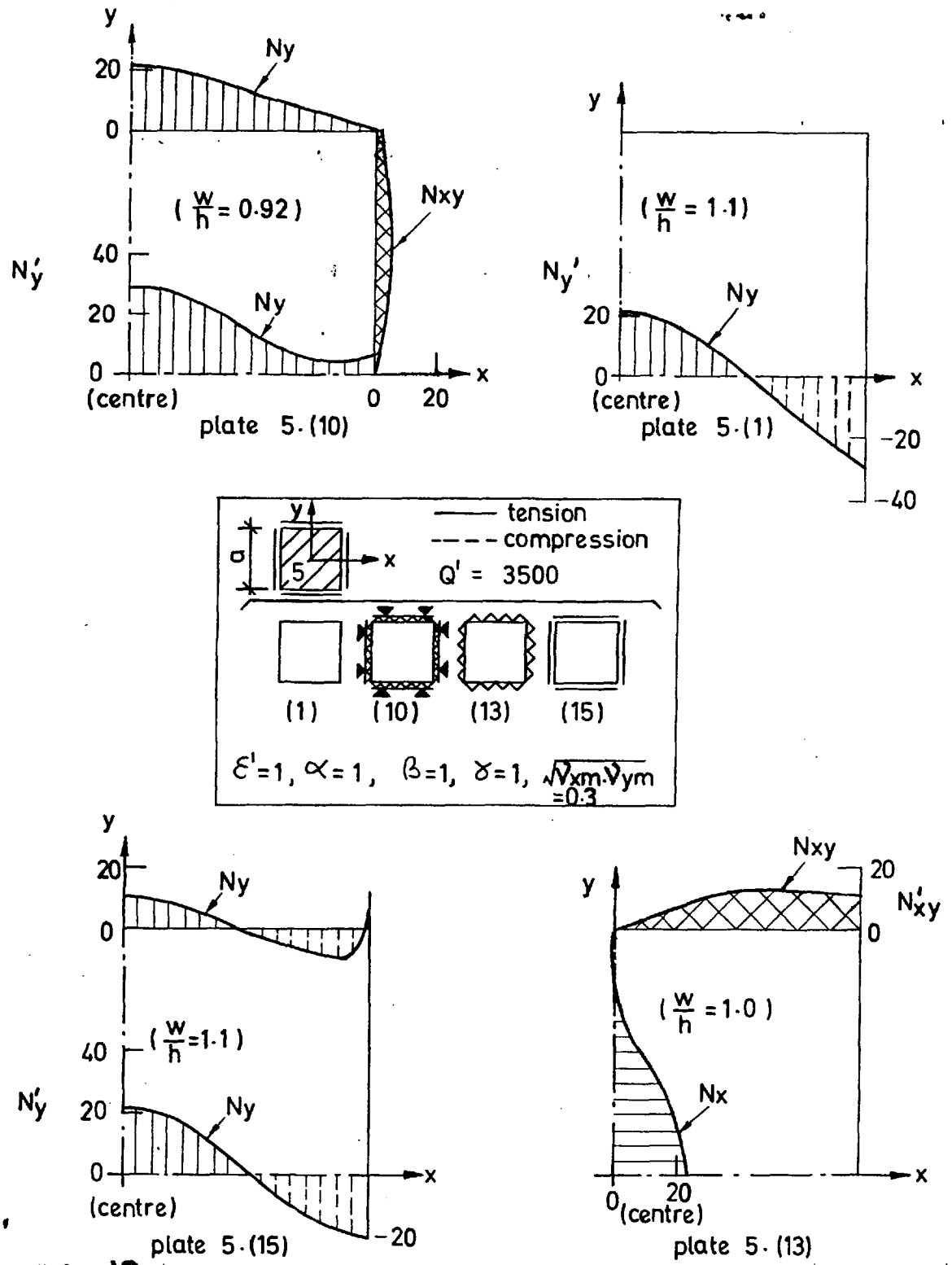


FIG. 12 Distribution of membrane stress along the centre lines and the boundaries of clamped plates under uniform transverse pressure.

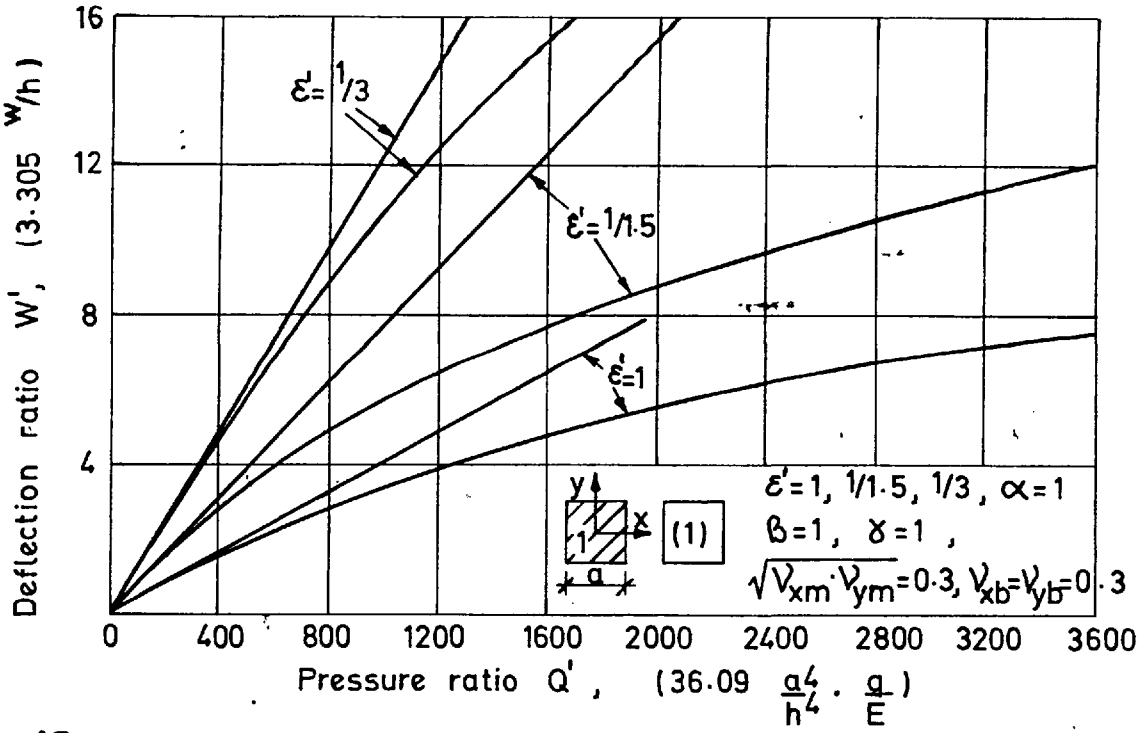


FIG. 13 Deflection at the centre of simply supported plates under uniform transverse pressure. (variation of aspect ratio.)

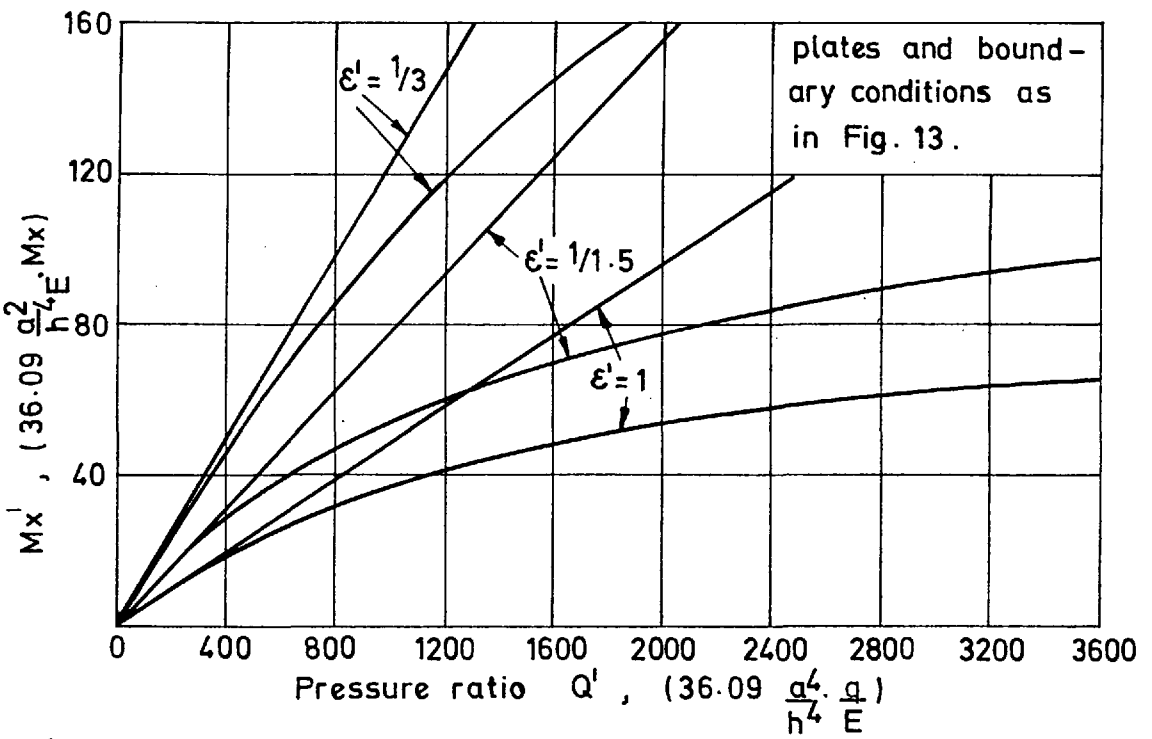


FIG. 14 Bending moment at the centre of simply supported plates under uniform transverse pressure. (variation of aspect ratio)

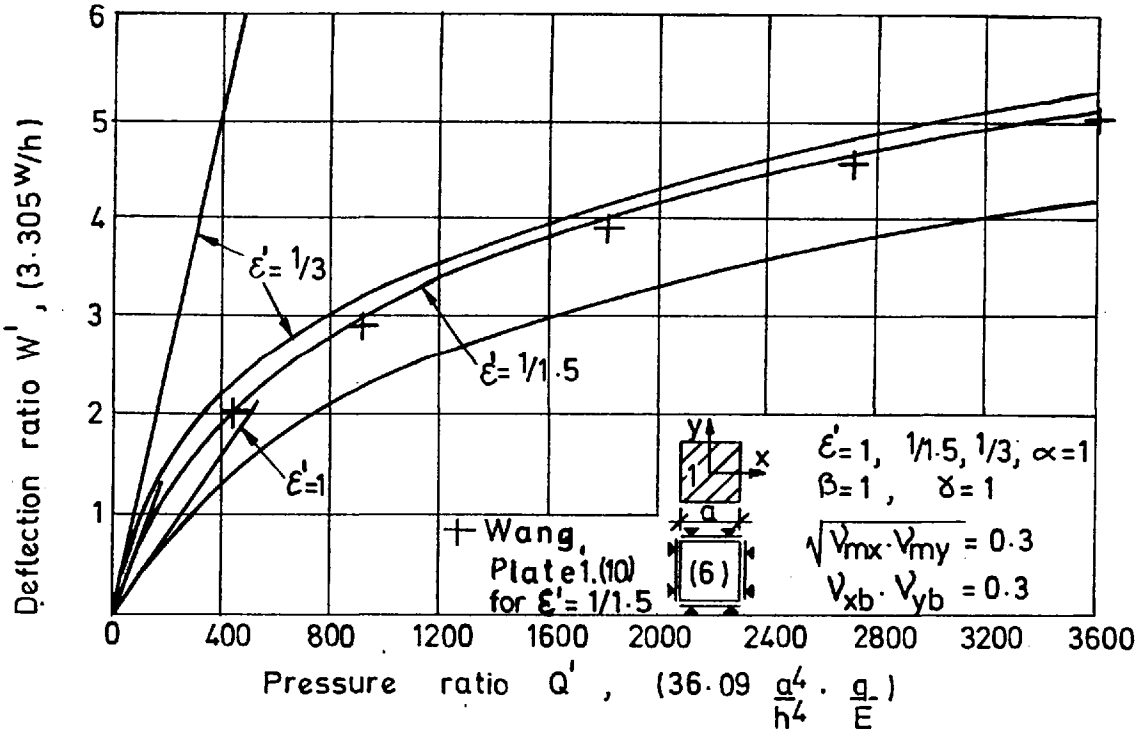


FIG. **15** Deflection at the centre of simply supported plates under uniform transverse pressure. (variation of aspect ratio.)

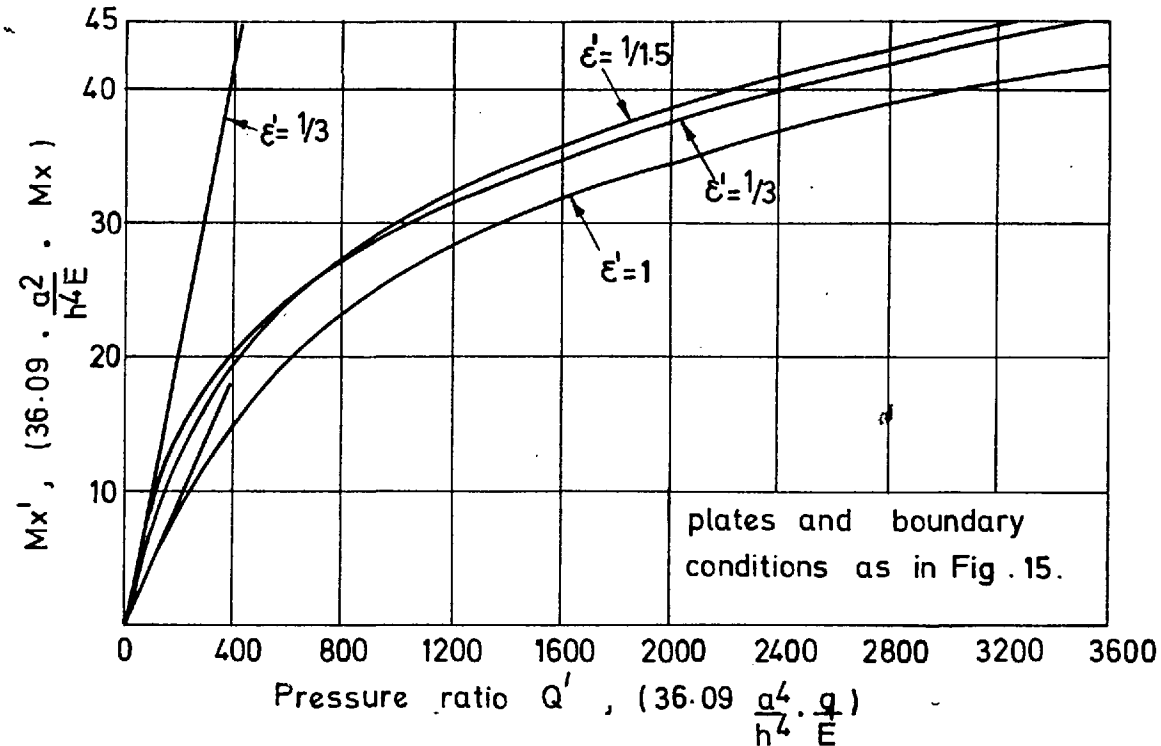


FIG **16** Bending at the centre of simply supported plates under uniform transverse pressure. (variation of aspect ratio.)

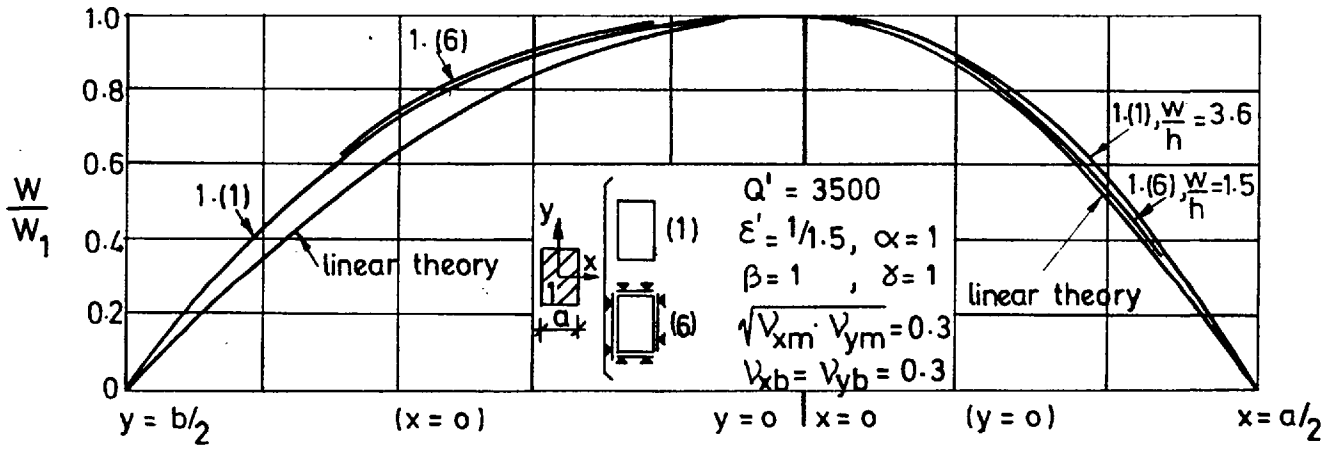


FIG. 17 Deflection profiles along the centre lines of simply supported plates under uniform transverse pressure ($\varepsilon' = 1/1.5$)

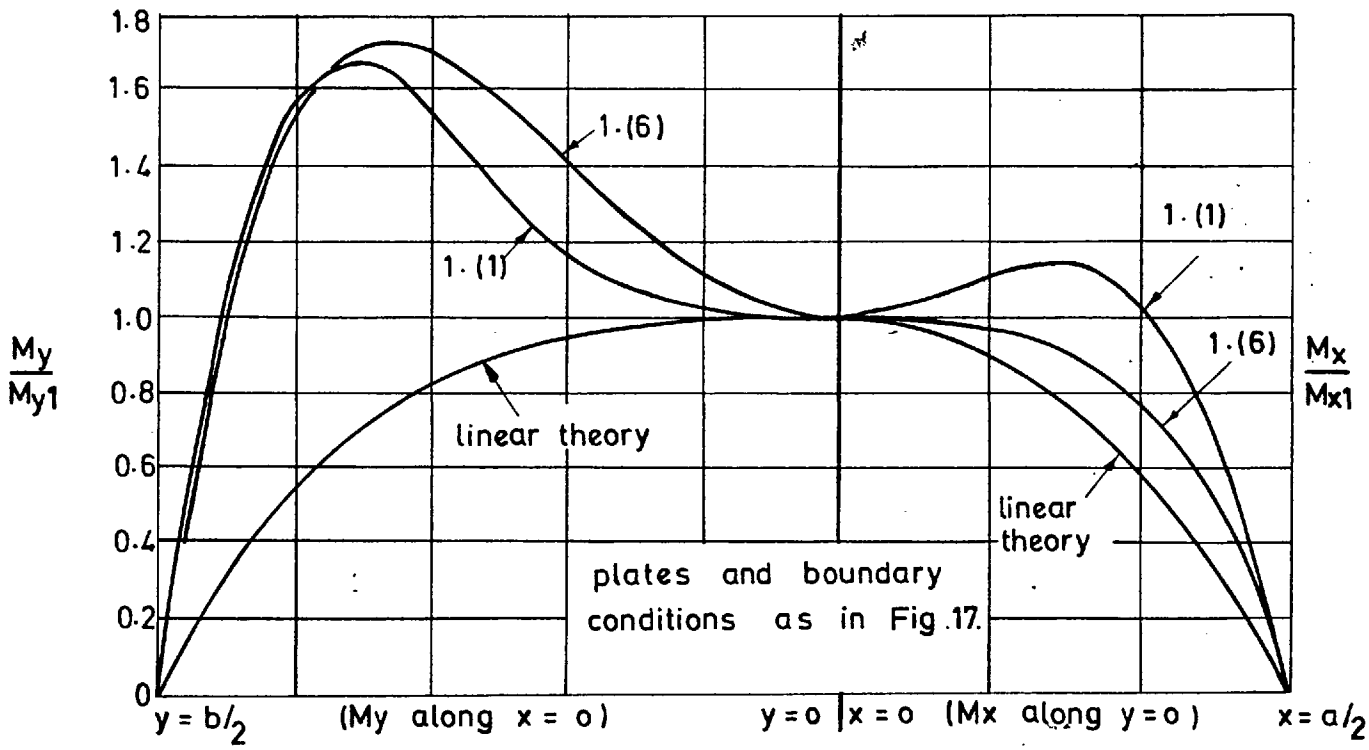


FIG. 18 Bending moment profiles along the centre lines of simply supported plates under uniform transverse pressure ($\varepsilon = 1/1.5$)

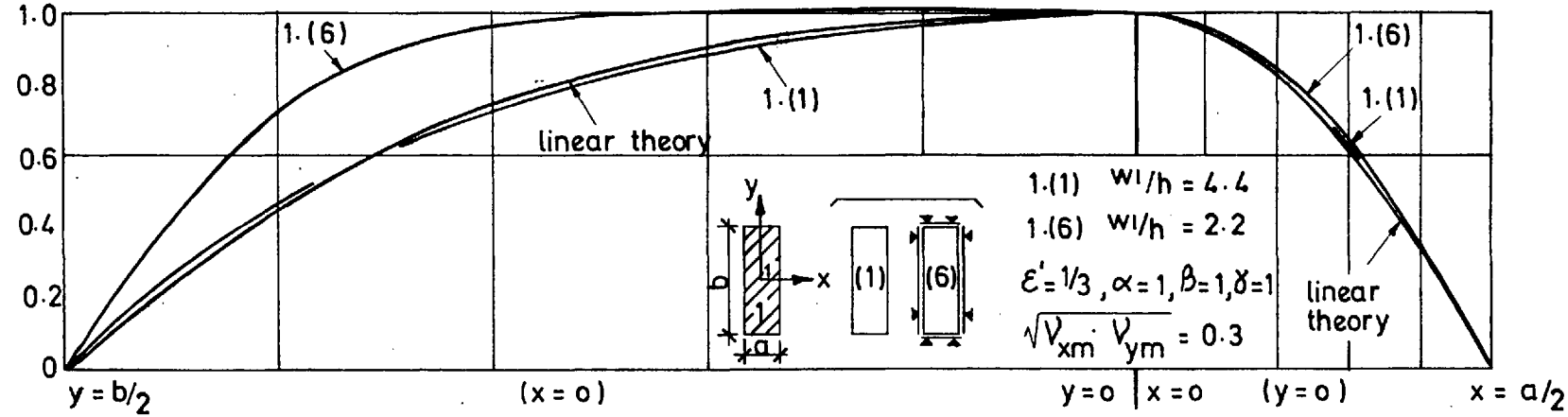


FIG. 19 Deflection profiles along the centre lines of simply supported plates under uniform transverse pressure ($\varepsilon' = 1/3$)

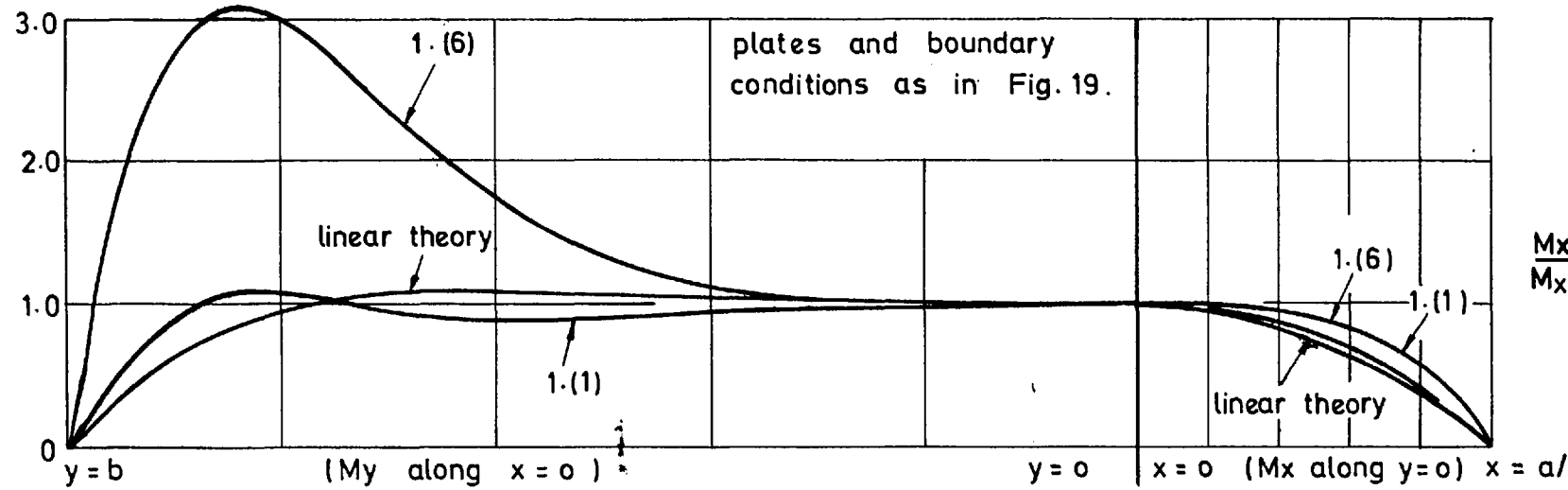


FIG. 20 Bending moment profiles along the centre lines of simply supported plates under uniform transverse pressure ($\varepsilon = 1/1.5$)

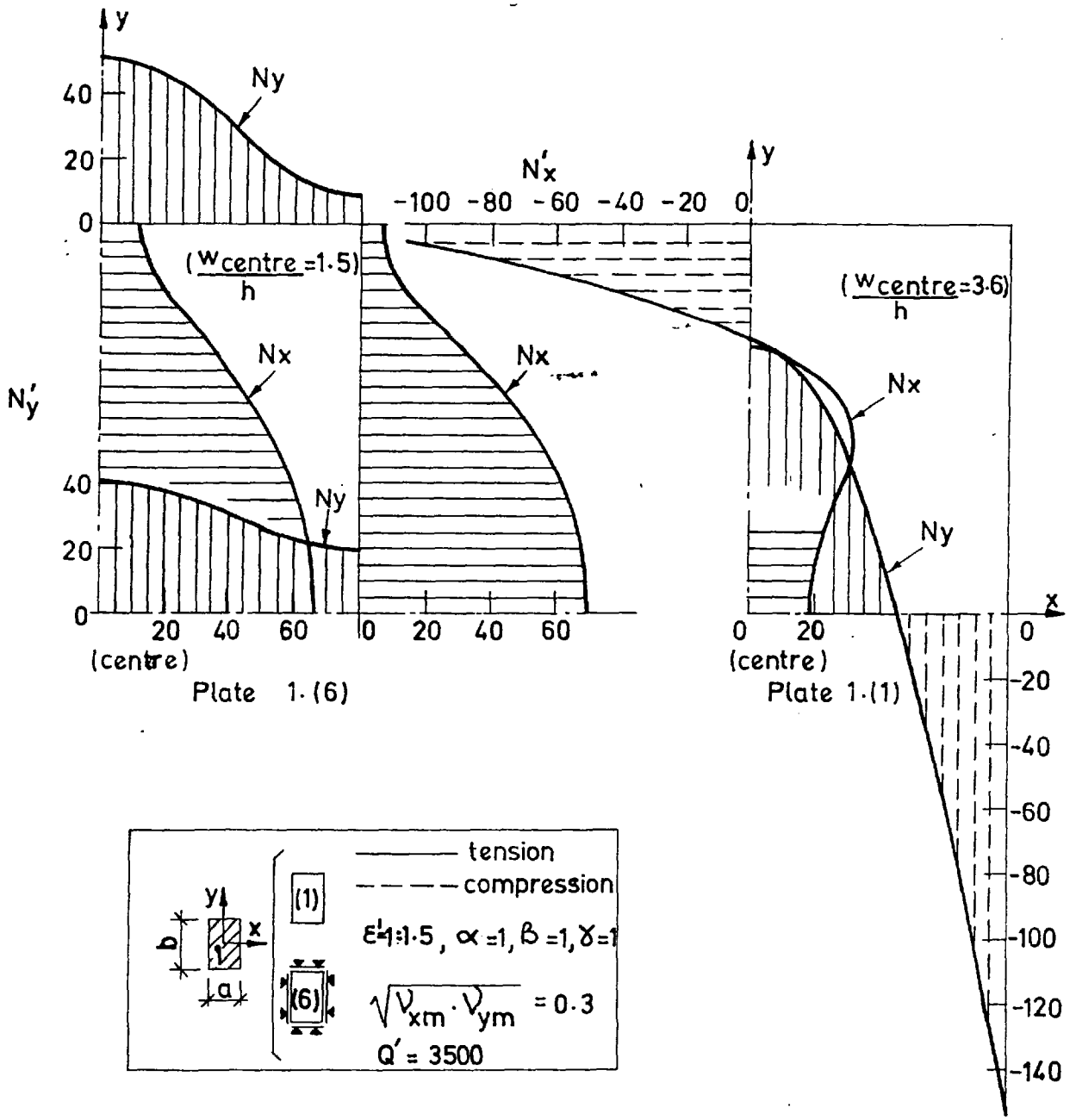


FIG. **21**. Distribution of membrane forces along the centre lines and the boundaries of simply supported plates under uniform transverse pressure ($\epsilon'=1:1.5$)

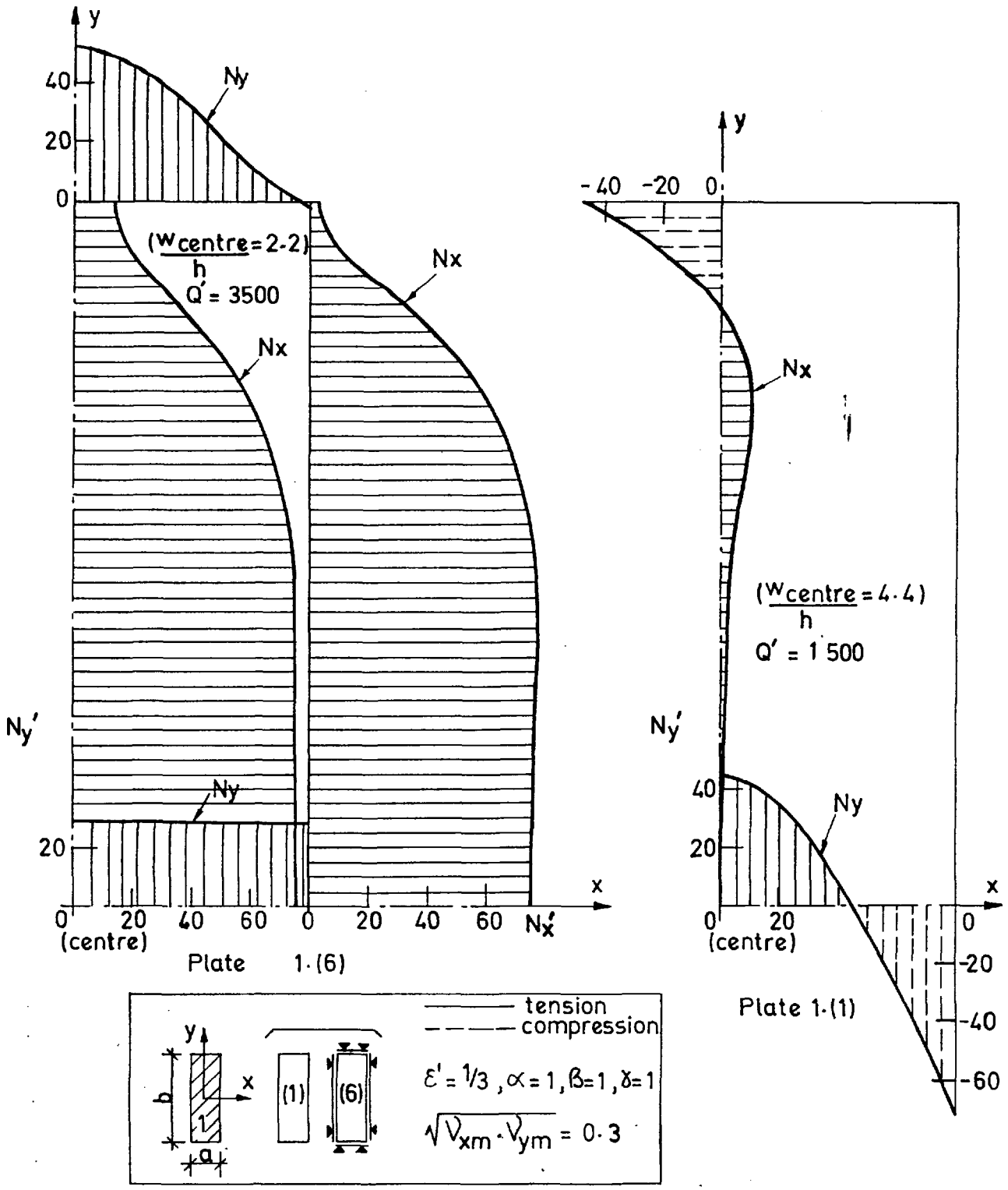


FIG. **22**. Distribution of membrane forces along the centre lines and the boundaries of simply supported plates under uniform transverse pressure ($\varepsilon' = 1/3$)

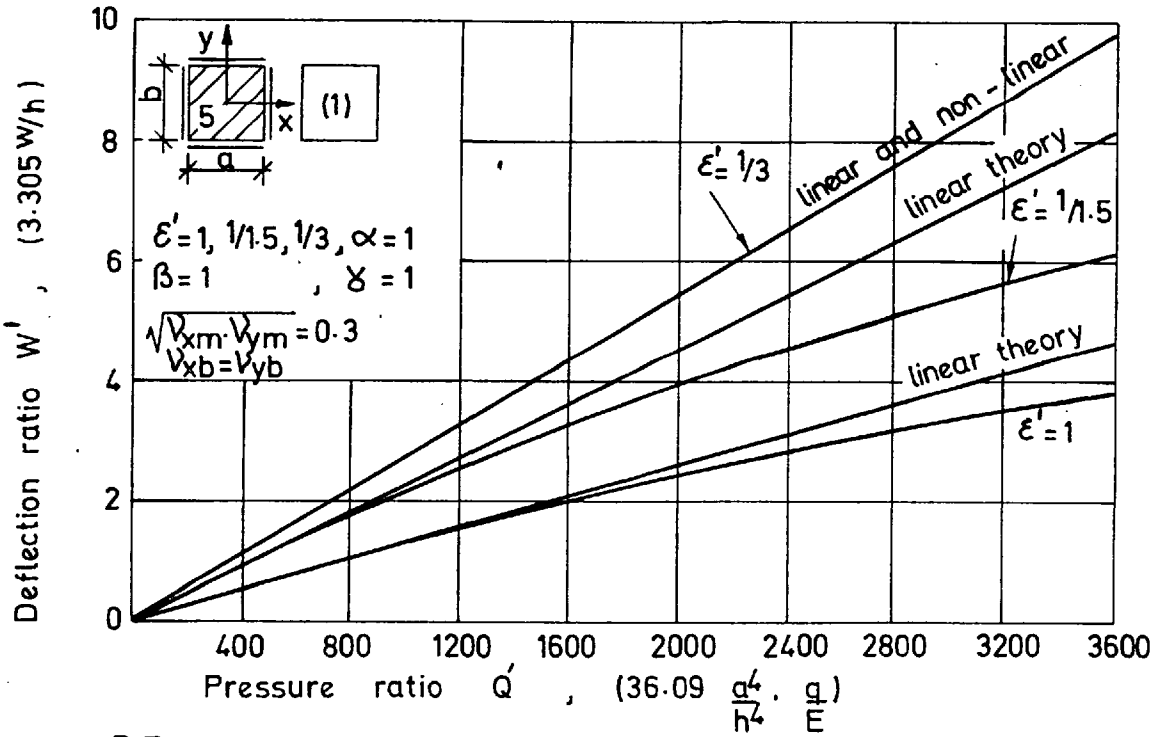


FIG. **23** Deflection at the centre of clamped plates under uniform transverse pressure. (variation of aspect ratio)

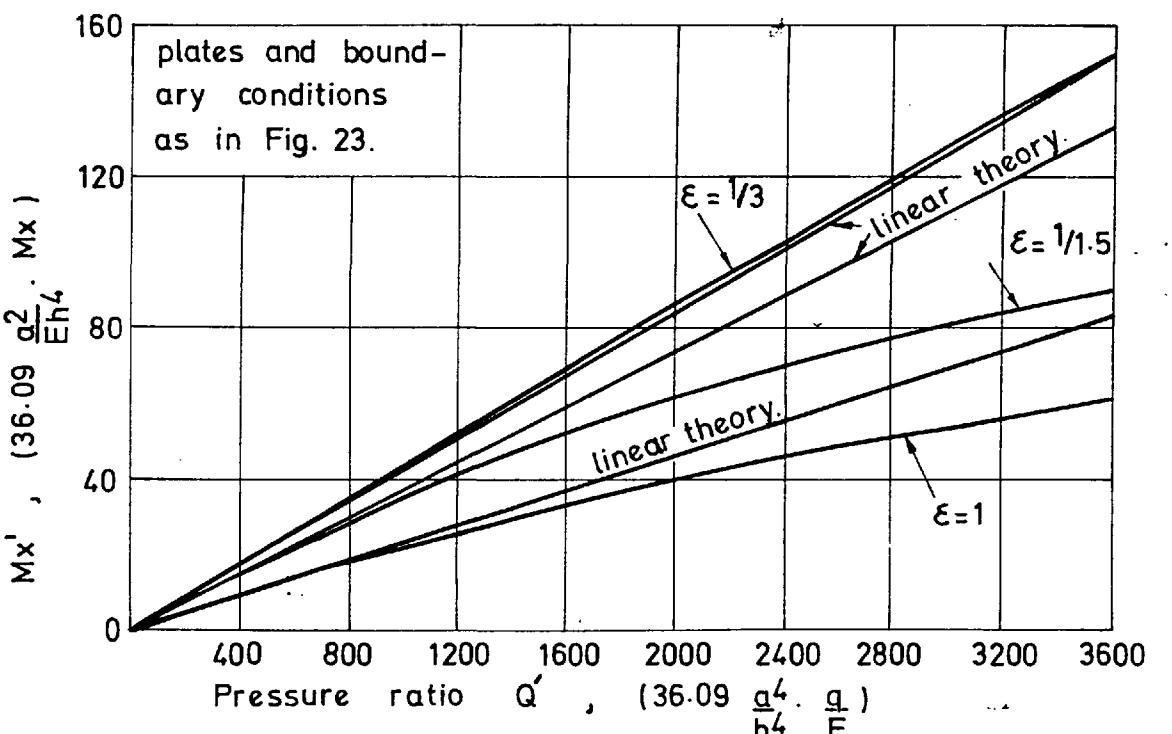


FIG. **24** Bending moment at the centre of clamped plates under uniform transverse pressure. (variation of aspect ratio)

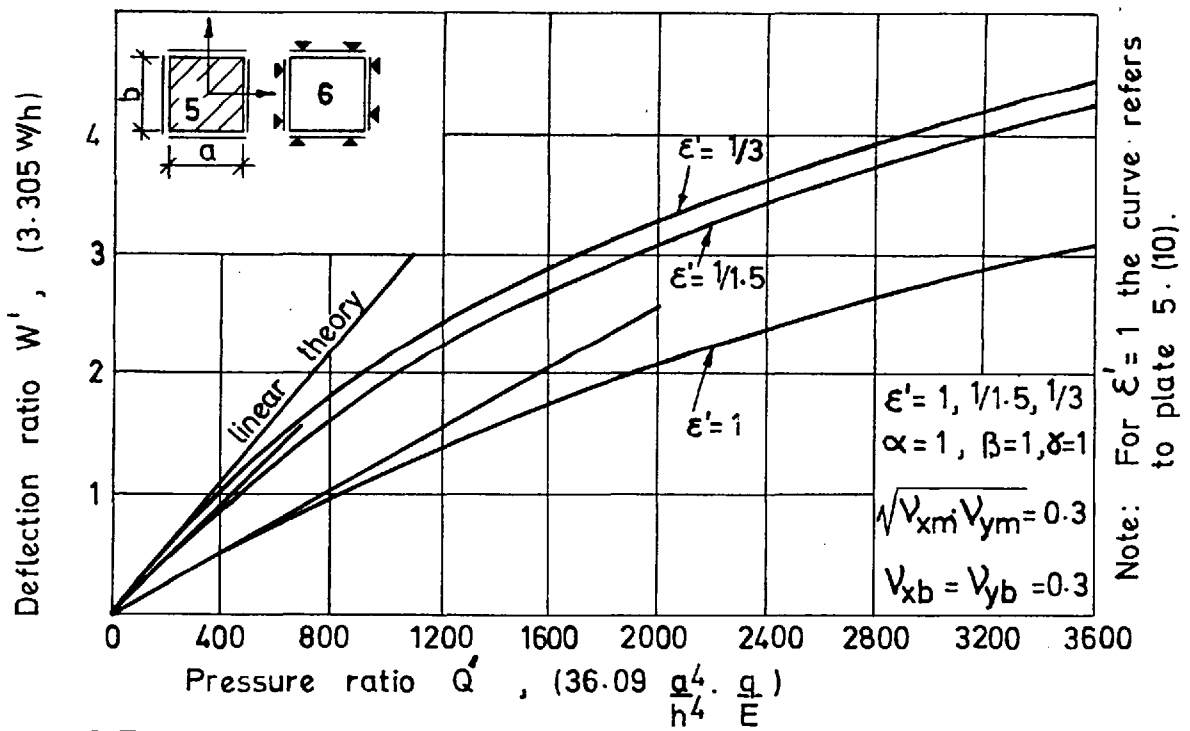


FIG. **25** Deflection at the centre of clamped plates under uniform transverse pressure. (variation of aspect ratio)

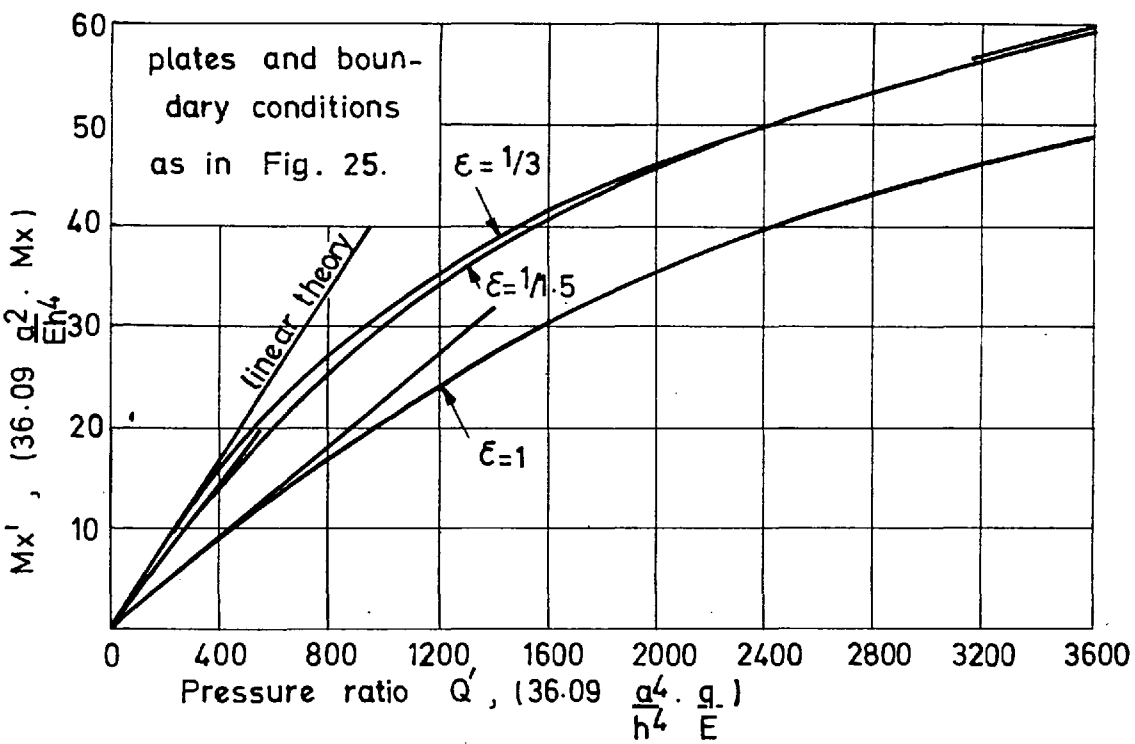


FIG. **26** Bending moment at the centre of clamped plates under uniform transverse pressure. (variation of aspect ratio)

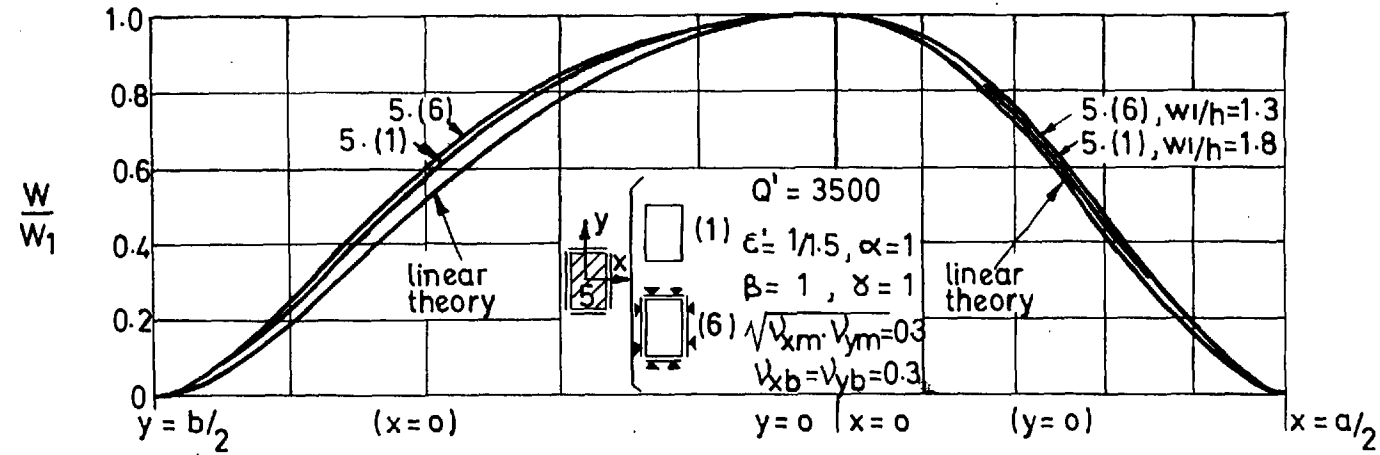


FIG. **27** Deflection profiles along the centre lines of clamped plates under uniform transverse pressure ($\varepsilon' = 1/1.5$)

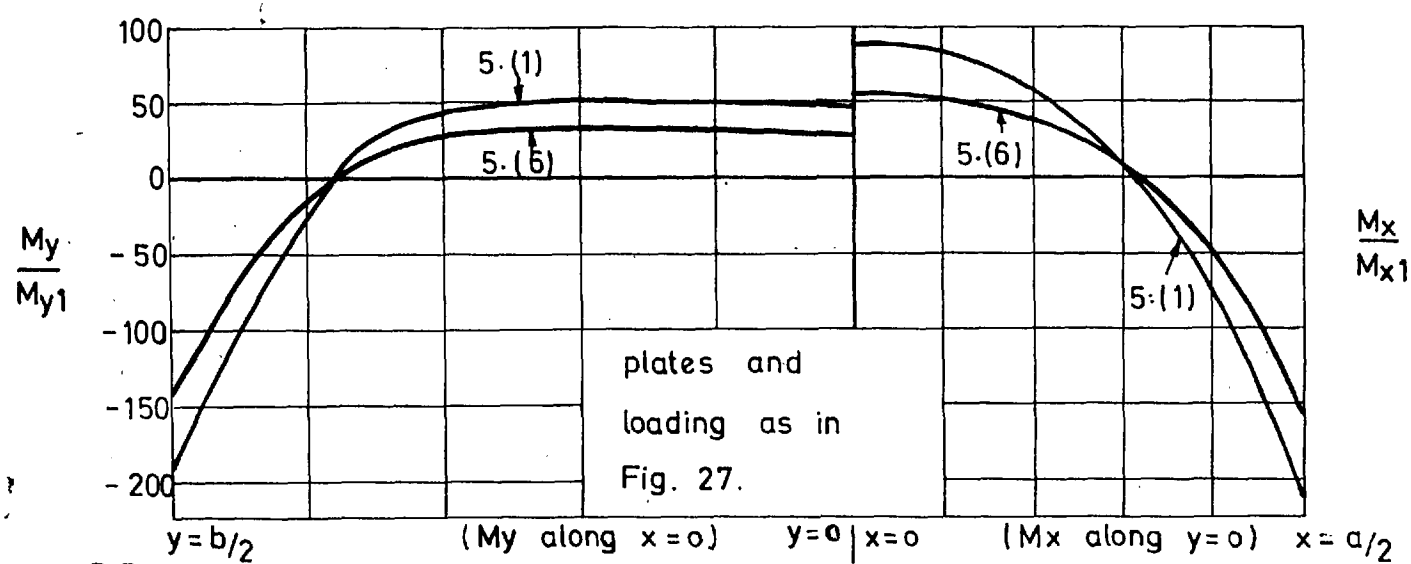


FIG. **28** Bending moment profiles along the centre lines of clamped plates under uniform transverse pressure ($\varepsilon = 1/1.5$)

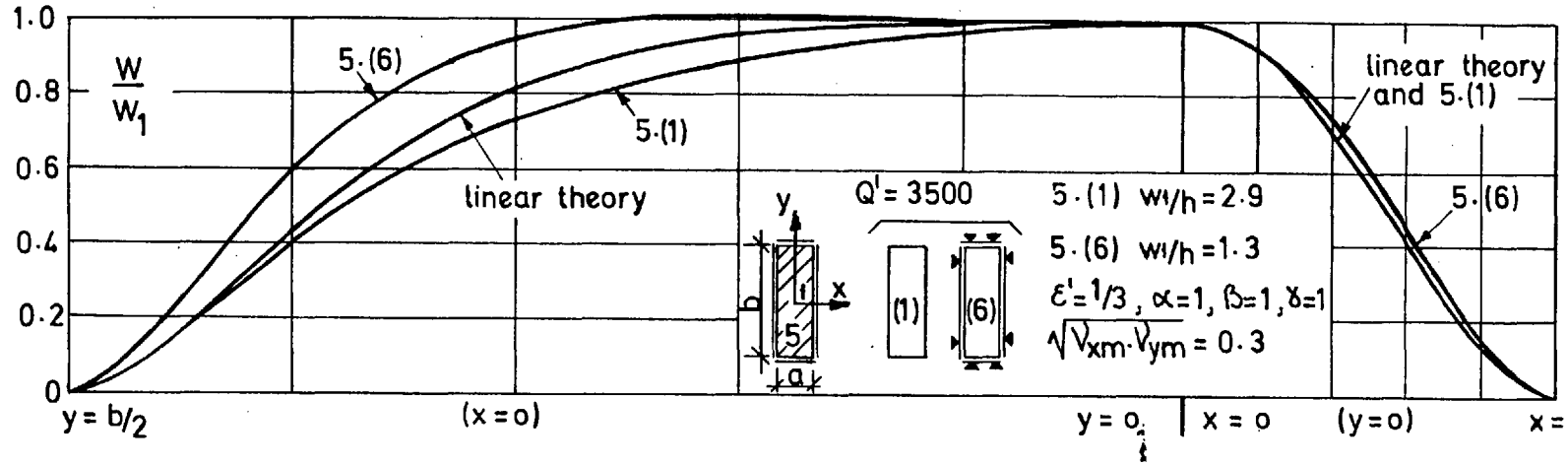


FIG. 29 Deflection profiles

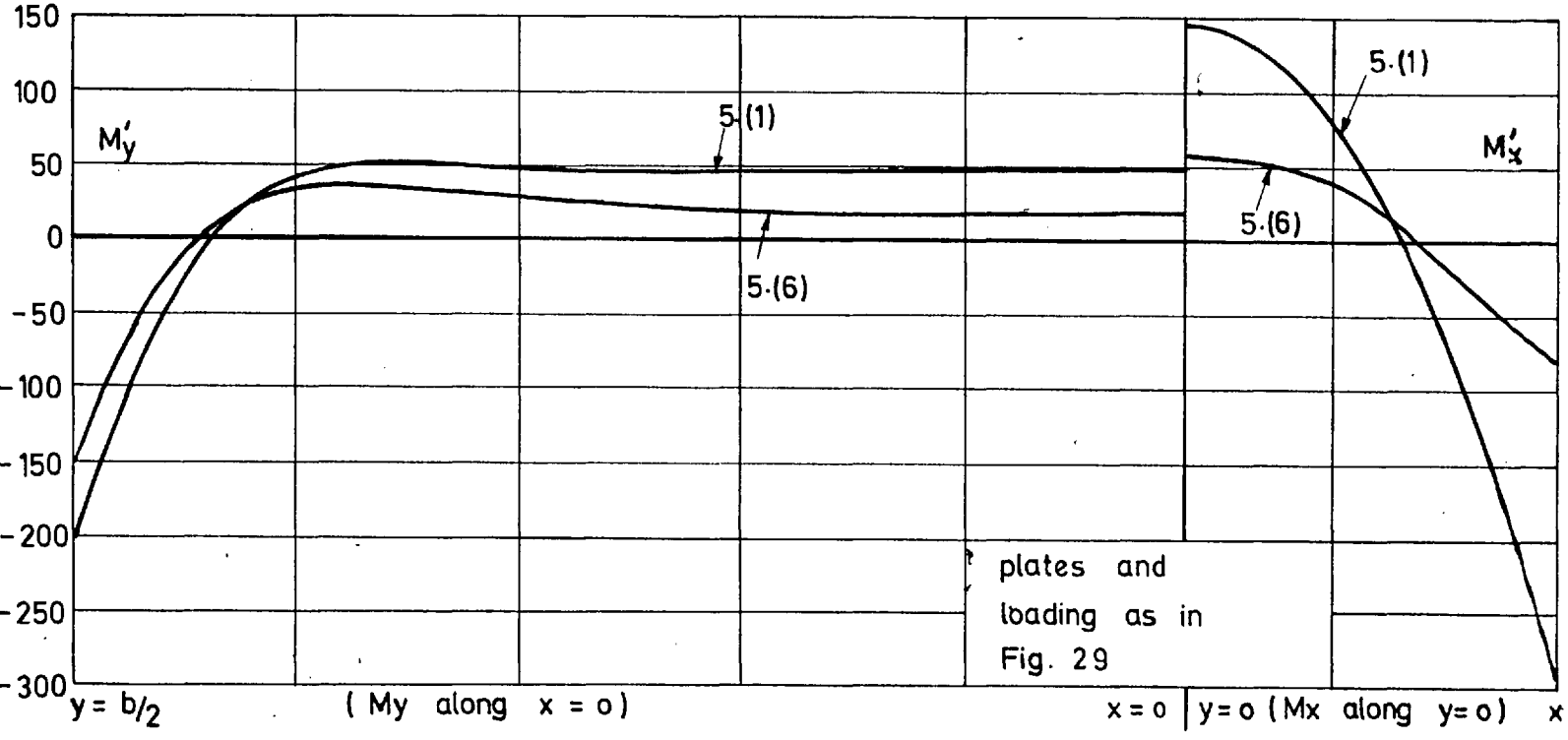


FIG. 30 Distribution of bending moment.

Deflection and bending moment profiles along the centre lines of clamped plates under uniform transverse pressure ($\epsilon = 1/3$)

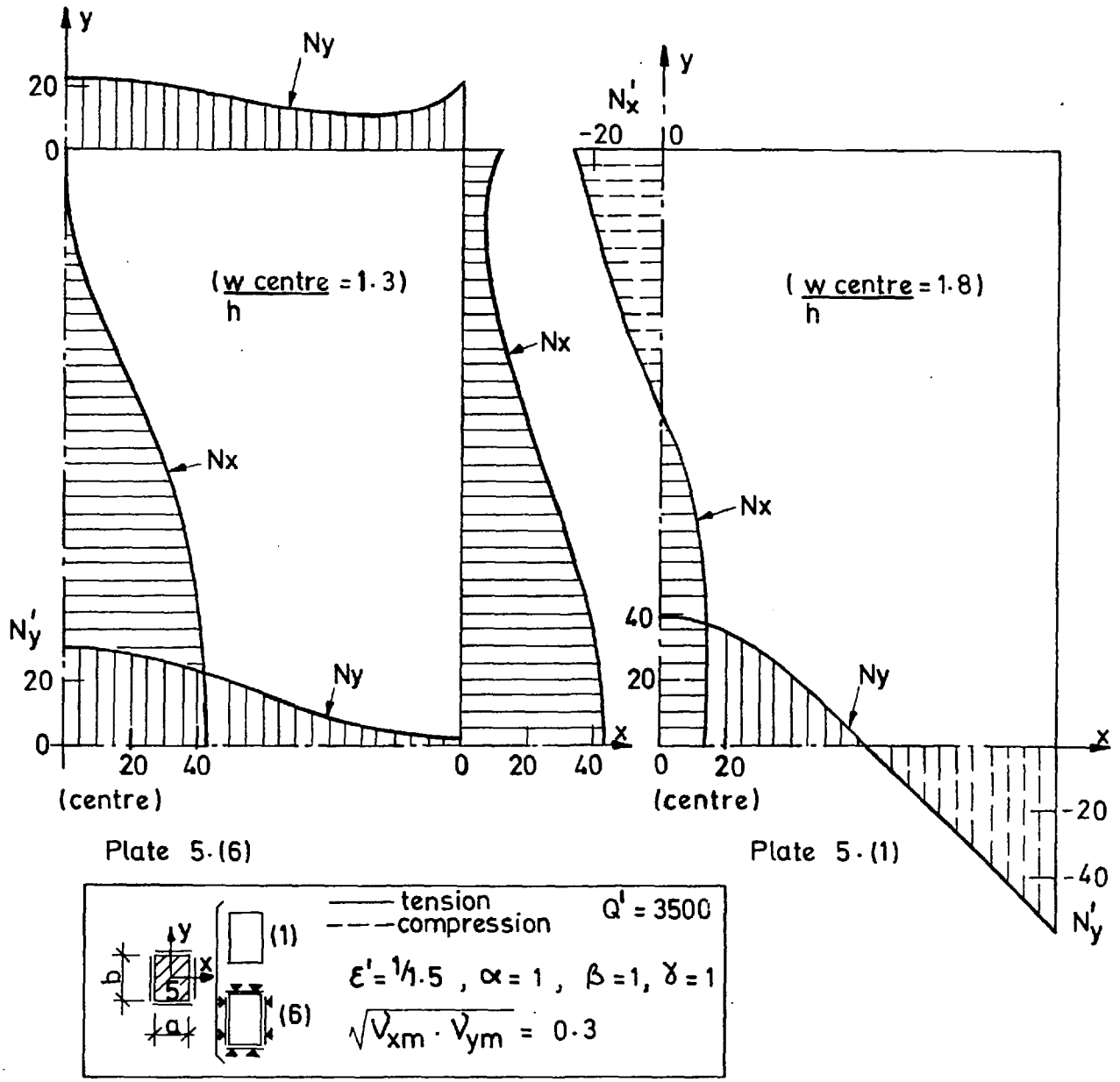


FIG. **31** Distribution of membrane forces along the centre lines and the boundaries of clamped plates under uniform transverse pressure ($\varepsilon' = 1/1.5$.)

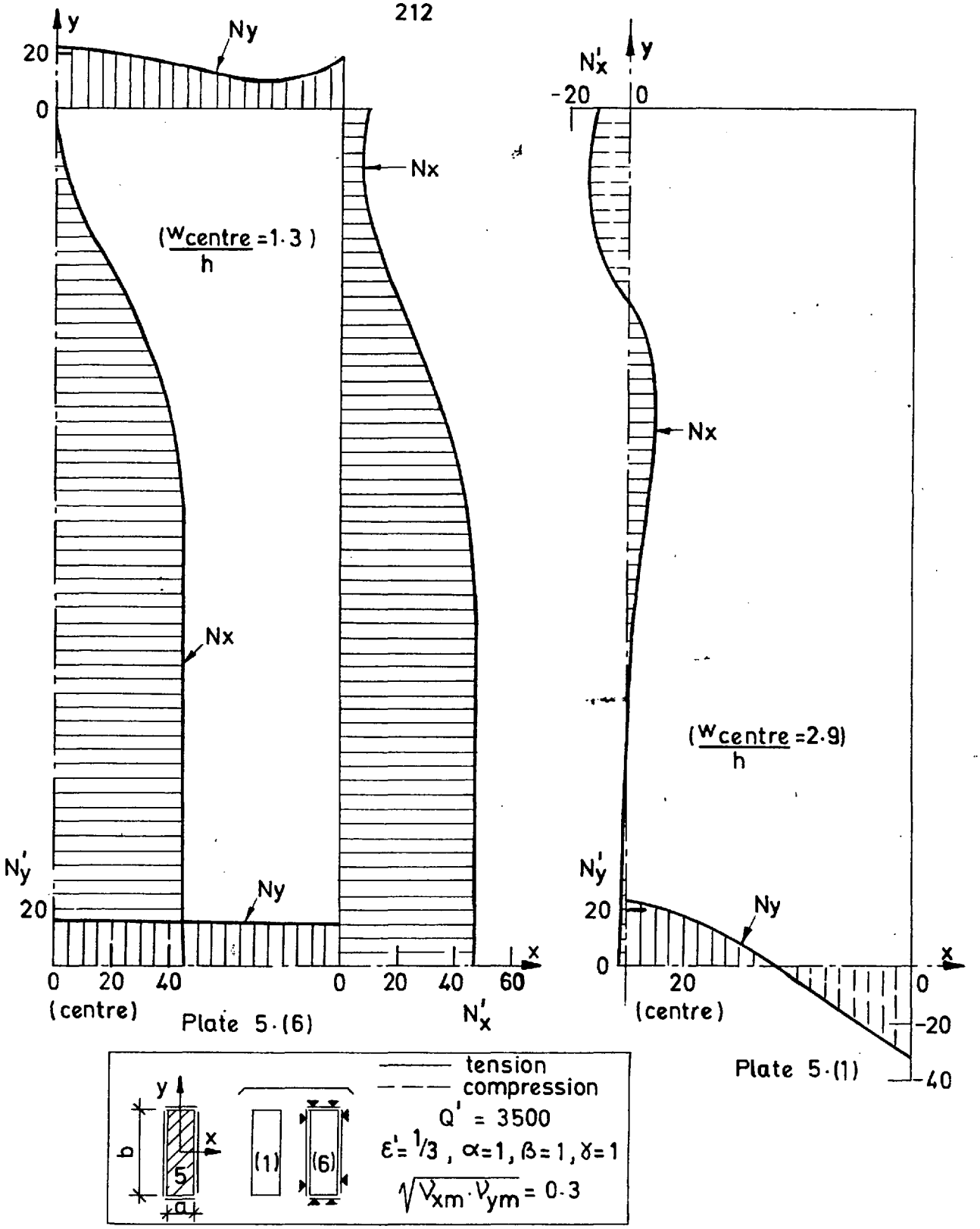


FIG. **32** Distribution of membrane forces along the centre lines and boundaries of clamped plates under uniform transverse pressure ($\varepsilon' = 1/3$)

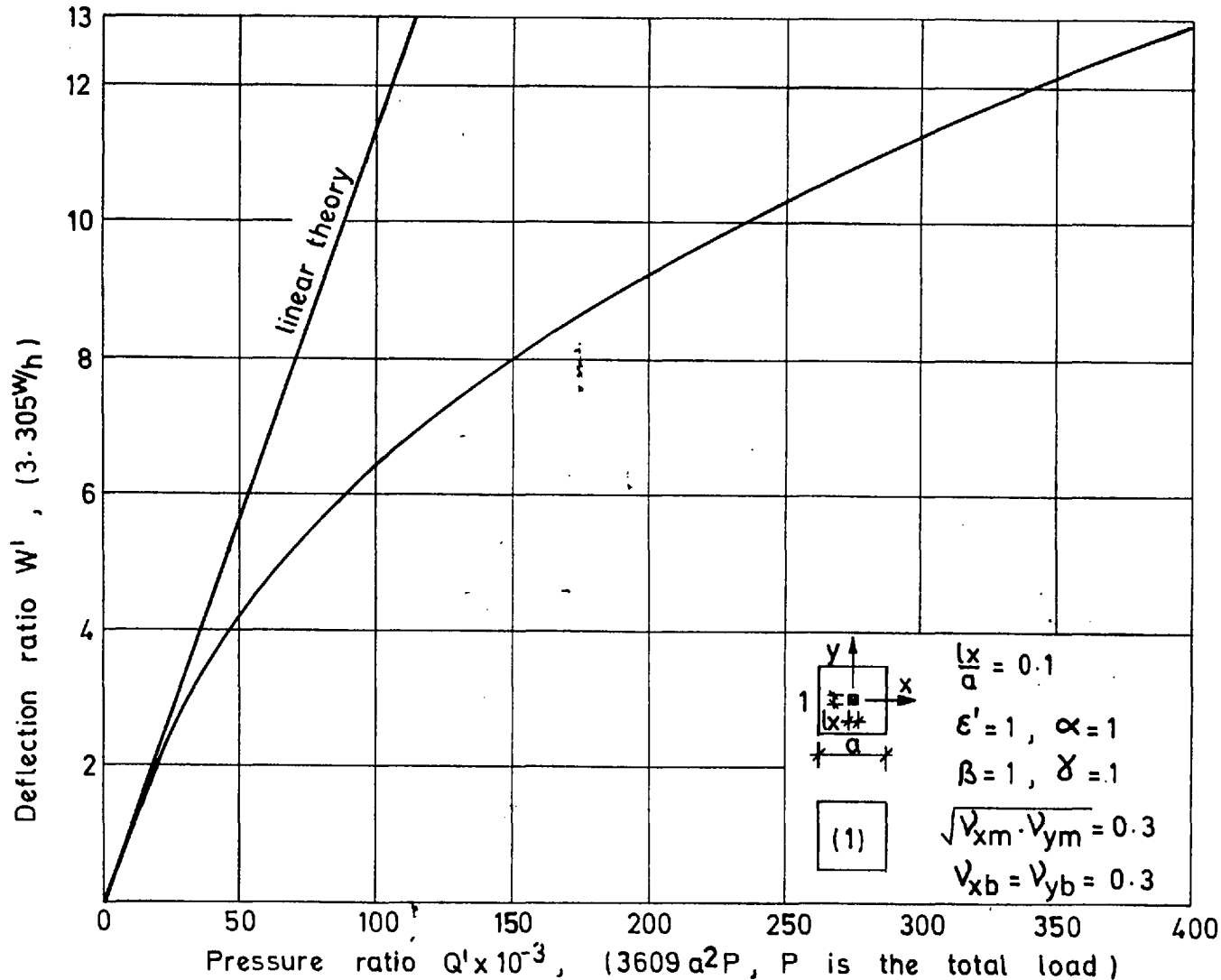


FIG. **33** Deflection at the centre of a simply supported plate under a central patch load ($\frac{lx}{a} = 0.1$)

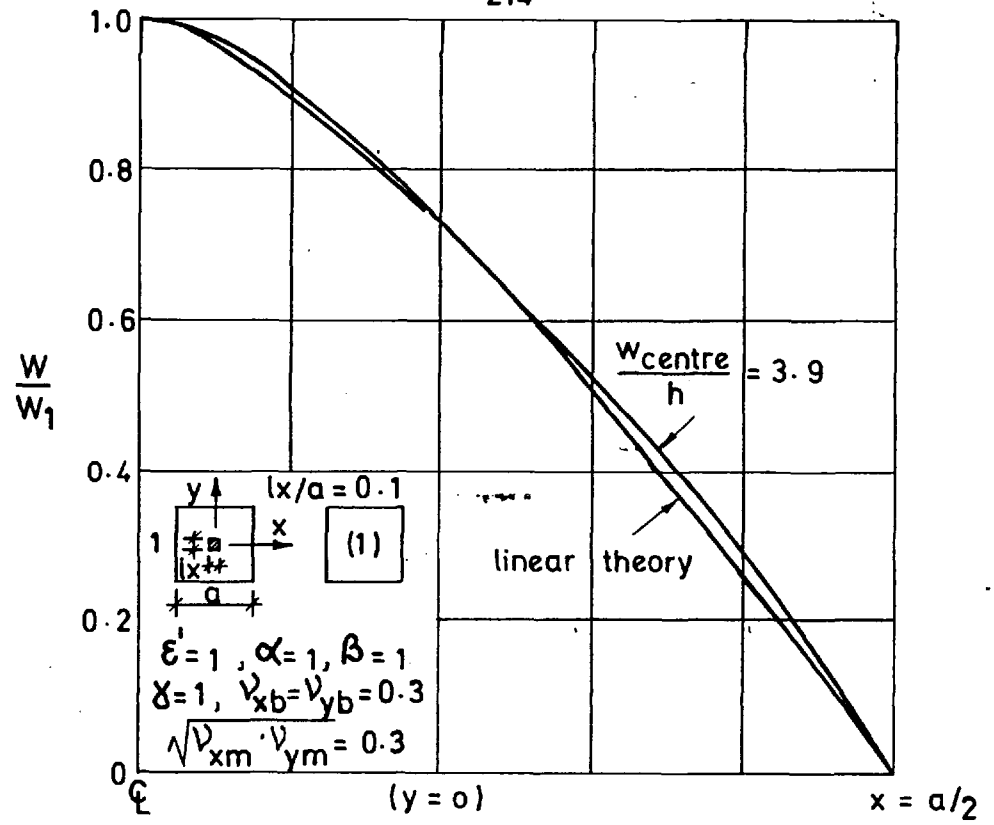


FIG. **34** Deflection profiles along the centre line of simply supported plates under a central patch load ($l_x = l_y$, $\frac{l_x}{a} = 0{\cdot}1$)

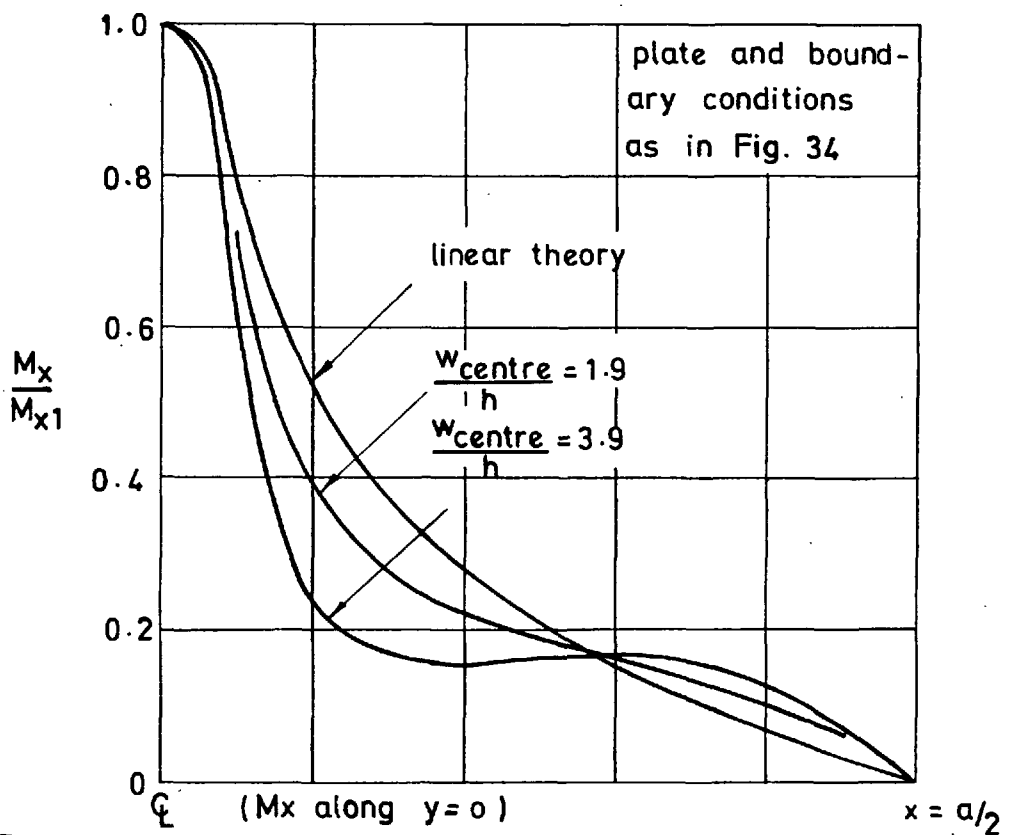


FIG. **35** Bending moment profiles along the centre line of a square simply supported plate under a central patch load.

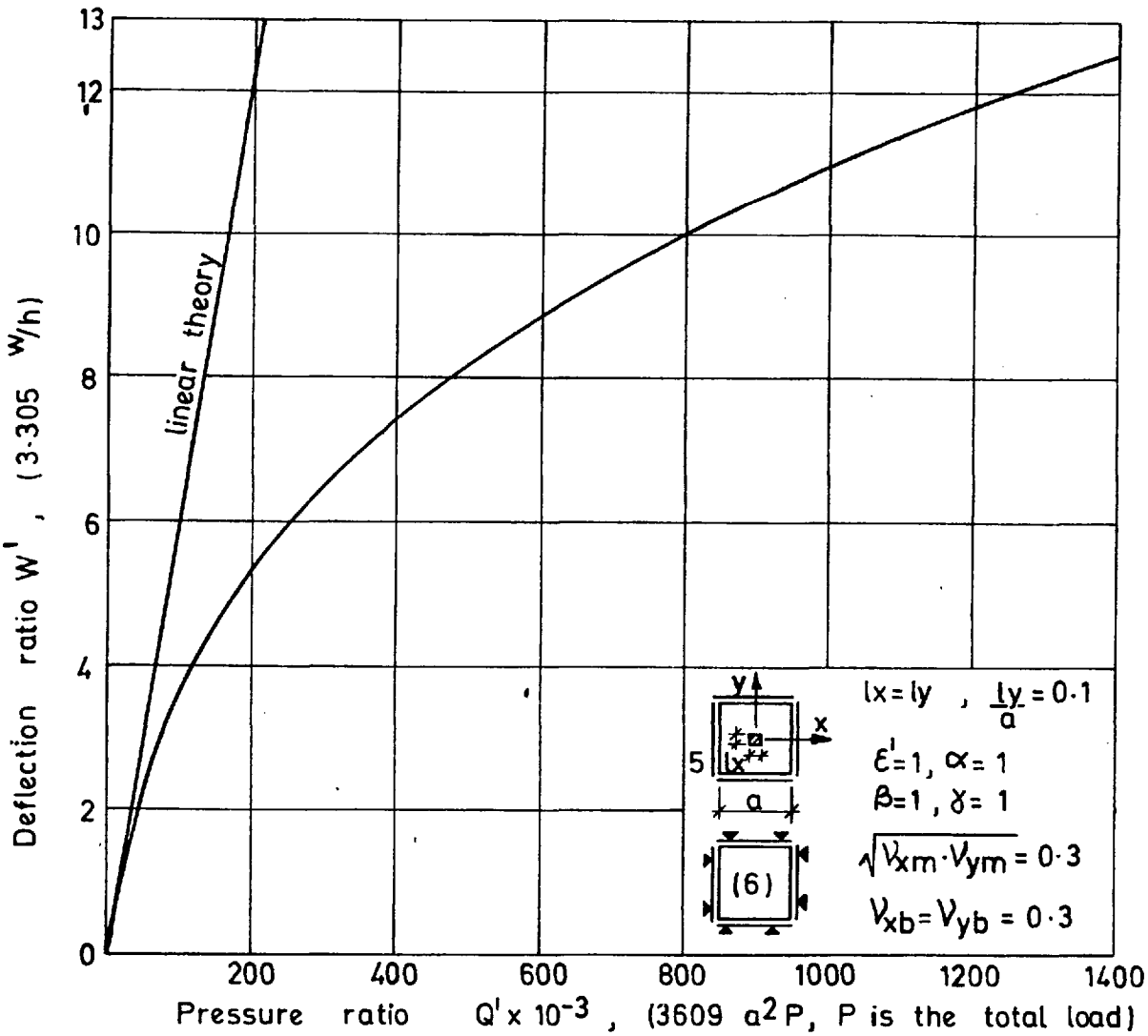


FIG. **36** Deflection at the centre of a clamped plate under a central patch load $(\frac{lx}{a} = 0{\cdot}1)$

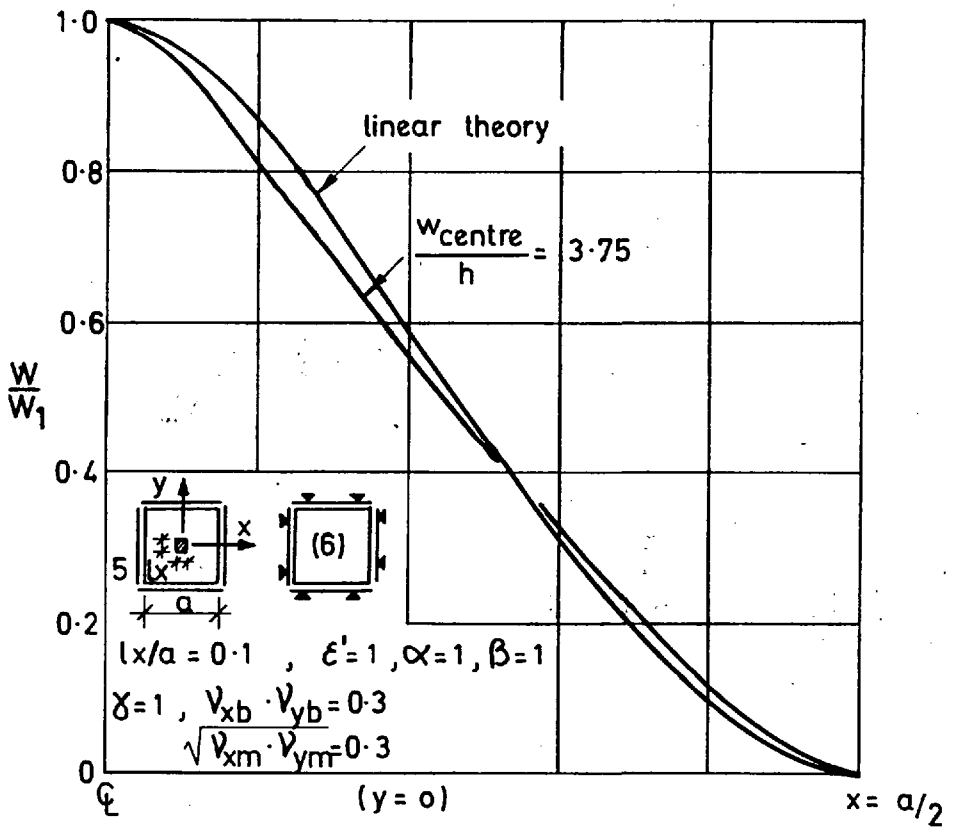


FIG. **37**. Deflection profiles along the centre lines of clamped plates under a central patch load ($l_x = l_y$, $l_x/a = 0{\cdot}1$)

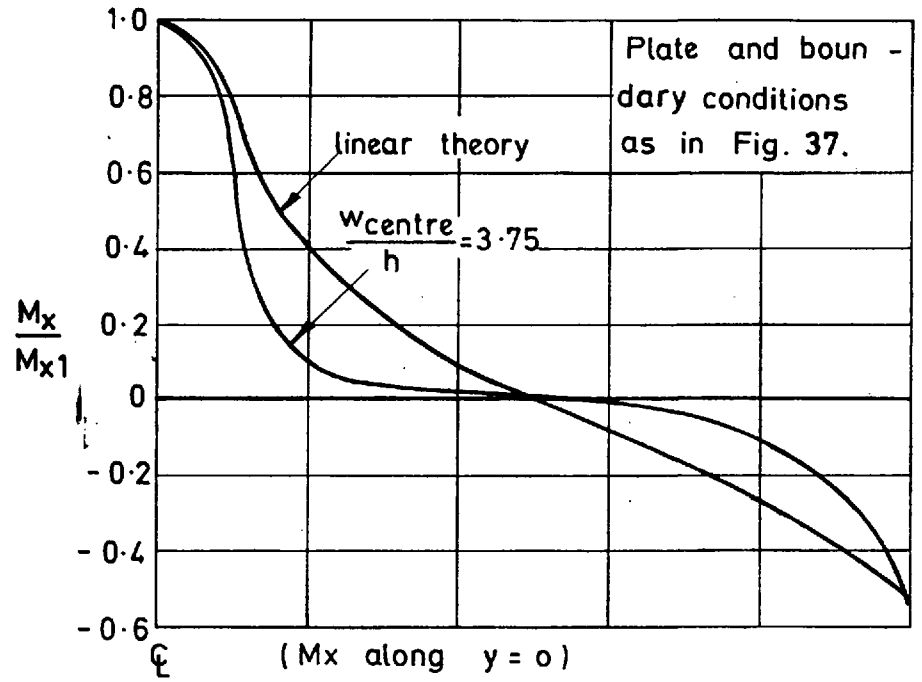


FIG. **38** Bending moment profiles along the centre line of a square clamped plate under a central patch load.

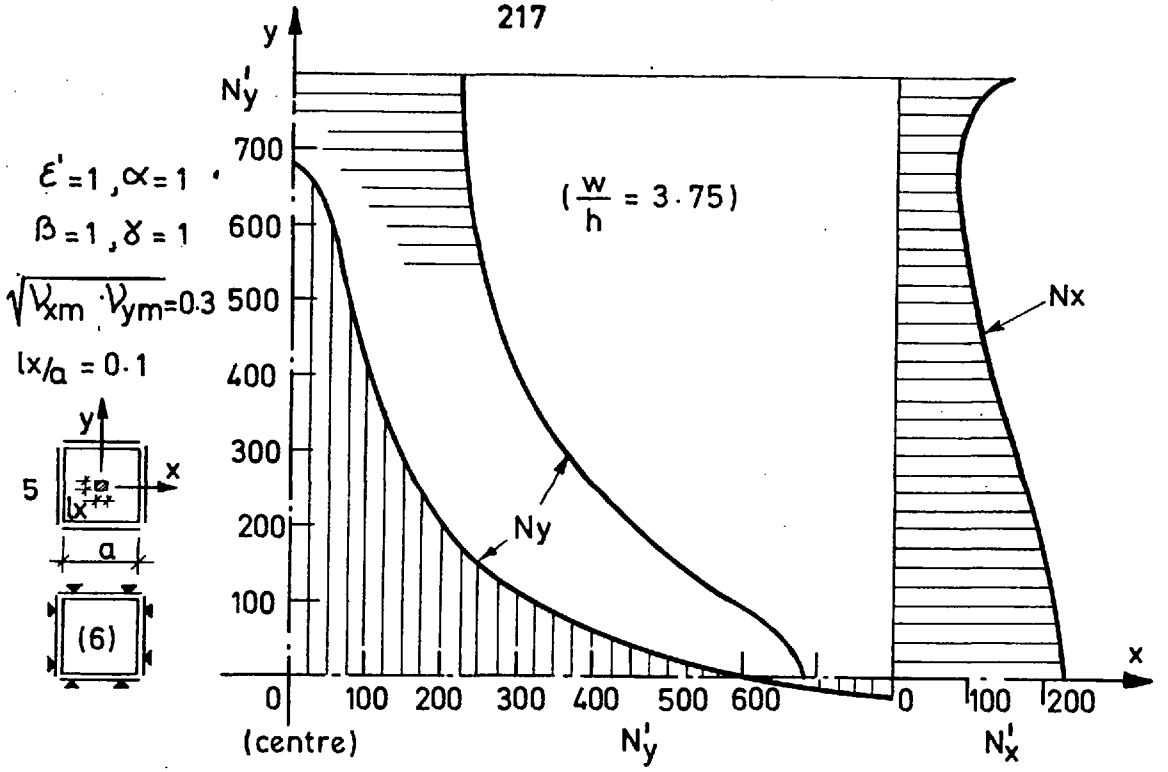


FIG. **39** Distribution of membrane stress along the centre lines and boundaries of clamped plates under a central patch load.

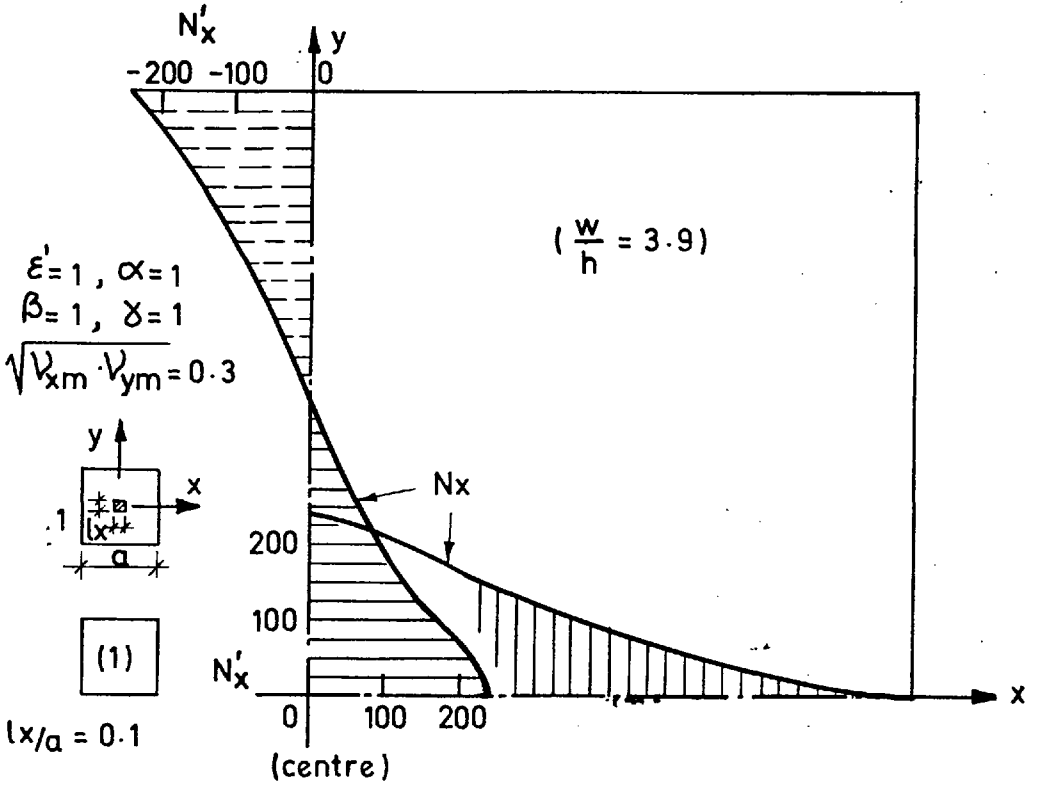


FIG. **40** Distribution of membrane stress along the centre lines of simply supported plates under a central patch load.

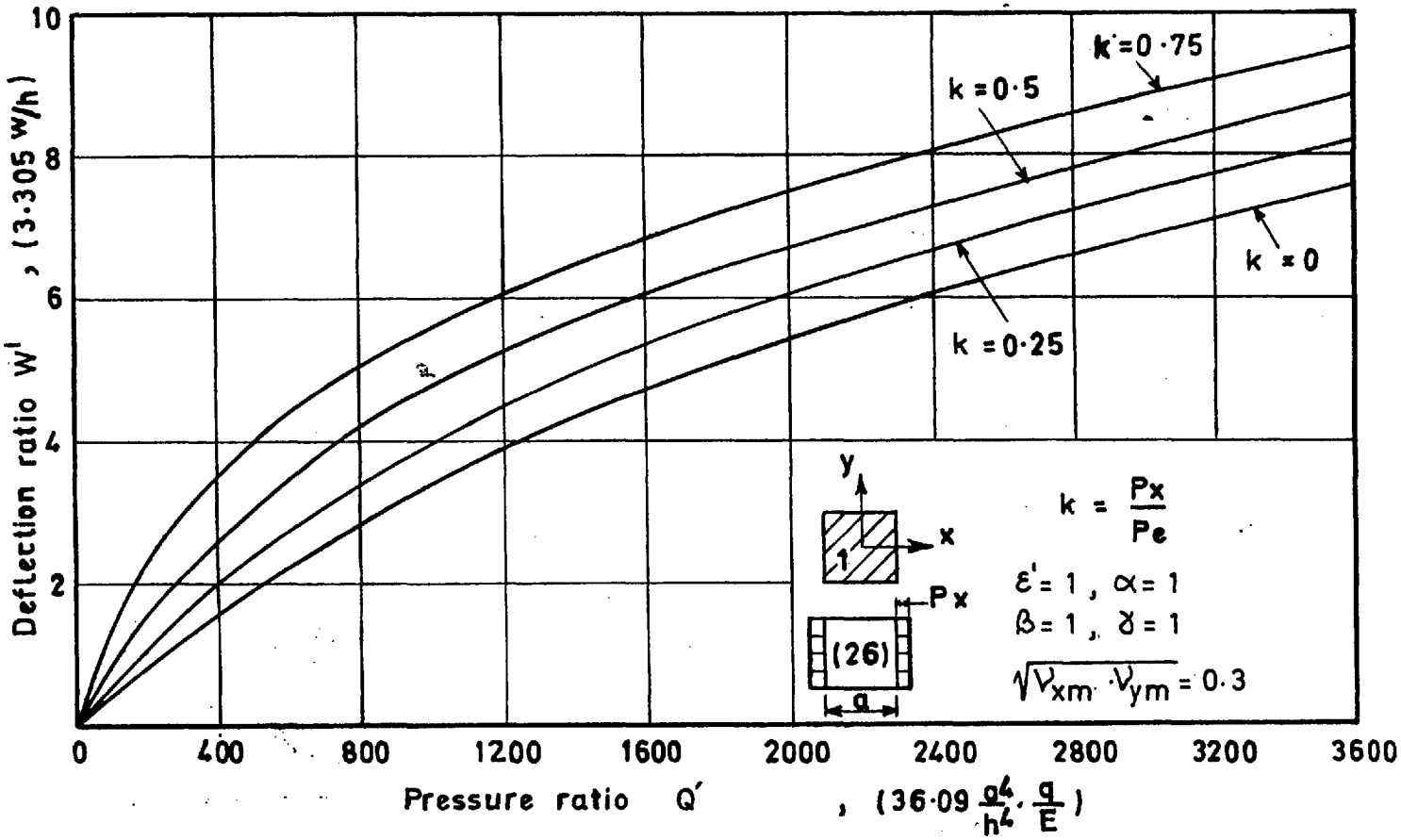


Fig. 41 Deflection at the centre of simply supported plates (Uniform edge compression plus U.D.L.)

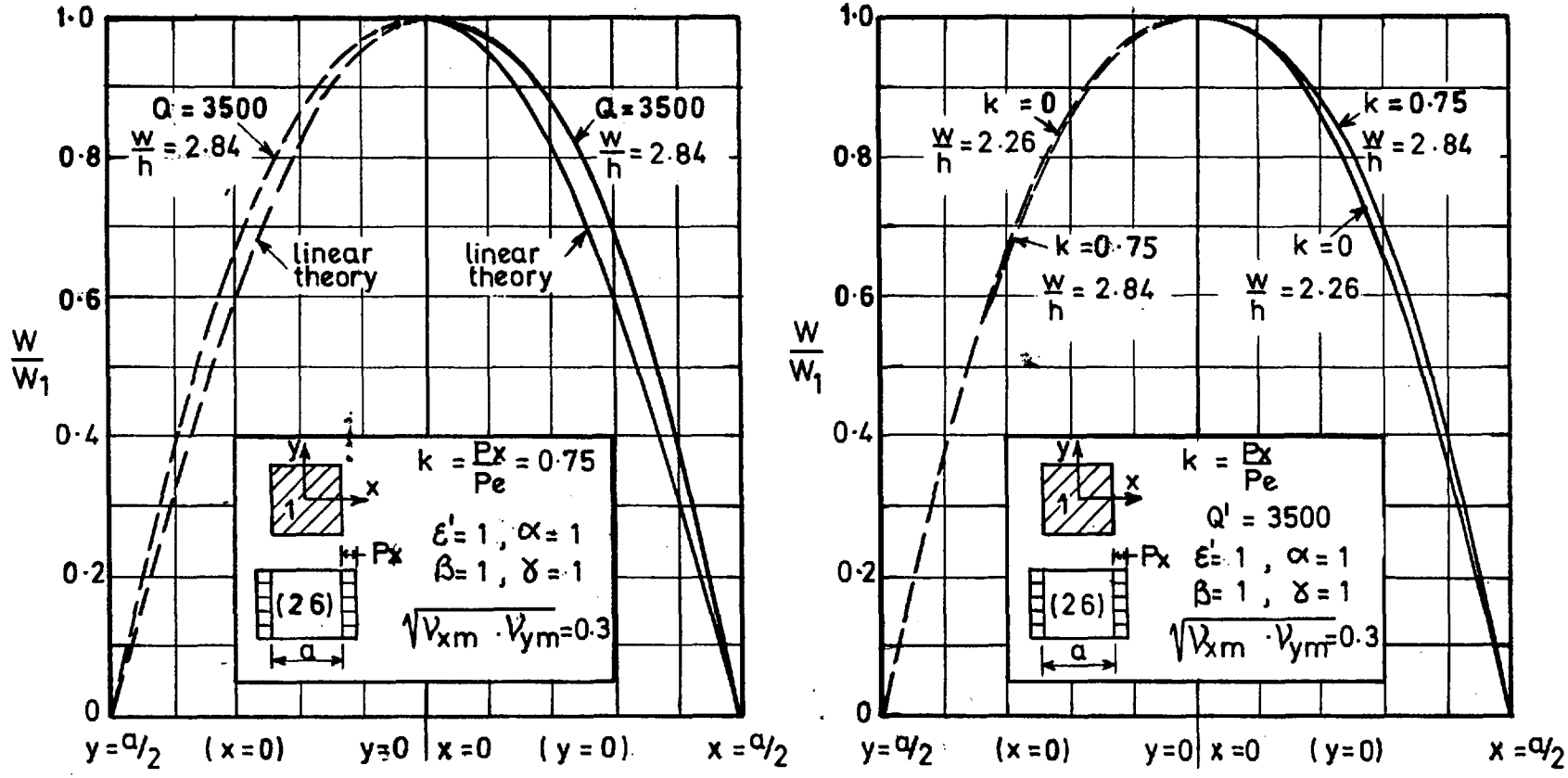


Fig. **42** Deflection profiles along the centre lines of simply supported plates (Uniform edge compression plus U.D.L.)

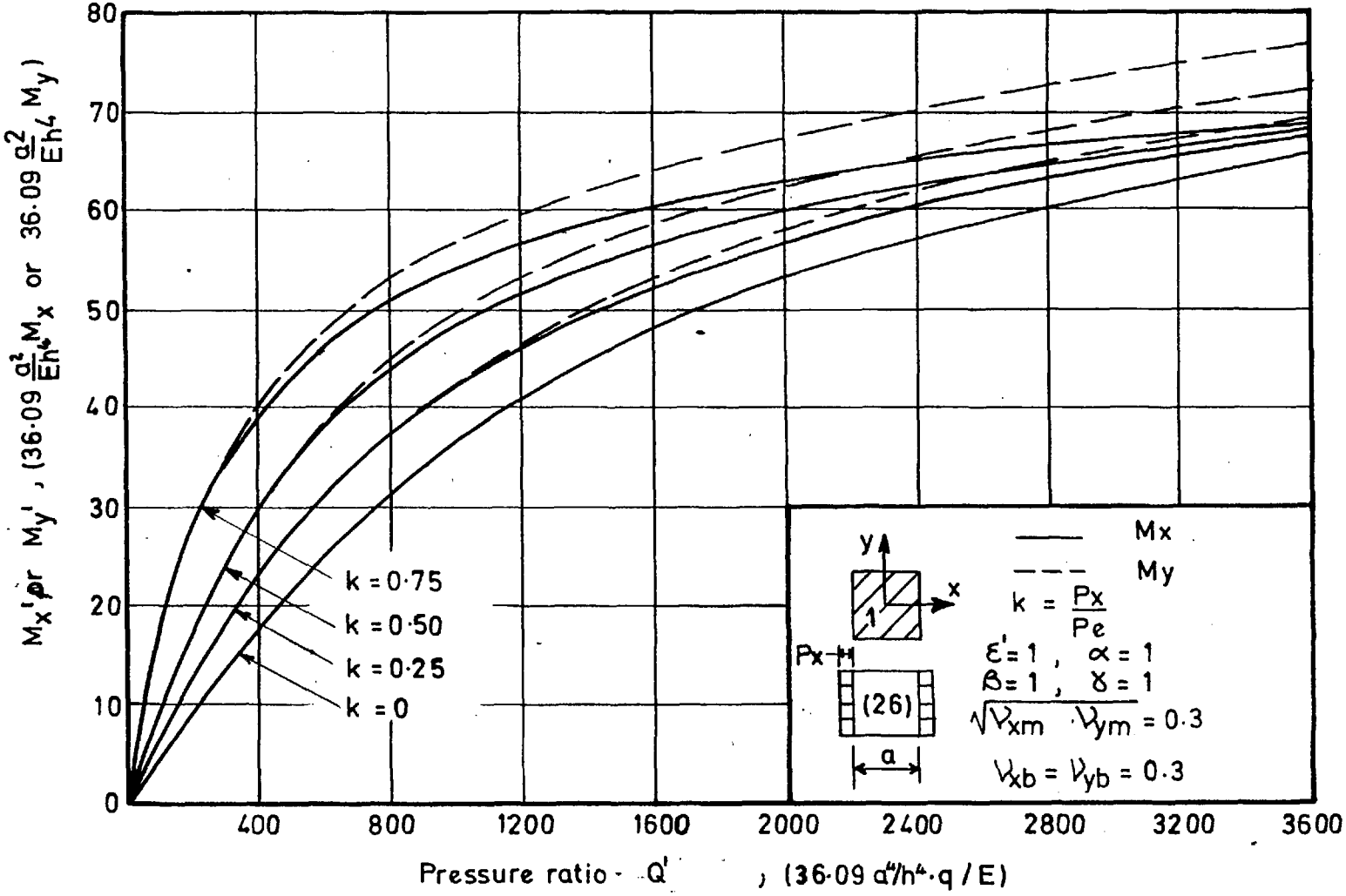


Fig.43 Bending moment at the centre of simply supported square plates (Uniform edge compression plus U.D.L.)

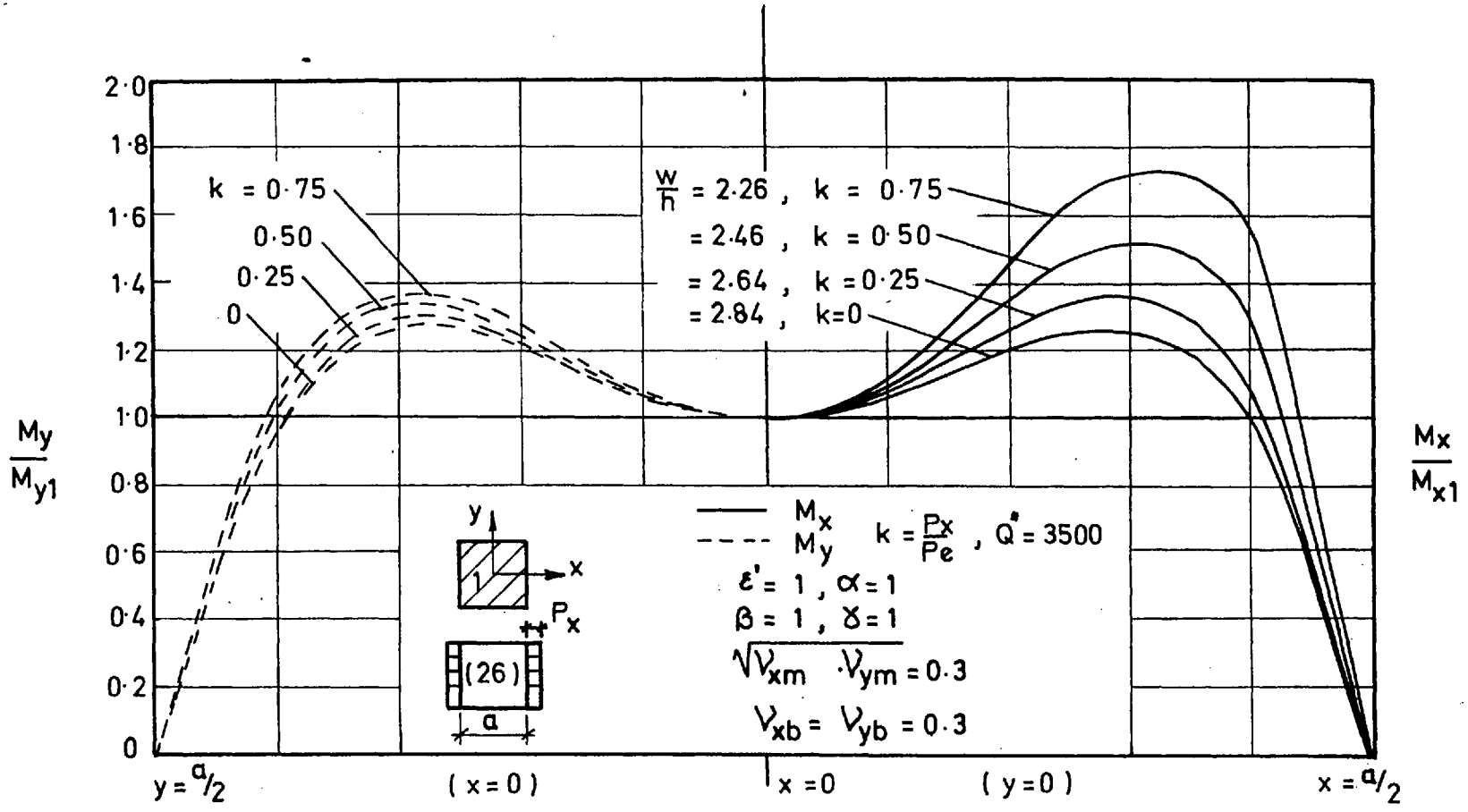


FIG. 44 Bending moment profiles along the centre lines of a simply supported square plate (Uniform edge compression plus U.D.L.)

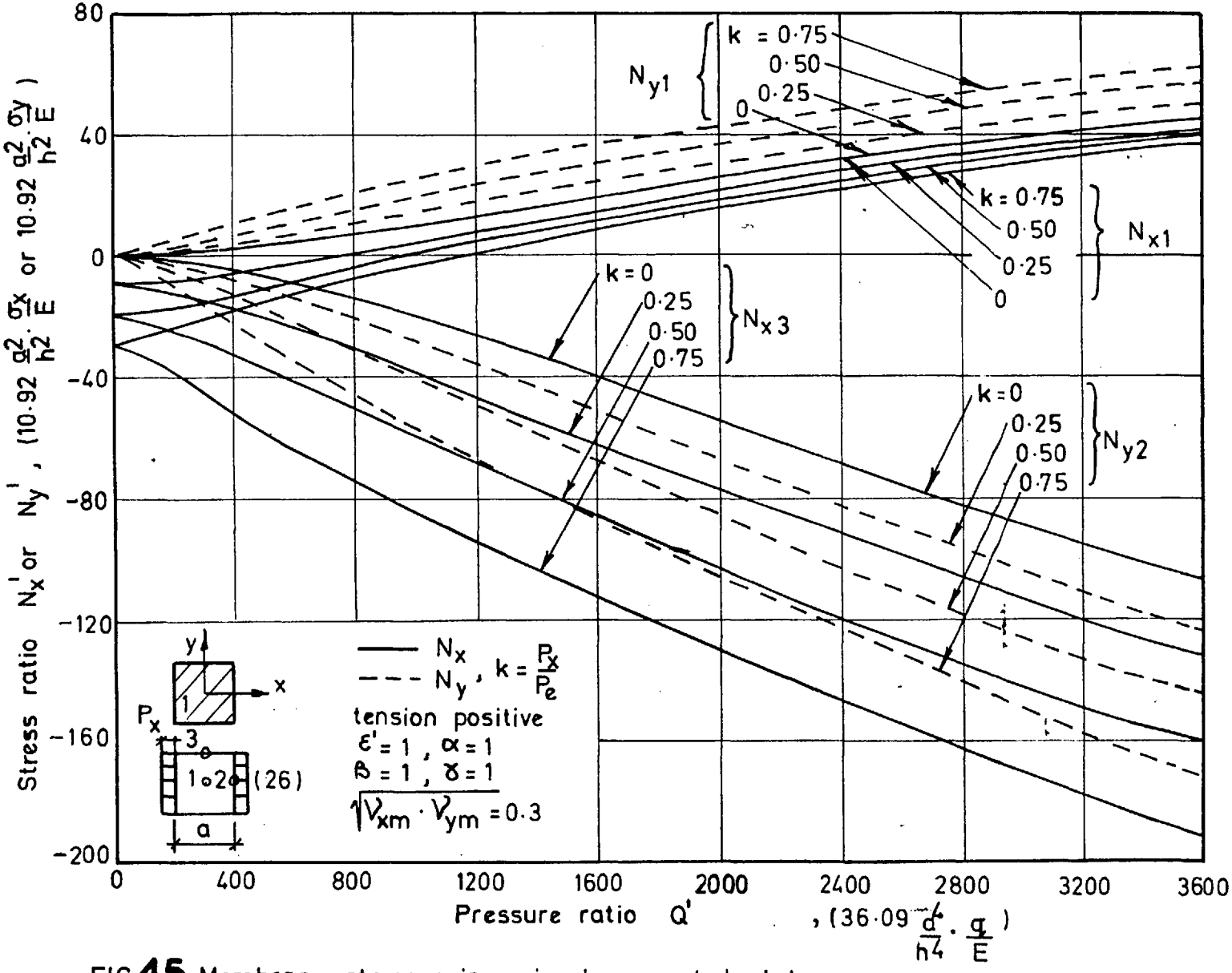


FIG.**45** Membrane stresses in simply supported plates
(Uniform edge compression plus U.D.L.)

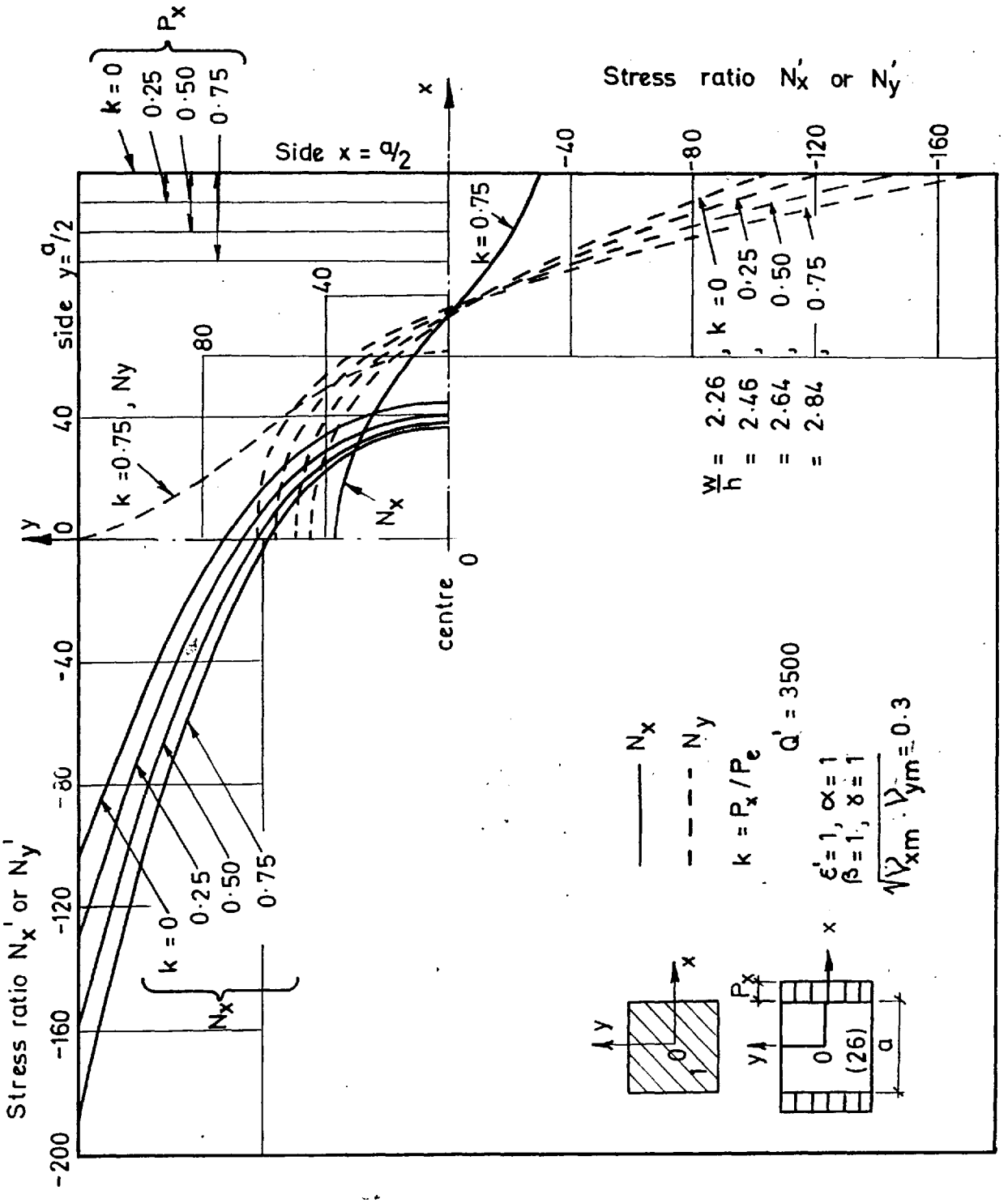


FIG. **46** Membrane stresses along the centre lines of simply supported plates. (Uniform edge compression plus U.D.L.)

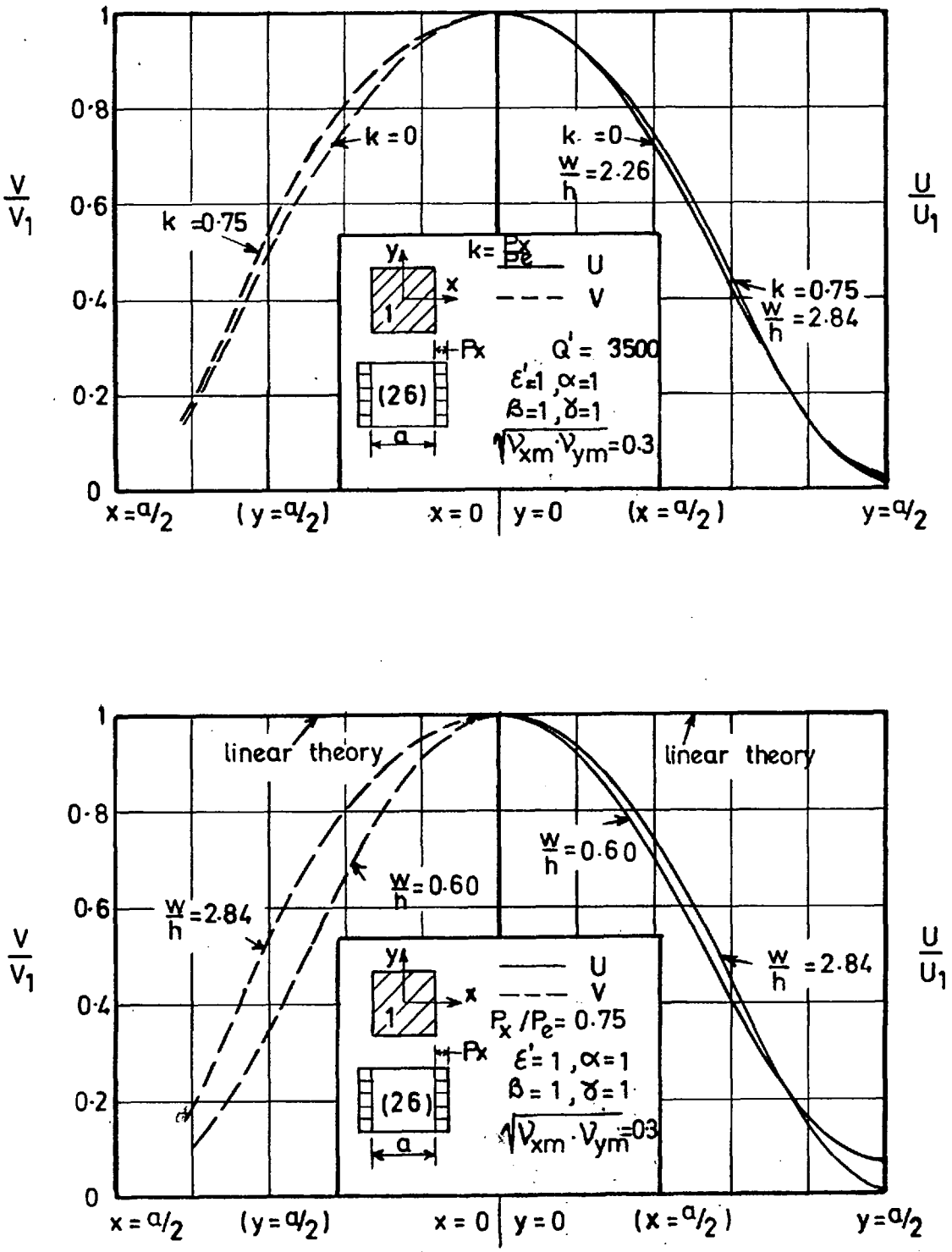


FIG 47 Extensional displacement profiles at the boundaries of simply supported square plates.
(Uniform edge compression plus U.D.L.)

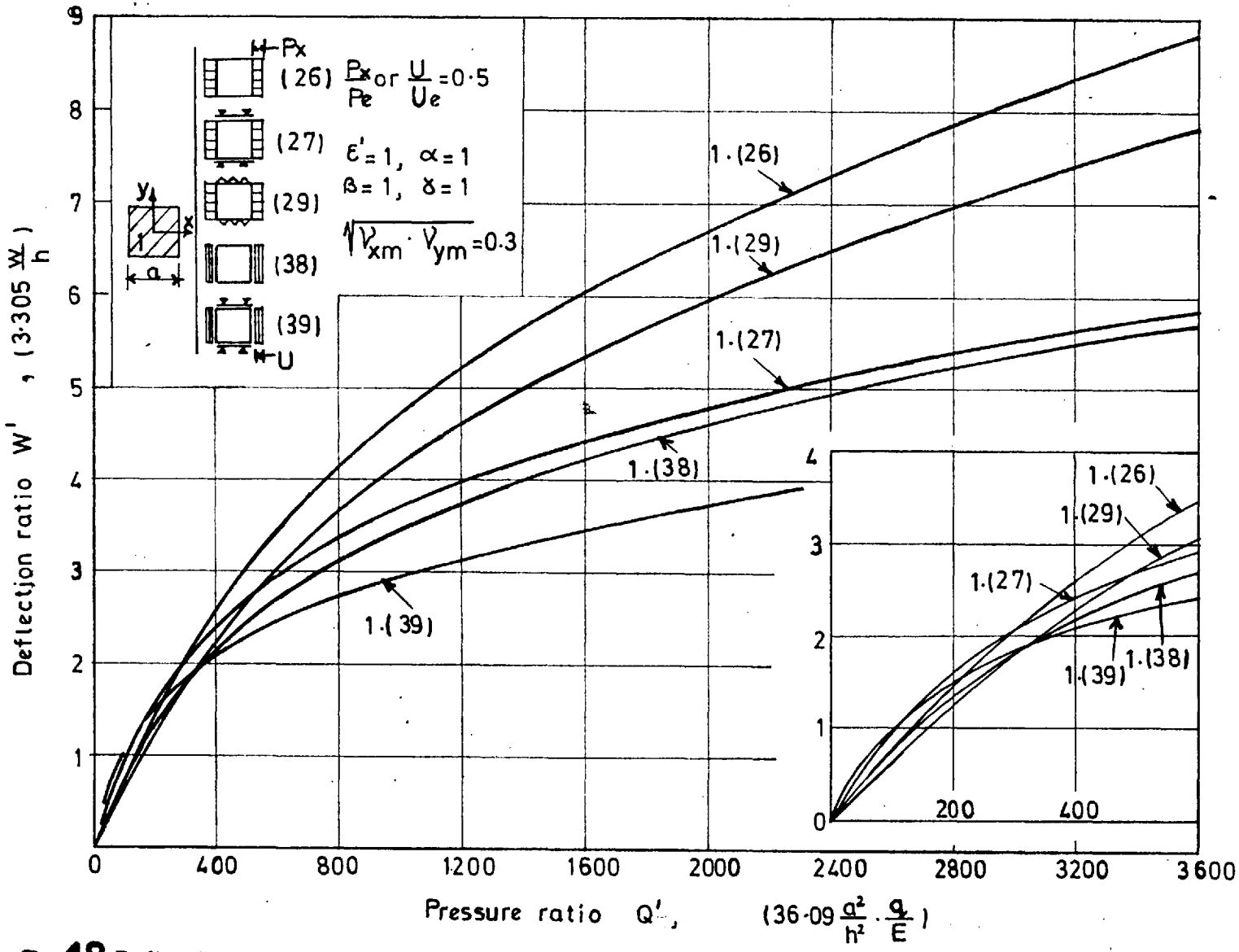


Fig.48 Deflection at the centre of simply supported plates
(Uniform edge compression or displacement plus U.D.L.)

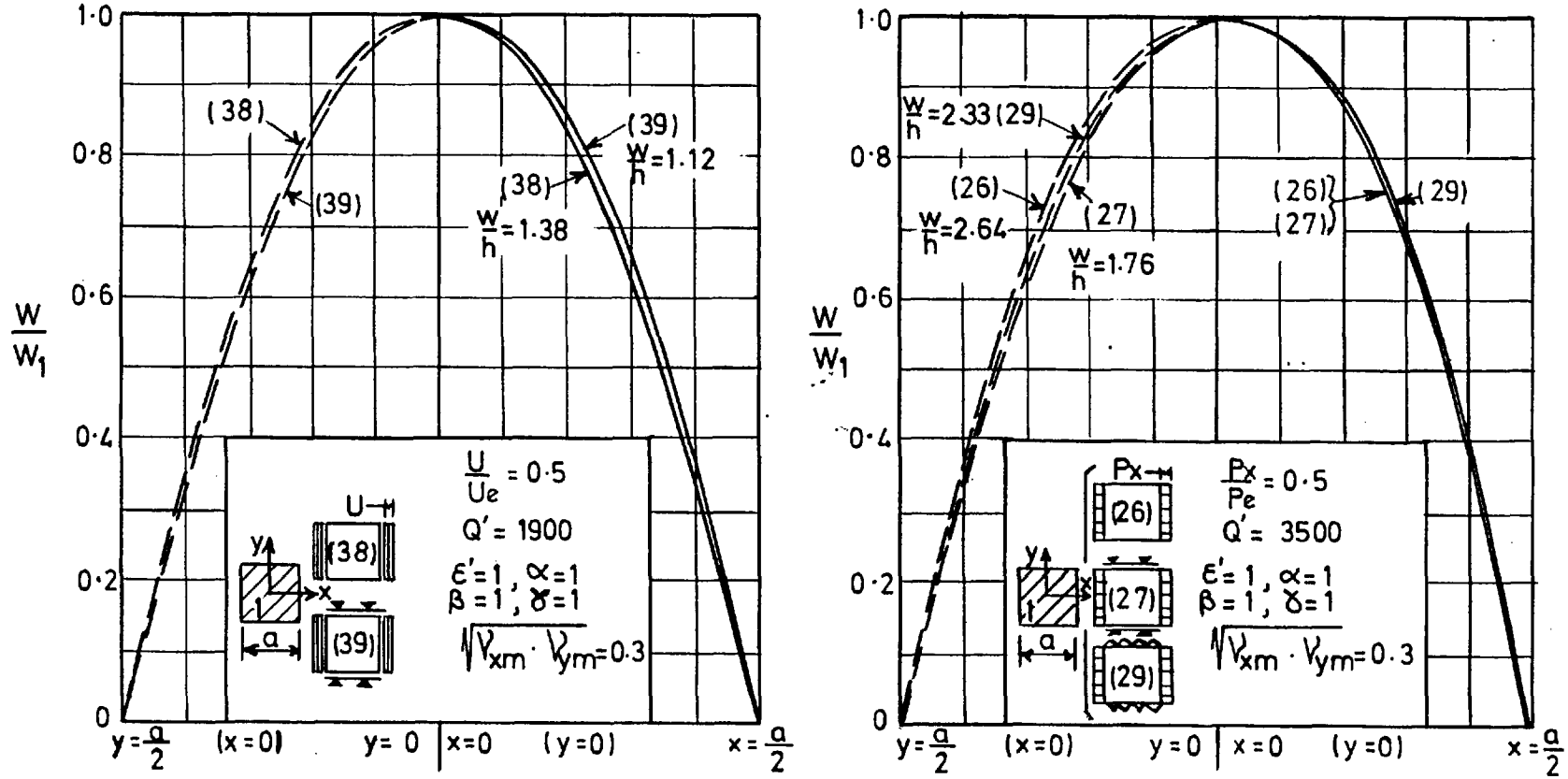


Fig 49 Deflection profiles along the centre lines of simply supported square plates (U.D.L plus uniform edge compression or displacement)

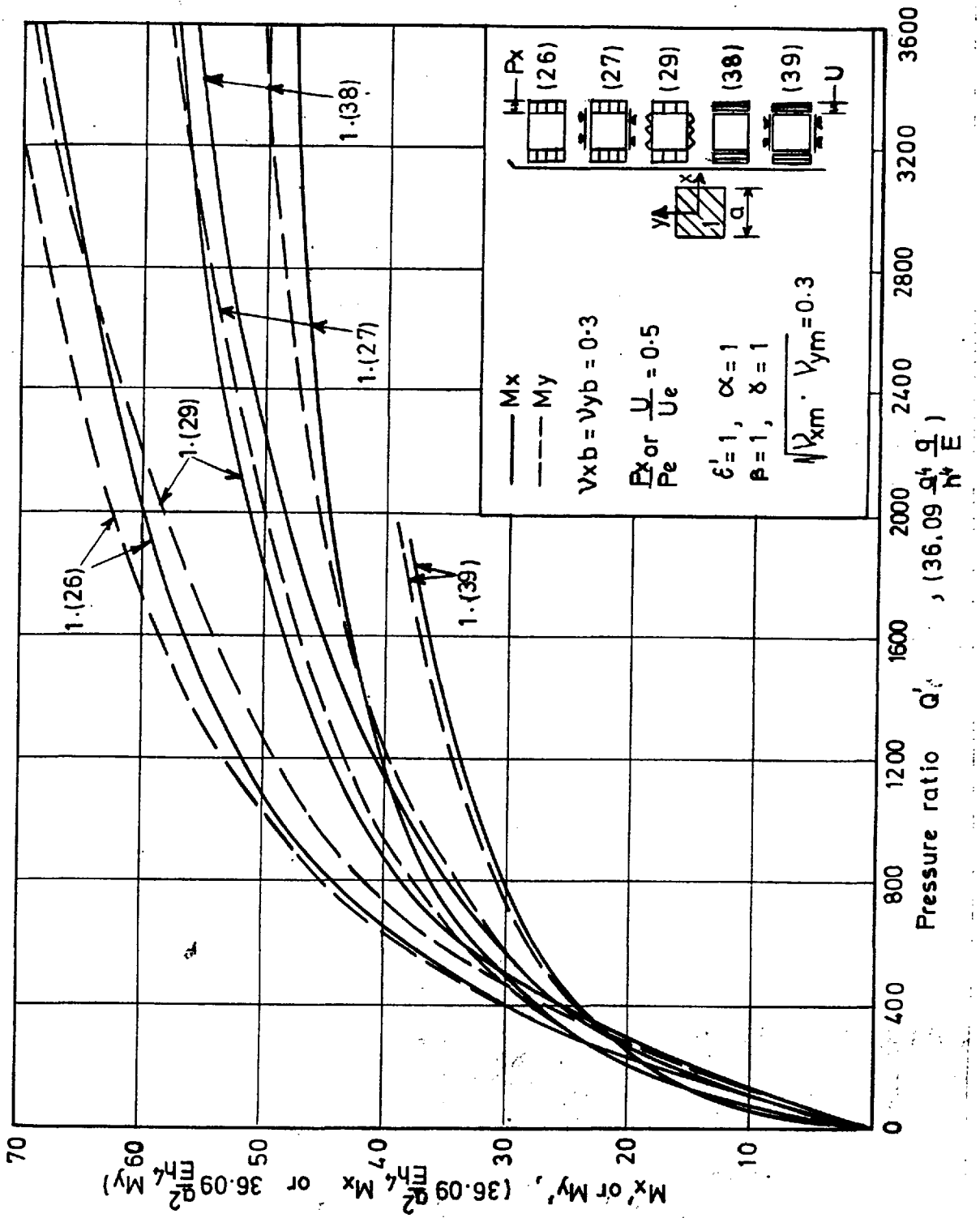
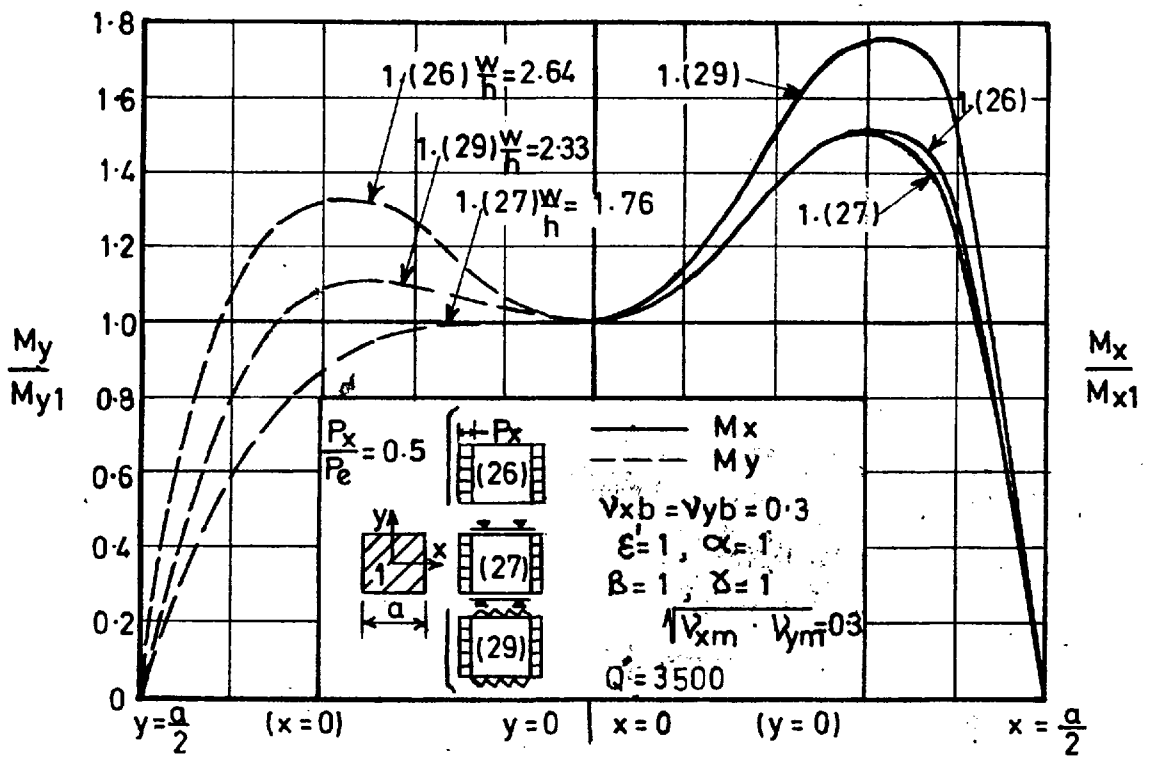
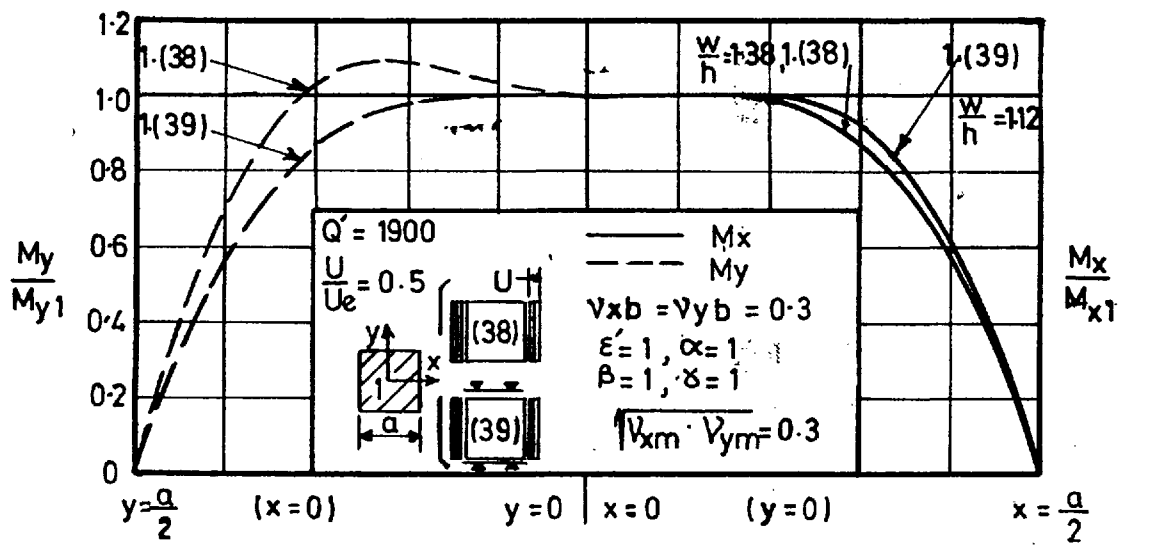


Fig. 50 Bending moment at the centre of simply supported square plates

(Uniform edge compression—or displacement, plus U.D.L.)



i) Uniform edge compression



ii) Uniform edge displacement

Fig 51 Bending moment profiles along the centre lines of a simply supported square plate (U.D.L plus uniform edge compression or displacement.)

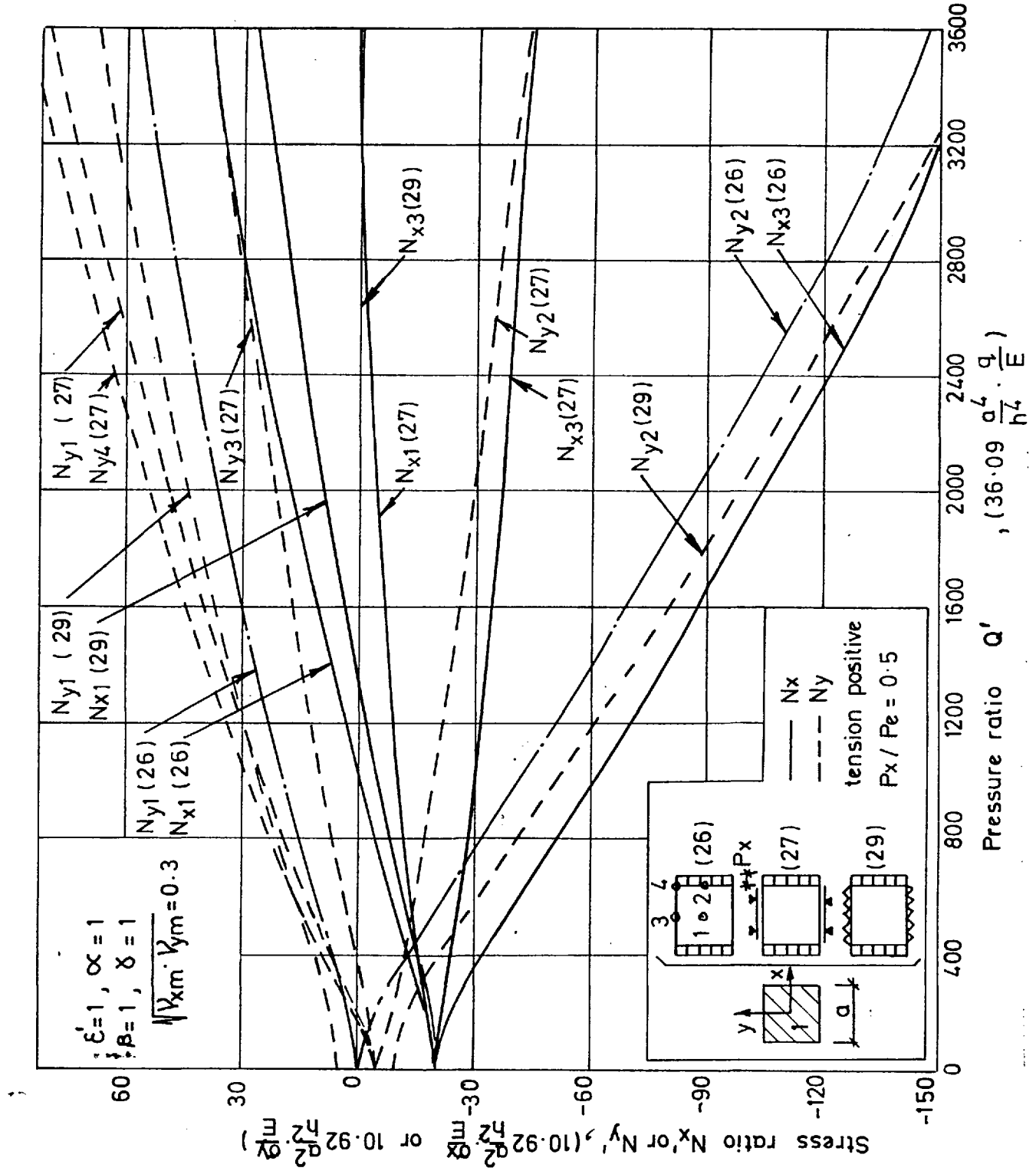


FIG. **52** Membrane stresses in simply supported plates
(U.D.L. plus a uniform edge compression)

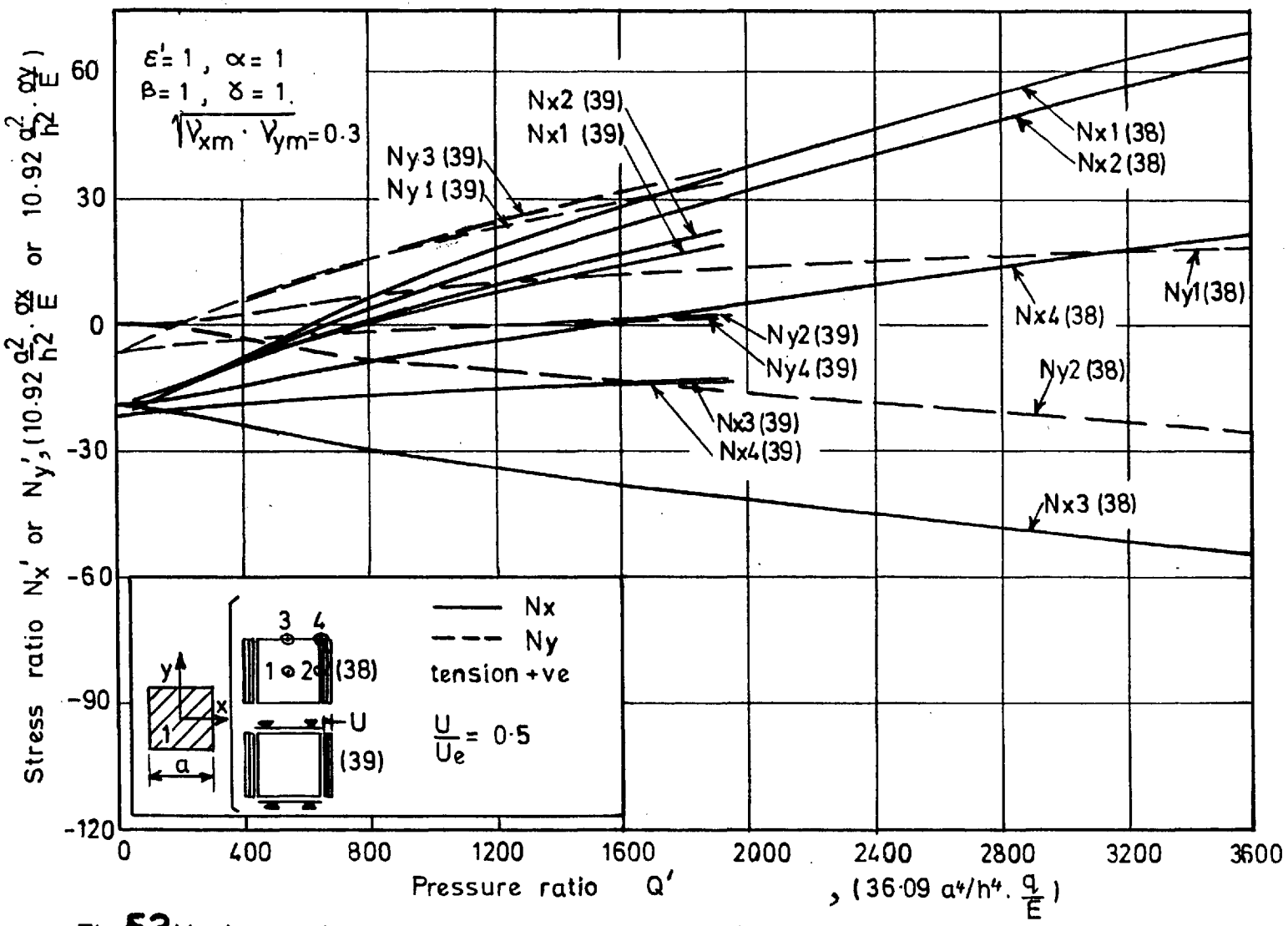


Fig. 53 Membrane stresses in simply supported plates
(Uniform edge displacement plus U.D.L.)

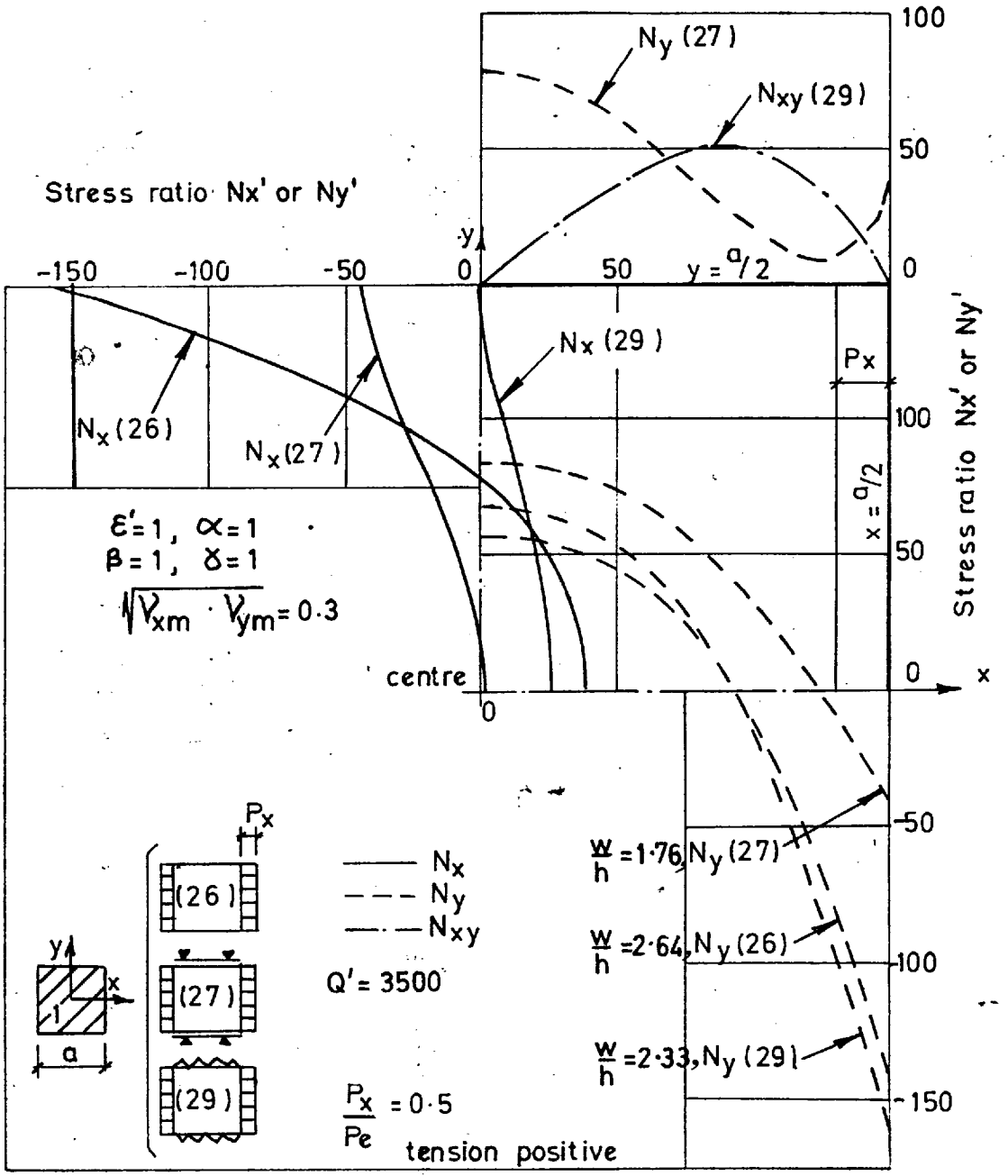


FIG. 54 Membrane stresses along the centre lines and boundary of simply supported square plates.
(Uniform edge compression plus U.D.L.)

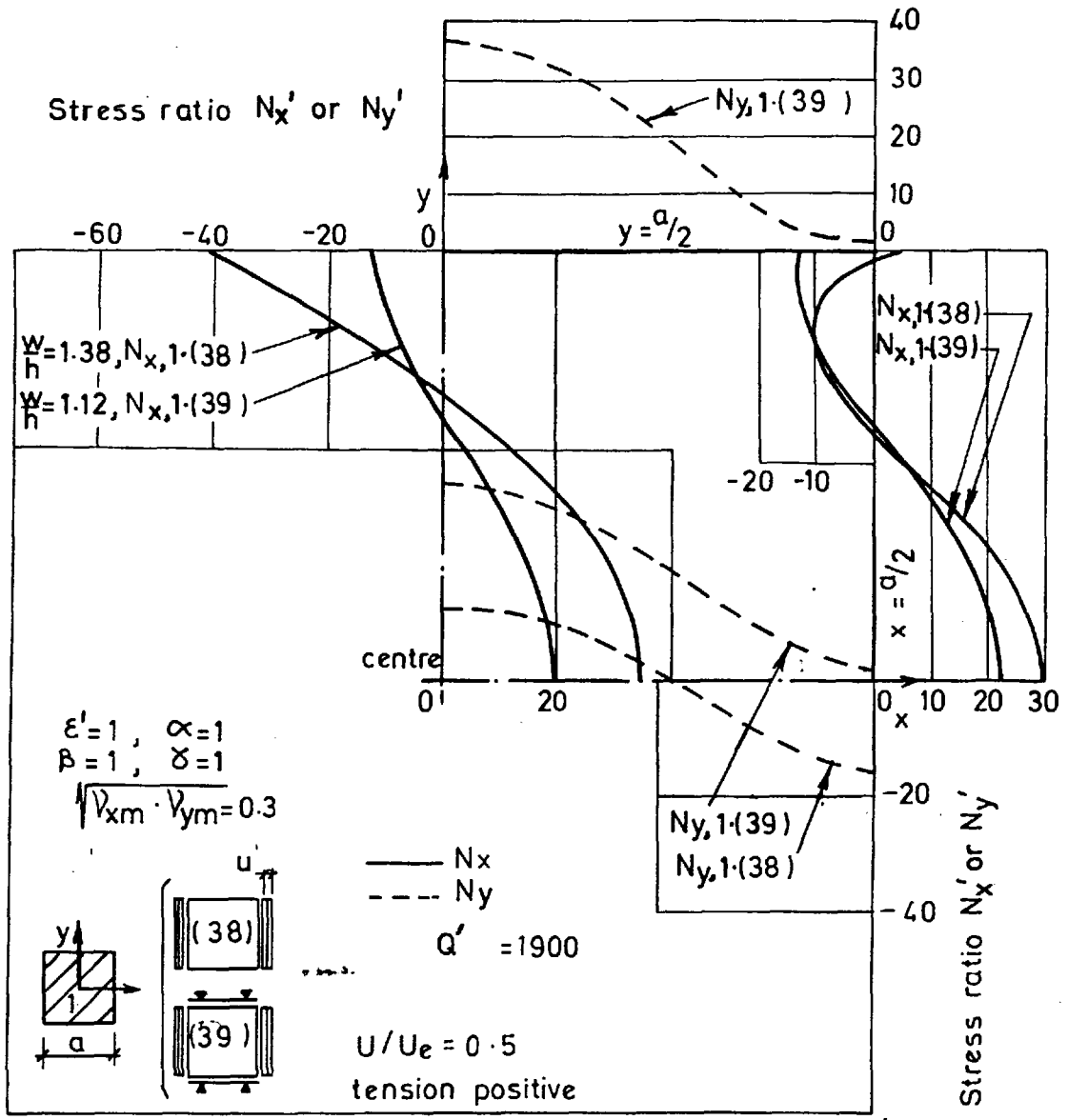


FIG. **55** Membrane stresses along the centre lines and boundaries of simply supported square plates

(Uniform edge displacement plus U.D.L.)

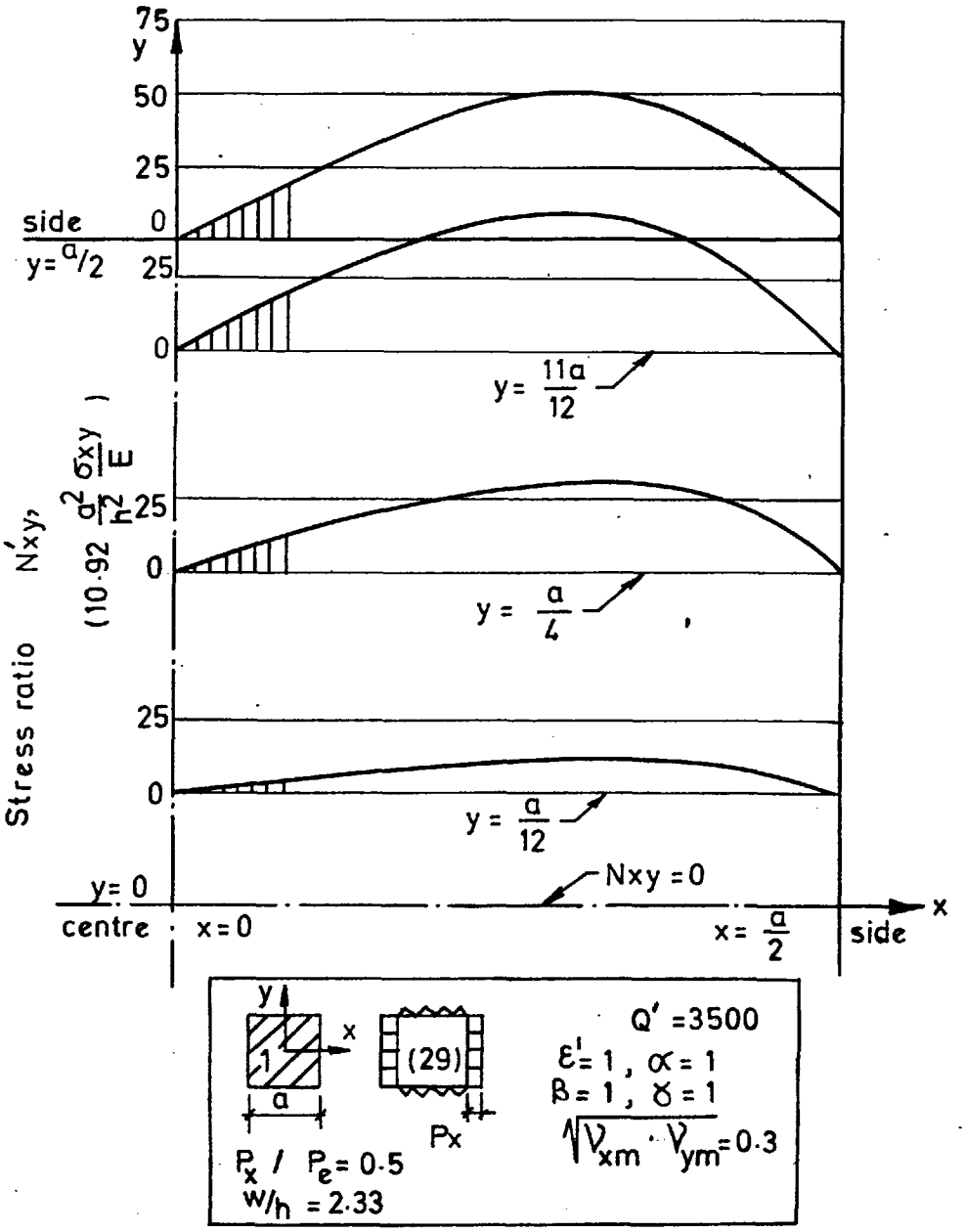


FIG. **56** Shear stresses in simply supported square plates.

(Uniform edge compression plus U.D.L.)

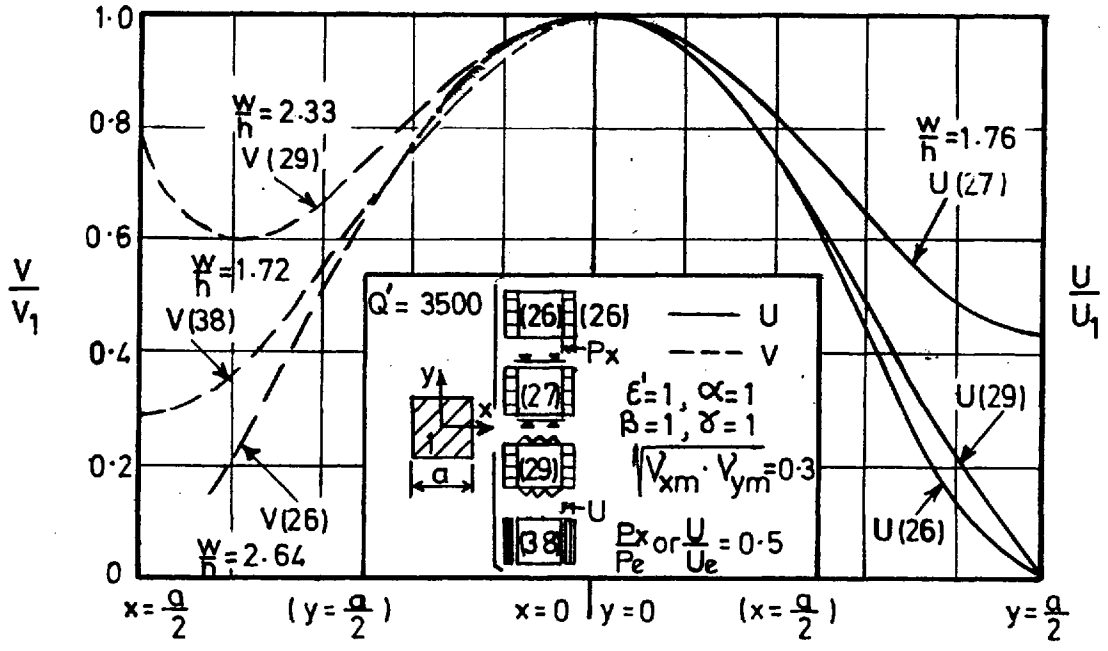


Fig. **57** Extensional displacement profiles at the boundaries of simply supported square plates.
(Uniform edge compression–or displacement plus U.D.L)

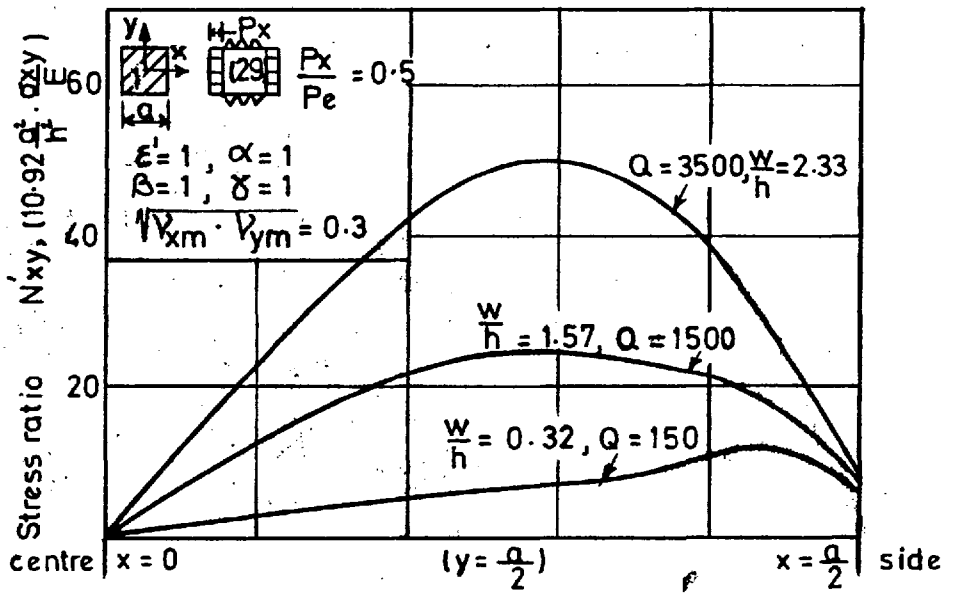


Fig. **58** Shear stress at the boundary of simply supported square plates (Uniform edge compression plus U.D.L)

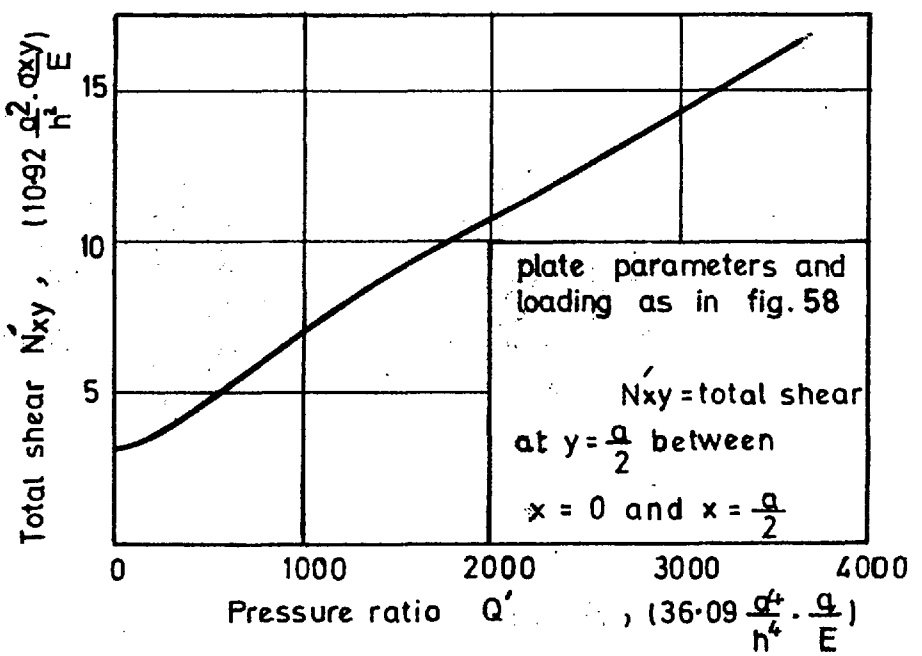


Fig. **59** Total shear force at the boundary of simply supported square plates (Uniform edge compression plus U.D.L)

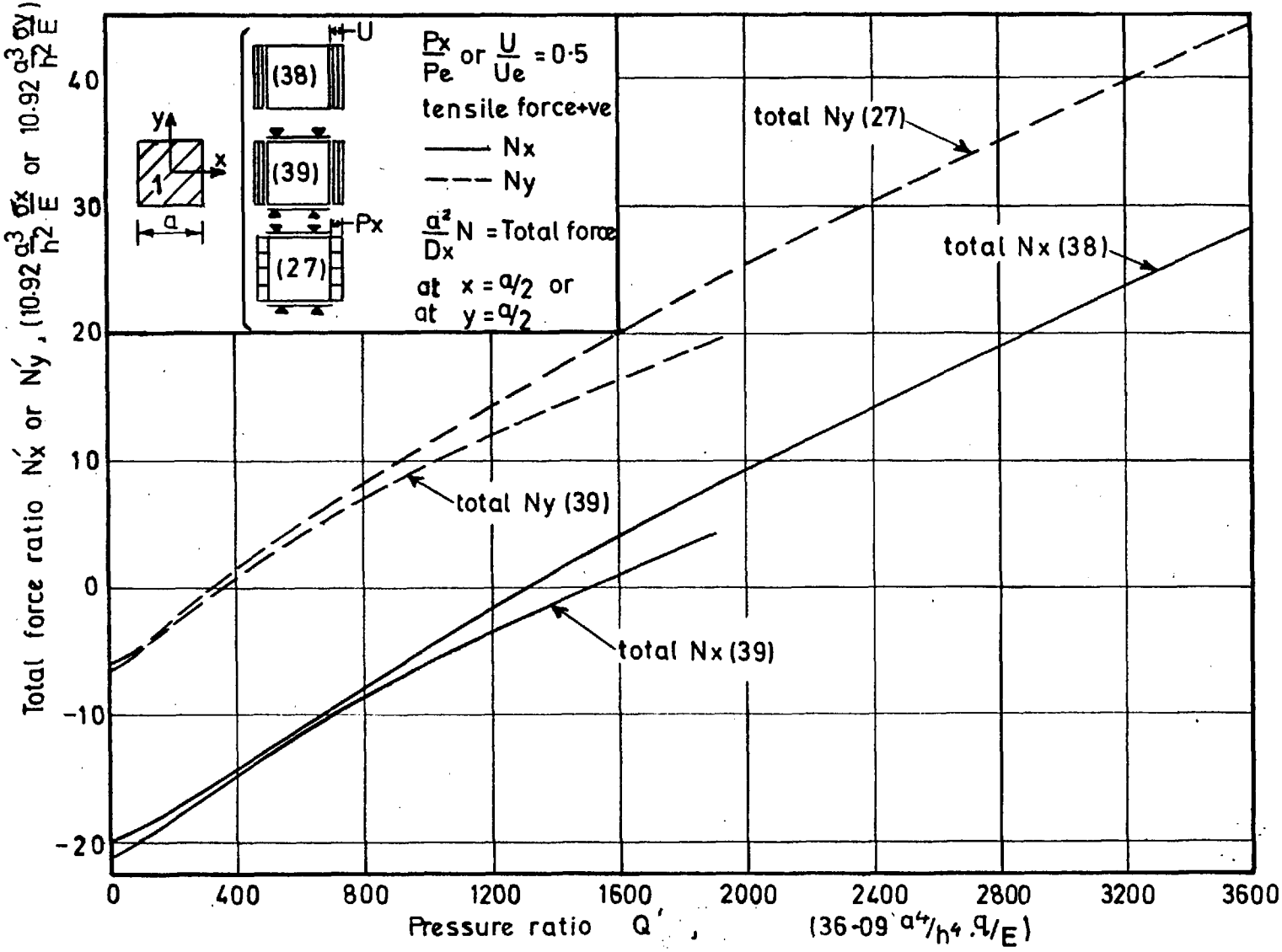


Fig. 60 Total extensional forces at the boundaries of simply supported plates (Uniform edge compression-or displacement, plus U.D.L)

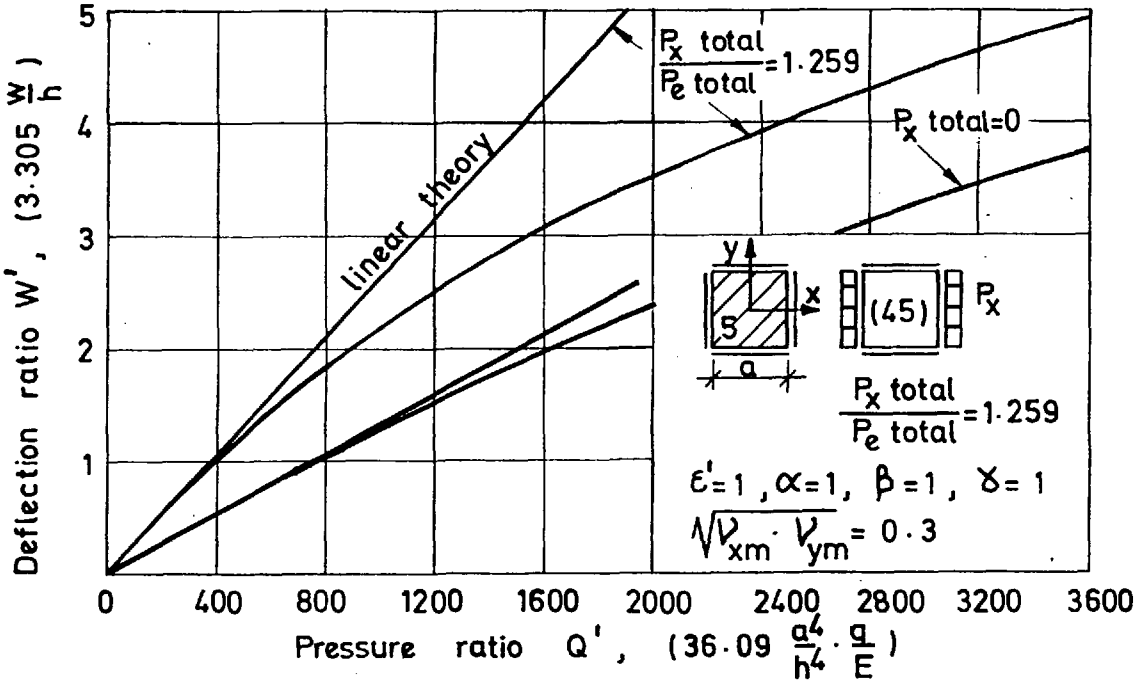


FIG. 61 Clamped plate under combined loading. Deflection at centre.

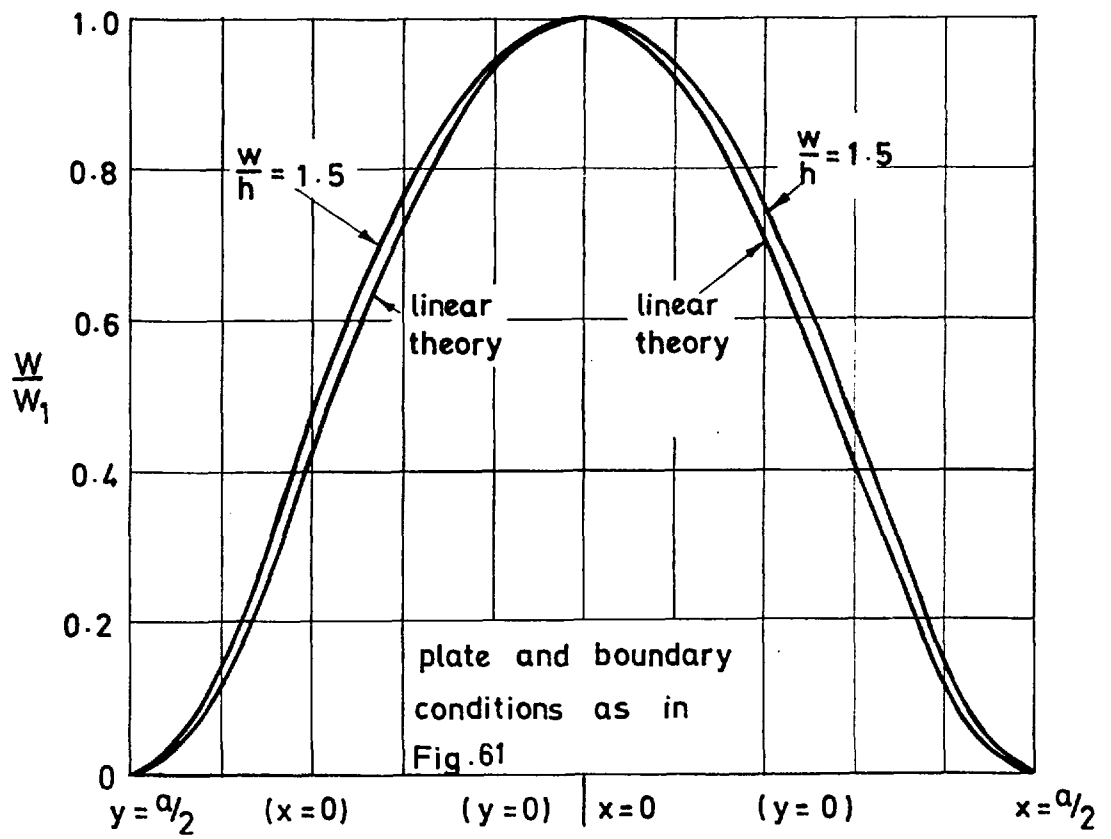


FIG. 62 Clamped plate under combined loading. Deflection profile along the centre lines.

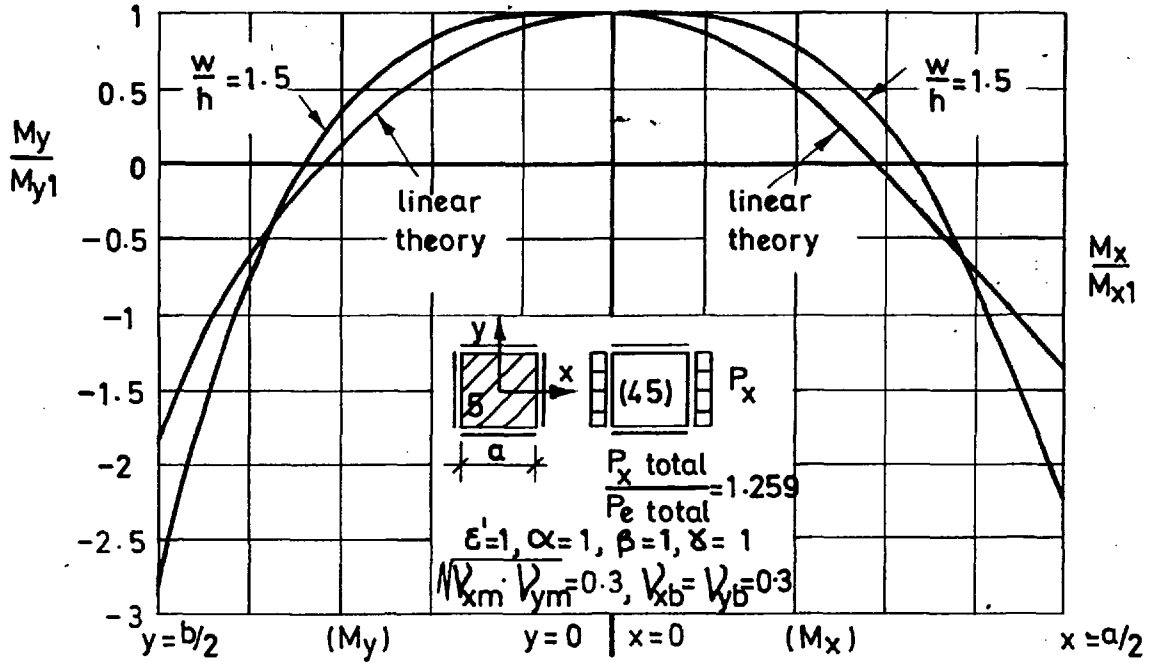


FIG. 63 Clamped plate under combined loading. Bending moment profiles along the centre lines.

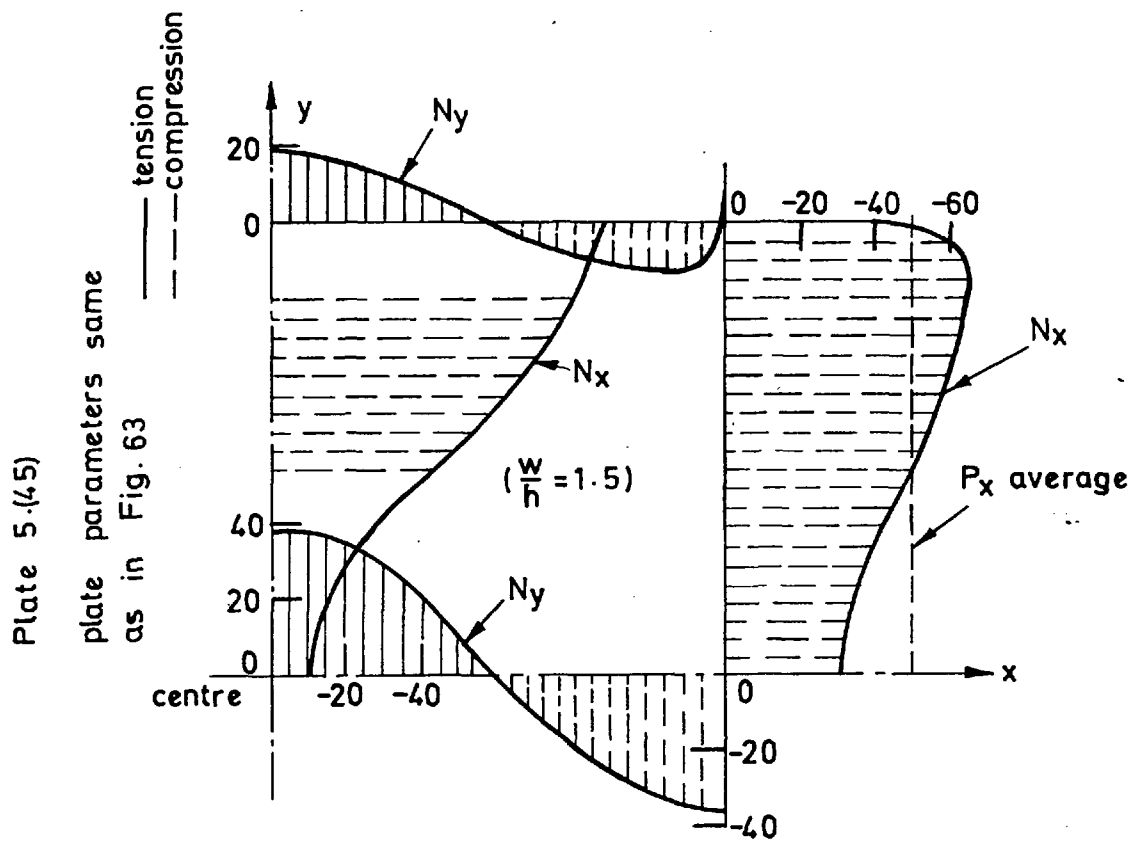


FIG. 64 Clamped plate under combined loading. Distribution of membrane stress.

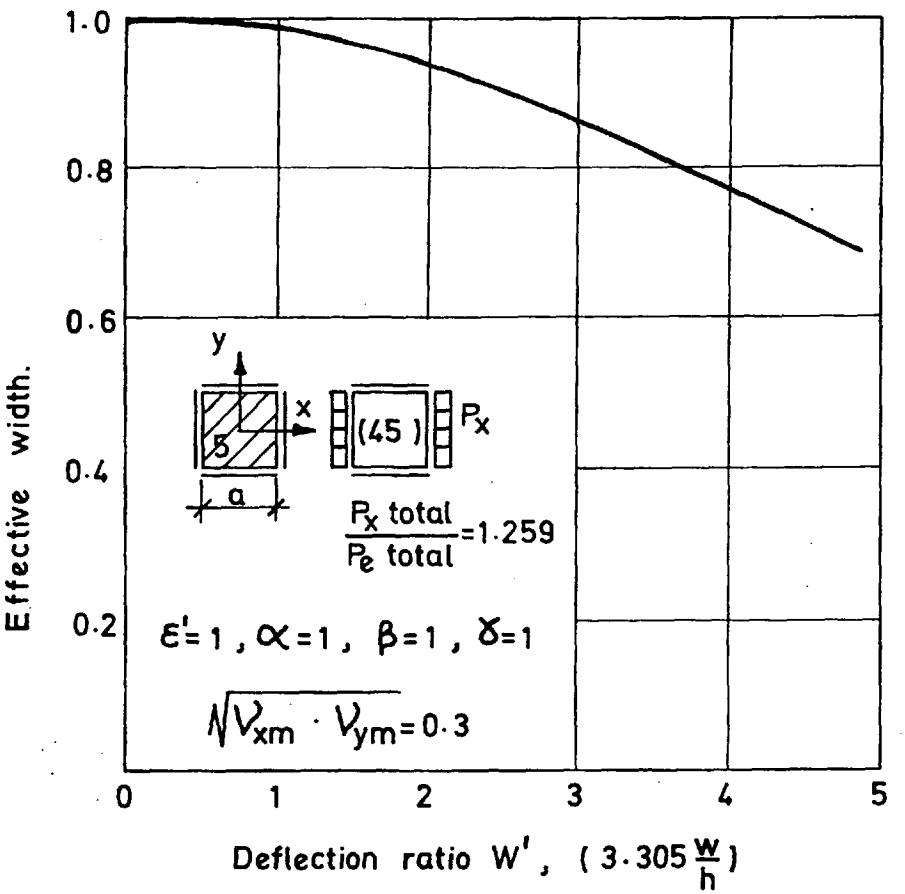


FIG. 65 Clamped plate under combined loading. Variation of effective width with central deflection.

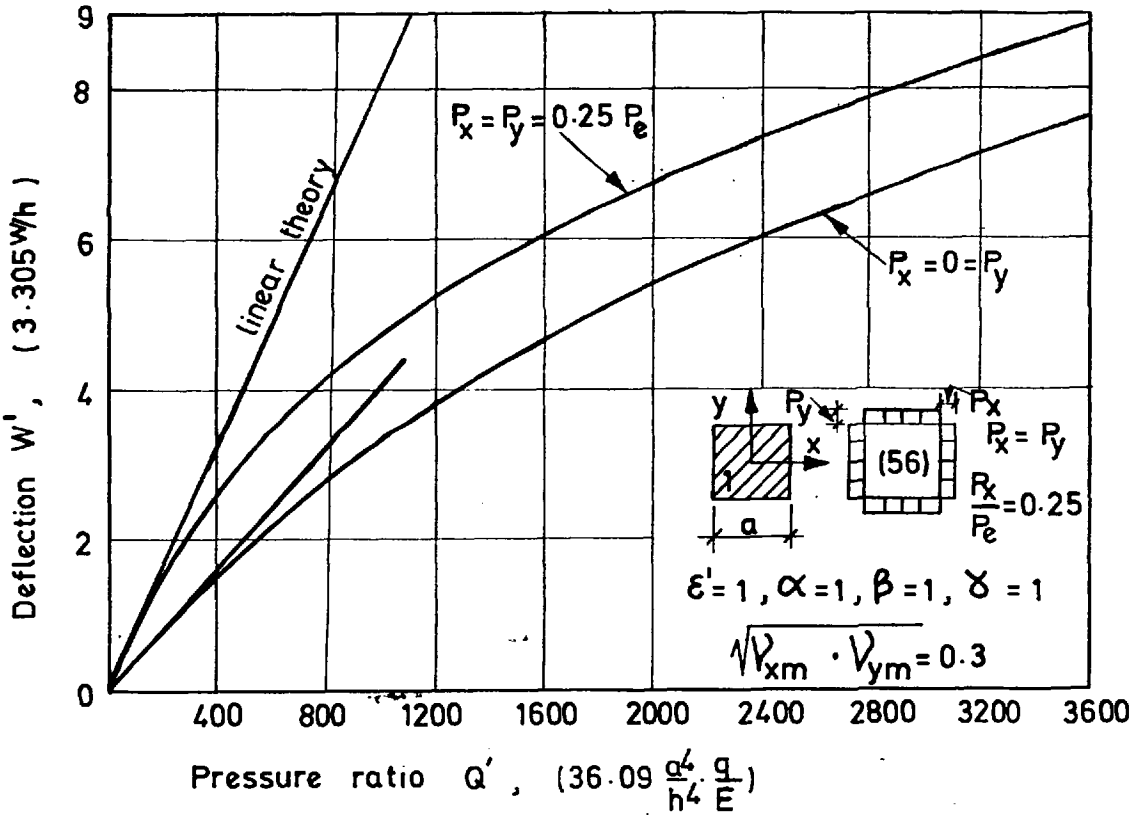


FIG. 66 Simply supported plate under combined loading. Deflection at centre.

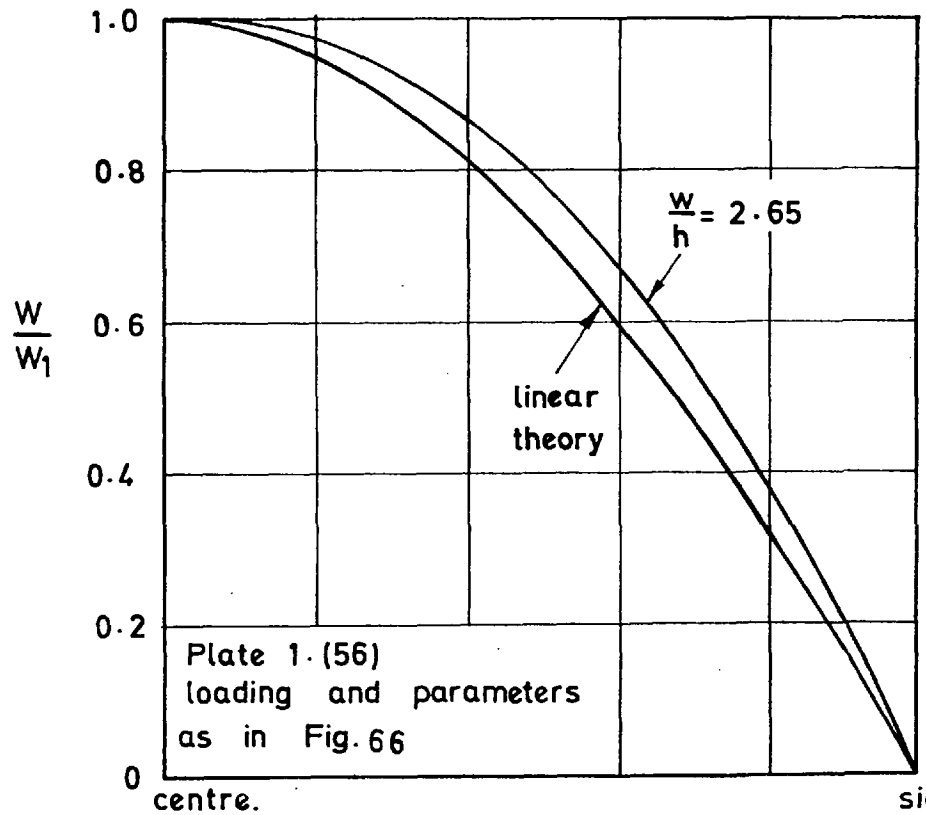


FIG. 67 Simply supported plate under combined loading. Deflection profile along the centre lin

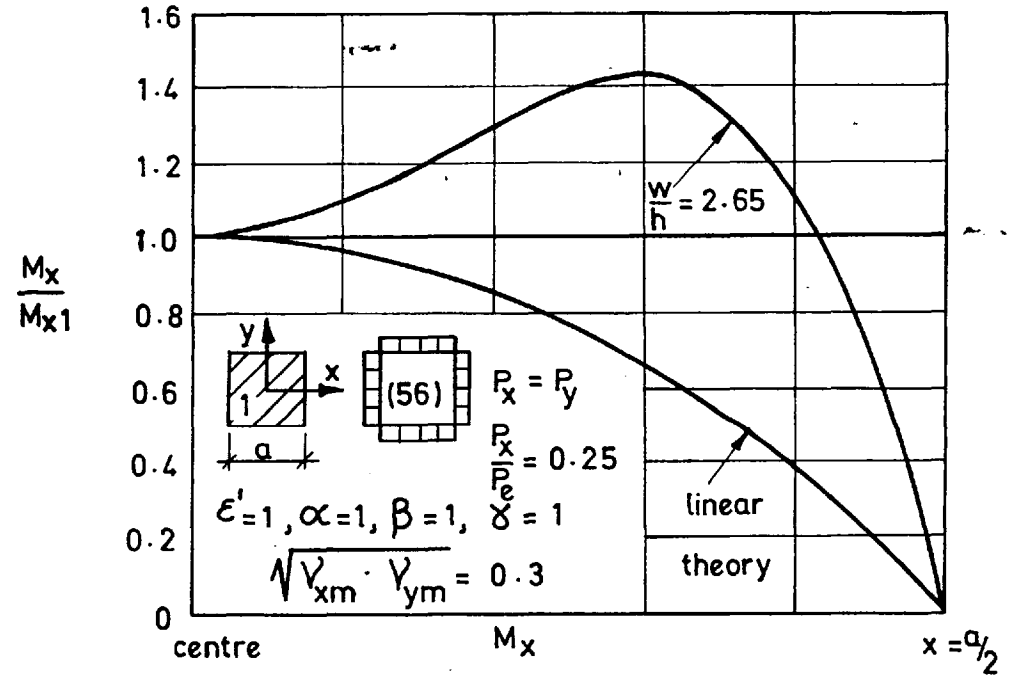


FIG. 68 Simply supported plate under combined loading. Bending moment profiles along the centre line.

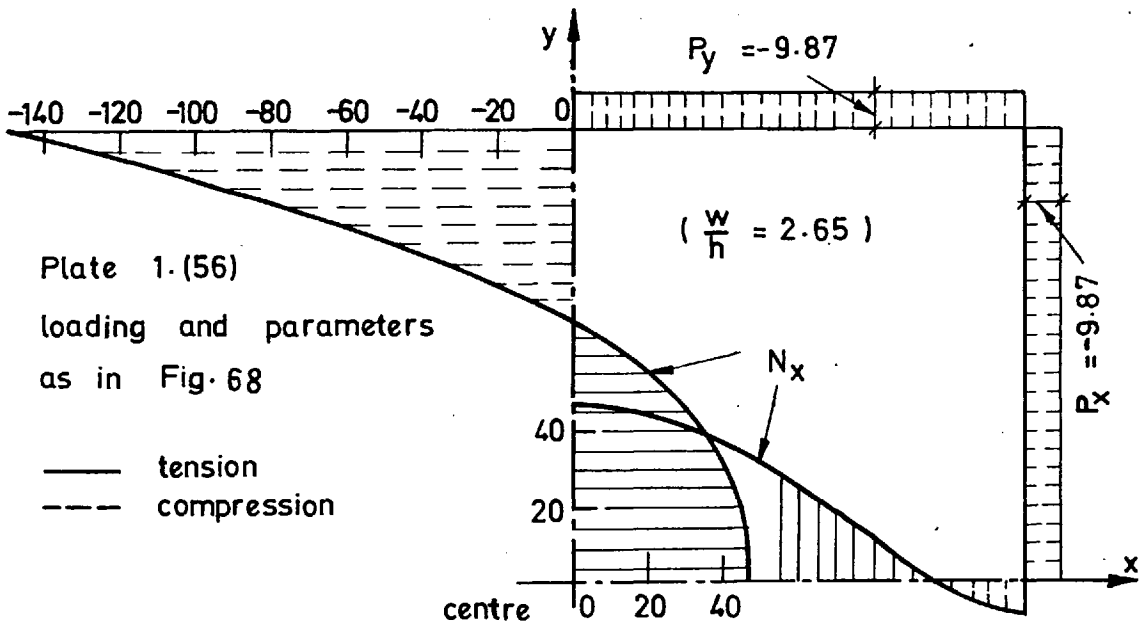


FIG. 69 Simply supported plate under combined loading. Distribution of membrane stress along the centre lines and the boundary.

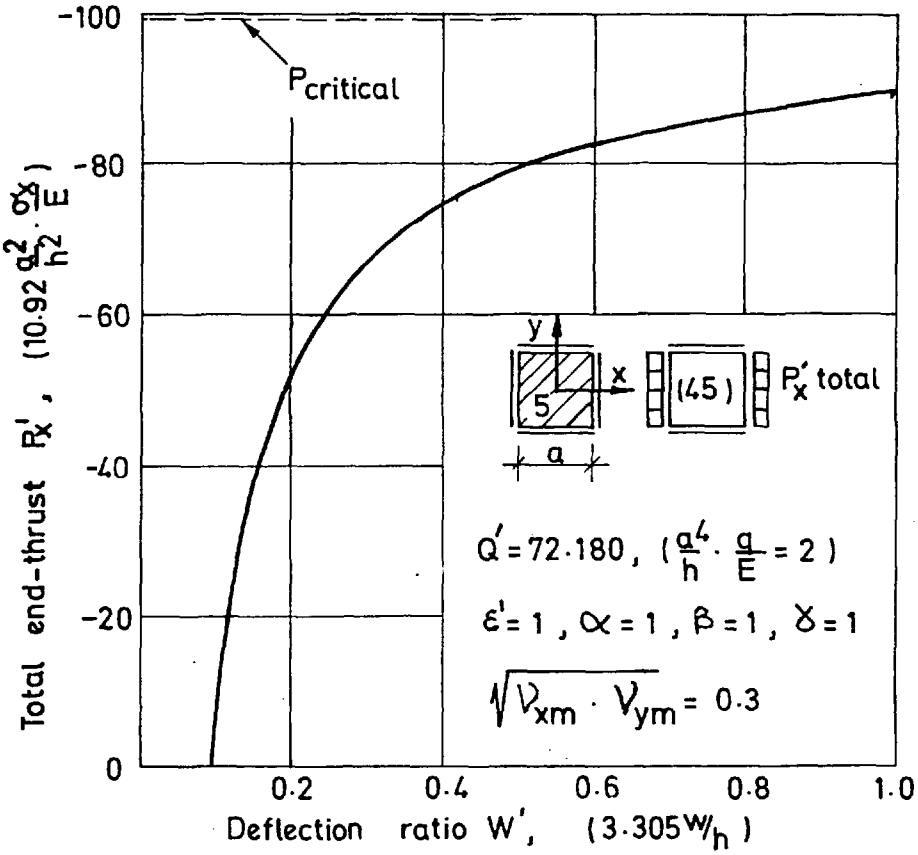


FIG. 70 Clamped plate under combined loading. Deflection at centre.

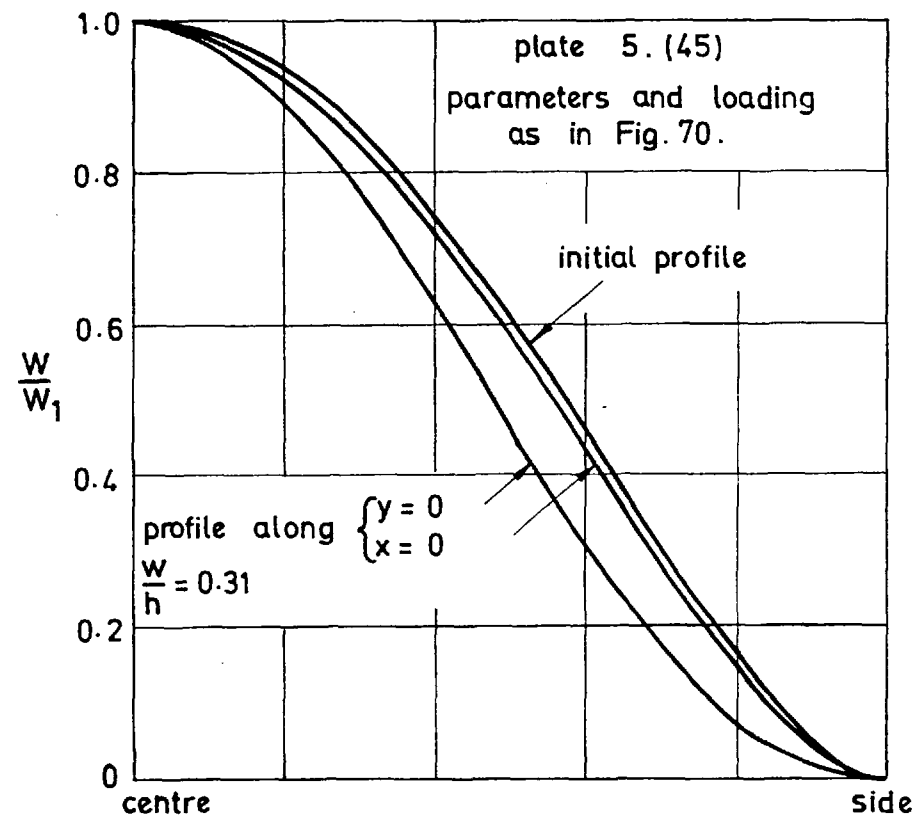


FIG. 71 Clamped plate under combined loading. Deflection profiles along the centre lines.

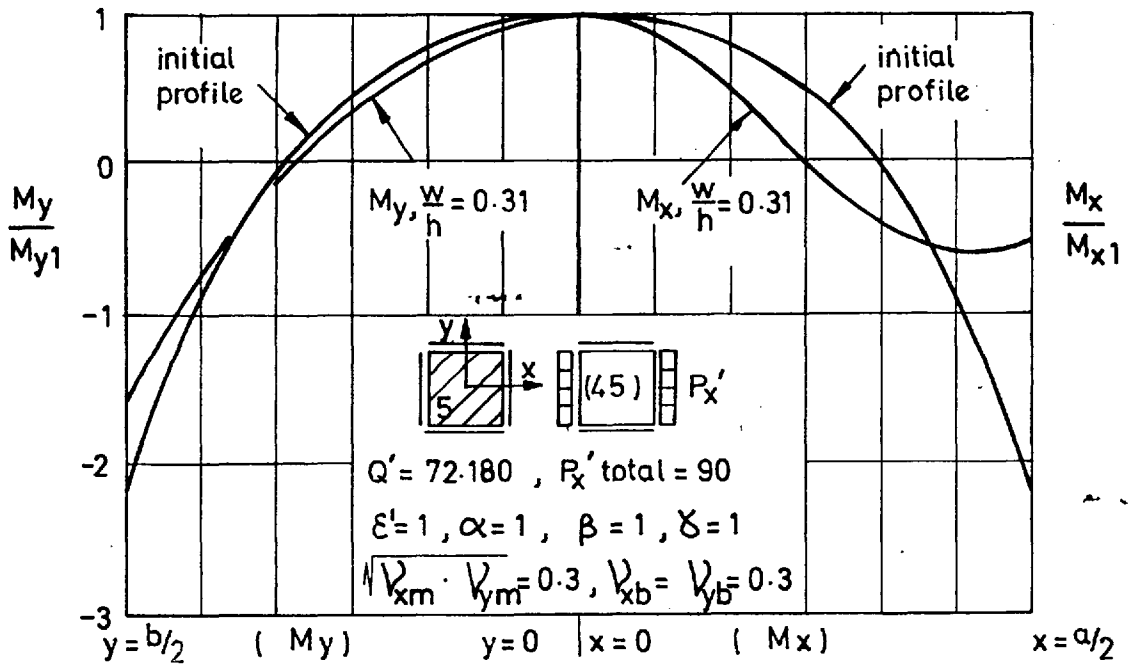


FIG. **72** Clamped plate under combined loading. Bending moment profiles along the centre lines.

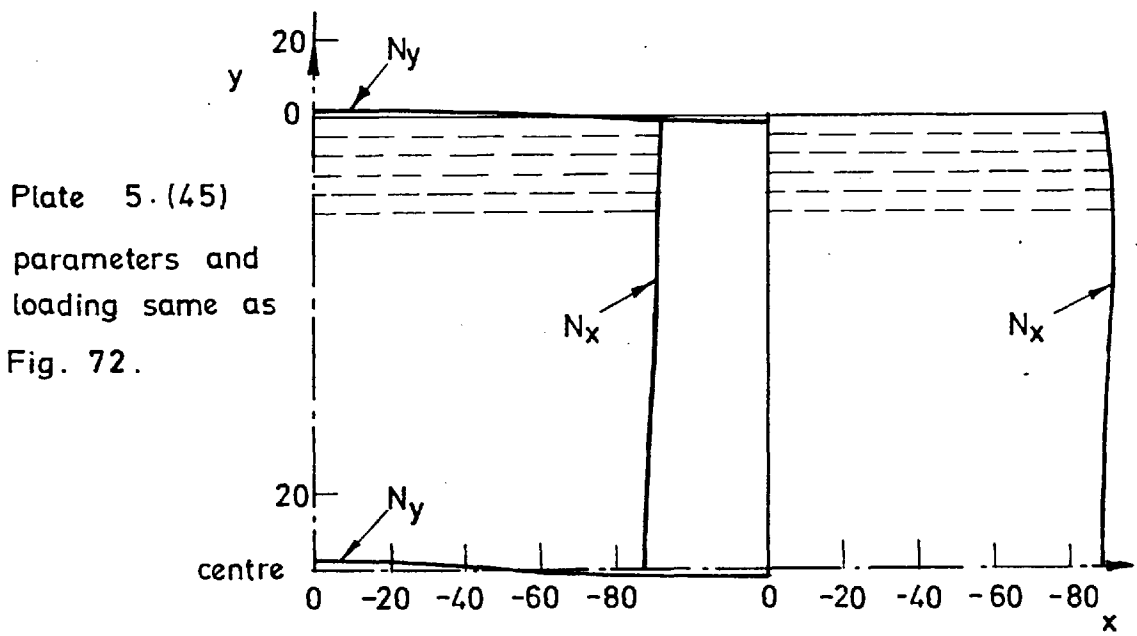


FIG. **73** Clamped plate under combined loading. Distribution of membrane stress.

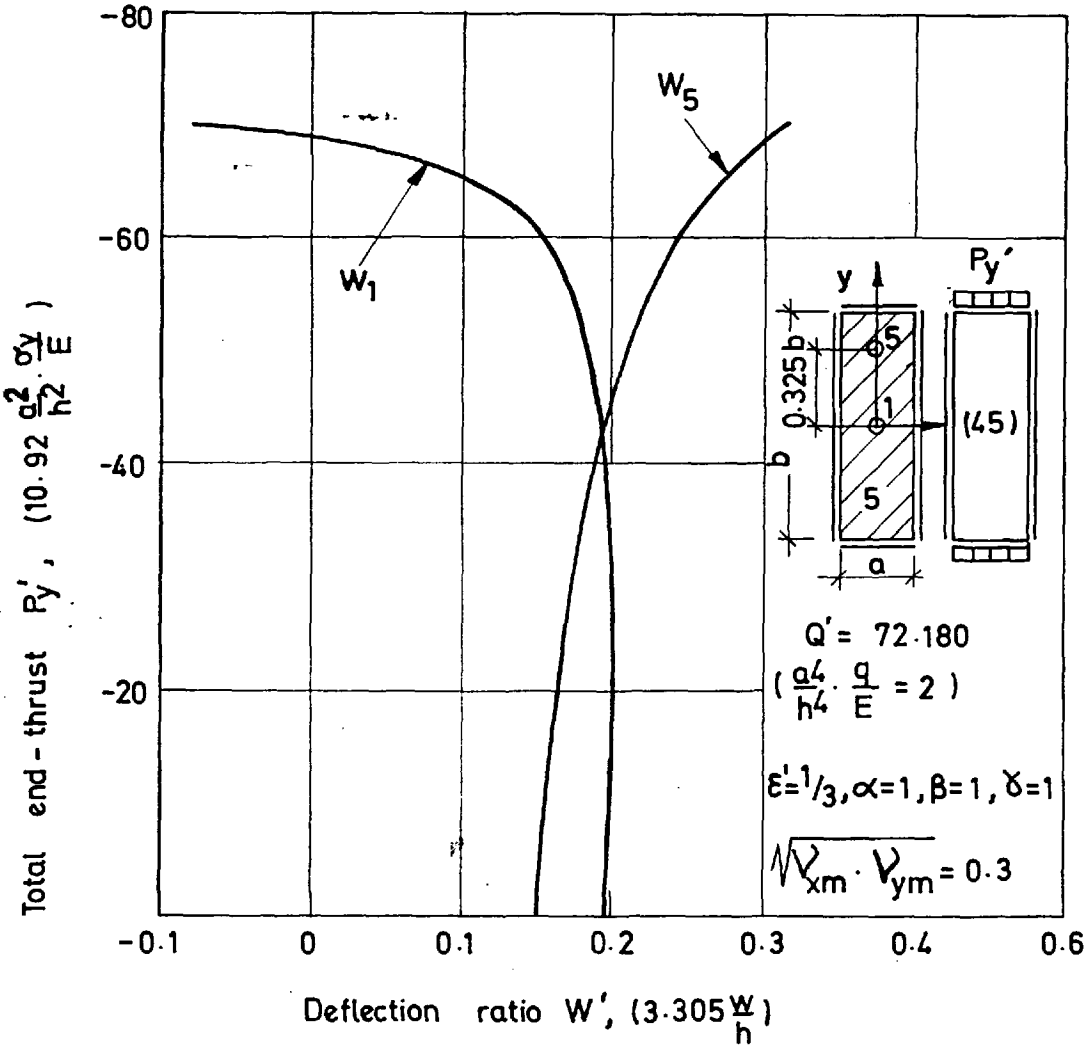


FIG. **74** Clamped plate under combined loading.
Deflection at centre, and at point (x = 0, y = 0·325b)

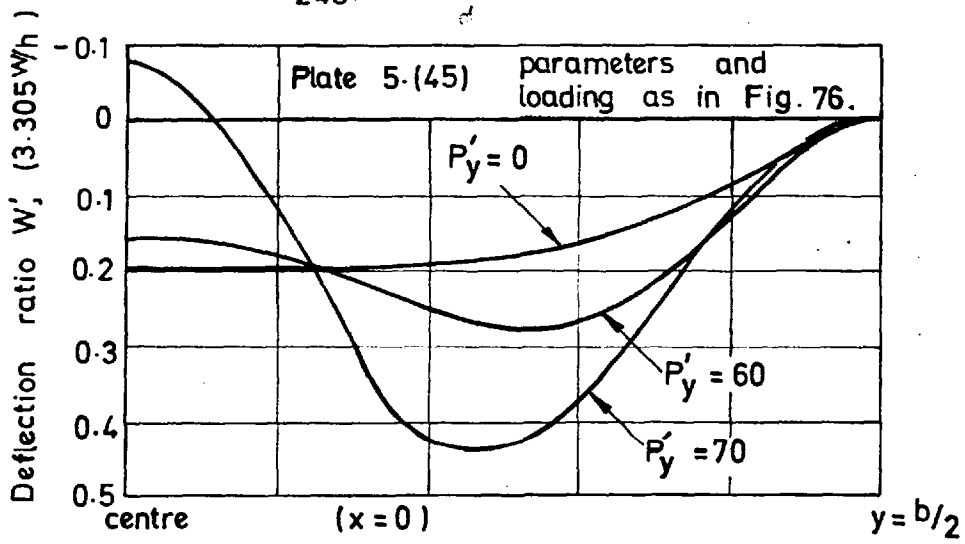


FIG. 75 Clamped plate under combined loading.
Deflection profiles along the centre line.

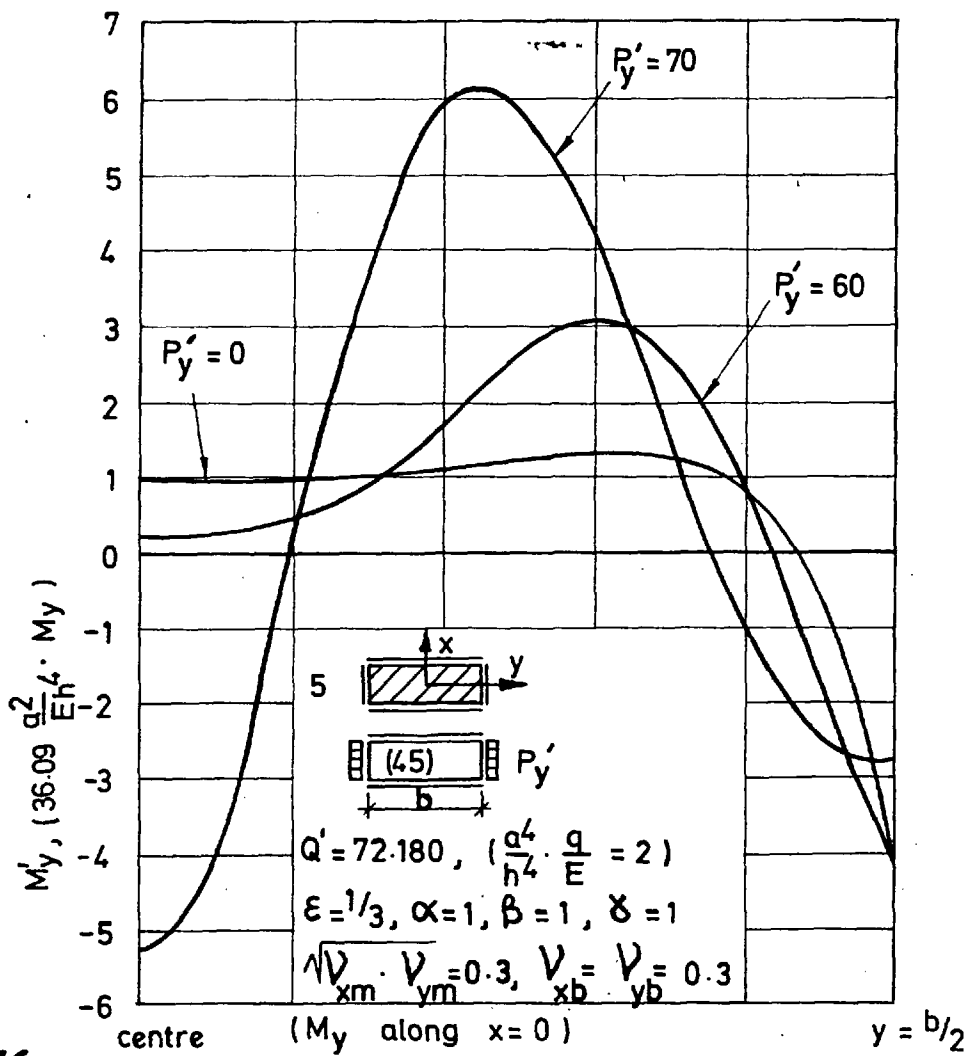


FIG. 76. Clamped plate under combined loading.
Bending moment profiles along the centre line.

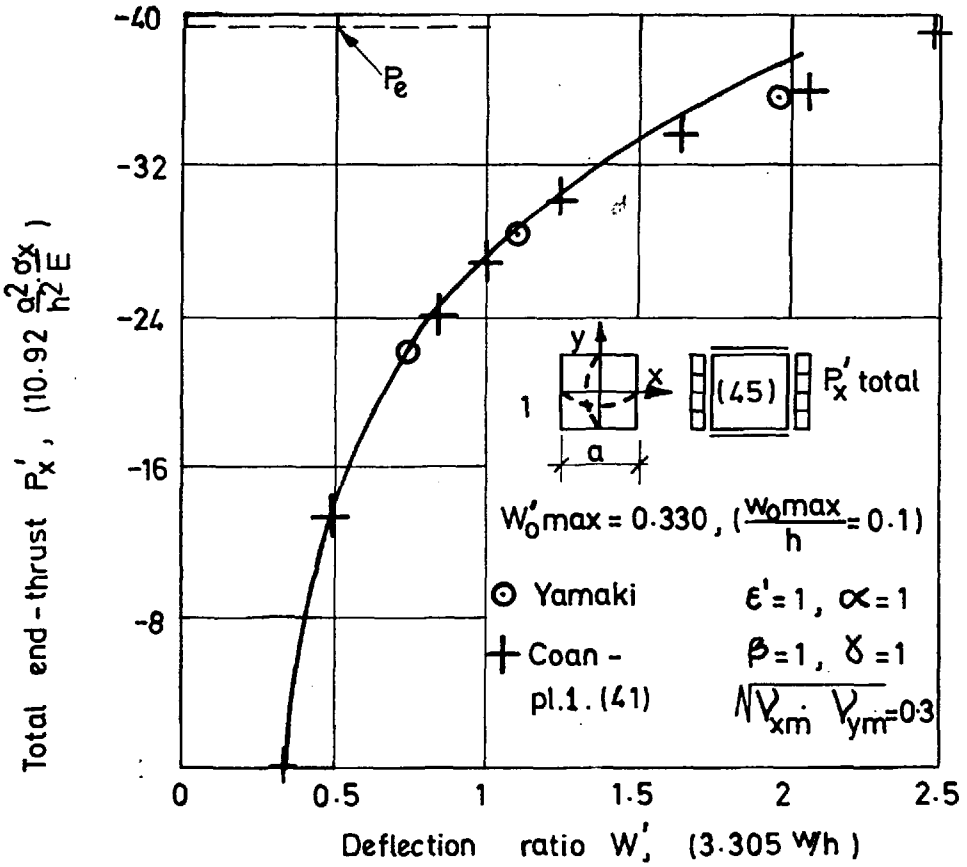


FIG. **77** Initially deformed simply supported plate under end-thrust. Deflection at centre.

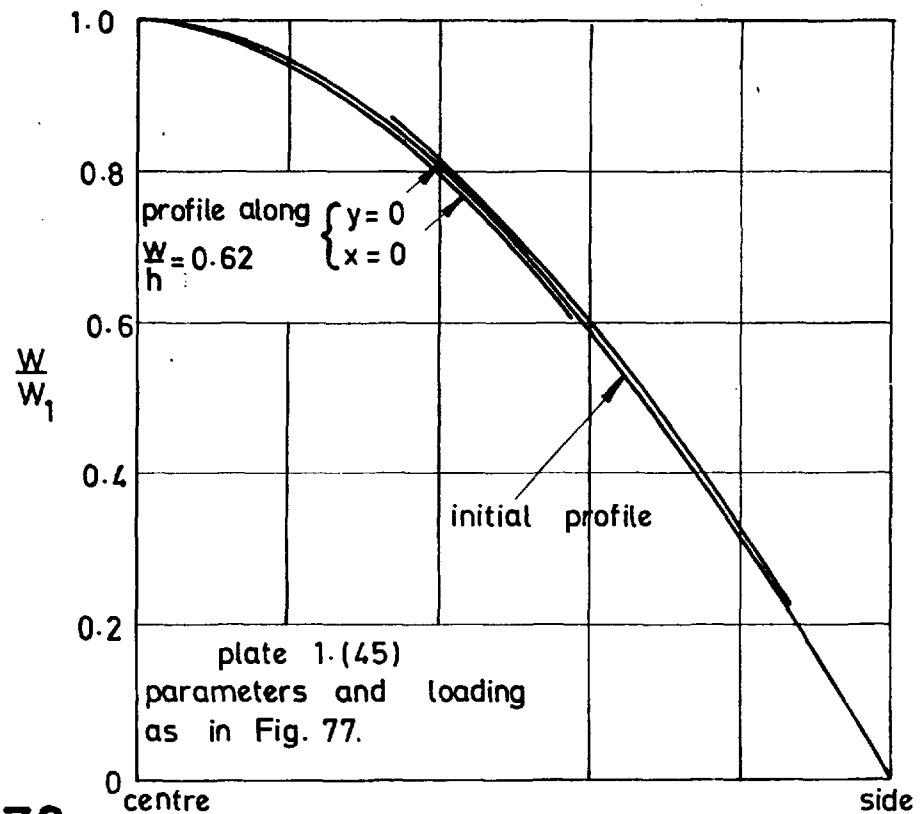


FIG. **78** Initially deformed simply supported plate under end-thrust. Deflection profiles along the centre lines.

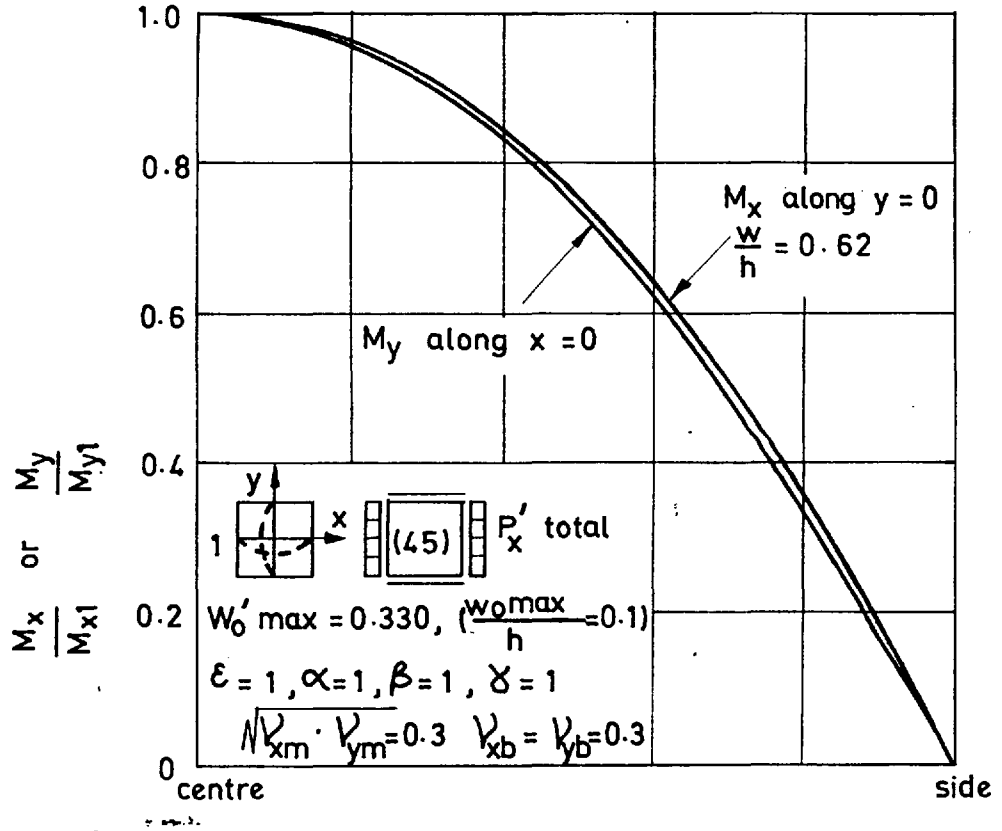


FIG. **79** Initially deformed simply supported square plate under edge-compression. Bending moment profiles along the centre lines.

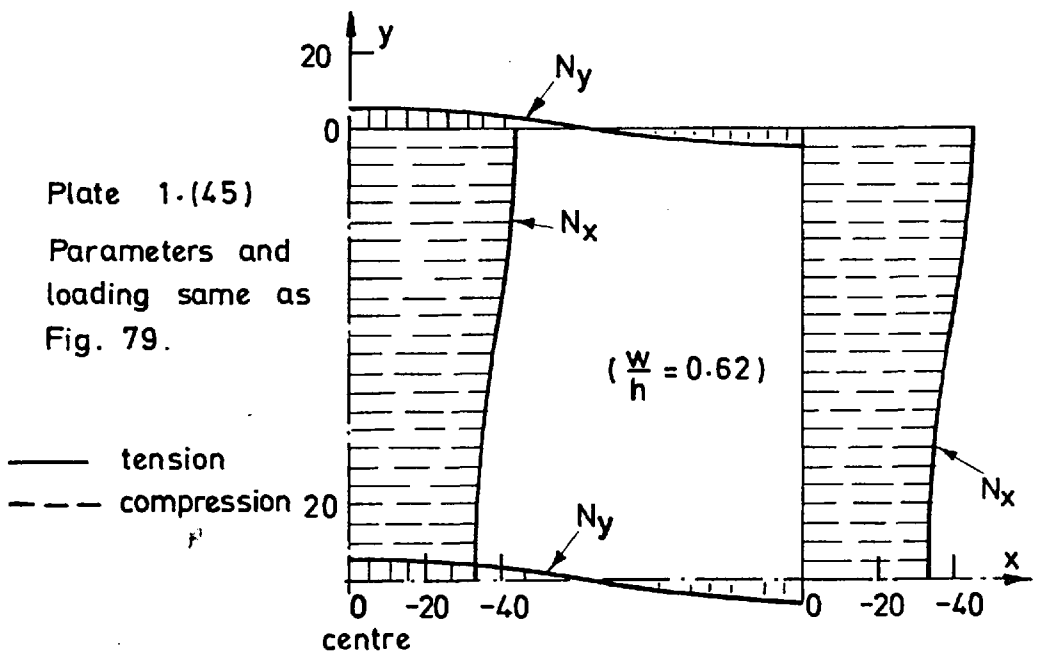


FIG. **80** Initially deformed simply supported plate under edge-compression. Distribution of membrane stress.

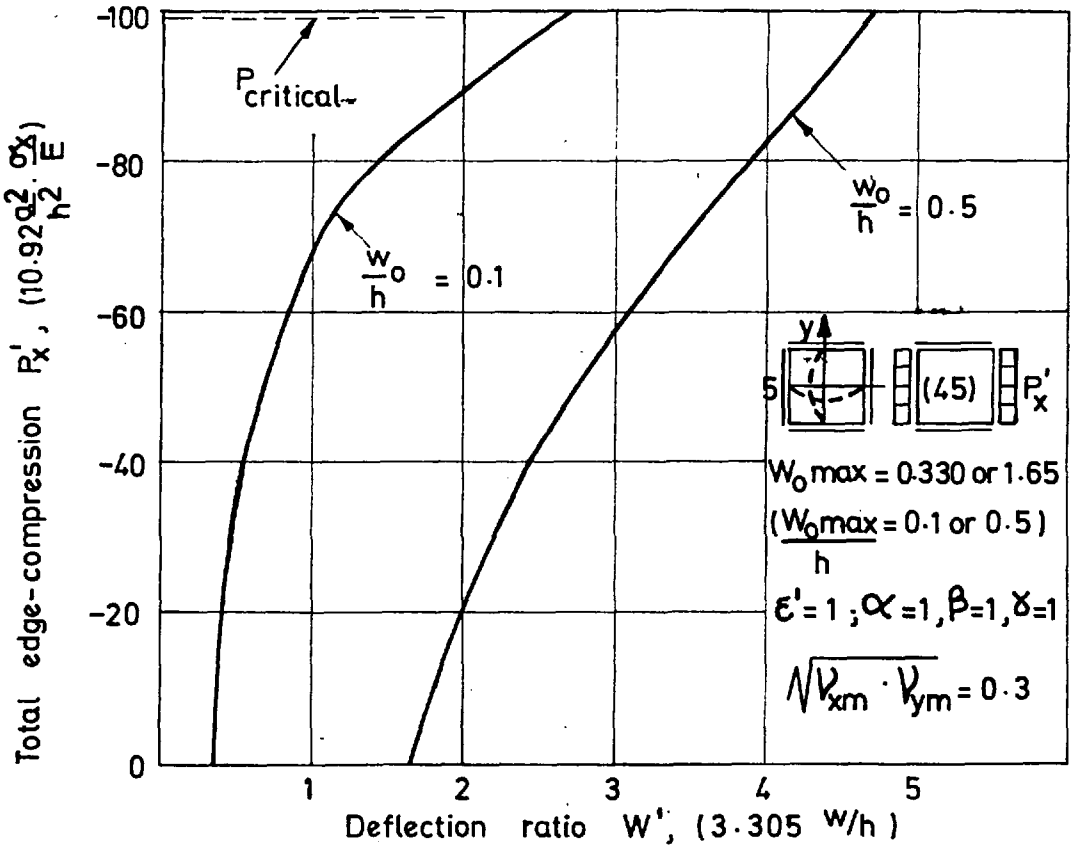


FIG. 81 Initially deformed clamped plate under edge-compression Deflection at centre.

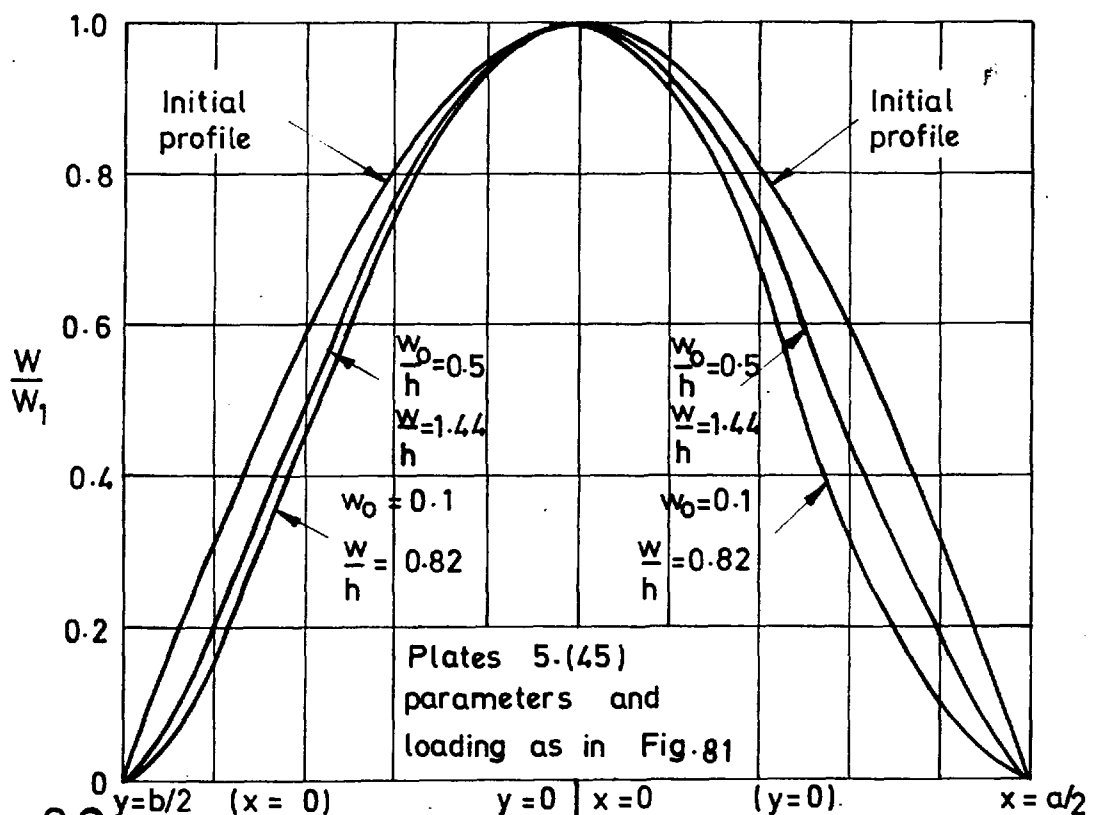


FIG. 82 Initially deformed clamped plates under edge-compression Deflection profiles along the centre lines.

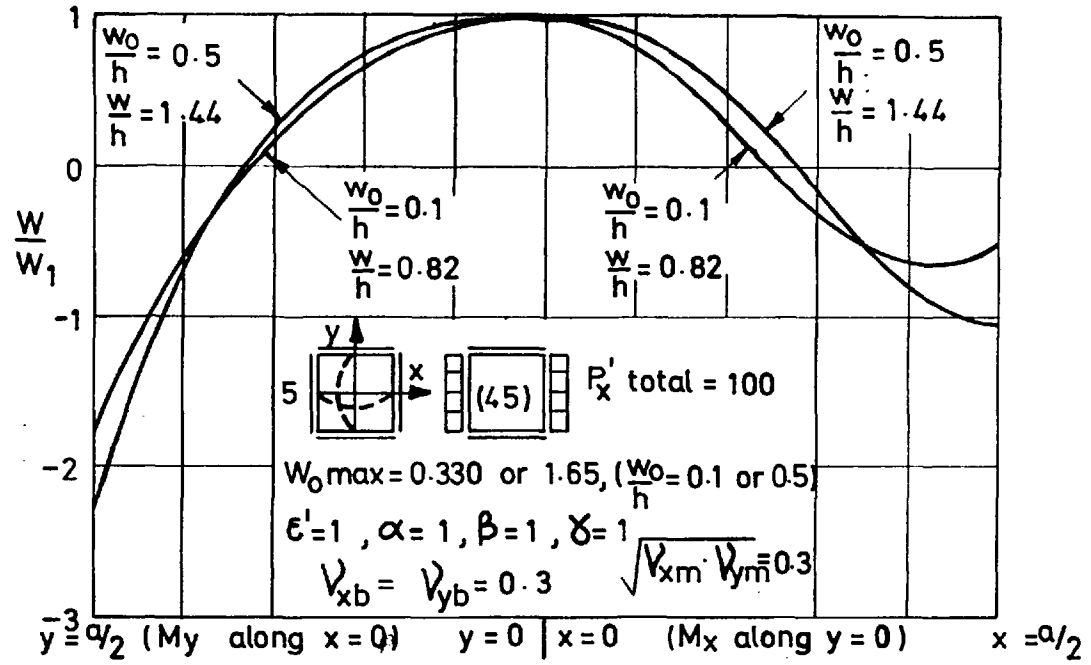


FIG. 83 Initially deformed clamped square plate under edge – compression. Bending moment profiles along the centre lines.

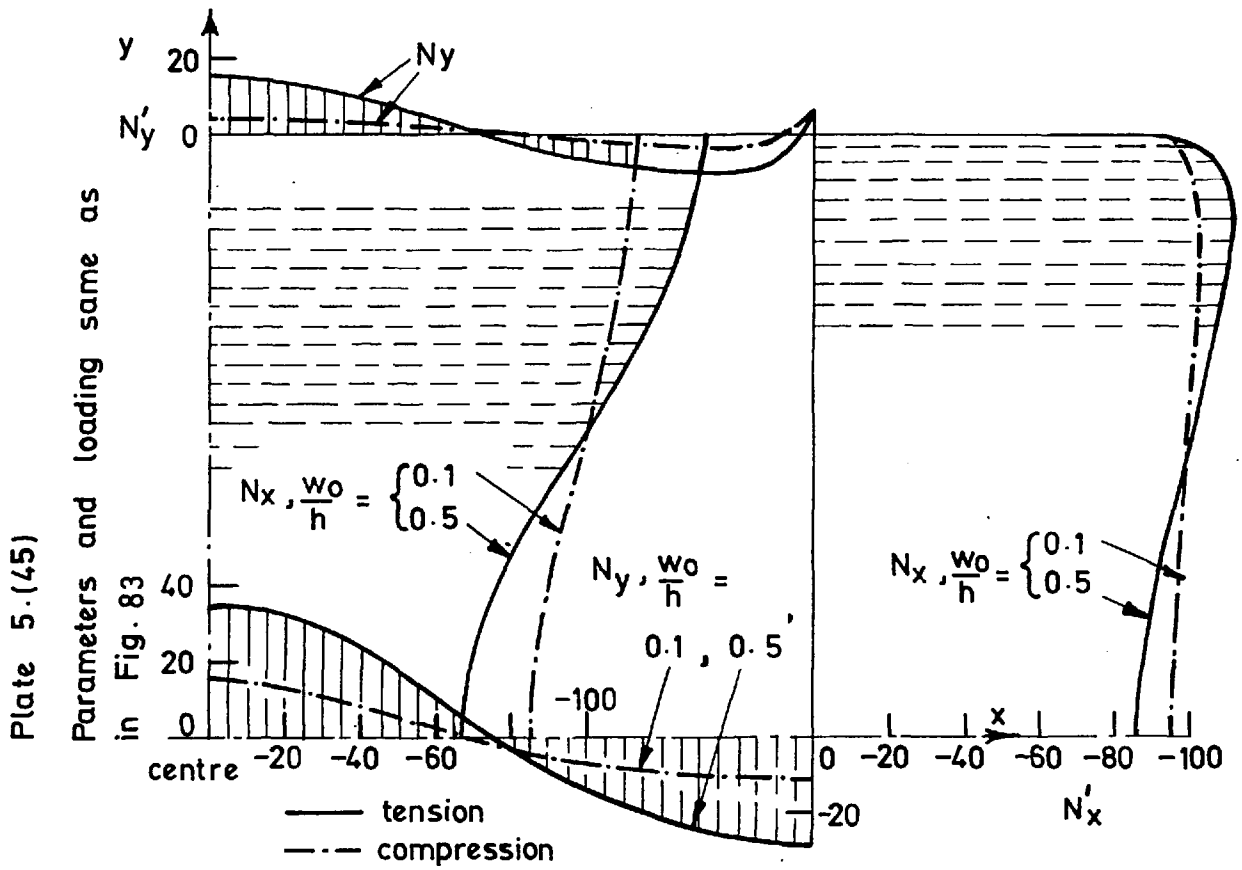


FIG. 84 Initially deformed clamped plate under edge – compression. Distribution of membrane stress.

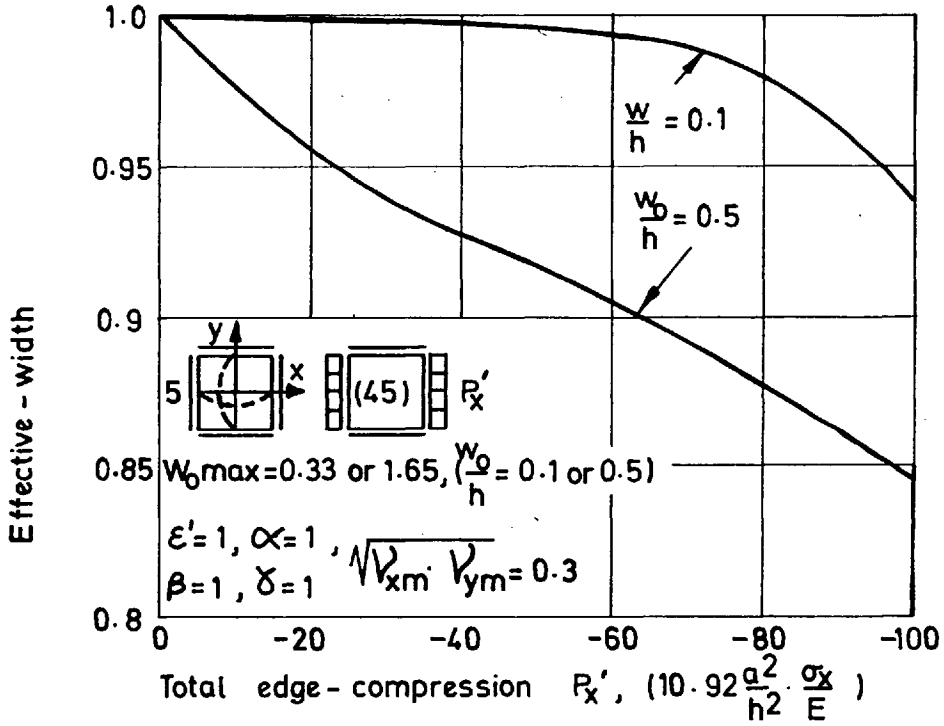


FIG. **85** Initially deformed clamped plate under edge-compression. Variation of effective width with edge-compression.

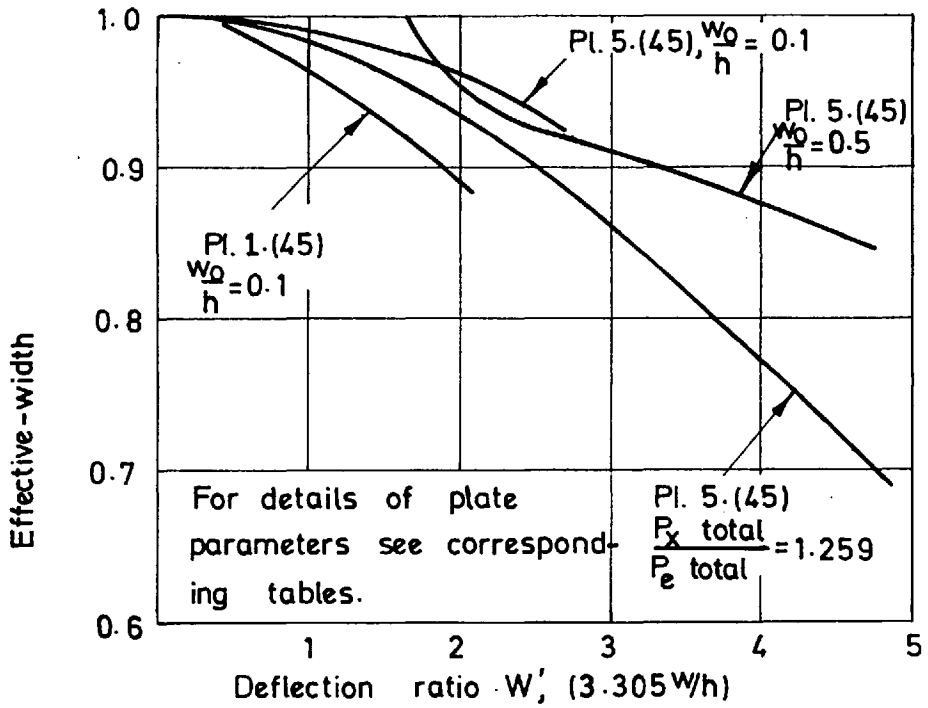


FIG. **86** Plates under edge-compression. Variation of effective - width with central deflection.

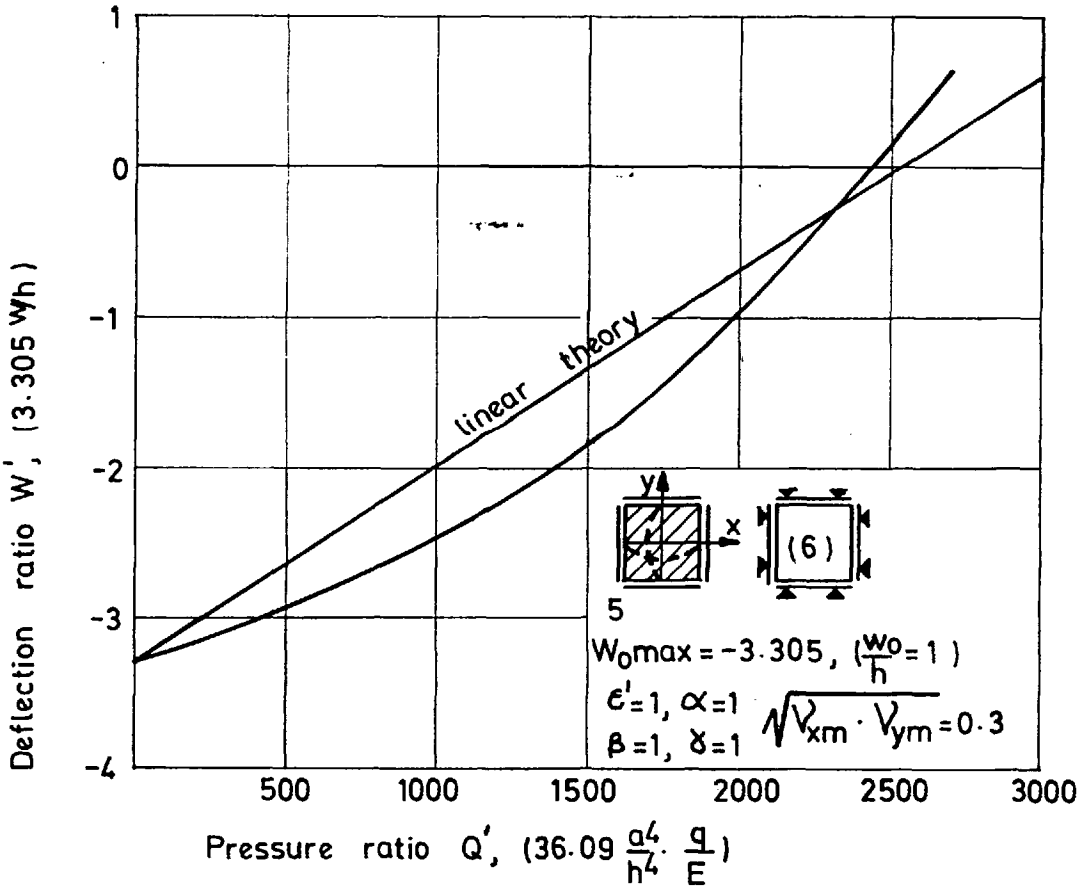


FIG. **87** Initially deformed clamped plate under transverse pressure. Deflection at centre.

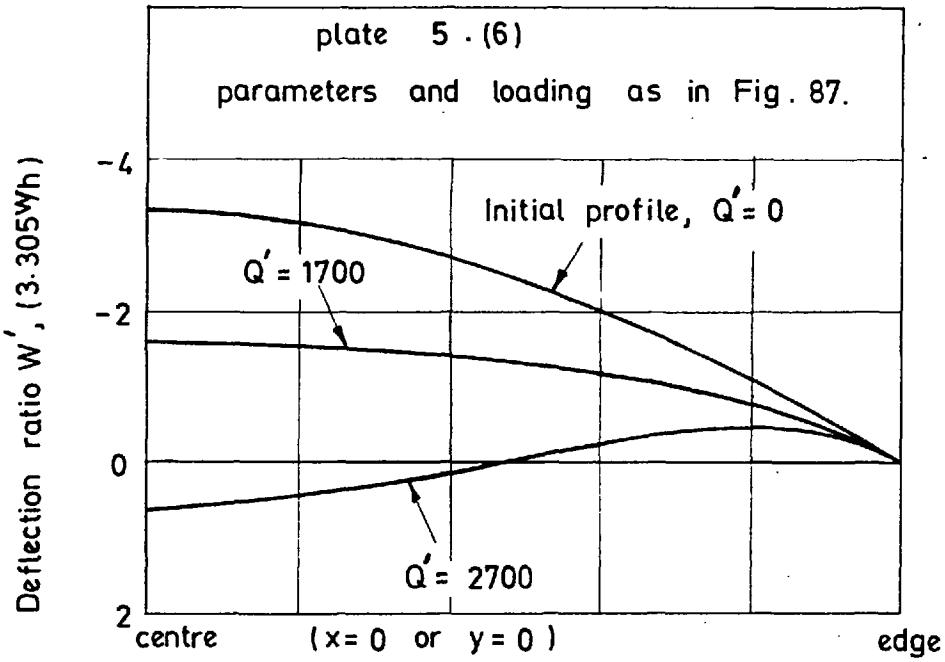


FIG. **88** Initially deformed clamped plate under transverse pressure. Deflection profiles along the centre lines.

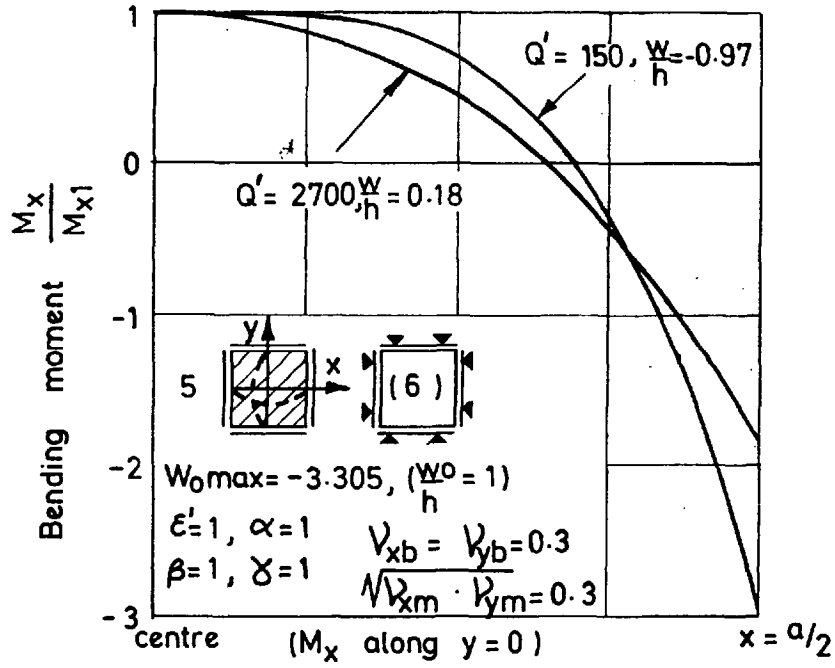


FIG. **89** Initially deformed clamped plate under transverse pressure. Bending moment profiles along the centre line.

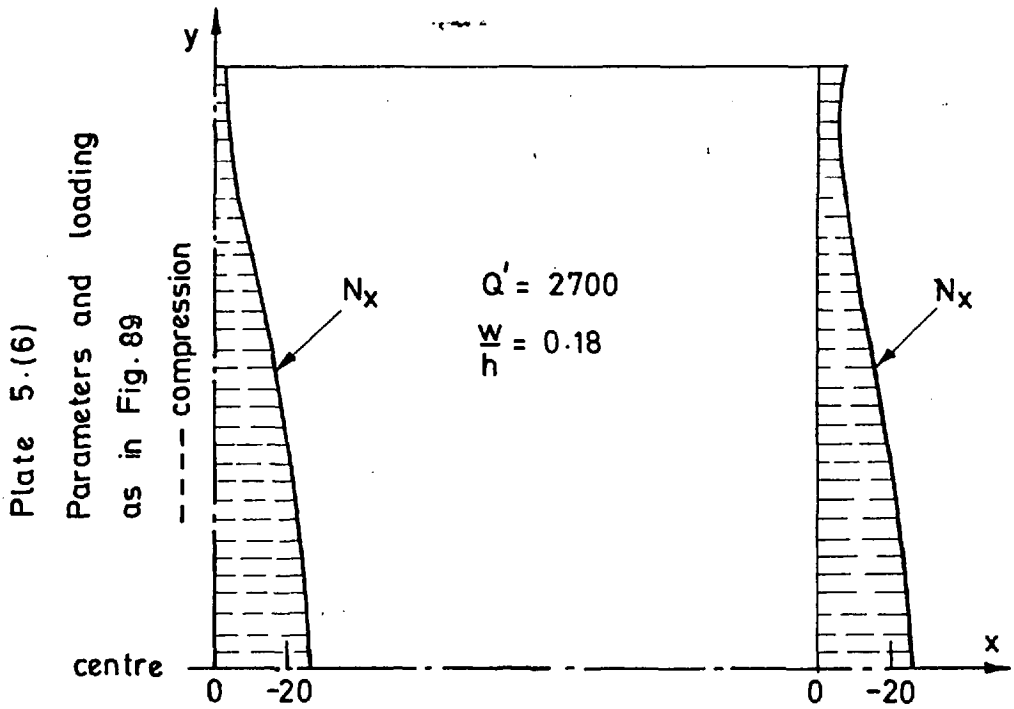
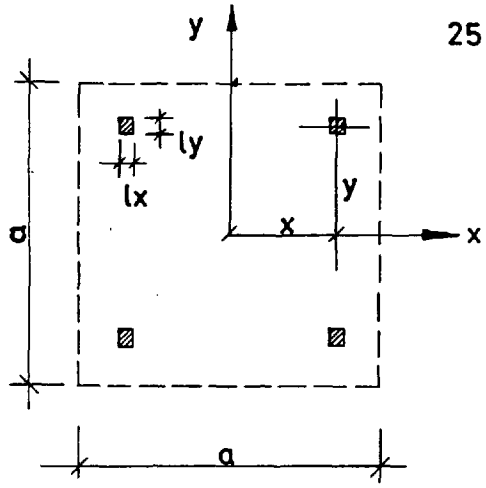


FIG. **90** Initially deformed clamped plate under transverse pressure. Distribution of membrane stress.



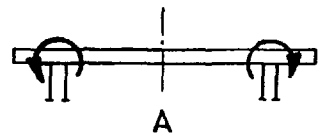
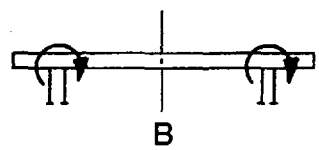
$lx = ly$

$\frac{lx}{a} = \frac{1}{20}$

$x = y$

$V_{xb} = V_{yb} = 0$

mesh 32 x 32, graded

case	$\frac{x}{a}$	mesh No.	$M_t = k_1 D_x \theta_x$ k_1 present solution	k_1 equi-valent beam.	max. moment * +ve k_2	-ve k_3
 A symmetrical	0.2	6	1.93	2.50	2.77	-1.78
	0.35	7	1.18	1.43	2.83	-1.75
	0.44	8	0.69	1.14	4.35	-0.84
 B antisymmetrical	0.2	6	2.58	10.00	2.16	-2.32
	0.35	7	3.17	5.71	2.49	-2.01
	0.44	8	1.52	4.55	4.21	-0.87

Note :

For +ve moment tension at top.

M_t = total applied moment at column - slab junction in x - direction.

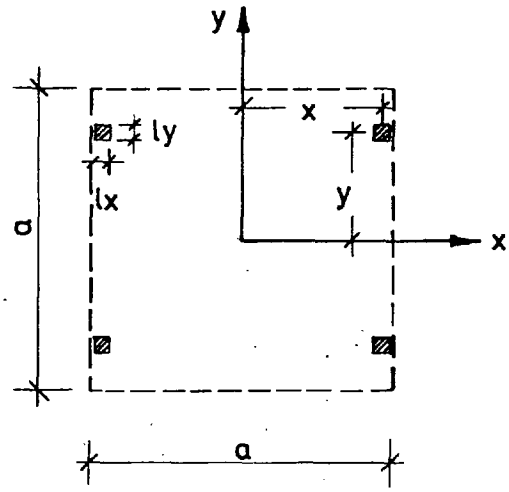
θ_x = rotation of slab in x - direction at top of column.

k_2, k_3 ratios of average applied moment,

e.g. max. +ve $M_x = k_2 \frac{2Mt}{a}$ * for position see text.

FIG. **92** Square slab on four columns.

Applied moment Mx at column - slab - junction.



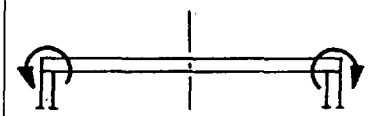
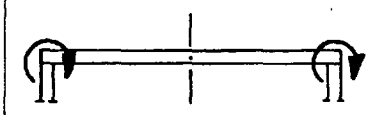
$lx = ly$

$\frac{lx}{a} = \frac{1}{20}$

$x = 0.44a$

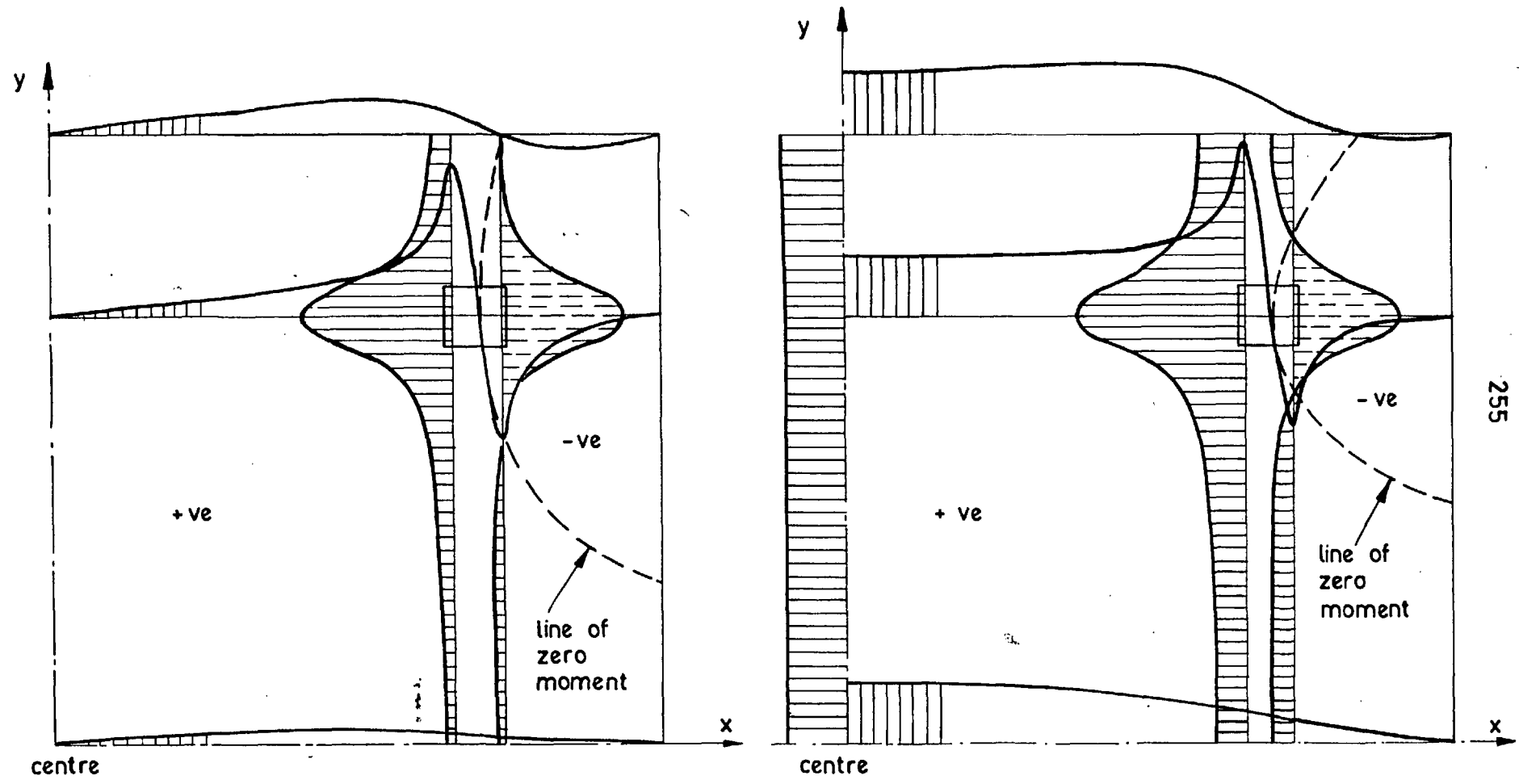
$V_{xb} = V_{yb} = 0$

mesh : 32 x 32 , graded

case	$\frac{y}{a}$	No. mesh	$M_t = k_1 D_x \theta_x$ k_1		max. moment	
			present solution	equi – valent beam	+ ve k_2	-ve k_3
 C symmetrical	0.2	10	0.69	1.14	3.22	-0.88
	0.35	9	0.86	1.14	3.27	-0.88
	0.44	8	0.88	1.14	4.35	-0.84
 D antisymmetrical	0.2	10	1.50	4.55	3.13	-0.90
	0.35	9	1.80	4.55	3.17	-0.89
	0.44	8	1.52	4.55	4.21	-0.87

Note : for notation see notes on Figure 92.

FIG. 93 Square slab on four columns.
Applied moment M_x at column - slab junction.



ii) case B, (antisymmetrical)

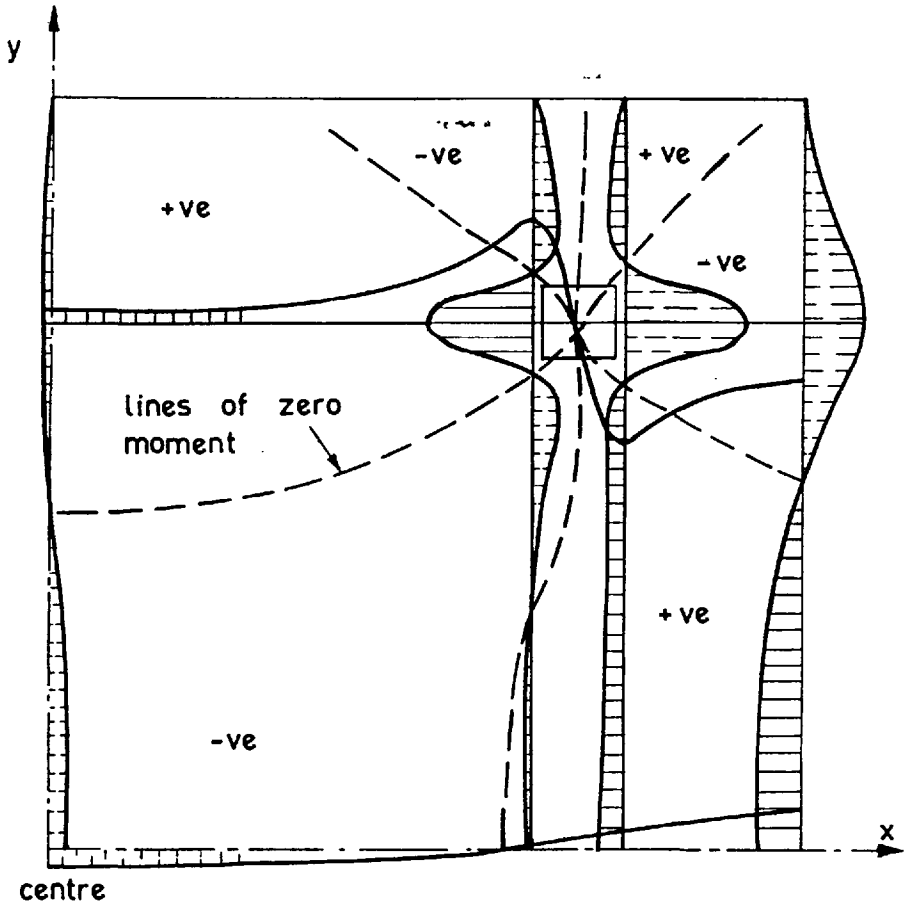
i) case A, (symmetrical)

$\frac{x}{a} = 0.35$, $\frac{lx}{a} = \frac{1}{20}$, scale : 1 cm ≡ average applied moment, $\left(\frac{2Mt}{a}\right)$ *

* see note on figure 92.

$V_{xb} = V_{yb} = 0$

FIG. **94** Square slab on four columns. Distribution, in the slab, of an applied moment Mx at the column - slab junction.



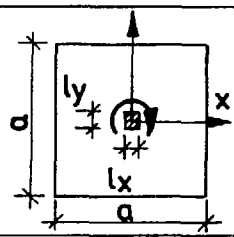
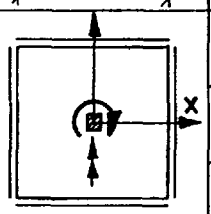
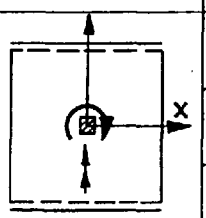
case A, (symmetrical)

$\frac{x}{a} = 0.35$, $\frac{lx}{a} = \frac{1}{20}$, $V_{xb} = V_{yb} = 0$

scale : 1 cm. $\equiv \frac{1}{2}$ average applied moment, $(\frac{Mt}{a})^*$

* see notes on figure 92.

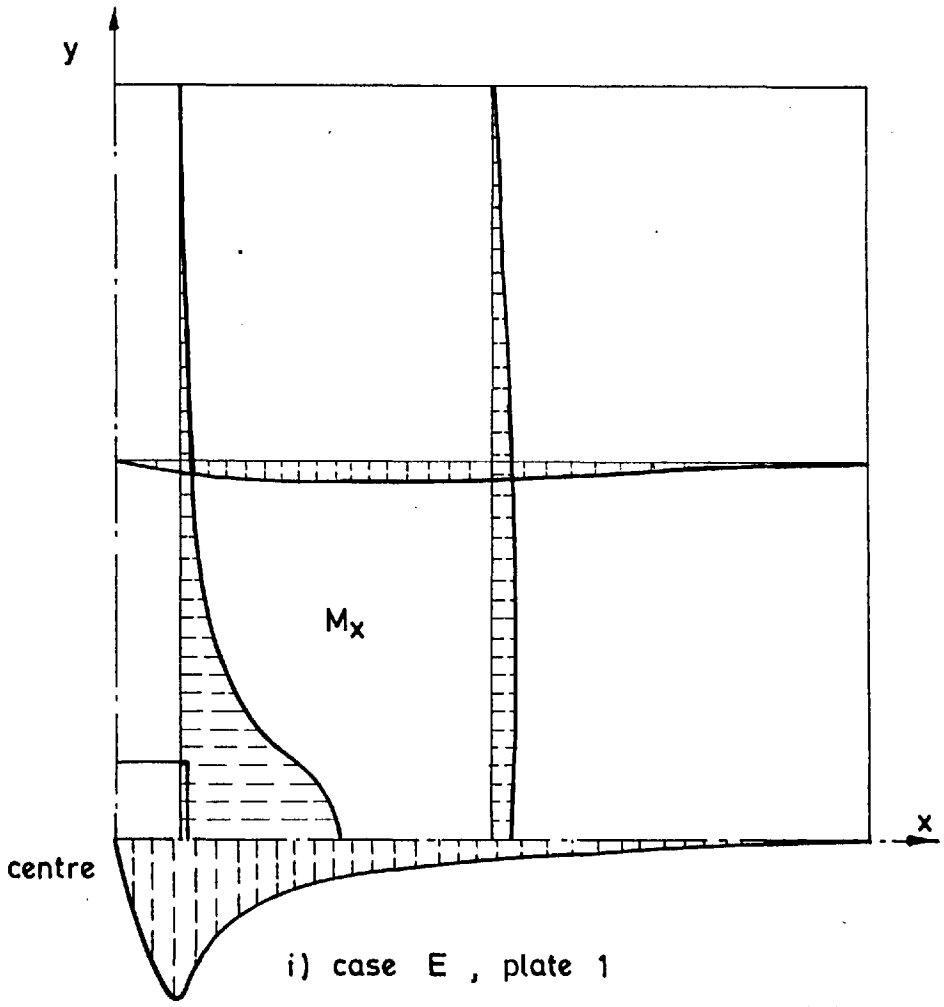
FIG. **95** Square slab on four columns.
Distribution of bending moment My in the slab, due to an applied moment Mx at the column–slab junction.

$\nu_{xb} = \nu_{yb} = 0$	$l_x = l_y$	mesh 32x32	$M_t = k_1 D_x \theta$ k_1		max. * moment
case	$\frac{lx}{a}$	mesh No.	present solution	equivalent beam	$M_x = k_2 \frac{M_t}{a}$ k_2
E plate 1 	0.05	11	4.17	–	−4.54
	0.1	12	5.53	–	−2.18
	0.15	13	6.78	–	−1.40
F plate 5 	0.05	11	4.25	–	−4.54
	0.1	12	6.24	–	−2.18
	0.15	13	7.87	–	−1.41
G plate 4 	0.05	11	4.10	16	−4.53
	0.1	12	5.40	16	−2.16
	0.15	13	6.59	16	−1.37

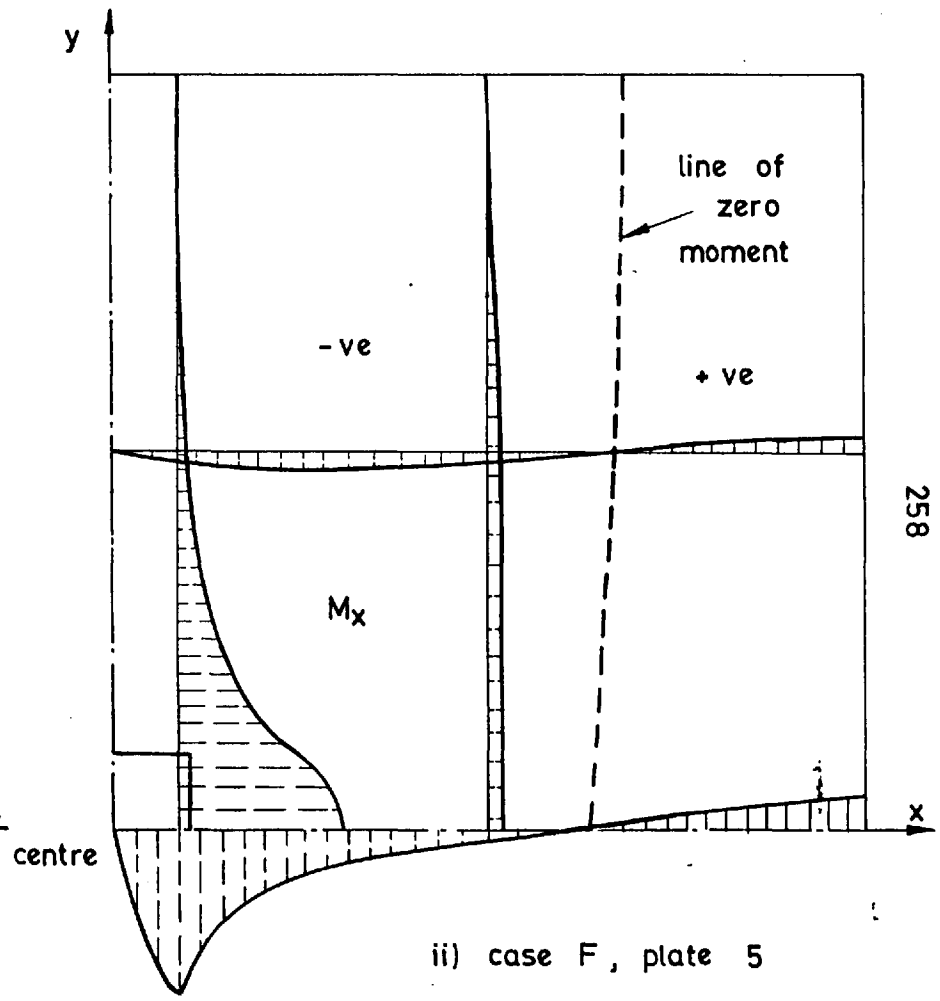
* M_t = total applied moment at column - slab junction in x – direction

* For position see figures and text.

FIG. 96 Square slab on central column.
Applied moment M_t at column - slab junction.



i) case E , plate 1

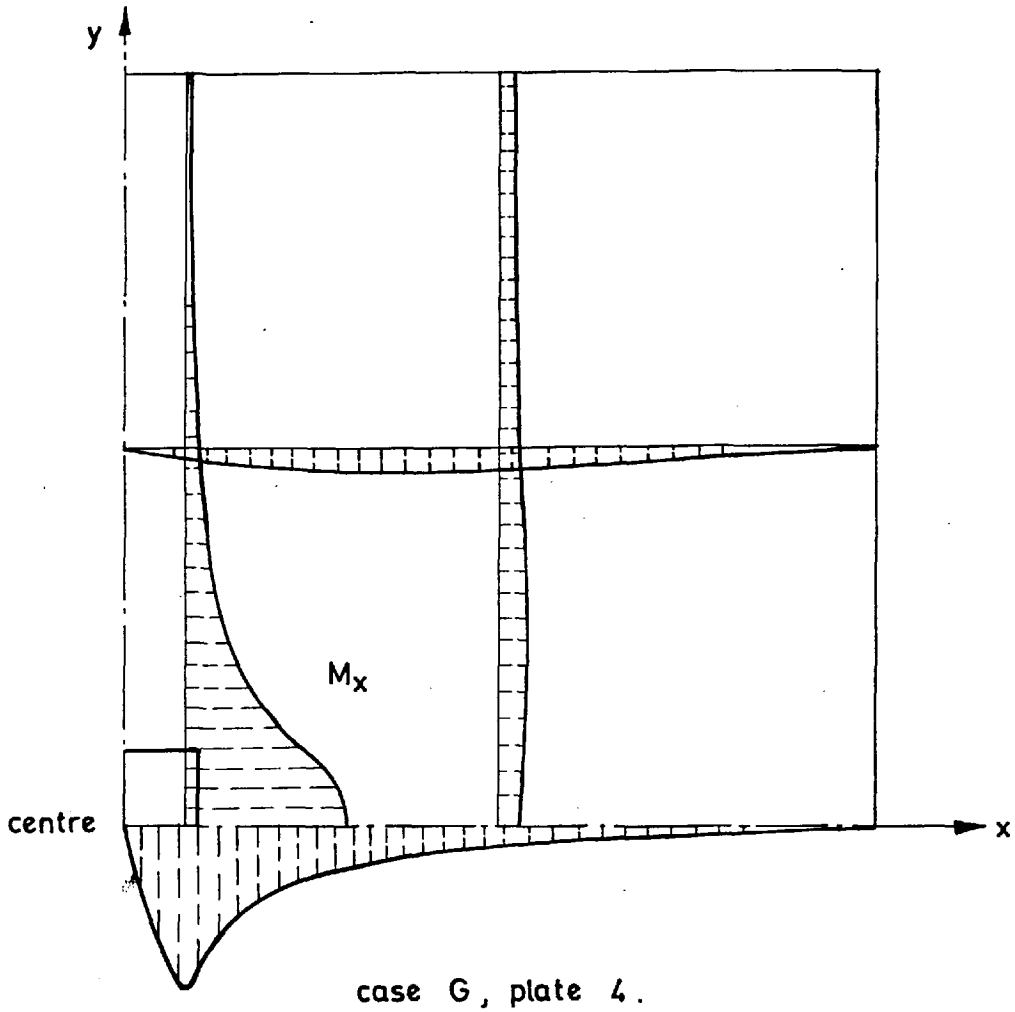


ii) case F , plate 5

$V_{xb} = V_{yb} = 0$, $l_x = l_y$, $\frac{l_x}{a} = 0{\cdot}1$, scale : 1 cm $\equiv \frac{Mt}{a}$ (average moment)

FIG. **97**

Square slab on central column. Distribution, in the slab, of an applied moment Mt (in x - direction) at column - slab junction.



case G, plate 4.

$V_{xb} = V_{yb} = 0$, $l_x = l_y$, $\frac{l_x}{a} = 0{\cdot}1$

Scale 1 cm $\equiv \frac{Mt}{a}$ (average moment)

FIG **98** Square slab on central column. Distribution, in the slab, of an applied moment Mt (in x - direction) at column - slab junction.

mesh No.	1	2		3		4		5
number of sub-divisions	12 x 12	12 x 20		12 x 20		12 x 20		16 x 16
mesh lengths along	x - x and y - y	x - x	y - y	x - x	y - y	x - x	y - y	x - x and y - y
Mesh lengths are given from the centre to the side as ratios of the average mesh length	1·125	1·125	1	1	1·5	1·125	1·5	0·5333
	1·125	1·125	1	1	1·5	1·125	1·5	0·5333
	1·125	1·125	1	1	1·5	1·125	1·5	0·7334
	1·125	1·125	1	1	1	1·125	1	1·2
	1	1	1	1	1	1	1	1·5
	0·5	0·5	1	1	1	0·5	1	1·5
			1		1		1	1·25
			1		0·5		0·5	0·75
			1		0·5		0·5	
			1		0·5		0·5	

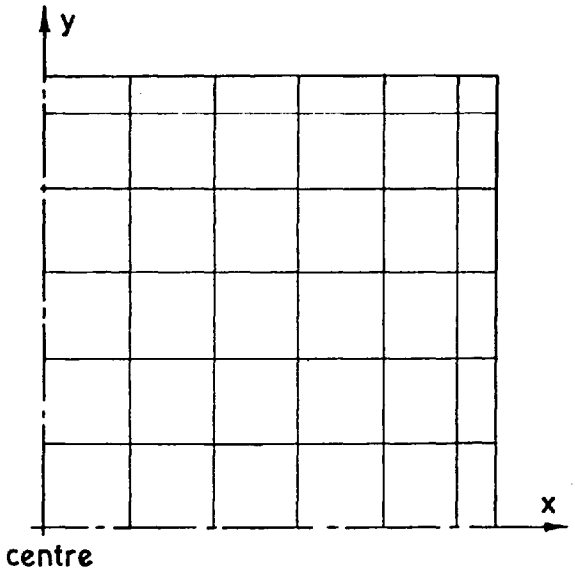
FIG. 99 Graded meshes.

mesh No.	6	7	8	9		10	
mesh lengths along	x - x and y - y	x - x and y - y	x - x and y - y	x - x	y - y	x - x	y - y
Mesh lengths are given from the centre to the side as ratios of the average mesh length. number of divisions 32 x 32	1.80	2.00	2.00	2.00	2.00	2.00	1.80
	1.50	2.00	2.00	2.00	2.00	2.00	1.50
	1.50	2.10	2.00	2.00	2.10	2.00	1.50
	0.64	2.00	1.50	1.50	2.00	1.50	0.64
	0.32	1.50	1.50	1.50	1.50	1.50	0.32
	0.32	0.64	1.50	1.50	0.64	1.50	0.32
	0.32	0.32	1.20	1.20	0.32	1.20	0.32
	0.32	0.32	1.00	1.00	0.32	1.00	0.32
	0.32	0.32	0.80	0.80	0.32	0.80	0.32
	0.32	0.32	0.58	0.58	0.32	0.58	0.32
	0.64	0.32	0.32	0.32	0.32	0.32	0.64
	1.50	0.32	0.32	0.32	0.32	0.32	1.50
	1.50	0.64	0.32	0.32	0.64	0.32	1.50
	2.00	1.00	0.32	0.32	1.00	0.32	2.00
	2.00	1.20	0.32	0.32	1.20	0.32	2.00
	1.00	1.00	0.32	0.32	1.00	0.32	1.00

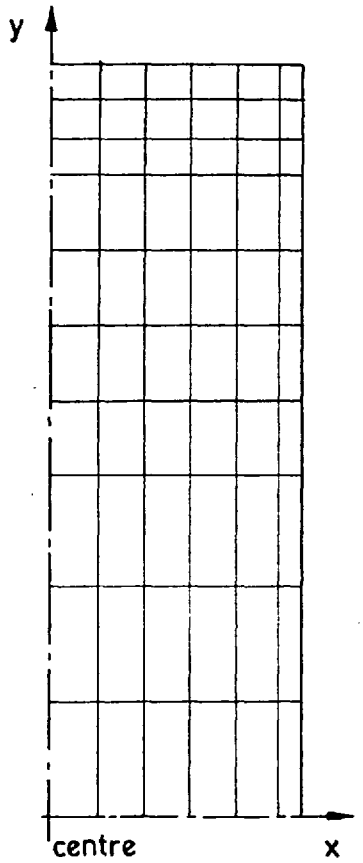
FIG. 100 Graded meshes.

mesh. No.	11	12	13
mesh lengths along	x - x and y - y	x - x and y - y	x - x and y - y
Mesh lengths are given from the centre line to the side as ratios of average mesh length. Subdivision of plate 32 x 32.	0.32	0.45714	0.53333
	0.32	0.45714	0.53333
	0.32	0.45714	0.53333
	0.54	0.45714	0.53333
	0.90	0.57144	0.53333
	1.10	1.10	0.83335
	1.50	1.50	1.50
	1.50	1.50	1.50
	1.50	1.50	1.50
	1.50	1.50	1.50
	1.50	1.50	1.50
	1.50	1.50	1.50
	1.50	1.50	1.50
	1.00	1.00	1.0
	0.50	0.50	0.50
	0.50	0.50	0.5

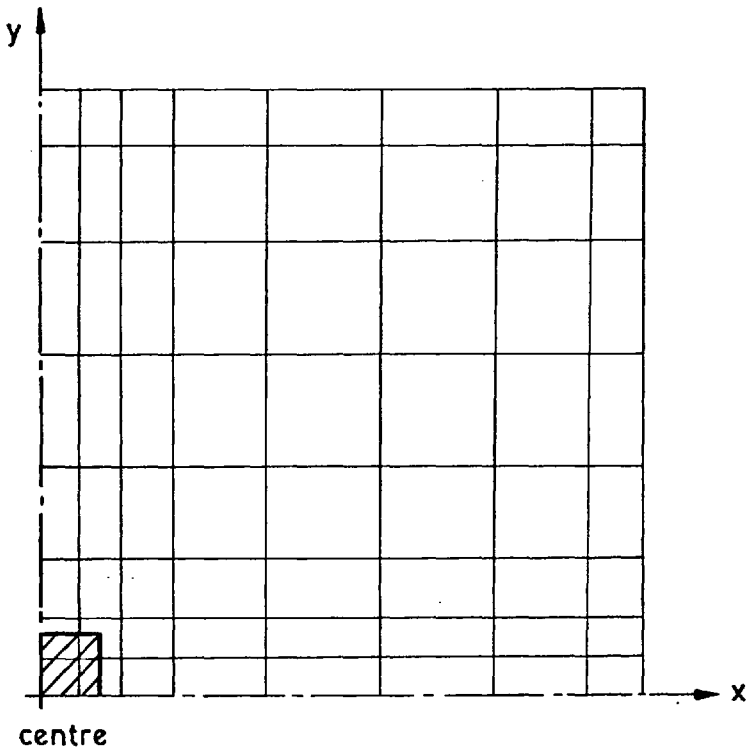
FIG. 101 Graded meshes.



mesh No. 1.

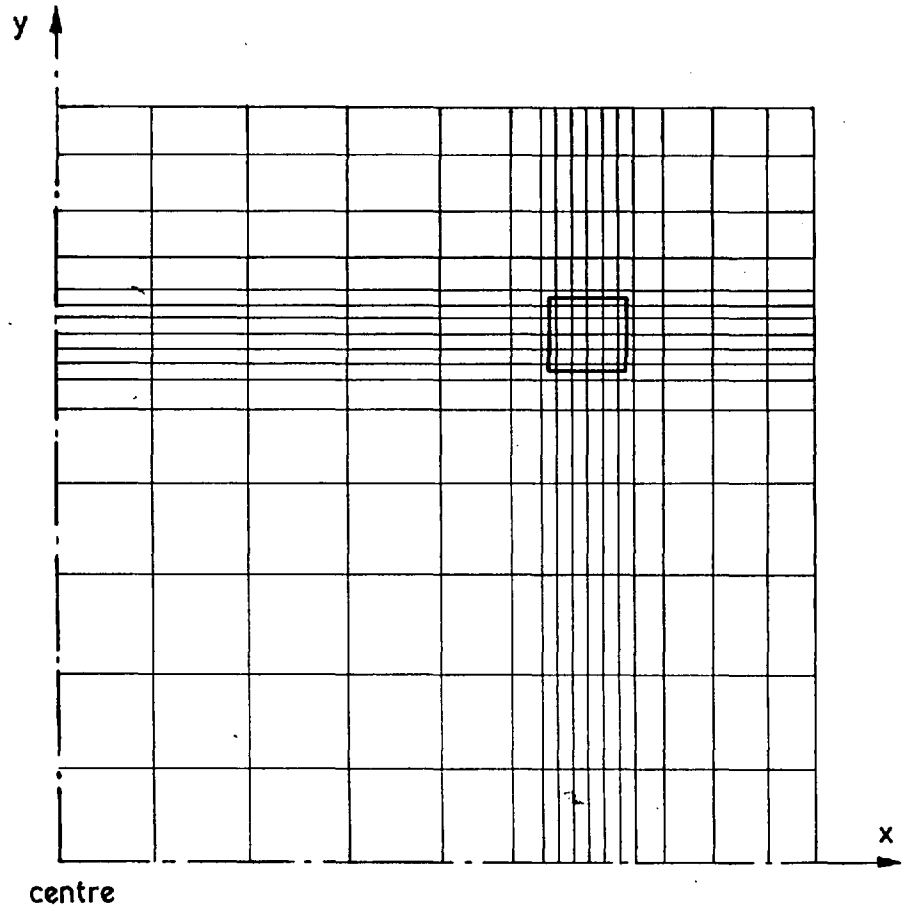


mesh No. 4.

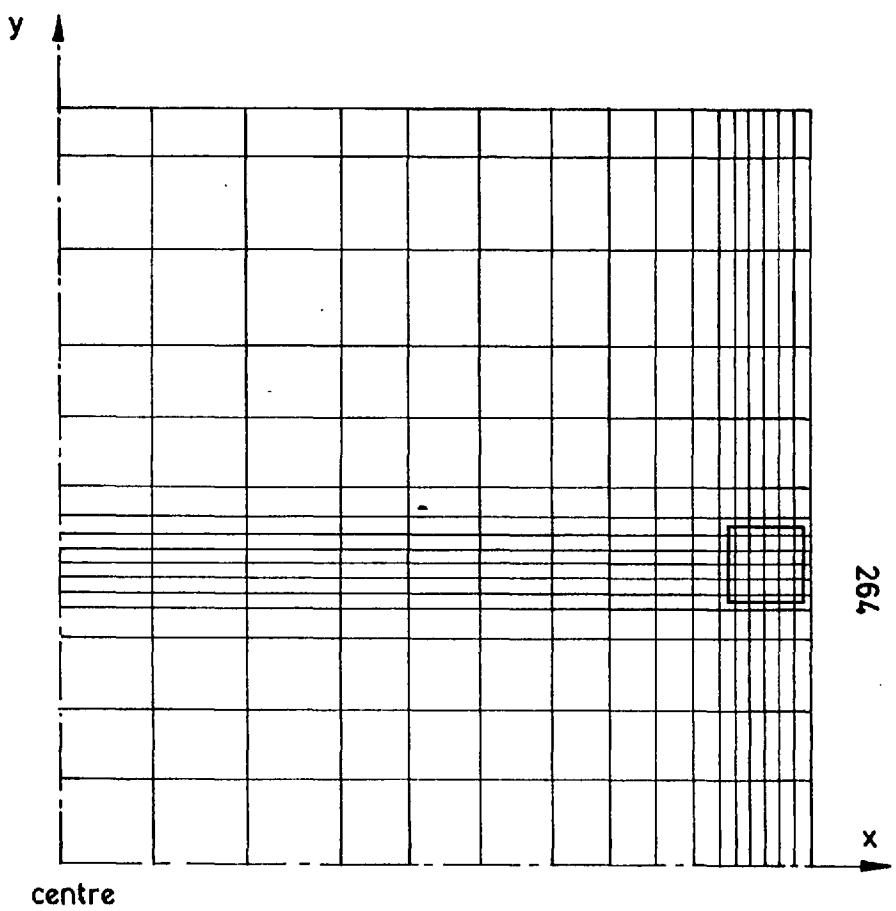


mesh No. 5.

FIG. 102

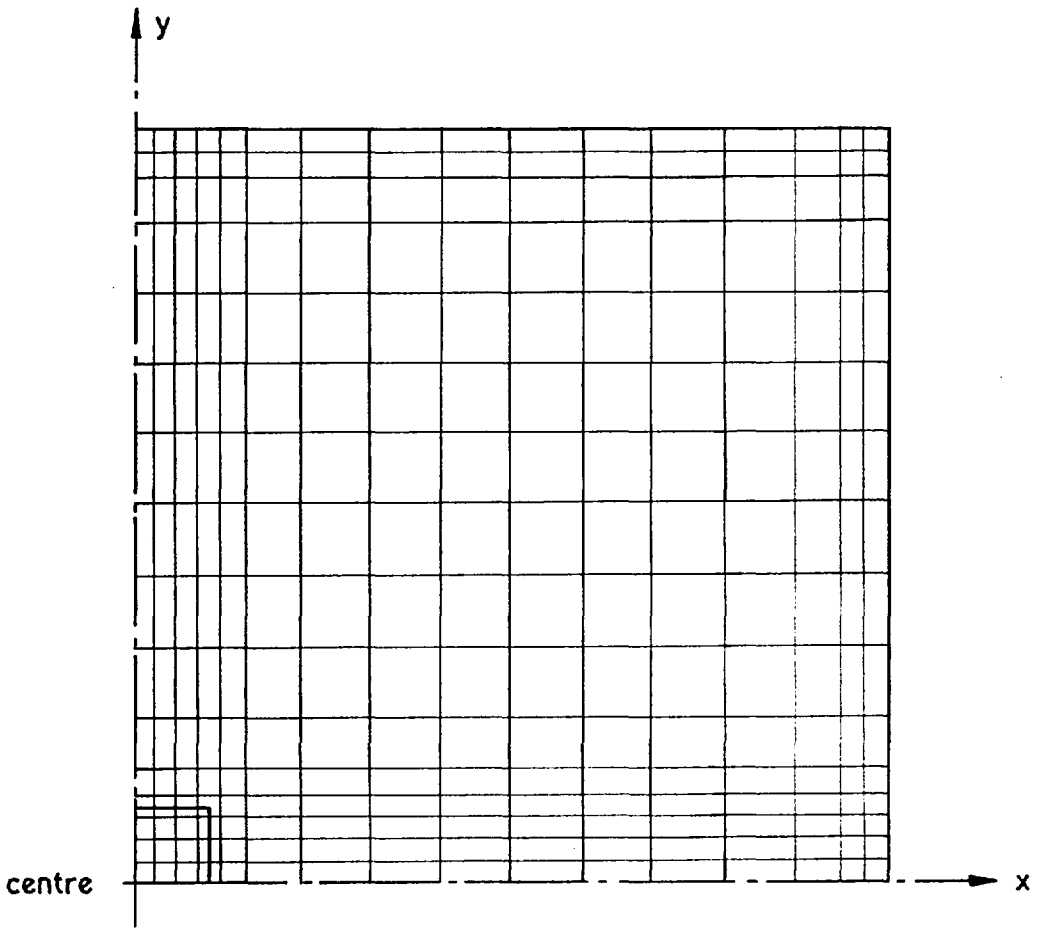


mesh No. 7.



mesh No. 10.

FIG. 103



mesh No. 12.

FIG. 104

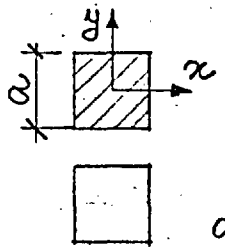


TABLE 1

plate 1.(1)

mesh: 12×12
equal

accuracy: 0.5%

$\varepsilon' = 1, \alpha = 1$

$\beta = 1, \gamma = 1$

$\sqrt{\nu_{xm} \cdot \nu_{ym}} = 0.3$

$\nu_{xb} = \nu_{yb} = 0.3$

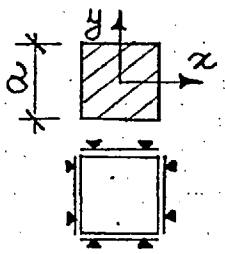


TABLE 2

plate 1.(6)

mesh: 12×12
equal

accuracy: 0.5%

$\varepsilon' = 1, \alpha = 1$

$\beta = 1, \gamma = 1$

$\sqrt{\nu_{xm} \cdot \nu_{ym}} = 0.3$

$\nu_{xb} = \nu_{yb} = 0.3$

Q'	W_1'	M_{x1}', M_{y1}'	N_{x1}', N_{y1}'	N_{x3}', N_{y2}'	U_2', V_3'	W_1'	M_{x1}', M_{y1}'	N_{x1}', N_{y1}'	N_{x3}', N_{y2}'	N_{x2}', N_{y3}'	N_{x4}', N_{y4}'	total N_x' or N_y' at the edge
linear	4.06×10^{-3}	4.76×10^{-2}	0	0	0	4.06×10^{-3}	4.76×10^{-2}	0	0	0	0	0
150	0.605	7.08	0.370	-0.675	-0.808	0.582	6.80	1.059	0.189	1.080	0.228	0.321
400	1.556	17.92	2.38	-4.42	-6.44	1.325	15.20	5.222	0.972	5.380	1.109	1.600
750	2.698	30.05	6.89	-13.20	-33.32	2.014	22.53	11.70	2.295	12.20	2.432	3.630
1100	3.625	38.80	12.31	-24.31	-116.3	2.488	27.22	17.98	3.672	18.91	3.667	5.632
1500	4.509	46.23	18.35	-37.60	-246.0	2.888	30.94	24.80	5.254	26.29	4.966	7.836
1900	5.260	51.86	24.09	-51.03	-460.2	3.216	33.86	31.02	6.776	33.10	6.107	9.872
2300	5.913	56.21	29.57	-64.50	-733.8	3.494	36.25	36.82	8.256	39.51	7.137	11.79
2700	6.462	59.24	35.28	-78.75	-955.8	3.737	38.28	42.30	9.702	45.60	8.085	13.62
3100	7.012	62.51	39.86	-91.22	-1086	3.952	40.04	47.52	11.12	51.42	8.965	15.37
3500	7.473	64.65	44.92	-104.8	-1388	4.116	41.24	53.10	12.62	57.64	9.907	17.24

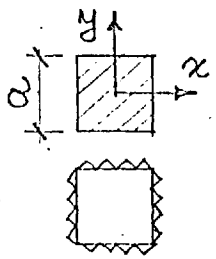


TABLE 3

plate 1.(13)

mesh : 12×12 equal

accuracy : 0.5%

$\varepsilon' = 1,\ \alpha = 1$

$\beta = 1,\ \gamma = 1$

$\sqrt{\nu_{xm} \cdot \nu_{ym}} = 0.3$

$\nu_{xb} = \nu_{yb} = 0.3$

Q'	W_1'	or M'_{x1} M'_{y1}	or N'_{x1} N'_{y1}	total N'_{xy} at the edge	or U'_2 V'_3
linear	4.06×10^{-3}	4.76×10^{-2}	0	0	0
150	0.600	7.01	0.576	0.151	-0.310
400	1.487	17.04	3.41	0.907	-1.88
750	2.441	26.95	9.04	2.46	-5.21
1100	3.158	33.57	14.96	4.17	-8.98
1 500	3.803	38.91	21.44	6.12	-13.41
1 900	4.335	42.88	27.48	8.01	-17.84
2 300	4.792	46.00	33.15	9.84	-22.23
2 700	5.194	48.56	38.49	11.61	-26.58
3 100	5.555	50.72	43.57	13.32	-30.87
3 500	5.883	52.58	48.41	14.99	-35.12

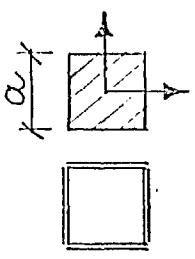


TABLE 4

plate 1.(15)

mesh : 12×12 equal

accuracy : 0.5%

$\varepsilon' = 1,\ \alpha = 1$

$\beta = 1,\ \gamma = 1$

$\sqrt{\nu_{xm} \cdot \nu_{ym}} = 0.3$

$\nu_{xb} = \nu_{yb} = 0.3$

W_1'	or M'_{x1} M'_{y1}	or N'_{x1} N'_{y1}	or N'_{x3} N'_{y2}	or N'_{x2} N'_{y3}	or N'_{x4} N'_{y4}	or U' V'
4.06×10^{-3}	4.76×10^{-2}	0	0	0	0	0
0.601	7.04	0.430	-0.468	0.452	-0.428	-0.232
1.510	17.44	2.63	-2.89	2.81	-2.69	-1.45
2.516	28.30	7.19	-8.00	7.91	-7.68	-4.07
3.281	35.91	12.09	-13.64	13.68	-13.52	-7.05
3.968	42.25	17.49	-19.99	20.35	-20.50	-10.52
4.530	47.08	22.53	-26.03	26.85	-27.55	-13.93
5.007	50.96	27.22	-31.73	33.10	-34.57	-17.24
5.425	54.21	31.61	-37.12	39.13	-41.54	-20.47
5.797	57.00	35.74	-42.25	44.93	-48.44	-23.61
6.133	59.45	39.66	-47.13	50.53	-55.30	-26.67

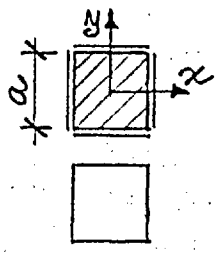


TABLE 5

plate 5.(1)

mesh: 12×12 graded No.1

accuracy: 0.5%

$\varepsilon' = 1,\ \alpha = 1$

$\beta = 1,\ \delta = 1$

$\sqrt{\nu_{xm} \cdot \nu_{ym}} = 0.3$

$\nu_{xb} = \nu_{yb} = 0.3$

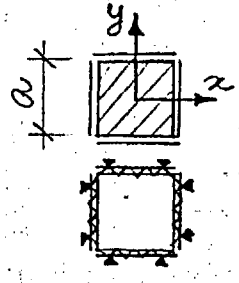


TABLE 6

plate 5. (10)

mesh: 16×16 equal

accuracy: 0.5%

$\varepsilon' = 1,\ \alpha = 1$

$\beta = 1,\ \delta = 1$

$\sqrt{\nu_{xm} \cdot \nu_{ym}} = 0.3$

$\nu_{xb} = \nu_{yb} = 0.3$

Q'	W_1'	M_{x1}' or M_{y1}'	M_{x2}' or M_{y3}'	N_{x1}' or N_{y1}'	N_{x3}' or N_{y2}'	U_2' or V_3'	W_1'	M_{x1}' or M_{y1}'	M_{x2}' or M_{y3}'	N_{x1}' or N_{y1}'	N_{x3}' or N_{y2}'	N_{x2}' or N_{y3}'	N_{x4}' or N_{y4}'	total $\frac{N_x'}{2}$ or $\frac{N_y'}{2}$ at the edge	total $N_{xy}'/2$ at the edge
linear	1306×10^{-3}	2.291×10^{-2}	-5.016×10^{-2}	0	0	0	1.259×10^{-3}	2.261×10^{-2}	-5.132×10^{-2}	0	0	0	0	0	0
150	0.196	3.43	-7.52	0.0633	-0.0780	-0.0244	0.188	3.38	-7.69	0.1156	0.0226	0.0752	0.0010	0.0218	0.0064
400	0.520	9.10	-20.02	0.445	-0.550	-0.172	0.497	8.91	-20.39	0.8020	0.1572	0.5239	0.0069	0.1515	0.0444
750	0.965	16.79	-37.37	1.527	-1.895	-0.595	0.909	16.13	-37.64	2.661	0.5253	1.751	0.023	0.5057	0.1475
1100	1.394	24.03	-54.25	3.157	-3.954	-1.24	1.286	22.55	-54.04	5.282	1.054	3.512	0.046	1.012	0.2934
1500	1.858	31.64	-73.06	5.543	-7.034	-2.22	1.671	28.84	-71.63	8.908	1.799	5.998	0.0781	1.726	0.4961
1900	2.294	38.48	-91.22	8.330	-10.73	-3.41	2.012	34.14	-88.09	12.86	2.633	8.778	0.1136	2.520	0.7181
2300	2.700	44.59	-108.7	11.39	-14.90	-4.76	2.315	38.62	-103.5	16.98	3.523	11.74	0.1509	3.364	0.9502
2700	3.080	50.02	-125.6	14.61	-19.44	-6.25	2.586	42.44	-118.2	21.15	4.444	14.81	0.1891	4.235	1.186
3100	3.435	54.86	-141.9	17.92	-24.25	-7.85	2.832	45.74	-132.0	25.31	5.384	17.95	0.2275	5.121	1.427
3500	3.768	59.18	-157.6	21.28	-29.26	-9.53	3.057	48.61	-145.3	29.42	6.331	21.10	0.2659	6.012	1.655

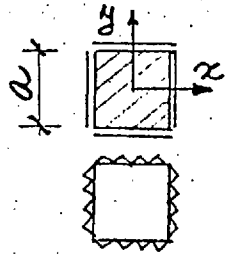


TABLE 7

plate 5.(13)

mesh : 12×12 equal

accuracy: 0.5%

$\varepsilon'=1, \alpha=1$

$\beta=1, \gamma=1$

$\sqrt{\nu_{xm}\cdot\nu_{ym}}=0.3$

$\nu_{xb}=\nu_{yb}=0.3$

Q'	W_1'	or M_{x1}' M_{y1}'	or M_{x2}' M_{y3}'	or N_{x1}' N_{y1}'	total $N_{xy}'/2$ at the edge	or U_2' V_3'
linear	1.258×10^{-3}	2.24×10^{-2}	-5.12×10^{-2}	0	0	0
150	0.1886	3.36	-7.68	0.0796	0.0147	-0.0196
400	0.5001	8.88	-20.41	0.558	0.103	-0.138
750	0.9232	16.29	-37.93	1.89	0.352	-0.471
1100	1.324	23.13	-54.91	3.85	0.724	-0.973
1500	1.749	30.15	-73.51	6.66	1.26	-1.71
1900	2.139	36.31	-91.24	9.84	1.89	-2.58
2300	2.495	41.64	-108.1	13.34	2.60	-3.56
2700	2.825	46.38	-124.3	16.83	3.32	-4.59
3100	3.125	50.44	-139.6	20.55	4.10	-5.70
3500	3.408	54.14	-154.5	24.08	4.87	-6.82

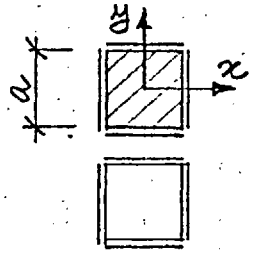


TABLE 8

plate 5. (15)

mesh : 12×12 graded, No. 1

accuracy : 0.5%

$\varepsilon'=1, \alpha=1$

$\beta=1, \gamma=1$

$\sqrt{\nu_{xm}\cdot\nu_{ym}}=0.3$

$\nu_{xb}=\nu_{yb}=0.3$

W_1'	or M_{x1}' M_{y1}'	or M_{x2}' M_{y3}'	or N_{x1}' N_{y1}'	or N_{x3}' N_{y2}'	or N_{x2}' N_{y3}'	or N_{x4}' N_{y4}'	or U' V'
1.306×10^{-3}	2.29×10^{-2}	-5.02×10^{-2}	0	0	0	0	0
0.1958	3.43	-7.52	0.0683	-0.0611	0.0284	0.0225	-0.0172
0.5198	9.09	-20.01	0.479	-0.430	0.201	0.158	-0.121
0.9627	16.74	-37.28	1.64	-1.47	0.691	0.543	-0.417
1.386	23.89	-54.14	3.37	-3.05	1.44	1.13	-0.867
1.841	31.33	-72.82	5.88	-5.38	2.58	2.00	-1.53
2.264	37.96	-90.81	8.78	-8.11	3.94	3.04	-2.33
2.655	43.82	-108.1	11.93	-11.13	5.49	4.21	-3.21
3.016	49.00	-124.7	15.23	-14.36	7.19	5.47	-4.17
3.352	53.57	-140.8	18.61	-17.72	9.00	6.82	-5.18
3.664	57.64	-156.4	22.00	-21.16	10.90	8.23	-6.23

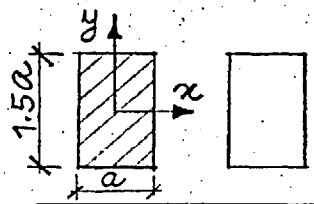


TABLE 9

plate 1.(1)

mesh: 12×20 equal

accuracy: 0.5%

$\varepsilon' = 1/1.5$, $\alpha = 1$

$\beta = 1$, $\gamma = 1$

$\sqrt{\nu_{xm} \cdot \nu_{ym}} = 0.3$

$\nu_{xb} = \nu_{yb} = 0.3$

Q'	W_1'	M_{x1}'	M_{y1}'	N_{x1}'	N_{x3}'	N_{y1}'	N_{y2}'
linear	7.732×10^{-3}	8.085×10^{-2}	4.979×10^{-2}	0	0	0	0
150	1.141	11.88	7.28	0.436	-0.966	1.038	-1.809
400	2.826	28.79	17.26	2.336	-6.050	6.019	-10.56
750	4.650	45.62	26.47	5.491	-17.56	15.80	-27.97
1100	6.063	57.54	32.66	8.092	-31.25	25.81	-46.03
1500	7.371	67.71	37.87	10.44	-48.00	36.85	-66.16
1900	8.466	75.60	41.96	12.67	-65.18	47.47	-85.57
2300	9.419	82.01	45.37	14.57	-82.37	57.46	-104.2
2700	10.27	87.40	48.34	16.31	-99.35	67.02	-122.1
3100	10.98	91.26	50.41	18.31	-117.1	77.14	-147.1
3500	11.82	96.85	54.19	18.77	-132.0	84.06	-154.2

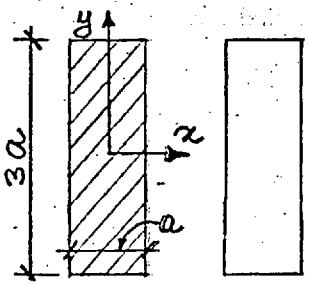


TABLE II

plate 1.(1)

mesh: 12×20 graded, No 3

accuracy: 0.5%

$\varepsilon' = 1/3$, $\alpha = 1$

$\beta = 1$, $\gamma = 1$

$\sqrt{\nu_{xm} \cdot \nu_{ym}} = 0.3$

$\nu_{xb} \cdot \nu_{yb} = 0.3$

W_1'	M_{x1}'	M_{y1}'	N_{x1}'	N_{x3}'	N_{y1}'	N_{y2}'
1.228×10^{-2}	1.187×10^{-1}	4.067×10^{-2}	0	0	0	0
1.836	17.76	6.122	-0.078	-0.611	0.631	-0.983
4.796	46.40	16.28	-0.226	-4.185	4.557	-7.228
8.511	82.08	29.28	-0.166	-13.87	14.66	-23.50
11.67	111.90	40.33	0.002	-27.69	27.58	-44.42
14.67	139.17	49.64	0.936	-46.67	44.15	-71.63

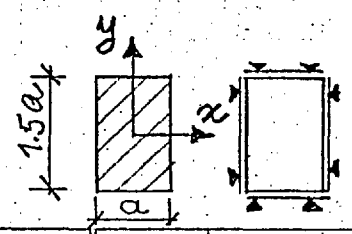


TABLE 10

plate : 1.(6)

mesh : 12×20

equal

accuracy : 0.5%

$\varepsilon = 1/1.5$, $\alpha = 1$

$\beta = 1$, $\gamma = 1$

$\sqrt{D_{xm} \cdot D_{ym}} = 0.3$

$D_{xb} = D_{yb} = 0.3$

Q'	W_1'	M_{x1}'	M_{y1}'	N_{y1}'	N_{y2}'	N_{x1}'	N_{x2}'	N_{y3}'	N_{y4}'	N_{x3}'	N_{x4}'
linear	7.732×10^{-3}	8.085×10^{-2}	4.979×10^{-2}	0	0	0	0	0	0	0	0
150	1.010	10.45	6.32	1.632	0.564	2.827	2.888	1.766	0.497	0.340	0.372
400	1.999	20.22	11.75	5.880	2.226	10.053	10.42	6.631	1.679	1.329	1.308
750	2.705	26.61	14.72	12.06	4.891	20.40	21.33	14.04	3.231	2.991	2.611
1100	3.245	31.38	16.84	16.87	7.291	28.28	29.78	20.15	4.253	4.305	3.555
1500	3.688	35.11	18.33	22.09	9.844	36.75	38.90	26.91	5.266	5.898	4.534
1900	4.037	37.96	19.39	26.98	12.38	44.60	47.39	33.33	6.132	7.459	6.409
2300	4.333	40.34	20.26	31.55	14.82	51.90	55.29	39.41	6.873	8.977	6.190
2700	4.594	42.43	21.02	35.85	17.15	58.71	62.69	45.18	7.514	10.45	6.893
3100	4.776	43.75	21.37	40.49	19.65	66.10	70.68	51.35	8.220	12.03	7.654

TABLE 12

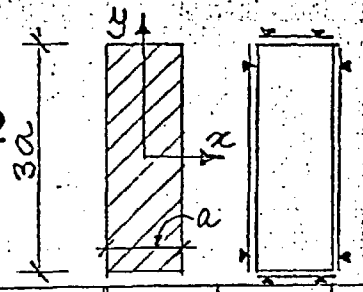


plate 1.(6)

mesh : 12×20

graded, No.3

accuracy: 0.5%

$\varepsilon = 1/3$, $\alpha = 1$

$\beta = 1$, $\gamma = 1$

$\sqrt{\nu_{xm} \cdot \nu_{ym}} = 0.3$

$\nu_{xb} = \nu_{yb} = 0.3$

Q'	W_1'	M_{x1}'	M_{y1}'	N_{y1}'	N_{y2}'	N_{x1}'	N_{x2}'	N_{y3}'	N_{y4}'	N_{x3}'	N_{x4}'
linear	1.228×10^{-2}	1.187×10^{-1}	4.067×10^{-2}	0	0	0	0	0	0	0	0
150	1.317	12.53	4.03	1.420	1.232	4.625	4.669	2.011	0.723	0.442	0.344
400	2.223	20.67	6.30	4.395	4.062	13.35	13.49	6.845	1.408	1.526	0.955
750	2.916	26.64	7.98	8.031	7.632	23.18	23.47	13.29	1.773	3.031	1.506
1 100	3.394	30.62	9.12	11.26	10.81	31.62	31.92	19.23	1.755	4.485	1.853
1 500	3.819	34.10	10.14	14.64	14.13	40.27	40.63	25.54	1.497	6.093	2.107
1 900	4.167	36.91	10.98	17.77	17.21	48.20	48.61	31.48	1.095	7.653	2.264
2 300	4.461	39.24	11.67	20.76	20.14	55.70	56.16	37.15	0.613	9.183	2.360
2 700	4.428	41.35	12.30	23.55	22.88	62.67	63.17	42.50	0.059	10.66	2.400
3 100	4.966	43.23	12.86	26.24	25.52	69.34	69.88	47.66	-0.531	12.12	2.404
3 500	5.184	44.94	13.38	28.81	28.04	75.71	76.29	52.61	-1.520	13.54	2.379

TABLE 13

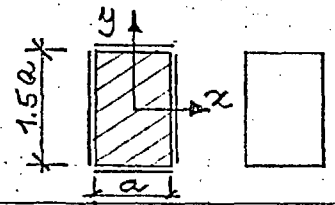


plate: 5.(1)
mesh: 12×20
graded, No.2
accuracy: 0.5%

$\varepsilon' = 1/15$, $\alpha = 1$
$\beta = 1$, $\gamma = 1$
$\sqrt{\nu_{xm} \cdot \nu_{ym}} = 0.3$
$\nu_{xb} = \nu_{yb} = 0.3$

Q'	W_1'	M_{x1}'	M_{y1}'	M_{x2}'	M_{y3}'	N_{x1}'	N_{y1}'	N_{y2}'	N_{x3}'
linear	2.260×10^{-3}	3.671×10^{-2}	2.065×10^{-2}	-7.427×10^{-2}	-5.819×10^{-2}	0	0	0	0
150	0.339	5.50	3.09	-11.13	-8.73	0.066	0.141	-0.191	-0.065
400	0.897	14.52	8.14	-29.53	-23.24	0.454	0.980	-1.33	-0.456
750	1.651	26.54	14.74	-54.63	-43.43	1.49	3.29	-4.49	-1.78
1 100	2.359	37.56	20.63	-78.62	-63.37	2.91	6.62	-9.10	-3.31
1 500	3.107	48.84	26.43	-104.5	-85.76	4.75	11.26	-15.61	-5.94
1 900	3.788	58.73	31.31	-128.7	-107.7	6.74	16.58	-23.17	-9.18
2 300	4.414	67.49	35.51	-151.5	-129.1	8.67	22.19	-31.24	-12.92
2 700	4.990	75.30	39.15	-173.1	-150.0	10.51	27.97	-39.67	-17.08
3 100	5.525	82.33	42.37	-193.6	-170.4	12.27	33.82	-48.31	-21.60
3 500	6.024	88.69	45.26	-213.1	-190.3	13.92	39.70	-57.07	-26.42

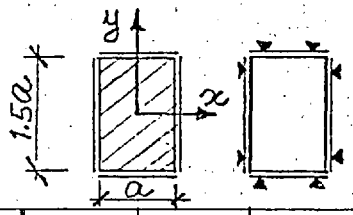


TABLE 14

plate: 5·(6)
mesh: 12×20.
graded, No. 2
accuracy: 0.5 %

$\varepsilon' = 1/1.5$, $\alpha = 1$
$\beta = 1$, $\gamma = 1$
$\sqrt{\nu_{xm} \cdot \nu_{ym}} = 0.3$
$\nu_{xb} = \nu_{yb} = 0.3$

Q'	w_1'	M'_{x1}	M'_{y1}	M'_{x2}	M'_{y3}	N'_{x1}	N'_{y1}	N'_{x2}	N'_{y2}	N'_{x3}	N'_{y3}	N'_{x4}	N'_{y4}
linear	2.260×10^{-3}	3.671×10^{-2}	2.065×10^{-2}	-7.427×10^{-2}	-5.819×10^{-2}	0	0	0	0	0	0	0	0
150	0.337	5.47	3.07	-11.10	-8.71	0.288	0.203	0.262	-0.003	-0.004	0.119	0.071	0.125
400	0.873	14.06	7.85	-29.02	-22.90	1.910	1.341	1.745	-0.013	-0.025	0.798	0.472	0.830
750	1.528	24.20	13.31	-52.01	-41.58	5.777	4.051	5.348	0.010	-0.075	2.491	1.453	2.535
1 100	2.069	32.15	17.38	-72.45	-58.76	10.49	7.350	9.849	0.124	-0.132	4.683	2.692	4.653
1 500	2.573	39.07	20.72	-93.15	-76.73	16.34	11.44	15.55	0.367	-0.197	7.556	4.278	7.325
1 900	2.994	44.53	23.20	-111.9	-93.39	22.07	15.44	21.29	0.729	-0.249	10.56	5.894	10.00
2 300	3.356	48.95	25.12	-129.1	-109.0	27.65	19.33	26.96	1.182	-0.288	13.64	7.513	12.65
2 700	3.672	52.64	26.65	-145.2	-123.7	33.03	23.08	32.52	1.708	-0.312	16.65	9.117	15.23
3 100	3.955	55.80	27.91	-160.4	-137.8	38.22	26.70	37.95	2.291	-0.322	19.87	10.70	17.76
3 500	4.212	58.57	28.99	-174.8	-151.2	43.22	30.18	43.22	2.917	-0.317	22.96	12.24	20.21

TABLE 15

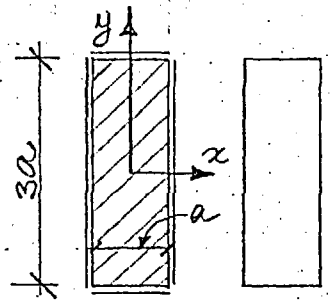


plate: S.(1)
mesh: 12×20
graded, No. 4
accuracy: 0.5%

$\varepsilon' = 1/3$, $\alpha = 1$
$\beta = 1.$, $\gamma = 1$
$\sqrt{\nu_{xm} \cdot \nu_{ym}} = 0.3$
$\nu_{xb} = \nu_{yb} = 0.3$

Q'	W'_1	M'_{x1}	M'_{y1}	M'_{x2}	M'_{y3}	N'_{x1}	N'_{y1}	N'_{y2}	N'_{x3}
linear	2.730×10^{-3}	4.232×10^{-2}	1.292×10^{-2}	-8.329×10^{-2}	-5.818×10^{-2}	0	0	0	0
150	0.409	6.35	1.94	-12.49	-8.23	0.016	0.026	0.032	-0.025
400	1.093	16.96	5.20	-33.35	-23.26	0.110	0.192	-0.237	-0.176
750	2.055	31.92	9.88	-62.67	-43.57	0.347	0.729	-0.913	-0.604
1 100	3.022	47.01	14.72	-92.15	-63.81	0.637	1.72	-2.19	-1.26
1 500	4.128	64.33	20.40	-125.9	-86.86	0.939	3.53	-4.56	-2.24
1 900	5.229	81.55	26.13	-159.5	-109.8	-1.14	6.13	-8.00	-3.44
2 300	6.326	98.80	32.09	-193.1	-132.8	-1.46	9.25	-12.14	-4.88
2 700	7.399	115.6	37.89	-226.7	-155.7	-1.60	13.21	-17.44	-6.49
3 100	8.443	131.9	43.57	-258.4	-178.6	-1.71	17.86	-23.70	-8.29
3 500	9.473	147.8	48.91	-290.4	-201.3	-150	22.86	-30.38	-10.49

TABLE 16

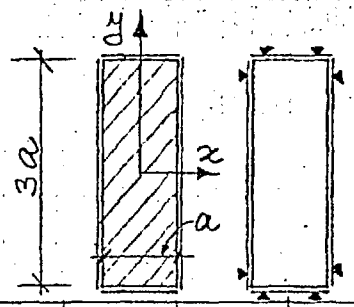


plate : 5.(6)
mesh : 12x20
graded, No. 4
accuracy : 0.5%

$\varepsilon' = 1/3$, $\alpha = 1$
$\beta = 1$, $\gamma = 1$
$\sqrt{\nu_{xm} \cdot \nu_{ym}} = 0.3$
$\nu_{xb} = \nu_{yb} = 0.3$

q'	W_1'	M_{x1}'	M_{y1}'	M_{x2}'	M_{y3}'	N_{x1}'	N_{y1}'	N_{x2}'	N_{y2}'	N_{x3}'	N_{y3}'	N_{x4}'	N_{y4}'
linear	2.730×10^{-3}	4.232×10^{-2}	1.292×10^{-2}	-8.329×10^{-2}	-5.818×10^{-2}	0	0	0	0	0	0	0	0
150	0.405	6.28	1.91	-12.41	-8.70	0.388	0.122	0.397	0.096	0.002	0.124	0.076	0.155
400	1.028	15.76	4.79	-31.97	-22.84	2.453	0.779	2.515	0.629	0.010	0.811	0.493	0.996
750	1.736	26.14	7.88	-55.93	-41.38	6.996	2.249	7.171	1.884	0.016	2.455	1.459	2.879
1100	2.287	33.75	10.12	-76.49	-58.43	12.19	3.969	12.49	3.417	0.017	4.524	2.612	5.042
1500	2.788	40.27	12.04	-97.11	-76.40	18.24	6.014	18.66	5.289	0.024	7.150	3.982	7.526
1900	3.201	45.34	13.53	-115.6	-93.10	24.14	8.056	24.68	7.189	0.046	9.919	5.330	9.814
2300	3.554	49.46	14.75	-132.7	-108.8	29.85	10.06	30.49	9.075	0.087	12.76	6.626	12.11
2700	3.864	52.93	15.77	-148.7	-123.7	35.36	12.03	36.10	10.93	0.150	15.64	7.864	14.83
3100	4.142	55.91	16.66	-163.9	-137.9	40.69	13.95	41.51	12.76	0.234	18.53	9.045	16.12
3500	4.394	58.53	17.43	-178.3	-151.5	45.85	15.84	46.75	14.55	0.337	21.44	10.17	17.94

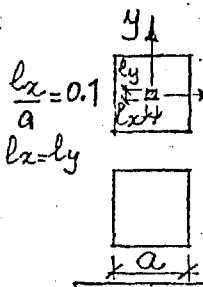


TABLE 17

Plate 1.(1)
mesh: 16×16
graded, No 5
accuracy: 0.5%

$\varepsilon' = 1$, $\alpha = 1$
$\beta = 1$, $\gamma = 1$
$\sqrt{\nu_{xm} \cdot \nu_{ym}} = 0.3$
$\nu_{xb} = \nu_{yb} = 0.3$

Q'	W_1'	M_{x1}', M_{y1}'	N_{x1}', N_{y1}'	N_{x3}', N_{y2}'	U_2', V_3'
linear	1.148×10^{-4}	2.874×10^{-2}	0	0	0
25 000	2.532	64.96	9.75	-10.78	-4.73
50 000	4.236	112.9	26.58	-29.19	-13.09
100 000	6.448	183.0	61.28	-66.41	-30.99
150 000	8.008	237.9	93.96	-100.6	-48.56
200 000	9.258	284.9	124.9	-132.3	-65.78
250 000	10.32	326.6	154.6	-161.9	-82.73
300 000	11.26	364.6	183.3	-190.1	-99.47
350 000	12.12	399.9	210.8	-216.4	-115.9
400 000	12.90	432.6	237.8	-241.9	-132.2

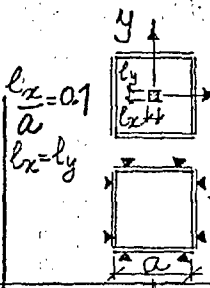


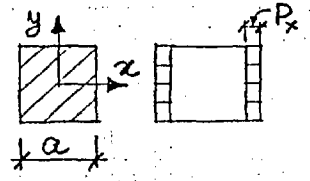
TABLE 18

Plate 5.(6)
mesh: 16×16
graded, No 5
accuracy = 0.5%

$\varepsilon' = 1$, $\alpha = 1$
$\beta = 1$, $\gamma = 1$
$\sqrt{\nu_{xm} \cdot \nu_{ym}} = 0.3$
$\nu_{xb} = \nu_{yb} = 0.3$

Q'	W'	M_{x1}', M_{y1}'	M_{x2}', M_{y3}'	N_{x1}', N_{y1}'	N_{x3}', N_{y2}'	N_{x2}', N_{y3}'	N_{x4}', N_{y4}'	total N_x' or N_y' at $\frac{1}{2}$ the edge
linear	5.538×10^{-6}	2.336×10^{-4}	-1.234×10^{-4}	0	0	0	0	0
75 000	3.042	139.6	-71.0	37.11	-2.925	14.33	12.35	4.802
150 000	4.600	228.4	-113.3	85.94	-5.886	32.46	26.58	10.74
300 000	6.518	356.2	-174.4	176.9	-9.816	64.65	49.37	21.04
450 000	7.842	454.2	-223.3	260.4	-12.48	92.95	67.95	29.98
600 000	8.886	535.5	-266.0	338.8	-14.56	118.7	84.21	38.07
750 000	9.762	605.9	-304.8	413.1	-16.32	142.6	98.96	45.61
900 000	10.52	668.2	-340.8	484.4	-17.88	165.0	112.6	52.69
1 050 000	11.20	724.0	-374.4	553.3	-19.34	186.5	125.6	59.37
1 200 000	11.81	775.3	-406.4	619.5	-20.69	206.8	137.8	65.90
1 350 000	12.38	822.4	-437.0	683.8	-21.99	226.3	149.5	72.09

TABLE 19



$\frac{P_x}{P_e} = 0.25$

Plate 1. (26)
mesh : 12×12 uniform
accuracy: 0.5%

$\varepsilon' = 1$, $\alpha = 1$
$\beta = 1$, $\gamma = 1$
$\sqrt{\nu_{xm} \cdot \nu_{ym}} = 0.3$
$\nu_{xb} \cdot \nu_{yb} = 0.3$

Q'	W_1'	M_{X1}'	M_{Y1}'	N_{X1}'	N_{X3}'	N_{Y1}'	N_{Y2}'	U'	V'
linear	0.00544	0.06493	0.06519	-9.869	-9.869	0	0	-4.935	1.480
150	0.805	9.54	9.57	-9.20	-11.07	0.67	-1.20	-6.38	1.48
400	1.993	23.01	23.14	-5.96	-17.05	3.89	-7.22	-20.79	0.56
750	3.272	35.91	36.21	0.34	-29.42	10.14	-19.67	-101.6	-7.85
1100	4.252	44.43	44.92	6.64	-42.78	16.36	-33.18	-239.3	-23.84
1 500	5.150	51.17	51.88	13.42	-58.12	23.02	-48.75	-443.6	-48.97
1 900	5.896	56.00	56.92	19.72	-73.25	29.18	-64.12	-715.1	-83.91
2 300	6.540	59.68	60.79	25.58	-88.01	34.91	-79.17	-1053	-128.9
2 700	7.113	62.63	63.92	31.06	-102.3	40.24	-93.81	-1458	-184.1
3 100	7.584	64.39	65.85	36.85	-117.5	45.87	-109.3	-1773	-227.3
3 500	8.142	67.62	69.22	40.64	-129.0	49.52	-121.1	-2131	-277.8

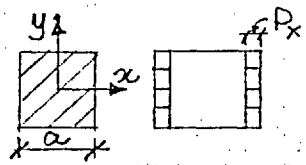


TABLE 20

$\frac{P_x}{P_e} = 0.5$

Plate 1.(26)
mesh: 12×12
uniform
accuracy: 0.5%

$\varepsilon' = 1, \alpha = 1$
$\beta = 1, \delta = 1$
$\sqrt{\nu_{xm}\nu_{ym}} = 0.3$
$\nu_{xb} = \nu_{yb} = 0.3$

Q'	W_1'	M_{x1}'	M_{y1}'	N_{x1}'	N_{x3}'	N_{y1}'	N_{y2}'
linear	8.253×10^{-3}	10.02×10^{-2}	10.08×10^{-2}	-19.740	-19.740	0	0
150	1.176	-14.09	-14.19	-18.23	-22.39	1.45	-2.67
400	2.646	30.19	30.57	-12.75	-32.58	6.92	-12.97
750	4.036	43.11	43.97	-5.04	-48.28	14.44	-28.98
1 100	5.013	50.45	51.81	2.20	-64.15	21.45	-45.30
1 500	5.871	55.70	57.57	9.79	-81.82	28.72	-63.58
1 900	6.592	59.52	61.86	16.51	-98.39	35.09	-80.82
2 300	7.112	60.99	63.77	23.82	-116.5	42.05	-99.62
2 700	7.743	64.36	67.50	28.66	-130.0	46.54	-113.9
3 100	8.185	65.47	68.95	34.71	-146.1	52.23	-130.7
3 500	8.729	68.18	71.96	38.81	-158.5	56.60	-143.8

TABLE 21

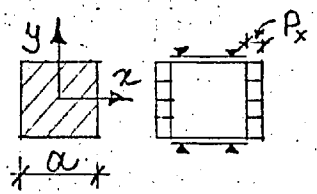
plate 1.(26)

$\frac{P_x}{P_e} = 0.75$

(Plate parameters the same as in table 20)

W_1'	M_{x1}'	M_{y1}'	N_{x1}'	N_{x3}'	N_{y1}'	N_{y3}'
16.806×10^{-3}	20.87×10^{-2}	20.97×10^{-2}	-29.609	-29.609	0	0
1.977	23.59	23.86	-25.60	-36.68	3.97	-7.13
3.561	39.15	40.14	-17.02	-53.10	12.33	-23.92
4.951	50.27	52.25	-8.30	-71.80	20.60	-43.44
5.855	55.56	58.43	-0.40	-89.83	27.98	-62.46
6.671	59.47	63.21	7.41	-108.7	35.17	-82.59
7.359	62.30	66.78	14.29	-126.2	41.42	-101.4
7.961	64.50	69.64	20.53	-142.7	47.04	-119.1
8.501	66.31	72.02	26.28	-158.3	52.17	-136.1
8.901	66.70	72.92	32.56	-175.2	57.83	-154.2
9.406	68.65	75.32	37.13	-188.6	61.84	-168.8

TABLE 22



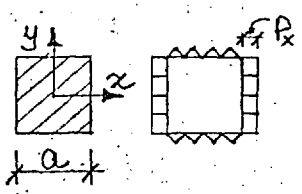
$\frac{P_x}{P_e} = 0.5$

plate 1.(27)
mesh: 12×12 uniform
accuracy: 0.5%

$\varepsilon = 1$, $\alpha = 1$
$\beta = 1$, $\gamma = 1$
$\sqrt{\nu_{xm} \cdot \nu_{ym}} = 0.3$
$\nu_{xb} = \nu_{yb} = 0.3$

Q'	W_1'	M_{x1}'	M_{y1}'	N_{x1}'	N_{x3}'	N_{y1}'	N_{y2}'	total N_y' at the edge
linear	11.893×10^{-3}	14.66×10^{-2}	14.70×10^{-2}	-19.739	-19.739	-5.922	-5.922	-2.96
150	1.375	16.52	16.67	-18.28	-21.36	-0.96	-7.90	-1.80
400	2.422	27.60	28.29	-15.33	-24.76	9.85	-12.23	0.79
750	3.310	35.77	37.36	-12.55	-28.13	21.22	-16.81	3.67
1100	3.855	39.71	42.34	-10.11	-27.66	31.77	-21.09	6.44
1500	4.329	42.54	46.38	-7.78	-34.05	42.47	-25.44	9.33
1900	4.717	44.48	49.55	-5.79	-36.57	52.06	-29.37	12.01
2300	5.049	45.87	52.18	-4.04	-38.79	60.86	-32.99	14.52
2700	5.342	46.91	54.43	-2.47	-40.79	69.04	-36.37	16.91
3100	5.541	46.91	55.66	-0.73	-42.97	77.86	-40.03	19.47
3500	5.813	47.92	57.83	0.45	-44.48	84.56	-42.84	21.53

TABLE 23



$\frac{P_x}{P_e} = 0.5$

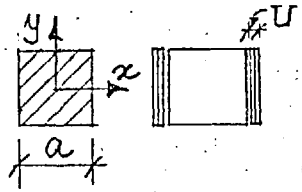
plate 1.(29)
mesh: 12×12 uniform
accuracy : 0.5 %

$\varepsilon' = 1$, $\alpha = 1$
$\beta = 1$, $\gamma = 1$
$\sqrt{D_{xm} \cdot D_{ym}} = 0.3$
$\nu_{xb} = \nu_{yb} = 0.3$

Q'	W_1'	M_{x1}'	M_{y1}'	N_{x1}'	N_{xy}'	N_{y1}'	N_{y2}'	total N_{xy}' *
linear	6.933×10^{-3}	8.213×10^{-2}	8.459×10^{-2}	-20.294	0	5.038	-9.322	-2.816
150	1.063	11.69	12.07	-19.26	0	6.44	-11.84	3.05
400	2.301	25.61	26.78	-15.21	0	11.93	-22.18	3.99
750	3.545	36.92	39.34	-9.22	0	20.11	-38.98	5.51
1100	4.428	43.38	47.11	-3.58	0	27.82	-56.10	7.04
1500	5.198	47.83	53.03	2.38	0	35.97	-75.42	8.75
1900	5.843	50.96	57.57	7.66	0	43.18	-93.66	10.36
2300	6.401	53.27	61.23	12.47	0	49.75	-111.1	11.88
2700	6.896	55.02	64.26	16.93	0	55.83	-128.0	13.35
3100	7.343	56.41	66.87	21.11	0	61.52	-144.4	14.76
3500	7.699	56.84	68.47	25.62	0	67.64	-161.8	16.26

* Total N_{xy} of the sides $y = \pm b/2$, between $x = 0$ and $x = a/2$

TABLE 24



$\frac{U}{U_e} = 0.5$

plate 1.(38)
mesh : 12×12 uniform
accuracy: 0.5%

$\varepsilon' = 1$, $\alpha = 1$
$\beta = 1$, $\delta = 1$
$\sqrt{\nu_{xm} \cdot \nu_{ym}} = 0.3$
$\nu_{xb} = \nu_{yb} = 0.3$

Q'	W_1'	M_{x1}'	M_{y1}'	N_{x1}'	N_{x3}'	N_{y1}'	N_{y2}'
linear	8.253×10^{-3}	10.02×10^{-2}	10.08×10^{-2}	-19.739	-19.739	0	0
150	1.094	13.12	13.17	-16.58	-20.98	0.91	-1.03
400	2.195	25.52	25.50	-7.87	-24.41	3.25	-3.77
750	3.012	33.71	33.29	4.69	-29.32	6.38	-7.59
1 100	3.635	39.68	38.72	14.47	-33.13	8.57	-10.39
1 500	4.148	44.24	42.54	24.99	-37.23	10.82	-13.30
1 900	4.555	47.65	45.12	34.71	-41.02	12.81	-15.90
2 300	4.899	50.46	47.06	43.70	-44.52	14.58	-18.22
2 700	5.203	52.88	48.58	52.06	-47.79	16.17	-20.31
3 100	5.415	54.30	49.04	61.09	-51.33	17.93	-22.58
3 500	5.696	56.61	50.46	67.93	-54.01	19.12	-24.17

TABLE 25

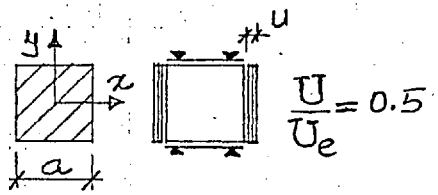


Plate 1. (39)
mesh: 12x12 uniform
accuracy: 0.5%

$\varepsilon' = 1$, $\alpha = 1$
$\beta = 1$, $\gamma = 1$
$\sqrt{\upsilon_{xm} \cdot \upsilon_{ym}} = 0.3$
$\upsilon_{xb} \cdot \upsilon_{yb} = 0.3$

Q'	W_1'	M_{x1}'	M_{y1}'	N_{x1}'	N_{x3}'	N_{y1}'	N_{y2}'	N_{y3}'	N_{y4}'	total $\frac{N_y'}{2}$ at the edge
linear	14.653×10^{-3}	18.16×10^{-2}	18.21×10^{-2}	-21.691	-21.691	-6.507	-6.507	-6.507	-6.507	-3.254
150	1.288	15.53	15.61	-16.91	-20.88	-1.74	-5.71	-1.71	-5.45	-1.83
400	2.098	24.39	24.58	-9.81	-19.55	5.33	-4.37	5.61	-3.94	0.35
750	2.617	29.24	29.55	-0.91	-17.70	14.17	-2.53	14.97	-2.15	3.15
1100	3.047	33.19	33.59	5.77	-16.15	20.81	-0.98	22.17	-0.87	5.30
1500	3.409	36.28	36.76	12.73	-14.44	27.71	0.72	29.79	0.40	7.58
1900	3.694	38.57	39.14	19.18	-12.78	34.12	2.37	36.86	1.55	9.71

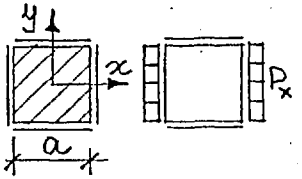


TABLE 26

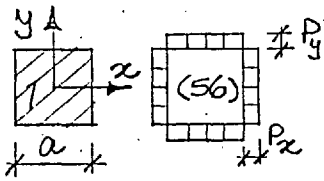
$\frac{P_x(\text{total at } x=\pm a/2)}{P_e(\text{total at } x=\pm a/2)} = 1.259$

Plate 5. (45)
mesh: 12x12 graded, No.1
accuracy: 0.5%

$\varepsilon' = 1$, $\alpha = 1$
$\beta = 1$, $\gamma = 1$
$\sqrt{\nu_{xm} \cdot \nu_{ym}} = 0.3$
$\nu_{xb} = \nu_{yb} = 0.3$

Q'	W_1'	M_{x1}'	M_{x2}'	M_{y1}'	M_{y3}'	N_{x1}'	N_{x3}'	N_{y1}'	N_{y2}'	N_{x2}'	N_{x4}'	U'	V'	effective width
linear	2.627×10^{-3}	5.421×10^{-2}	-7.138×10^{-2}	5.071×10^{-2}	-9.331×10^{-2}	-49.694	-49.694	0	0	-49.694	-49.694	-24.847	7.4541	1
150	0.392	8.06	-10.66	7.55	-13.93	-49.39	-49.95	0.31	-0.24	-49.59	-49.60	-24.91	7.389	0.997
400	1.009	20.55	-27.91	19.27	-36.23	-47.74	-51.39	2.02	-1.59	-49.02	-49.10	-25.30	7.028	0.982
750	1.758	34.84	-50.23	32.78	-64.36	-43.93	-54.78	5.94	-4.77	-47.63	-47.90	-26.21	6.159	0.941
1100	2.368	45.50	-70.37	43.01	-88.86	-39.32	-58.98	10.65	-8.76	-45.81	-46.39	-27.36	5.053	0.908
1500	2.945	54.59	-91.39	51.89	-113.6	-33.98	-64.03	16.11	-13.60	-43.49	-44.55	-28.77	3.682	0.863
1900	3.429	61.46	-110.8	58.73	-135.7	-28.77	-69.11	21.39	-18.50	-41.02	-42.64	-30.23	2.263	0.822
2300	3.848	66.85	-129.0	64.19	-156.0	-23.79	-74.09	26.41	-23.35	-38.48	-40.72	-31.69	0.831	0.786
2700	4.219	71.20	-146.2	68.70	-174.9	-19.07	-78.94	31.16	-28.12	-35.87	-38.78	-33.14	-0.598	0.750
3100	4.552	74.81	-162.7	72.49	-192.6	-14.56	-83.66	35.64	-32.78	-33.25	-36.84	-34.58	-2.020	0.718
3500	4.857	77.86	-178.6	75.76	-209.5	-10.27	-88.24	39.93	-37.34	-30.60	-34.88	-36.01	-3.43	0.690

TABLE 27



$P_x = P_y$

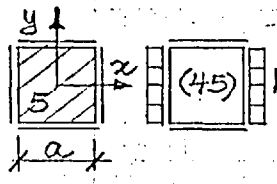
$\frac{P_x}{P_e} = 0.25$

Plate : 1.(56)
mesh : 12×12
uniform
accuracy : 0.5%

$\varepsilon' = 1, \alpha = 1$
$\beta = 1, \gamma = 1$
$\sqrt{\upsilon_{xm} \cdot \upsilon_{ym}} = 0.3$
$\upsilon_{xb} = \upsilon_{yb} = 0.3$

Q'	W_1'	M_{x1}' or M_{y1}'	N_{x1}' or N_{y1}'	N_{x3}' or N_{y2}'
linear	8.253×10^{-3}	10.05×10^{-2}	-9.8696	-9.8696
150	1.177	14.15	-8.36	-12.53
400	2.649	30.46	-2.94	-22.71
750	3.997	43.03	5.17	-39.39
1 100	4.967	50.56	12.37	-55.61
1 500	5.843	56.36	19.61	-73.22
1 900	6.573	60.58	26.07	-89.94
2 300	7.207	63.84	31.94	-105.9
2 700	7.772	66.49	37.37	-121.3
3 100	8.285	68.71	42.44	-136.1
3 500	8.756	70.62	47.21	-150.4

TABLE 28



$Q' = 72.180$

$\left(\frac{a^4}{h^4}\cdot\frac{q}{E} = 2\right)$

plate : 5. (45)

mesh : 12×12 graded, No.1

accuracy = 0.5 %

$\varepsilon' = 1, \alpha = 1, \beta = 1, \gamma = 1$

$\sqrt{\nu_{xm}\cdot\nu_{ym}} = 0.3$

$\nu_{xb} = \nu_{yb} = 0.3$

$P_x'/2$ total	W_1'	M_{x1}'	M_{y1}'	M_{x2}'	M_{y3}'	N_{x1}'	N_{y1}'	N_{x2}'	N_{y2}'	N_{x3}'	N_{x4}'	N_{y3}'	U'	V'	Effective width
0	0.0943	1.653	1.653	-3.621	-3.621	0.0158	0.0158	0.0066	-0.014	-0.014	0.0052	0.0066	-0.004	-0.004	—
-4	0.102	1.83	1.82	-3.77	-3.89	-7.98	0.019	-7.99	-0.018	-8.02	-7.99	0.0076	-4.005	1.195	0.999
-8	0.112	2.05	2.02	-3.95	-4.20	-15.98	0.021	-15.99	-0.018	-16.02	-15.99	0.0083	-8.005	2.395	0.999
-12	0.124	2.33	2.27	-4.15	-4.59	-23.97	0.029	-23.99	-0.024	-24.02	-23.99	0.0107	-12.007	3.593	0.999
-16	0.139	2.67	2.58	-4.40	-5.07	-31.96	0.037	-31.99	-0.031	-32.03	-31.99	0.0131	-16.009	4.792	0.999
-20	0.156	3.13	2.98	-4.69	-5.69	-39.95	0.049	-39.98	-0.039	-40.04	-39.98	0.0164	-20.011	5.989	0.999
-23	0.176	3.57	3.37	-4.95	-6.28	-45.94	0.061	-45.98	-0.049	-46.05	-45.98	0.0198	-23.014	6.887	0.999
-26	0.199	4.14	3.58	-5.27	-7.04	-51.92	0.080	-51.97	-0.062	-52.07	-51.98	0.0246	-26.017	7.783	0.999
-29	0.229	4.90	4.50	-5.67	-8.02	-57.89	0.108	-57.97	-0.081	-58.09	-57.97	0.0314	-29.023	8.678	0.999
-32	0.269	5.96	5.38	-6.18	-9.36	-63.85	0.154	-63.95	-0.112	-64.12	-63.96	0.0419	-32.032	9.571	0.999
-36	0.352	8.18	7.21	-7.18	-12.15	-71.74	0.274	-71.92	-0.193	-72.22	-71.92	0.0677	-36.055	10.75	0.999
-40	0.510	12.45	10.66	-8.93	-17.42	-79.44	0.560	-79.85	-0.403	-80.47	-79.83	0.1313	-40.12	11.90	0.999

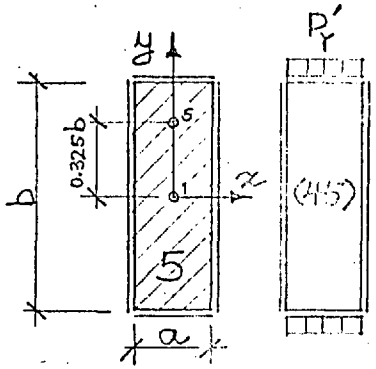


TABLE 29

$Q' = 72.180$

$\left(\frac{a^4}{h^4}\cdot\frac{q}{E} = 2\right)$

Plate: 5. (45)

mesh: 12×20 graded, No.3

accuracy: 0.5%

$\varepsilon' = 1/3$, $\alpha = 1$

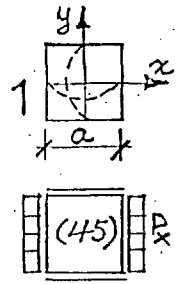
$\beta = 1$, $\gamma = 1$

$\sqrt{\nu_{xm}\cdot\nu_{ym}} = 0.3$

$\nu_{xb} = \nu_{yb} = 0.3$

$P_Y'/2$ total	W_1'	W_5'	M_{X1}'	M_{Y1}'	M_{X2}'	M_{Y3}'	N_{X1}'	N_{Y1}'	N_{X2}'	N_{Y2}'	N_{X3}'	N_{Y3}'	V'	U'	Effective width
0	0.197	0.148	3.05	0.932	-6.01	-4.20	0.0279	0.0036	0.0302	-0.0026	-0.0621	0.0039	-0.00931	-0.0276	——
-4	0.198	0.153	3.07	0.918	-6.03	-4.20	0.0265	-7.997	0.0291	-8.002	-0.0651	-7.996	-12.010	1.171	1.000
-8	0.198	0.160	3.07	0.897	-6.04	-4.21	0.0244	-15.998	0.0274	-16.001	-0.0685	-15.996	-24.011	2.370	1.000
-14	0.197	0.171	3.04	0.841	-5.99	-4.22	0.0192	-28.000	0.0230	-27.999	-0.0747	-27.996	-42.012	4.168	1.000
-20	0.193	0.188	2.94	0.733	-5.83	-4.22	0.0095	-40.007	0.0147	-39.996	-0.0836	-39.996	-60.014	5.9657	1.000
-25	0.182	0.209	2.74	0.555	-5.49	-4.23	-0.0057	-50.006	0.0014	-49.993	-0.0958	-49.997	-75.017	7.463	1.000
-30	0.154	0.244	2.30	0.119	-4.62	-4.18	-0.0283	-60.001	-0.0266	-59.999	-0.1220	-60.003	-90.025	8.958	1.000
-35	-0.077	0.313	-0.62	-5.09	2.16	-2.74	-0.107	-69.99	-0.147	-70.89	-0.349	-70.02	-105.11	10.425	0.999

TABLE 30



Initially deformed plate.

$W_o = W_{omax} \cos \pi X \cos \pi Y$

$W_{omax} = 0.3305$

$\left(\frac{W_{omax}}{h} = 0.1\right)$

Plate 1. (45)

mesh: 12×12

uniform

accuracy : 0.5%

$\varepsilon' = 1, \alpha = 1$

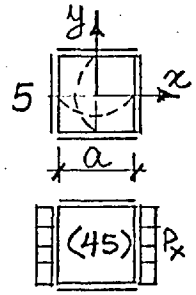
$\beta = 1, \gamma = 1$

$\sqrt{\nu_{xm}' \nu_{ym}} = 0.3$

$\nu_{xb} = \nu_{yb} = 0.3$

$P_x'/2$ total	W_1'	M_{x1}'	M_{y1}'	N_{x1}'	N_{y1}'	N_{x2}'	N_{y2}'	N_{x3}'	N_{x4}'	N_{y3}'	U'	V'	Effective-width
0	0.3305	0	0	0	0	0	0	0	0	0	0	0	—
−3	0.3898	0.756	0.756	−5.974	0.0256	−5.976	−0.0265	−6.026	−6.021	0.0241	−3.0124	0.8876	0.996
−6	0.4735	1.820	1.820	−11.86	0.143	−11.86	−0.149	−12.15	−12.12	0.135	−6.0696	1.7304	0.988
−9	0.6014	3.444	3.445	−17.68	0.316	−17.70	−0.328	−18.33	−18.26	0.299	−9.1536	2.5464	0.983
−12	0.8135	6.124	6.128	−23.31	0.692	−23.34	−0.720	−24.72	−24.58	0.656	−12.338	3.2624	0.973
−15	1.191	10.84	10.86	−28.36	1.639	−28.43	−1.711	−31.17	−31.39	1.563	−15.804	3.6960	0.949
−18	1.812	18.38	18.47	−32.10	3.884	−32.23	−4.092	−40.10	−39.38	3.761	−19.935	3.4647	0.903
−19	2.054	21.22	21.37	−32.95	5.015	−33.08	−5.308	−43.30	−42.41	4.890	−21.518	3.1822	0.883

TABLE 31



Initially deformed plate

$W_o = W_{omax} \cos \pi X \cdot \cos \pi Y$

$W_{omax} = 0.3305$

$\left(\frac{W_{omax}}{h} = 0.1\right)$

plate 5.(45) $\varepsilon' = 1$, $\alpha = 1$

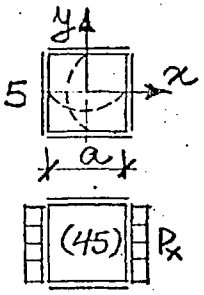
mesh: 12×12 $\beta = 1$, $\gamma = 1$

graded, No.1 $\sqrt{\nu_{xm} \cdot \nu_{ym}} = 0.3$

accuracy: 0.5% $\nu_{xb} = \nu_{yb} = 0.3$

$P_x'/2$ total	W_1'	M_{x1}'	M_{y1}'	M_{x2}'	M_{y3}'	N_{x1}'	N_{y1}'	N_{x2}'	N_{y2}'	N_{x3}'	N_{x4}'	N_{y3}'	U'	V'	Effective width
0	0.3305	0	0	0	0	0	0	0	0	0	0	0	0	0	—
-5	0.3646	0.670	0.663	-1.095	-1.142	-9.982	0.0177	-9.991	-0.0162	-10.02	-9.999	0.00091	-5.0053	1.4947	0.9997
-15	0.4617	2.692	2.593	-3.736	-4.367	-29.83	0.169	-29.92	-0.147	-30.15	-29.99	0.0785	-15.046	4.454	0.9977
-25	0.6357	6.642	6.166	-7.435	-10.14	-49.50	0.519	-49.79	-0.425	-50.44	-49.93	0.2110	-25.131	7.372	0.9955
-35	1.023	16.23	14.33	-13.59	-23.17	-68.25	1.867	-69.39	-1.395	-71.54	-69.66	0.6132	-35.429	10.105	0.9913
-40	1.420	25.52	22.72	-18.67	-36.86	-76.38	3.910	-78.83	-2.785	-83.17	-79.19	1.135	-40.837	11.238	0.9877
-45	2.018	42.23	35.76	-46.44	-58.44	-82.22	8.501	-87.62	-5.813	-96.88	-88.02	2.199	-46.761	11.955	0.9862
-50	2.717	60.46	48.73	-31.57	-85.65	-85.46	16.05	-95.61	-10.71	-11.31	-95.95	3.881	-53.302	12.204	0.9862

TABLE 32



Initially deformed plate

$W_0 = W_{0max} \cos \pi X \cdot \cos \pi Y$

$W_{0max} = 1.6525$

$\left(\frac{W_{0max}}{h} = 0.5\right)$

plate 5.(45) $\quad \varepsilon = 1, \ \alpha = 1$

mesh : 12×12 $\quad \beta = 1, \ \gamma = 1$

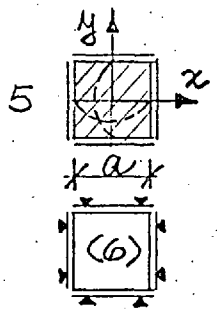
graded, No1 $\quad \sqrt{\nu_{xm} \cdot \nu_{ym}} = 0.3$

accuracy : 0.5% $\quad \nu_{xb} = \nu_{yb} = 0.3$

$P'_x/2$ total	W'_1	M'_{x1}	M'_{y1}	M'_{x2}	M'_{y3}	N'_{x1}	N'_{y1}	N'_{x2}	N'_{y2}	N'_{x3}	N'_{x4}	N'_{y3}	U'	V'	Effective width
0	1.6525	0	0	0	0	0	0	0	0	0	0	0	0	0	—
-5	1.815	3.148	3.116	-5.274	-5.494	-9.561	0.441	-9.774	-0.405	-10.41	-9.984	0.228	-5.1314	1.3687	0.974
-15	2.208	10.927	10.563	-16.60	-19.15	-26.62	3.45	-28.35	-3.08	-33.13	-29.73	1.69	-15.983	3.5221	0.938
-25	2.765	22.417	21.041	-29.96	-39.14	-42.08	8.22	-46.35	-7.09	-57.34	-49.05	3.75	-27.231	5.3020	0.918
-35	3.490	37.599	34.135	-44.51	-67.00	-54.57	16.30	-63.19	-13.62	-84.48	-67.58	7.023	-39.27	6.3603	0.891
-40	3.895	45.982	41.039	-51.66	-83.77	-59.51	21.83	-71.07	-18.01	-99.43	-76.42	9.206	-45.658	6.5679	0.876
-45	4.322	54.692	47.984	-58.52	-102.4	-63.76	28.19	-78.62	-23.03	-115.2	-84.96	11.72	-52.272	6.5921	0.861
-50	4.739	62.895	54.294	-64.63	-121.9	-67.27	35.45	-85.79	-28.74	-132.0	-93.18	14.62	-59.138	6.4157	0.845

TABLE 33

$\varepsilon' = 1,\ \alpha = 1$
$\beta = 1,\ \gamma = 1$
$\sqrt{\nu_{xm} \cdot \nu_{ym}} = 0.3$
$\nu_{xb} = \nu_{yb} = 0.3$



5

Initially deformed plate

$W_o = W_{omax} \cos \pi X \cdot \cos \pi Y$

$W_{omax} = -3.305$

$\left(\frac{W_{omax}}{h} = -1\right)$

Plate 5. (6)
mesh: 12×12.
graded, N01
accuracy: 0.5%

Q'	W_1'	M_{x1}' or M_{y1}'	M_{x2}' or M_{y3}'	N_{x1}' or N_{y1}'	N_{x3}' or N_{y2}'	N_{x2}' or N_{y3}'	N_{x4}' or N_{y4}'	total $\frac{N_x'}{2}$ or $\frac{N_y'}{2}$ at the edge
0	-3.305	0	0	0	0	0	0	0
linear	$W_o + 1.306\times10^{-3}$	—	—	0	0	0	0	0
150	-3.200	1.559	-4.65	-1.950	-0.0121	-1.614	-0.989	-0.495
400	-3.019	4.459	-12.75	-5.285	-0.0306	-4.330	-2.625	-1.330
575	-2.867	6.752	-18.69	-7.618	-0.0467	-6.260	-3.762	-1.924
750	-2.715	9.212	-24.77	-10.11	-0.0639	-8.289	-4.928	-2.549
925	-2.543	13.58	-31.37	-12.48	-0.0925	-10.224	-6.007	-3.146
1100	-2.360	15.30	-38.17	-15.007	-0.129	-12.28	-7.110	-3.780
1300	-2.123	19.59	-46.62	-17.79	-0.194	-14.58	-8.268	-4.487
1500	-1.855	24.61	-55.76	-20.58	-0.295	-16.92	-9.338	-5.205
1700	-1.545	30.51	-65.83	-23.22	-0.459	-19.23	-10.23	-5.910
2000	-0.983	41.88	-83.27	-26.43	-0.914	-22.43	-10.93	-6.866
2300	-0.304	55.73	-103.8	-27.56	-1.771	-24.68	-10.24	-7.488
2700	0.604	73.51	-132.7	-24.59	-3.486	-25.09	-6.759	-7.473